

# The BUMP model of response planning: a neuroengineering account of speed-accuracy tradeoffs, velocity profiles, and physiological tremor in movement

**Author:**

Bye, Robin Trulssen

**Publication Date:**

2009

**DOI:**

<https://doi.org/10.26190/unsworks/20328>

**License:**

<https://creativecommons.org/licenses/by-nc-nd/3.0/au/>

Link to license to see what you are allowed to do with this resource.

Downloaded from <http://hdl.handle.net/1959.4/43542> in <https://unsworks.unsw.edu.au> on 2024-04-23

# THE UNIVERSITY OF NEW SOUTH WALES



SYDNEY • AUSTRALIA

## THE BUMP MODEL OF RESPONSE PLANNING A NEUROENGINEERING ACCOUNT OF SPEED-ACCURACY TRADEOFFS, VELOCITY PROFILES, AND PHYSIOLOGICAL TREMOR IN MOVEMENT

A THESIS SUBMITTED FOR THE DEGREE OF  
DOCTOR OF PHILOSOPHY (ELECTRICAL ENGINEERING)

By  
Robin Trulssen Bye (2259735)

*Supervisor:* Dr. Peter D. Neilson  
*Co-supervisor:* Dr. Megan D. Neilson

School of Electrical Engineering and Telecommunications,  
The University of New South Wales.

January 2009

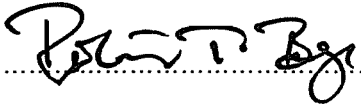
This page is intentionally left blank.

#### **COPYRIGHT STATEMENT**

'I hereby grant the University of New South Wales or its agents the right to archive and to make available my thesis or dissertation in whole or part in the University libraries in all forms of media, now or here after known, subject to the provisions of the Copyright Act 1968. I retain all proprietary rights, such as patent rights. I also retain the right to use in future works (such as articles or books) all or part of this thesis or dissertation.

I also authorise University Microfilms to use the 350 word abstract of my thesis in Dissertation Abstract International (this is applicable to doctoral theses only).

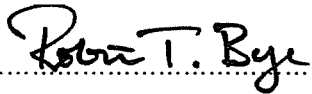
I have either used no substantial portions of copyright material in my thesis or I have obtained permission to use copyright material; where permission has not been granted I have applied/will apply for a partial restriction of the digital copy of my thesis or dissertation.'

Signed ..... 

Date ..... 23/6/09 .....

#### **AUTHENTICITY STATEMENT**

'I certify that the Library deposit digital copy is a direct equivalent of the final officially approved version of my thesis. No emendation of content has occurred and if there are any minor variations in formatting, they are the result of the conversion to digital format.'

Signed ..... 

Date ..... 23/6/09 .....

I hereby declare that this submission is my own work and to the best of my knowledge it contains no materials previously published or written by another person, nor material which to a substantial extent has been accepted for the award of any other degree or diploma at UNSW or any other educational institution, except where due acknowledgement is made in the thesis. Any contribution made to the research by others, with whom I have worked at UNSW or elsewhere, is explicitly acknowledged in the thesis.

I also declare that the intellectual content of this thesis is the product of my own work, except to the extent that assistance from others in the project's design and conception or in style, presentation and linguistic expression is acknowledged.

Ålesund, 23/6/09

Robin T. Bye

Robin Trulssen Bye

---

## Abstract

---

Speed-accuracy tradeoffs, velocity profiles, and physiological tremor are fundamental characteristics of human movement. The principles underlying these phenomena have long attracted major interest and controversy. Each is well established experimentally but as yet they have no common theoretical basis. It is proposed that these three phenomena occur as the direct consequence of a movement response planning system that acts as an intermittent optimal controller operating at discrete intervals of  $\sim 100$  ms. The BUMP model of response planning describes such a system. It forms the kernel of adaptive model theory which defines, in computational terms, a basic unit of motor production or BUMP. Each BUMP consists of three processes: (i) analysing sensory information, (ii) planning a desired optimal response, and (iii) executing that response. These processes operate in parallel across successive sequential BUMPs. The response planning process requires a discrete time interval in which to generate a minimum acceleration trajectory of variable duration, or horizon, to connect the actual response with the predicted future state of the target and compensate for executional error. BUMP model simulation studies show that intermittent adaptive optimal control employing two extremes of variable horizon predictive control reproduces almost exactly findings from several authoritative human experiments. On the one extreme, simulating spatially-constrained movements, a receding horizon strategy results in a logarithmic speed-accuracy tradeoff and accompanying asymmetrical velocity profiles. On the other extreme, simulating temporally-constrained movements, a fixed horizon strategy results in a linear speed-accuracy tradeoff and accompanying symmetrical velocity profiles. Furthermore, simulating ramp movements, a receding horizon strategy closely reproduces

experimental observations of 10 Hz physiological tremor. A 100 ms planning interval yields waveforms and power spectra equivalent to those of joint-angle, angular velocity and electromyogram signals recorded for several speeds, directions, and skill levels of finger movement. While other models of response planning account for one or other set of experimentally observed features of speed-accuracy tradeoffs, velocity profiles, and physiological tremor, none accounts for all three. The BUMP model succeeds in explaining these disparate movement phenomena within a single framework, strengthening this approach as the foundation for a unified theory of motor control and planning.

---

## Publications and conference presentations

---

- Bye, R. T., & Neilson, P. D. (2006). Adaptive model theory: A simulation study of speed-accuracy tradeoff in aimed movements. Poster presentation at the Brain Sciences UNSW "what's hot" Symposium, Sydney, Australia.
- Bye, R. T., & Neilson, P. D. (2007). Variable horizon predictive control in the central nervous system predicts the speed-accuracy tradeoffs and velocity profiles observed in rapid aimed movements. Poster presentation at the 8th Motor Control and Human Skills Conference, Fremantle, Australia.
- Bye, R. T., & Neilson, P. D. (2008). The BUMP model of response planning: Variable horizon predictive control accounts for the speed-accuracy tradeoffs and velocity profiles of aimed movement. *Human Movement Science*, 27(5), 771–798.
- Bye, R. T., & Neilson, P. D. (2009). The BUMP model of response planning: Intermittent optimal control accounts for 10 Hz physiological tremor. Poster presentation to be held at the 9th Motor Control and Human Skills Conference, Hobart, Australia.



---

## Acknowledgements

---

I am deeply indebted to my supervisors, Drs. Peter D. Neilson and Megan D. Neilson, for their superb guidance and support. With their vast knowledge on anything from human movement science and control systems theory to human interrelations and ethics they have been inspirational on an academic as well as a personal level. I strongly hope that we will continue our collaboration in the time ahead.

I am also grateful for the aid in supervision by Dr. Beatrix Vereijken at the Human Movement Science Programme at the Norwegian University of Science and Technology. My visits to Trondheim were valuable and provided new insights to my research.

I wish to express my gratitude to the postgraduate coordinator, Dr. Chee Y. Kwok, and the head of school, Dr. Tim Hesketh, for showing great flexibility in accommodating my stay in Norway.

Finally, I would like to thank Svein M. Olsen and Jayshri Master, whose work informed this thesis.

Helene, I dedicate this thesis to you.

Robin Trulssen Bye  
Ålesund, Norway, 19 February 2009

---

## Contents

---

Chapter 1	Introduction	1
1.1	Motivation . . . . .	1
1.2	The BUMP model of response planning . . . . .	2
1.3	Aim and hypothesis . . . . .	3
1.4	Thesis outline . . . . .	4
Chapter 2	The BUMP model of response planning	5
2.1	The origin of adaptive model theory . . . . .	5
2.1.1	Closed-loop theory . . . . .	7
2.1.2	Motor programming and schema theories . . . . .	8
2.1.3	Impulse-variability theory . . . . .	10
2.1.4	Dynamical oscillatory theories . . . . .	12
2.2	Influential models of response planning . . . . .	13
2.2.1	The deterministic iterative-corrections model . . . . .	13
2.2.2	The stochastic optimised-submovements model . . . . .	15
2.3	Overview of the BUMP model . . . . .	20
2.3.1	Planning in terms of sensory consequences . . . . .	22
2.3.2	Response execution . . . . .	24
2.3.3	Minimum acceleration approach . . . . .	25
2.3.4	Intermittency in trajectory generation . . . . .	27
2.3.5	Information processing bottleneck . . . . .	29
2.3.6	Double stimulus reaction time experiments . . . . .	30
2.3.7	Serial reaction time experiments . . . . .	32

2.3.8	Continuous-stimulus tracking experiments . . . . .	35
2.3.9	Input-output characteristics in visual tracking . . . . .	36
2.3.10	The isochrony principle . . . . .	37
2.3.11	The quantum of motor control . . . . .	38
2.4	Optimal trajectory generation . . . . .	41
2.4.1	Ballistic trajectories . . . . .	44
2.4.2	Non-ballistic trajectories . . . . .	48
2.4.3	Solution to the redundancy problem . . . . .	49
2.4.4	Synchronous operation of multiple OTGs . . . . .	52
2.5	Variable horizon predictive control . . . . .	55
2.5.1	Receding and fixed horizon control . . . . .	56
2.6	Noise in the motor system . . . . .	58
Chapter 3	Study I: Speed-accuracy tradeoffs and velocity profiles	60
3.1	Literature review . . . . .	60
3.1.1	Logarithmic speed-accuracy tradeoff . . . . .	62
3.1.2	Linear speed-accuracy tradeoff . . . . .	64
3.1.3	Velocity profiles in aimed movements . . . . .	65
3.2	Predictions of the BUMP model . . . . .	67
3.2.1	Logarithmic speed-accuracy tradeoff . . . . .	67
3.2.2	Asymmetrical velocity profiles . . . . .	76
3.2.3	Linear speed-accuracy tradeoff . . . . .	76
3.2.4	Symmetrical velocity profiles . . . . .	79
3.3	Method . . . . .	79
3.3.1	Description of simulator . . . . .	80
3.3.2	Simulator settings . . . . .	81
3.4	Results and conclusions . . . . .	83
3.4.1	Logarithmic speed-accuracy tradeoff . . . . .	83
3.4.2	Asymmetrical velocity profiles . . . . .	85
3.4.3	Linear speed-accuracy tradeoff . . . . .	89

3.4.4	Symmetrical velocity profiles . . . . .	91
3.5	Discussion . . . . .	93
3.5.1	Logarithmic speed-accuracy tradeoff . . . . .	93
3.5.2	Linear speed-accuracy tradeoff . . . . .	94
3.5.3	Velocity profiles . . . . .	95
Chapter 4	Study II: Physiological tremor	97
4.1	Literature review . . . . .	97
4.1.1	Introduction . . . . .	97
4.1.2	Mechanisms of physiological tremor . . . . .	98
4.1.3	The degree of contribution depends on the condition . . . . .	106
4.1.4	Functional significance of central oscillations . . . . .	114
4.2	Method . . . . .	118
4.2.1	Description of simulator . . . . .	119
4.2.2	Experiment 1 . . . . .	120
4.2.3	Experiment 2 . . . . .	121
4.2.4	Experiment 3 . . . . .	122
4.2.5	Experiment 4 . . . . .	122
4.2.6	Summary of simulator settings . . . . .	123
4.3	Results . . . . .	123
4.3.1	Experiment 1 . . . . .	123
4.3.2	Experiment 2 . . . . .	127
4.3.3	Experiment 3 . . . . .	134
4.3.4	Experiment 4 . . . . .	138
4.3.5	Conclusions . . . . .	138
4.4	Discussion . . . . .	143
4.4.1	Velocity of movements . . . . .	143
4.4.2	Visual feedback and skill level . . . . .	144
4.4.3	Bandwidth of tremor . . . . .	146
4.4.4	Handedness and flexion versus extension movements . . . . .	147

4.4.5	Oscillations during position holding . . . . .	147
4.4.6	Pulsatile motor output . . . . .	149
Chapter 5	General discussion	150
5.1	Comparison with other models . . . . .	150
5.1.1	Speed-accuracy tradeoff . . . . .	150
5.1.2	Velocity profiles . . . . .	152
5.2	Challenges from experiment . . . . .	153
5.2.1	Glitches in rapid movements . . . . .	153
5.2.2	Fitts' law in unsighted movements . . . . .	154
5.3	Modelling issues . . . . .	154
5.3.1	Continuous-time versus discrete-time modelling . . . . .	154
5.3.2	Model parameters . . . . .	155
5.3.3	Choice of response planning interval . . . . .	155
5.3.4	Genuine results or consequences of system design? . . . . .	156
5.3.5	Analytical proofs . . . . .	156
5.3.6	Choice of sampling rates . . . . .	157
5.3.7	Choice of noise constants . . . . .	158
5.4	Implications of the BUMP model . . . . .	159
5.4.1	Predictive control . . . . .	159
5.4.2	Optimal control and strategy selection . . . . .	160
5.4.3	Neuroanatomy of the intermittent optimal controller . . . . .	161
5.4.4	Synchronisation and binding . . . . .	161
5.4.5	Phase coding . . . . .	162
5.5	Concluding remarks . . . . .	163
References		165
Appendix A	Properties of logarithmic functions	192
A.1	Changing the base of a logarithm . . . . .	192
A.2	Logarithm of a fraction . . . . .	193

Appendix B Block diagrams of the simulator	195
B.1 Simulator used for Study I . . . . .	195
B.2 Simulator used for Study II . . . . .	198
Appendix C CD-ROM content	201

---

## List of Tables

---

3.1	Settings for simulations of human aimed movements . . . . .	82
3.2	Goodness of fit for receding horizon control simulations . . . . .	85
3.3	Asymmetrical velocity profiles . . . . .	87
3.4	Groups of fixed horizon control step movements . . . . .	91
4.1	Settings for simulations of human ramp movements . . . . .	123

---

## List of Figures

---

2.1	Basic unit of motor production (BUMP). . . . .	28
2.2	Relationship between BUMPs and the PRP . . . . .	31
2.3	Grouping of stimuli . . . . .	31
2.4	Reaction time for S3 in a serial reaction time experiment . . . . .	32
2.5	Minimum reaction time for S3 . . . . .	33
2.6	Maximum reaction time for S3 . . . . .	34
2.7	Sensory “chunking” . . . . .	35
2.8	S-shaped response trajectories . . . . .	43
2.9	Ballistic movement trajectories . . . . .	46
2.10	Non-ballistic movement trajectories . . . . .	48
2.11	Discrete-time equivalent of double integrator system . . . . .	49
2.12	Optimal $N$ -step desired response trajectory . . . . .	51
2.13	The optimal trajectory generator (OTG). . . . .	53
2.14	The $2 \times 2$ matrix transformation $y = \mathbf{M}x$ . . . . .	53
2.15	Example of receding horizon control . . . . .	56
2.16	Example of fixed horizon control . . . . .	57
3.1	Position, velocity, and acceleration trajectories . . . . .	68
3.2	Reaching task using receding horizon control . . . . .	70
3.3	Reaching task using fixed horizon control . . . . .	77
3.4	Endpoint error for receding horizon control simulations . . . . .	84
3.5	Comparison between velocity profiles in handwriting . . . . .	86
3.6	Velocity profiles for receding horizon control simulations . . . . .	88
3.7	Endpoint standard deviation for fixed horizon control simulations . . . . .	90



3.8	Velocity profiles for fixed horizon control simulations . . . . .	92
4.1	Human ramp and hold movements . . . . .	124
4.2	Simulated ramp and hold movements with visual feedback . . . . .	125
4.3	Simulated ramp and hold movements without visual feedback . . . . .	126
4.4	Human ramp and hold movements (M.S. and A.P.) . . . . .	128
4.5	Power spectra of eight human subjects . . . . .	128
4.6	Simulated ramp movements, position (M.S. and A.P.) . . . . .	129
4.7	Simulated ramp movements, velocity (M.S. and A.P.) . . . . .	130
4.8	Simulated ramp movements, acceleration (M.S. and A.P.) . . . . .	131
4.9	Simulated ramp movements, power of acceleration (M.S. and A.P.) . . . . .	132
4.10	Simulated ramp movements, power of velocity (M.S. and A.P.) . . . . .	133
4.11	Four human ramp movements, position . . . . .	135
4.12	Four human ramp movements, velocity . . . . .	135
4.13	Simulated ramp movements with speeds 4, 10, 25, 62 deg/s . . . . .	136
4.14	Amplitude of submovements increases with ramp speed . . . . .	137
4.15	Human ramp movements, position and velocity (K.G.) . . . . .	139
4.16	Human ramp movements, power (K.G.) . . . . .	139
4.17	Simulated ramp movements, position (K.G.) . . . . .	140
4.18	Simulated ramp movements, velocity (K.G.) . . . . .	141
4.19	Simulated ramp movements, power of velocity (K.G.) . . . . .	142
B.1	Block diagram of simulator used for Study I . . . . .	196
B.2	Block diagram of simulator used for Study II . . . . .	200

---

# CHAPTER 1

## Introduction

---

### 1.1 Motivation

Computational models are an important tool for investigating human movements. Movement phenomena such as speed-accuracy tradeoffs, velocity profiles, and physiological tremor may be successfully reproduced by a model, however, in order not to be a mere line-fitting tool, the model must also be biologically feasible. If not contradicted by any physiological or anatomical facts or well-established experimental findings, the model is realistic and constitutes hypotheses of how human motor control is achieved. Predictions from the model can be compared with data from existing experiments or spawn the design and undertaking of new experiments. A match between model predictions and experimental data strengthens the model and its hypotheses, whereas a mismatch can be equally valuable, as one, or several, of the hypotheses represented by the model can be rejected.

The principles underlying speed-accuracy tradeoffs in aimed movement have attracted major interest and controversy both experimentally and theoretically for over a century. The two most prominent tradeoffs reported are the linear speed-accuracy tradeoff (Schmidt, Zelaznik, Hawkins, Frank, & Quinns, 1979) and the logarithmic speed-accuracy tradeoff known as Fitts' law (Fitts, 1954). While Fitts' law holds for movements emphasising spatial accuracy, the linear tradeoff occurs for movements emphasising both spatial and temporal accuracy. Typically, the first kind of movements produces asymmetrical velocity profiles, whereas the latter kind produces symmetrical velocity profiles (see Section 3.1 for a review).

Another fundamental characteristic of motor control is the phenomenon of physiological tremor. Under a variety of conditions, including rest, posture, and motion, any healthy person exhibits unintentional, small amplitude oscillations of body parts. While it is commonly accepted that physiological tremor consists of a passive mechanical-reflex component and an active central-neurogenic component, details such as topography, mechanism, and functional significance of a centrally originating network driving the oscillations are still under debate (see Section 4.1 for a review).

Any comprehensive theoretical model of movement control must be able to account for these well-established experimental results. The model presented in this thesis does exactly this. Conducting two simulation studies, one related to speed-accuracy tradeoffs and velocity profiles, and the other related to physiological tremor, it is shown that the BUMP<sup>1</sup> model of response planning is able to successfully reproduce and account for these phenomena. Uniquely, it provides a unifying theoretical bridge between seemingly disparate phenomena of human motor control.

## 1.2 The BUMP model of response planning

The BUMP model is a comprehensive, discrete-time computational model of response planning. The model can be considered the kernel of the larger coherent theoretical framework of adaptive model theory (AMT), a neuroengineering account of human movement control (Neilson, Neilson, & O'Dwyer, 1992).

Based on a meld of adaptive control theory and neuroscience, AMT addresses major issues in human movement science, including those of intermittency, redundancy, resources and nonlinear interactions (see Neilson & Neilson, 2005b, for review). The theory sets out a three-stage account of the information processing required for sensory analysis, response planning, and response execution and provides explicit biologically-feasible neural network implementations for each stage. It is therefore readily testable by comparing computational results from simulations

---

<sup>1</sup>Basic Unit of Motor Production

based on these networks with experimental observations from behavioural studies. In particular it has accounted for a variety of phenomena observed in the continuous movements of human tracking behaviour (Neilson, Neilson, & O'Dwyer, 1995), from whence the theory emerged. But it would seem to be equally applicable to discrete movement tasks where error correction and prediction are also known to be operative.

A key part of AMT is variable horizon predictive control. The theory posits a basic unit of motor production (BUMP), which is determined by an intermittently operating response planning system. At fixed intervals of time, sensory information about the position and velocity of the actual response as well as the predicted future state of the target is passed to the response planning system, which in turn generates an optimal response trajectory to reach the predicted future state of the target and to compensate for executional error. The ability to vary the duration, or prediction horizon, of each optimal trajectory gives rise to the concept of variable horizon predictive control. Thus, overall movement is seen as being comprised of one or several concatenated submovements, or BUMPs, each generated with its own prediction horizon.

### 1.3 Aim and hypothesis

The aim of this thesis is to develop and validate, by means of simulation, a response planning hypothesis that unifies and accurately predicts speed-accuracy tradeoffs, velocity profiles, and physiological tremor. This hypothesis is the foundation for the BUMP model.

It is proposed that the combination of signal-dependent noise in the nervous system and variable horizon predictive control accounts for speed-accuracy tradeoffs and velocity profiles of aimed movements. Specifically, this thesis examines the ability of a simulated implementation of the BUMP model to reproduce the well-known speed-accuracy results from studies of discrete movement along with the velocity profile findings from similar work. Theoretical accounts of these phenomena exist and will be discussed but to date there appears to be none that explicitly unifies

both sets of results by placing them within a broader account of response planning and control.

Furthermore, it is hypothesised that physiological tremor occurs as a direct result of intermittent response planning, where each cycle of tremor corresponds to a single BUMP. Specifically, this thesis investigates whether the BUMP model simulator is able to reproduce the 10 Hz physiological tremor observed in studies of slow finger movements.

## 1.4 Thesis outline

In addition to Chapter 1 (this chapter), which details motivation, the BUMP model, aim and hypothesis, and thesis outline, this thesis is divided into four other chapters. Chapter 2 begins by presenting the origin of adaptive model theory and models of motor control that have influenced the development of the BUMP model. The chapter proceeds with an overview of the BUMP model, with particular attention given to the concepts of optimal trajectory generation, variable horizon predictive control, and noise in the motor system. Chapter 3 and 4 are devoted to the two simulation studies upon which this thesis is based. Chapter 3 presents a simulation study of speed-accuracy tradeoffs and velocity profiles in aimed movement whereas Chapter 4 presents a simulation study of 10 Hz physiological tremor during ramp movements. Both chapters contain a review of the relevant literature, experimental method, results, conclusions, and discussion. The thesis is concluded with Chapter 5, which contains a general discussion including comparison with other models, challenges from experiment, modelling issues, some implications of the BUMP model, and concluding remarks.

---

## CHAPTER 2

### The BUMP model of response planning

---

While papers have been published based on the AMT framework for more than 30 years, the first paper that describes the BUMP model of response planning under that title appeared just recently and presented the results from the study in Chapter 3 (Bye & Neilson, 2008). However, much of the theoretical background material presented below has appeared in earlier papers that are cited where appropriate. The remaining material is based on knowledge and hypotheses accumulated over many years and was most recently summarised in an unpublished manuscript by Neilson (2000). The aim of this chapter is to clarify, correct, and to a minor degree extend the material where necessary. The end result is a detailed description of the BUMP model that represents the most up-to-date view of AMT and its response planning hypotheses. It should be noted that the theoretical aspects of the BUMP model most relevant for the studies in this thesis are presented in Chapter 3.2, in which some mathematical derivations and corresponding predictions of the BUMP model have been extended.

#### 2.1 The origin of adaptive model theory

The perceptual-motor loop is the major feedback loop involved in the control of purposive movement. Adaptive model theory (AMT) is a computational theory about information processing within this loop (e.g., Neilson, 1993; Neilson & Neilson, 1999, 2001, 2005b; Neilson, Neilson, & O'Dwyer, 1988a; Neilson et al., 1992, 1995; Neilson, Neilson, & O'Dwyer, 1997). Its purpose is to understand the neural

mechanisms of sensory-motor control to the extent that they can be reproduced in computer simulations and robotic systems. AMT aims to provide a comprehensive account of the feedforward and feedback control systems employed by the central nervous system (CNS) during control of movement. The theory was developed primarily to account for the behaviour of subjects performing visual tracking tasks but has proven equally applicable to discrete movement tasks where error correction and prediction are also known to be operative. In fact, AMT hypothesises that the same central processes are involved in the control of all purposive movements, including self-paced movements.

According to Abernethy & Sparrow (1992), research in motor behaviour has typically been inspired by one or more of the following four major theoretical positions: The closed-loop theory (Adams, 1971), motor programming and schema theories (e.g., Henry & Rogers, 1960; Keele, 1968; Schmidt, 1975), the asymmetric impulse-variability theory (Schmidt et al., 1979) and its symmetric modification (Meyer, Smith, & Wright, 1982), all of which belong to the movement systems approach, and dynamical oscillatory theories (e.g., Kelso, Holt, Rubin, & Kugler, 1981; Kugler, Kelso, & Turvey, 1982; Kugler & Turvey, 1987), which belong to the action systems approach. In the movement systems approach, movement kinematics are represented centrally, for example in the form of a motor program, schema, plan, or any other form. In the action systems approach, however, no such central representation exists. Rather, movements are an emergent property of the nonlinear dynamics of the motor system. While AMT has its origins in the mathematical theories of signals and systems, and asserts the existence of central representations involved in response planning and other information processing strategies, it nevertheless reconciles many aspects of the theories mentioned above. In what follows next, the reconciliation with each of these four theoretical positions will be presented.

### *2.1.1 Closed-loop theory*

While the idea that continuous feedback plays a role during control of movement was voiced at least as early as the turn of the previous century (Woodworth, 1899), the first consolidated theory involving feedback in both learning and control was provided by Adams (1971). Based on engineering principles and consistent with pre-existing knowledge on the role of feedback in learning and performance (e.g., Adams, 1968), the theory proposed that movement was controlled by continuous comparison between afferent information and a set of “sensory consequences” stored in memory from previous successful movements. Closed-loop theory explains many of the characteristics of human movements, with perhaps the best example being the deterministic iterative-corrections model of Crossman & Goodeve (1983), which successfully accounts for the logarithmic speed-accuracy tradeoff known as Fitts’ law (Fitts, 1954; Fitts & Peterson, 1964). Despite its success, the closed-loop theory ultimately lost its position as a motor control paradigm because of its inability to explain both the control of fast, ballistic movements with a duration less than the feedback time (e.g., Schmidt, 1976) as well as the control of movements in the complete absence of afferent information (Taub, 1976).

On the other hand, the notion of preplanning and open-loop control (Henry & Rogers, 1960) has been challenged by the problems of storage and novelty (Schmidt, 1976) as well as by the difficulties in explaining the ongoing error corrections in movements with long duration and slow velocity. AMT provides a unifying bridge between these two opposing approaches by recognising that sensorimotor control involves both feedback and feedforward control processes encompassing both peripheral and central processes operating interactively. As described in detail later in this thesis, feedback control via the perceptual-motor loop is seen as being comprised of a sequence of 100 ms preplanned responses executed open-loop. However, while one submovement is being executed, the next one is being planned. Thus, within each submovement the control system operates open-loop but execution errors are corrected by intermittent feedback operating with a reaction time delay.



### *2.1.2 Motor programming and schema theories*

Early open-loop control views argued that control of ballistic movements was performed by the use of a set of pre-planned efferent commands executed open-loop, that is, without afferent modifications (Abernethy & Sparrow, 1992). Henry & Rogers (1960) formalised this centralised control model into their memory drum theory, which later was superseded by the formalisation of the motor program by Keele (1968) as the backbone of open-loop control. Perhaps most notable of the anomalies of the motor program concept was the aforementioned storage and novelty problems. According to Keele (1968), specific neural commands were stored in the motor program. This gave rise to the storage problem, as it seems unrealistic, if not impossible, for the human brain to be able to store every single neural command necessary to generate any kind of movement. Moreover, it seems impossible to perform a novel movement without some feedback guidance, at least during learning. This gave rise to the novelty problem. In addition to this pair of problems, the motor program model as hypothesised by Keele (1968) suffered from a lack of explanation of the continuous error correction observed in long duration, slow velocity movements, in similar vein as closed-loop theory suffered from a lack of explanation of short duration, ballistic movements where feedback does not have the time to affect the response. As a consequence of these problems, motor behaviour research was driven toward a hybrid model approach. The best known and most persistent hybrid view is the schema theory of Schmidt (1975) and the parallel development of the generalised motor program (Schmidt, 1976, 1985). In schema theory, task-specific experience leads to the abstraction of the relationship between response specification, sensory consequences, and movement outcome. These relationships are stored in the control program and retrieved for execution of that particular movement class. The generalised motor program view extends the schema theory and argues that only those features of movement that are invariant over a range of different task conditions are stored centrally.

AMT incorporates similar ideas to schema theory and the generalised motor program. The theory proposes (e.g., Neilson et al., 1992, 1995, 1997; Neilson & Neilson, 2005b) that the nervous system includes distributed neural circuitry, most likely involving subcortical pathways through parts of the basal ganglia and cerebellum, which can function as parallel arrays of self-tuning neural adaptive filter circuits implementing the well-known least mean squares (LMS) algorithm (Widrow & Stearns, 1985). This LMS module is repeated hundreds of thousands of times within the cerebellar structure, with each module operating more or less independently in parallel with each other (Neilson & Neilson, 2005b). It is known from the signal processing literature (e.g., Widrow & Stearns, 1985; Haykin, 2002) that within a few tenths of a second, say, adaptive filters can automatically tune the parameters controlling their input-output dynamic relationships to form internal models of the nonlinear dynamic relationships between signals. Similarly, the neural adaptive filters hypothesised above can form internal models of the dynamic relationships between sensory-sensory, motor-motor, and sensory-motor signals. Once formed, these internal models can be employed for a variety of functions within sensory analysis systems, response execution systems, and even cognitive and response planning systems.

Importantly, AMT argues that the parameters controlling the input-output transmission characteristics of the adaptive filter circuits are represented centrally in the form of patterns of electrical activity within the cortex which modulate the basal ganglia and cerebellum circuits, probably via the substantia nigra and the dopaminergic system in the case of the basal ganglia and via the inferior olive climbing fibre system in the case of the cerebellum. Because of this, multiple slave copies of each neural adaptive filter can be established in various functional systems. Furthermore, the patterns of electrical activity can be stored into and retrieved from long-term memory and, as a result, the nervous system can establish a repertoire of internal models associated with previously learned skills. By retrieving these

models from memory, the nervous system can switch quickly from one set of models to another (Neilson et al., 1997; Neilson, Neilson, & O'Dwyer, 1998).

Moreover, AMT hypothesises that the neural adaptive filters are able to remove redundancy from incoming sensory signals and to extrapolate task-dependent orthogonal sensory feature signals corresponding to the degrees of freedom of the response being performed (Neilson, 1993; Neilson & Neilson, 2005b). It has been demonstrated how neural adaptive filter circuits can function as a self-organising synergy generator, or coordinative structure, able to transform central representations of motor commands encoded in terms of feature signals associated with each degree of freedom of the response into the large number of highly intercorrelated motor commands required by individual motor units (Neilson & Neilson, 2005b,a). Furthermore, it is suggested that these neural circuits are able to form internal models of both the forward and inverse dynamics of the multivariable non-linear relationships between motor commands, muscle tensions, body movements and sensory consequences (e.g., Neilson et al., 1992, 1997; Neilson & Neilson, 2001, 2005b). These models can function within a feedforward-feedback adaptive optimal control system that assures that the responses actually executed match as closely as possible the goal-oriented desired response trajectories generated centrally. Finally, AMT, like schema theory and the generalised motor program, has a learning emphasis and a focus on acquisition of skills and development of motor control.

### *2.1.3 Impulse-variability theory*

The impulse-variability model proposed by Schmidt et al. (1979), later termed the asymmetric impulse-variability model by Meyer et al. (1982), was largely developed in an attempt to explain Fitts' law by means of motor programming ideas. However, it was the linear speed-accuracy tradeoff the model would end up explaining successfully. The linear speed-accuracy tradeoff is observed in aimed movement tasks when the subject is instructed not only to minimize endpoint error but also to make the movement have a pre-specified duration (Schmidt et al., 1979; Meyer et al., 1982; Wright & Meyer, 1983). By letting subjects perform such time-constrained

aimed movements, Schmidt et al. (1979) found that their model was not particularly accurate for slower movements of duration 200–500 ms. On the contrary, the experimental results provided strong support for the model for fast movements with movement times of less than 200 ms, suggesting that the model was limited to rapid, preprogrammed movements without feedback error corrections. Thus, the model complemented closed-loop models (e.g., Crossman & Goodeve, 1983) that successfully explained slow movements with ongoing error corrections but failed for rapid, open-loop movements deprived of feedback. Theoretically, the asymmetric impulse-variability model posits a direct relationship between the type of errors produced in error tasks and the variability within the amplitude and duration of the initial force impulse applied to a limb. It assumes that the standard deviation (variability) of the amplitude of the force pulse and the standard deviation of the duration of the force pulse are proportional to their respective mean values. Criticisms of the theory are based on its oversimplification of actual movement dynamics as well as violations of probability theory and misapplication of physical laws (see Meyer et al., 1982). For example, Schmidt et al. (1979) assumed that the initial force-time curve is a square wave pulse with variable amplitude and duration, whereas accelerometer recordings show a more complex waveform that indicate that the forces underlying acceleration and deceleration are closer to being sinusoidal than square (Meyer et al., 1982). Furthermore, the asymmetric impulse-variability theory does not take into account the influence of the deceleration phase of the movement on the final placement error. Consequently, Meyer et al. (1982) developed a more realistic version of the theory, naming it the symmetrical impulse-variability model, indicating an inclusion of the deceleration phase of movements. This version of the theory accounted for the linear speed-accuracy tradeoff in time-constrained movements as well as other kinematic properties observed in fast movements (Meyer et al., 1982; Meyer, Abrams, Kornblum, Wright, & Smith, 1988). Moreover, the overlapping-impulse model (Meyer et al., 1982), an extension of the symmetrical

impulse-variability model, hypothesised that aimed movements generated by a series of miniature overlapping force pulses also would satisfy Fitts' law. AMT has much in common with the overlapping-impulse model. Both try to bridge theories concerned with speed-accuracy tradeoff in ballistic movements and theories concerned with performance of slower or more complex movements, such as those observed in pursuit or compensatory tracking.

#### *2.1.4 Dynamical oscillatory theories*

Whereas the theories discussed above all belong to the movement systems approach, the dynamical oscillatory theories belong to the action systems approach. This approach, which is also called the emergent approach or direct approach, arose largely out of the work of Kelso (1981); Kelso et al. (1981); Reed (1982); Kugler et al. (1982); Kugler (1986); Kugler & Turvey (1987); Saltzman & Kelso (1987). Movement kinematics are viewed as an emergent property of the underlying nonlinear dynamics of the motor system rather than being represented centrally in a motor program, plan, schema, or any other form. Thus, for any particular action, movement kinematics should be understood in terms of the collective physical properties of the functional muscle groups (Abernethy & Sparrow, 1992). Dynamical oscillatory theories (e.g., Kelso et al., 1981) are based on the idea that the behaviour of the motor system is that of an ensemble of limit cycle oscillators or periodic attractors. They attempt to explain the selection of action categories and transitions between different forms or phases of inter-limb coordination by using purely physical laws (e.g., Kugler, 1986).

AMT incorporates most of the points of view in the action systems school of motor control and learning. Specifically, it takes into account the nonlinear dynamics of the environment, of the body in interaction with the environment, of the biomechanical system and the neuromuscular system, and of the interactions between all of these. The lower levels of control posited in AMT include reflex mechanisms, postural responses, pattern generators, limit cycle oscillators, mass-spring attractors, self-organising coordinative structures, and all the emergent behaviour implied

by these nonlinear processes. However, at higher levels, AMT postulates the existence of central, possibly distributed, representations of orthogonalised sensory feature signals and of neural processes modulated by afferent input and memory that transform basic drives into a hierarchical structure of long-term to short-term goals. At the level of the most immediate sub-goal, the theory hypothesises central mechanisms that generate desired response trajectories and initiate descending commands that modulate the behaviour of lower level systems. It is exactly these latter hypotheses about central representation of movement kinematics that cause a philosophical rift with the protagonists of the action systems view.

## 2.2 Influential models of response planning

Before presenting the BUMP model of response planning, which lies at the core of AMT, it is instructive to examine its theoretical origin. Two models with which the BUMP model has a lot in common, namely the deterministic iterative-corrections model (Crossman & Goodeve, 1983) and the stochastic optimised-submovements model (Meyer et al., 1988), will be discussed next, including overviews, how these models are able to account for speed-accuracy tradeoffs observed in human aimed movements, and weaknesses of the models.

### 2.2.1 *The deterministic iterative-corrections model*

Whereas the logarithmic speed-accuracy tradeoff known as Fitts' law (see Chapter 3.1 for a review of speed-accuracy tradeoffs) originated in terms of information theory (Fitts, 1954; Fitts & Peterson, 1964), it is possible to derive this logarithmic relationship from feedback considerations. One of the most influential theories in accounting for Fitts' law by means of feedback has been the deterministic iterative-corrections model of Crossman & Goodeve (1983) and elaborated subsequently<sup>1</sup> by Keele (1968) and others (e.g., Meyer et al., 1982). The model assumes that movements consist of a sequence of discrete submovements made on the basis of

---

<sup>1</sup>The work by Crossman & Goodeve (1983) was first published in 1963.

sensory feedback. Each submovement travels a constant proportion  $p$  of the remaining distance to the centre of the target during a constant amount of time  $\Delta T$ . The submovement sequence ends when a submovement finishes inside the target region, that is, for a target with width  $W$ , within a distance of  $\frac{W}{2}$  of the target centre. Crossman & Goodeve called their model deterministic because it does not incorporate any variability due to stochastic noise in the neuromuscular system. Using a derivation similar to that of Crossman & Goodeve (1983) and Keele (1968), it can be shown that the aforementioned assumptions lead to a logarithmic speed-accuracy tradeoff: Let  $D$  denote the total distance to the target,  $T = k\Delta T$  the total movement time after  $k$  submovements,  $d_k$  the distance moved during the  $k$ -th submovement, and  $W_k$  the error or distance remaining to the target after  $k$  submovements. Then we obtain

$$\begin{aligned}
d_1 &= pD \Rightarrow \\
W_1 &= (1-p)D, \\
d_2 &= pW_1 = p(1-p)D \Rightarrow \\
W_2 &= W_1 - d_2 = (1-p)D - p(1-p)D \\
&= (1-p)(1-p)D = (1-p)^2 D, \\
&\vdots \\
W_k &= (1-p)^k D
\end{aligned} \tag{2.1}$$

for the error  $W_k$  after  $k$  submovements. Rearranging, substituting  $k = \frac{T}{\Delta T}$ , and taking logarithms on both sides, the expression for the movement time  $T$  after  $k$  submovements becomes

$$T = \Delta T \log_{(1-p)} \left( \frac{W_k}{D} \right) \tag{2.2}$$

For direct correspondence with Fitts' law, substitute  $p = 0.5$  into Eq. 2.2, let  $\Delta T = b$  and the  $k$ -th error equal half the target width, that is,  $W_k = \frac{W}{2}$ , and apply some

logarithmic properties<sup>2</sup> to get

$$T = b \log_{0.5} \left( \frac{W/2}{D} \right) \Leftrightarrow T = b \log_2 \left( \frac{2D}{W} \right) \quad (2.3)$$

Assuming that the time for the initial submovement differs from the other corrective submovements by a constant  $a$ , which is a reasonable assumption considering that the planning time for the first submovement is not part of the movement time, one may write

$$T = (k - 1)\Delta T + (\Delta T + a) = k\Delta T + a = b \log_2 \left( \frac{2D}{W} \right) + a, \quad (2.4)$$

which is identical to Fitts' law (Eq. 3.1, p. 62). As noted by Keele (1968), letting the duration of each submovement  $\Delta T$  equal 100 ms gives an “information rate” of 10 bits/s, which is close to the estimate of Fitts (1954).

The deterministic iterative-corrections model was eventually rejected because of empirical evidence against some of its key predictions. Not only can speed-accuracy tradeoffs be non-logarithmic, for example in the case of temporally constrained movements, but in addition, it has been shown that a logarithmic tradeoff can occur for movements containing only a single submovement and that submovements do not have constant duration and do not travel a constant proportion of the remaining distance. All of these findings contradict the predictions of the deterministic iterative-corrections model and therefore led to its downfall (Meyer et al., 1988; Meyer, Smith, Kornblum, Abrams, & Wright, 1990). Addressing these issues, Meyer et al. (1988) developed the stochastic optimised-submovements model, which is presented below.

### 2.2.2 The stochastic optimised-submovements model

The stochastic optimised-submovements model developed by Meyer et al. (1988) discards the idea that submovements have a fixed duration and move a fixed pro-

---

<sup>2</sup>To change the base of a logarithmic function, use the theorem  $\log_a(x) = \frac{1}{\log_b(a)} \log_b(x)$ . Combined with the identity  $\log_a(\frac{x}{y}) = -\log_a(\frac{y}{x})$ , Eq. 2.3 can be obtained. See Appendix A for proof of the theorem.



portion of the remaining distance to the target. It proposes that a movement begins with a primary submovement programmed to hit the centre of the target region. If the primary submovement ends within the target region, the movement is successful and the action terminates. If, on the other hand, the primary submovement overshoots or undershoots the target region, a secondary corrective submovement based on sensory feedback is made. Such an execution error is hypothesised to occur because of the presence of stochastic noise in the motor system, an idea that Crossman & Goodeve (1983) rejected. Accepting the hypothesis of stochastic noise, spatial variability will increase with movement velocity. Specifically, the model assumes that the distribution of the  $k$ -th submovement endpoints have a standard deviation  $S_k$  that is proportional to the average velocity  $V_k = \frac{D_k}{T_k}$  of the submovement:

$$S_k = KV_k = K\frac{D_k}{T_k}, \quad (2.5)$$

where  $D_k$  and  $T_k$  are the mean distance and the mean duration of the  $k$ th submovement, respectively, and  $K$  is a positive constant.

Moreover, Meyer and colleagues suggested that the average velocities of the submovements are programmed to minimise the average total movement duration  $T$ . For presentation purposes, assume that no more than two submovements are necessary to reach within the target region, although the model is by no means limited to this number. The total movement duration then becomes  $T = T_1 + T_2$ , where  $T_1$  and  $T_2$  denote the time of the primary and the secondary submovement, respectively. Selection of  $T_1$  and  $T_2$  constitutes an optimal control problem: If the primary submovement takes a long time, variability due to motor noise will be small, yielding greater spatial accuracy at the expense of increasing the total movement time. However, if the primary submovement is fast, the motor noise effect will cause greater execution errors, thus increasing the secondary submovement duration and hence, the overall movement duration. The stochastic optimised-submovements model predicts that the average total movement time  $T$  can be closely approximated

by

$$T = a + b\sqrt{\frac{D}{W}}, \quad (2.6)$$

where  $a$  and  $b$  are constants,  $D$  is the distance to the target, and  $W$  is the target width. Although Eq. 2.6 is not logarithmic, it still mimics Fitts' law because  $\sqrt{\frac{D}{W}}$  increases monotonically at a decreasing rate as  $\frac{D}{W}$  increases, and it even fits some experimental data better than a logarithmic function does (Kvålseth, 1980). Furthermore, the mean duration of the primary submovement  $T_1$  is predicted to mimic Fitts' law in the same fashion as do the average total movement time:

$$T_1 = a_1 + b_1\sqrt{\frac{D}{W}} \quad (2.7)$$

Hence, the secondary submovement is given by the remaining movement time:

$$T_2 = T - T_1 = a_2 + b_2\sqrt{\frac{D}{W}}, \quad (2.8)$$

where  $a_2 = a - a_1$  and  $b_2 = b - b_1$  are positive constants. Assuming that motor noise influences each submovement in the same fashion as for the primary and secondary submovements and that the mean durations of submovements are programmed to minimise the average total movement duration, the model can be extended to incorporate more than two submovements. According to Meyer et al. (1990), the average total movement time is then given by a quasi power function of the ratio  $\frac{D}{W}$  with an exponent of  $\frac{1}{k}$ :

$$T = a_k + b_k \left( \frac{D}{W} \right)^{\frac{1}{k}}, \quad (2.9)$$

where  $k$  is the maximum number of submovements for a particular movement task. Thus, the stochastic optimised-submovements model predicts a linear speed-accuracy tradeoff (see Chapter 3.1.2) for a single submovement, with  $T$  increasingly

approximating a logarithmic function as the number of submovements increases:

$$\begin{aligned}
T\Big|_{k=1} &= a_1 + b_1 \frac{D}{W} \\
T\Big|_{k=2} &= a_2 + b_2 \left(\frac{D}{W}\right)^{\frac{1}{2}} \\
T\Big|_{k=3} &= a_3 + b_3 \left(\frac{D}{W}\right)^{\frac{1}{3}} \\
&\vdots \\
\lim_{k \rightarrow \infty} T &= a + b \ln \left(\frac{D}{W}\right)
\end{aligned}$$

In essence, the stochastic optimised-submovements model encompasses one extreme case that implies Fitts' law exactly ( $k \rightarrow \infty$ ), another extreme case that implies a linear speed-accuracy tradeoff ( $k = 1$ ), and intermediate cases that approximate Fitts' law to varying degrees ( $1 < k < \infty$ ,  $k \in \mathbb{N}$ ).

Experimental data used to test the stochastic optimised-submovement model depend on the use of peaks and troughs in the velocity and acceleration profiles to detect the boundaries of submovements. However, such peaks and troughs do not necessarily define response boundaries. In handwriting and drawing movements, for instance, the tangential velocity varies linearly with the radius of curvature of the movement (Viviani & Terzuolo, 1982; Lui, 1993). This implies that peaks and troughs in the velocity and radius of curvature waveforms occur with the same relative spacing regardless of the total drawing time. In other words, the radius of curvature and velocity waveforms can be time-scaled, suggesting that variations in velocity and acceleration are related to the geometry of the movement trajectory rather than programming of submovements. Similar conclusions have been reached from frame-by-frame analysis of video recordings of baby reaching movements (Mathew & Cook, 1990). These observations cast doubt on the validity of the movement parsing algorithms developed by Meyer et al. (1988) to measure duration and extent of submovements, and consequently, undermine the experimental basis of the stochastic optimised-submovements model.

Another issue that is not addressed by the stochastic optimised-submovements model is the problem of redundancy (Bernstein, 1967). Even if the initial and final positions and velocities, the distance to the target, and the average velocity of each response trajectory are specified, there still remains an infinite number of possible response trajectories that would satisfy these specifications. The stochastic optimised-submovements model does not make any predictions about how and when the response trajectories are generated, nor their precise shape. AMT provides a solution to the redundancy problem by suggesting that the CNS uses task-dependent synergies to overcome this problem (see Neilson & Neilson, 2005b, for a review).

Finally, for each submovement, the stochastic optimised-submovements model hypothesises that noise in the motor system causes the deviation from the centre of the target, that is, the endpoint error, to be proportional to the average velocity of the submovement. If the error is smaller than half the target width, the movement has ended within the target region, and no further submovements are made. Otherwise, another error-correcting submovement has to be made. However, the model does not give any account of the time required by central processes to detect execution errors and to program and initiate corrective responses. Furthermore, because no reaction time interval pauses are observed in the position or velocity profiles of movements at submovement boundaries, it seems that the CNS is able to predict the error at the end of each submovement based on sensory feedback acquired during the early part of each submovement (see von Hofsten, 1980). The stochastic optimised-submovements model does not suggest that such predictions may be integrated into the programming of submovements. In the following sections, this and other issues will be dealt with within the theoretical framework of AMT. It will be shown that an optimal trajectory generator central to the BUMP model is capable of accounting for a wide range of experimental findings, including the logarithmic and the linear speed-accuracy tradeoffs and their associated asymmetrical and symmetrical bell-shaped velocity profiles, the relationship between tangential velocity and radius of curvature in three-dimensional movements, the isochrony

principle, biphasic and triphasic bursts of electromyography (EMG) records during fast movements, the psychological refractory period and the information processing bottleneck, planning in terms of end-point trajectories, task-dependent coordinate systems, motor synergies, optimisation of reaching movements and input-output transfer characteristics in visual tracking.

### 2.3 Overview of the BUMP model

Both common experience and experiments (e.g., Woodworth, 1899) indicate that human purposive movements can be corrected during the course of the movement. This is clearly fundamental to the theoretical understanding of speed-accuracy phenomena. This thesis takes a systems-oriented approach that dates back to World War II and the development of tracking control theory. Craik (1947, 1948) showed in his now famous papers that the human operator behaves like an error-correcting servomechanism in tracking tasks. The importance of error correction, and hence of feedback, was substantiated by Craik's colleague Vince (1948) in discrete aimed movements as well as in tracking tasks requiring continuous movement. This work showed clearly that humans respond intermittently in movement control tasks. Vince (1948) went on to suggest that there exists a psychological refractory period (PRP) during which the CNS is occupied and cannot respond to an incoming stimulus. This is supported by a wealth of results from discrete response, double stimulus reaction time experiments (e.g., Telford, 1931; Vince, 1948; Welford, 1967, 1980; Karlin & Kestenbaum, 1968; Kantowitz, 1974; McLeod, 1977; Pashler, 1984, 1992) that identify an information-processing bottleneck that gives rise to the PRP.

It is now well understood from these findings that during a reaction time interval, the CNS can plan an appropriate response to a stimulus while simultaneously executing a response to a previous stimulus and detecting and storing in memory a subsequent stimulus. Consequently, there must exist at least three processing systems within the perceptual-motor loop that are able to operate independently and in parallel, with interprocess communication via memory buffers. In AMT, these systems are termed the sensory analysis (SA), response planning (RP), and

response execution (RE) systems. Whereas detailed descriptions of the SA and RE systems can be found elsewhere (e.g., Neilson et al., 1992, 1997; Neilson & Neilson, 2005b), this thesis hypothesises that speed-accuracy tradeoff, velocity profiles, and physiological tremor all are movement phenomena explained by the BUMP model of response planning. Therefore, this thesis will focus mainly on the RP system and the processes of generating movement trajectories. Clearly, the planning of human movement responses involves many levels of processing. Here, the main concern is with the sensory-motor processes responsible for generating required trajectories as specified by cognition, motivation, and the like.

In addition to the aforementioned movement phenomena, the BUMP model is intended to account for behaviour of subjects in continuous-time visual tracking tasks, and at the same time, be consistent with findings of experiments concerned with self-paced movements, such as handwriting and reaching, and with findings of discrete-response experiments, such as double stimulus reaction time studies. The proposal for response planning put forward in the BUMP model has many elements in common with the deterministic iterative-corrections model (Crossman & Good-eve, 1983) and with the stochastic optimised-submovement model (Meyer et al., 1988) presented in Chapter 2.2. With respect to the systems-oriented literature it can be thought of as a discrete equivalent of the optimal control model of the human operator presented by Baron and colleagues (Baron & Kleinman, 1969; Baron, Kleinman, & Levison, 1970; Kleinman, Baron, & Levison, 1970, 1971), who hypothesised that the CNS acts as an optimal controller performing continuous error correction. The AMT approach addresses several limitations in that model (Neilson & Neilson, 1999), with perhaps the greatest difference being the introduction of intermittency.

The detailed description of the BUMP model have made the development of a computer simulator using MATLAB and Simulink software possible. For a variety of visual tracking tasks, the behaviour of the simulator model matches that of human

subjects. In the following, a qualitative description of the processes involved in response planning and trajectory generation will be presented.

### *2.3.1 Planning in terms of sensory consequences*

An important question in human movement science is whether response trajectories are planned with respect to kinematic or dynamic coordinates. Investigating this question, Wolpert, Ghahramani, & Jordan (1995) conducted an experiment involving point-to-point human arm movements. Their focus was on the minimum jerk model (Hogan, 1984; Flash & Hogan, 1985) and the minimum torque change model (Uno, Kawato, & Suzuki, 1989). Based on optimal control theory, both these models involve the minimisation of a cost function. For the minimum jerk model, the cost to be minimised is the first derivative of the Cartesian hand acceleration, or jerk, and thus, the model is based on kinematics<sup>3</sup>. For the minimum torque change model, the cost to be minimised is the first derivative of torque, or torque change, and thus, the model is based on dynamics<sup>4</sup>. Both models predict symmetrical bell-shaped velocity profiles, however, whereas the minimum jerk model predicts straight trajectories, the minimum torque change model predicts trajectories that vary across the workspace of the arm.

Using an adaptation paradigm, Wolpert et al. (1995) showed that these two models lead to different predictions about the arm trajectories when subjects are presented with a visual perturbation of the hand position. By altering the visual feedback of the hand such that the perturbation is zero at both ends of the movement and maximum at the midpoint, that is, the perceived straight-line trajectory is curved, adaptation should cause the actual trajectory to curve in the opposite direction if the trajectory is being planned in terms of kinematic coordinates, while no adaptation should occur if the trajectory is being planned in terms of dynamic

---

<sup>3</sup>By kinematics we mean the properties of motion, involving variables such as the position of joint angles or Cartesian hand coordinates and its derivatives.

<sup>4</sup>By dynamics we mean the forces required to produce motion given properties such as mass, inertia, and stiffness. The variables of interest are for example joint torques, external forces, and motor commands.

coordinates. Indeed, increasing the perceived curvature in both sagittal<sup>5</sup> and transverse<sup>6</sup> self-paced point-to-point arm movements resulted in significant corrective adaptation in both cases. Furthermore, when reducing the perceived curvature of transverse movements, which are already naturally curved, there was no significant adaptation. In this case, adaptation should occur only if the desired trajectory is curved and planned in kinematic coordinates. These results indicate that arm trajectories are planned in visually based kinematic coordinates and that the desired trajectory is a straight line in visual space. Wolpert et al. (1995) concluded that the results are incompatible with models based purely on dynamics such as the minimum torque change model and that spatial perception, as mediated by vision, plays a fundamental role in trajectory planning.

The AMT view on trajectory generation is consistent with the conclusions made by Wolpert et al. (1995). However, according to AMT, the desired trajectory is planned in the same high level sensory feature code in which the response feedback is encoded. The SA system is seen as being comprised of arrays of adaptive neural filters that automatically tune themselves to form internal models of the nonlinear dynamic relationships between sensory-sensory, sensory-motor, and motor-motor signals. Thus, the SA system removes redundancy from the millions of highly intercorrelated input signals and extracts a minimal set of orthogonal (independently varying) sensory and motor feature signals. Mathematically, this process is analogous to principal components analysis in statistics, or QR factorisation in matrix algebra. The orthogonal feature signals provide a task-dependent coordinate system that spans an  $M$ -dimensional vector space in which the desired response is planned. Thus,  $M$  is equal to the number of degrees of freedom (DOF) in the desired response.

---

<sup>5</sup>Wolpert et al. (1995) use “sagittal” to refer to movements made horizontally and in parallel with a vertical plane (the sagittal plane) passing through the standing body from front to back. Under non-perturbed conditions, this corresponds to moving a computer mouse such that its cursor on the screen moves along the  $y$ -axis.

<sup>6</sup>Wolpert et al. (1995) use “transverse” to refer to movements made horizontally across the body, that is, perpendicular to sagittal movements. Under non-perturbed conditions, this corresponds to moving a computer mouse such that its cursor on the screen moves along the  $x$ -axis.



The desired response<sup>7</sup> is denoted  $\mathbf{R}^*$  and may be described as a vector of coordinates  $\mathbf{R}^* = [R_1^* \ R_2^* \ \dots \ R_M^*]$ , where each coordinate  $R_i^*$  corresponds to a separate DOF of the response and can be planned independently of, and in parallel with, the others. A DOF in this context means a *control* DOF of movement, which is different from a *biomechanical* DOF. In an arm movement, there may be 25 biomechanical DOFs involved, including movements/rotations of the scapula, shoulder, elbow, forearm, wrist and fingers. However, by measuring all the 25 biomechanical DOFs as time signals in a reach and grasp task, it has been shown that this movement task only involve two independent control DOFs (Jeannerod, 1999; Smeets, Brenner, & Biegstraaten, 2002). That is, the 25 biomechanical DOFs cannot all be controlled independently (see Neilson & Neilson, 2005b, for details).

In the BUMP model, the coordinate system in which the  $\mathbf{R}^*$  trajectory is generated depends on the sensory consequences of the task. In a point-to-point arm movement such as that employed in the experiment of Wolpert et al. (1995), the desired response is being planned in terms of the trajectory of the endpoint of the hand. However, AMT proposes that the RP system may equally well plan a response to control the trajectory of the tip of the elbow, or the end of the nose, through space and time. Moreover, when an aircraft pilot operates a joystick to initiate a turn, the response is not planned in terms of the movement of the hand gripping the joystick *per se*, but rather, in terms of the attitude of the aircraft provided from sensory input, such as the the visual angle of the horizon or the roll-angle display on the instrument panel.

### 2.3.2 Response execution

During response execution, the  $\mathbf{R}^*$  trajectory must be translated into appropriate motor commands to activate lower level systems. According to AMT, these transformations are achieved within the RE system by adaptive neural filter models

---

<sup>7</sup>Throughout this thesis, the desired response is generally denoted in boldface,  $\mathbf{R}^*$ . However, to emphasise cases which involve only a single DOF, the desired response is denoted in nonbold italics,  $R^*$ .

of the appropriate inverse dynamics of the relationships between the motor commands, muscle tensions, body movements, and other sensory consequences. There is no more difficulty in translating a task-dependent  $\mathbf{R}^*$  trajectory into joint-angle space, say, than the well-known kinematic problem of translating the trajectory of the endpoint of the hand into joint-angle space. Indeed, an adaptive filter circuit able of modelling the input-output relationships of a multivariable nonlinear dynamic system can also be employed for the simpler problem of modelling the input-output relationships of a multivariable nonlinear algebraic, or kinematic, system. Throughout this thesis it is important to keep in mind that the  $\mathbf{R}^*$  trajectory is computed as an optimally smooth, minimum acceleration trajectory of desired sensory consequences. Thus, if the load on the muscles is predominantly inertial, the desired trajectory  $\mathbf{R}^*$  will correspond to a minimum force trajectory. However, in generating the  $\mathbf{R}^*$  trajectory, it is not necessary for the RP system to take into account the actual dynamics of the muscle control systems, biomechanical loads, and external systems being controlled. Rather, this is a task for the RE system, which utilises adaptive feedforward and feedback pathways for accurate modelling of these dynamics. Assuming that the models are accurate, the RE system translates the  $\mathbf{R}^*$  trajectory into the appropriate motor commands required to achieve it.

### *2.3.3 Minimum acceleration approach*

Although there exist an infinite number of possible hand trajectories in human aimed movements, studies show that humans tend to make movements along a straight path with a single-peaked, bell-shaped velocity profile (e.g., Bernstein, 1967; Flash & Hogan, 1985; Uno et al., 1989). Such invariant characteristics in human movements may be explained by adding extra constraints to the movement task, thus limiting the number of possible trajectories. In optimal control, a cost function is used for trajectory selection. The particular trajectory that minimises some cost is selected, where the cost may be related to parameters such as movement time, distance, velocity, energy, or acceleration (Nelson, 1983), rate of change of

acceleration or jerk (Hogan, 1984; Flash & Hogan, 1985), or rate of change of torque (Uno et al., 1989).

In agreement with Flash & Hogan (1985), AMT proposes that motor responses are generally planned as optimally smooth trajectories. However, whereas Flash & Hogan use a minimum jerk approach to generate such trajectories, AMT uses a minimum acceleration approach. This choice does not dismiss the minimum jerk approach; indeed, comparisons of minimum jerk and minimum acceleration trajectories in reach-and-grasp and tracking simulations based on the AMT framework using a stationary target (Gibson & Neilson, 1999; Jiang, Shen, & Neilson, 2002) show only very small differences in position. Nevertheless, the reason for using minimum acceleration instead of minimum jerk is twofold. First, for a predominantly inertial system like the arm and hand, minimising acceleration is equivalent to minimising energy. Proponents of AMT have previously discussed the importance of minimum energy in motor control (O'Dwyer & Neilson, 2000; Neilson & Neilson, 1999). In line with the extensive review by Sparrow & Newell (1998), who provide convincing evidence that performance of movement, and not just highly energy-demanding tasks but everyday motor skills, is constrained by the imperative to optimise the metabolic economy of movement, AMT suggests that creatures able to minimise their metabolic energy demands have an evolutionary advantage (Jiang et al., 2002). Second, AMT simulations of visual pursuit tracking (moving target) have shown that minimum acceleration trajectories are noticeably smoother than minimum jerk trajectories (Gibson & Neilson, 1999). This is due to the minimum jerk trajectories requiring the additional, and more difficult, prediction of acceleration in the future state (Neilson, 1993). Finally, it should be noted that when embedded in an intermittent response planning environment as presented here, minimisation of acceleration is not constrained by physics any more than minimisation of jerk.

### 2.3.4 Intermittency in trajectory generation

According to AMT, the processes of sensory analysis and response execution operate continuously, their inputs and outputs streaming in real time. In contrast, the response planning process operates on “chunks” of information. Via a memory buffer, the RP system receives the continuous output of the SA system as an intermittent input of refined afferent and reafferent information. Likewise, via a similar memory buffer, the RP system intermittently outputs a trajectory specification. This concatenates with earlier specifications, overwriting any part not yet executed, and thus provides continuous input to the RE system. Effectively, the intermittency introduced by the RP process means that the SA-RP-RE sequence proceeds in chunks. This leads to the concept of a *Basic Unit of Motor Production* or BUMP (Neilson et al., 1992, 1995), hence the BUMP model of response planning.

Specifically, the BUMP model hypothesises that the SA, RP, and RE processing systems operate independently and in parallel. Each BUMP corresponds to the discrete operation of the RP system that requires a fixed and finite interval of time in which to plan the trajectory for a future response. This planning is based on the information available from the SA buffer at the beginning of that interval, and the resulting trajectory is provided to the RE buffer at the end of that interval. The process then repeats. Thus, all purposive movements are seen as comprised of concatenated sequences of fixed duration submovements, where one submovement is being executed while the next one is being generated in light of feedback from the former submovement. A graphic representation of successive BUMPs is given in Fig. 2.1. Importantly, it is hypothesised that the trajectory that is generated during the fixed planning interval may have a time length considerably greater than the planning interval itself. In other words, trajectories may be planned that will run far into the future unless updated in a subsequent response planning interval.

A crucial part of this response planning hypothesis remains. AMT proposes that response planning occurs in a sequence of fixed time intervals. How long might

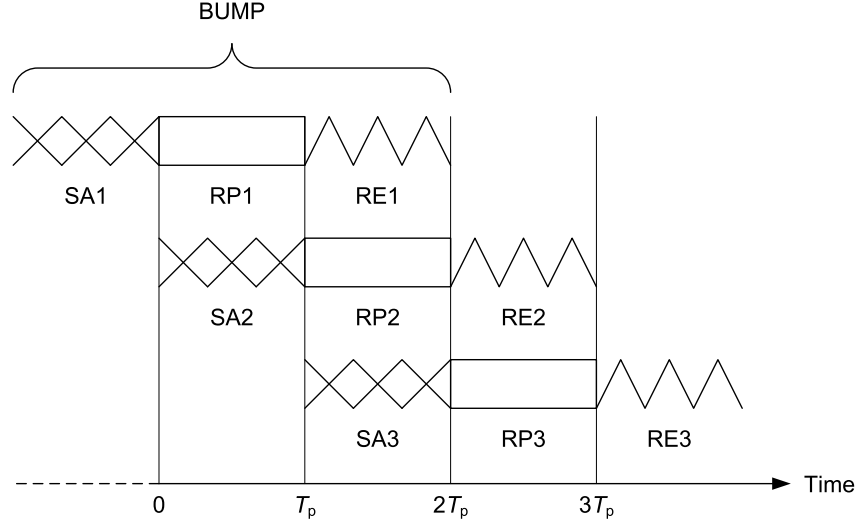


Figure 2.1: Basic unit of motor production (BUMP). During the response planning interval RP1 of fixed duration  $T_p$ , the RP system generates a desired response trajectory  $\mathbf{R1}^*$  based on sensory information available up to the end of the sensory analysis interval SA1. At the end of RP1,  $\mathbf{R1}^*$  is stored in working memory, ready for execution by the RE system. While the RE system executes  $\mathbf{R1}^*$  during the interval RE1, the RP system plans the next desired response trajectory  $\mathbf{R2}^*$  in parallel during the interval RP2, based on sensory information available up to the end of SA2. At the end of RP2, the desired response trajectory  $\mathbf{R2}^*$  is written into memory, overwriting the remainder of the desired response  $\mathbf{R1}^*$  not yet executed. The RE system then executes  $\mathbf{R2}^*$  during RE2 while the RP system plans yet another desired response trajectory during RP3. This process iterates, thus producing a sequence of overlapping BUMPs as illustrated.

these intervals be? Since they intentionally introduce refractoriness and intermittency into the AMT account of movement control, the corresponding behavioural data are relevant, as are estimates of probable time constraints in the nervous system. Estimates of time delay for proprioceptive feedback vary between 100 and 200 ms (van Beers, Haggard, & Wolpert, 2004). A similar range for visual feedback processing in motor tasks is indicated by Schmidt & Lee (1999). According to Stark (1968), the average refractory period for saccadic eye movements is 200 ms. Consistent with these figures are the intermittency at a frequency around 10 Hz observed in EMG activity and velocity profiles of slow finger movements (Vallbo & Wessberg, 1993). Recently, there has been shown a strong coherence between discontinuities at 6–9 Hz in finger movements and synchronised activity in cerebello-thalamo-cortical loops (Gross et al., 2002). In fact, Gross et al. suggest coupling of activity in

this 6–9 Hz range represents the neural mechanism for the intermittent control of continuous movements. Moreover, an RP interval in the range of 100–200 ms is consistent with average PRPs of 50–100 ms typically found in double stimulation reaction time experiments (e.g., Telford, 1931; Vince, 1948; Welford, 1967, 1980; Karlin & Kestenbaum, 1968; Kantowitz, 1974; McLeod, 1977; Pashler, 1984, 1992).

The choice of an RP interval in the 100–200 ms range in simulation studies has yielded good agreement with results of visual tracking experiments (Neilson et al., 1988a; Neilson, Neilson, & O’Dwyer, 1993; Neilson et al., 1995). It is also consistent with work by Cathers, O’Dwyer, & Neilson (1996) which shows that the upper limit of the visual tracking bandwidth is in the range 2.0–4.0 Hz. In light of the above information, the RP interval  $T_p$  in the simulation experiments presented in Chapter 3 and 4 is set to 100 ms.

### *2.3.5 Information processing bottleneck*

Experiments of Welford (1967, 1980) and subsequently Pashler (1984, 1992) have demonstrated the existence of an information processing bottleneck associated with response selection. This phenomenon is related to the PRP observed in double stimulus reaction time experiments. Pashler (1984, 1992) showed that the bottleneck occurs *after* perceptual processing; manipulations that increase the time required for perceptual processing of the second stimulus do not alter the PRP, whereas manipulations that alter the time required for response selection do. It appears that the RP system becomes unable, or refractory, to plan a response to a subsequent stimulus until it has completed planning the first. The time the second stimulus is being held in working memory by the SA system waiting for the RP system to become available corresponds to the PRP. According to AMT, this information processing bottleneck is the most important single factor limiting the performance of the perceptual-motor loop in visual tracking because it introduces a central time delay that, together with transmission delays and movement times, limits the bandwidth of visual tracking to 2.0–4.0 Hz. The only means available to compensate for time delays within this loop is by anticipating the future position

of the target, that is, by means of prediction. Investigations have shown that the inherent predictability of stochastic target signals used in visual tracking is essentially zero 300 ms ahead when the bandwidth of the spectrum of the signals exceeds 2.0–4.0 Hz, corresponding to the bandwidth at which subjects cease to be able to generate coherent tracking responses (Neilson et al., 1993).

### *2.3.6 Double stimulus reaction time experiments*

The relationship between BUMPs and the PRP for double stimulus reaction time experiments is illustrated in Fig. 2.2. At the beginning of such an experiment, the subject is alert and waiting for the first stimulus S1. In effect, after S1 arrives there is only a short interval of transmission time  $T_t = 10$  ms, say, required for perceptual processing before the RP system begins planning an appropriate response R1 to S1. The duration of the planning interval RP1 is fixed at  $T_p = 100$  ms, say. If a second stimulus S2 is presented during the planning interval RP1, the RP system will be busy generating R1 and will not be available to plan a response R2 to S2. Consequently, S2 will be held in working memory by the SA system until the RP system has completed planning R1. The RP system will then commence planning R2. The amount of time that S2 is held in working memory corresponds to the PRP described in double stimulation reaction time experiments. This time equals the increase in reaction time to S2 over the time interval that would be required if S2 was presented alone. From Fig. 2.2 it is evident that the PRP will be in a range from  $0^+$  ms (if S2 arrives just before RP1 has finished) to  $T_p - T_t = 100 - 10 = 90$  ms (if S2 arrives just after RP1 has started).

Suppose, however, that two stimuli are presented within a single planning interval RP1, as depicted in Fig. 2.3. According to AMT, the RP system can respond in a single reaction time interval to the two stimuli as if they were one. Pashler (1992) showed that the RP system is able to generate assemblages of motor behaviour as a single response without repeatedly employing the bottleneck mechanism. This grouping phenomenon of responding to two closely time-spaced stimuli (interstimulus interval less than  $T_p = 100$  ms) as if they were one has also been demonstrated

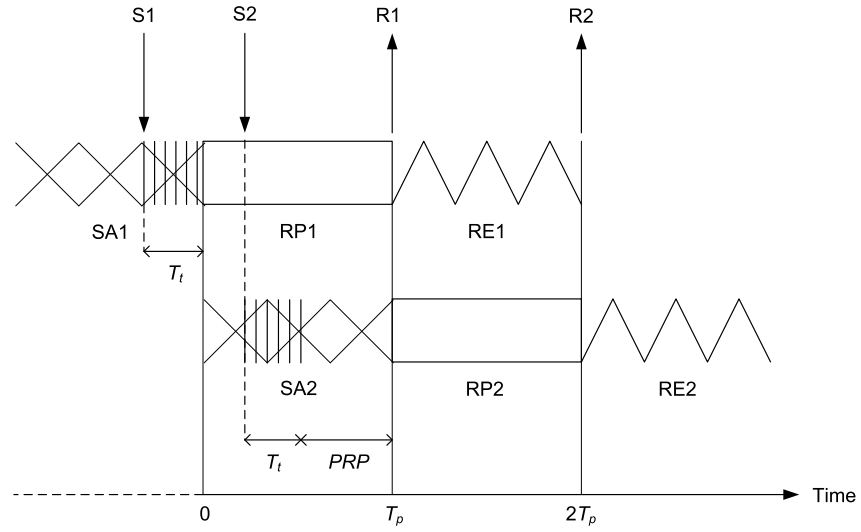


Figure 2.2: Relationship between basic units of motor production (BUMPs) and the psychological refractory period (PRP). S1 is the first stimulus, S2 is the second stimulus, R1 is the response to S1, R2 is the response to S2,  $T_t$  is the transmission time for stimulus signals (illustrated by vertical bars), and  $PRP$  is the duration corresponding to the psychological refractory period. Note that  $T_t$ , which typically is in the range 10–20 ms, has been exaggerated for clarity. After some perceptual processing of S2 with duration  $T_t$ , S2 is being held in working memory for a period of time  $PRP$ , during which the RP system is busy planning a response R1 to S1. When the RP system has finished planning R1 and passed the information to the RE system, the RP system becomes available and plans a second response R2 to S2 during the second response planning interval RP2.

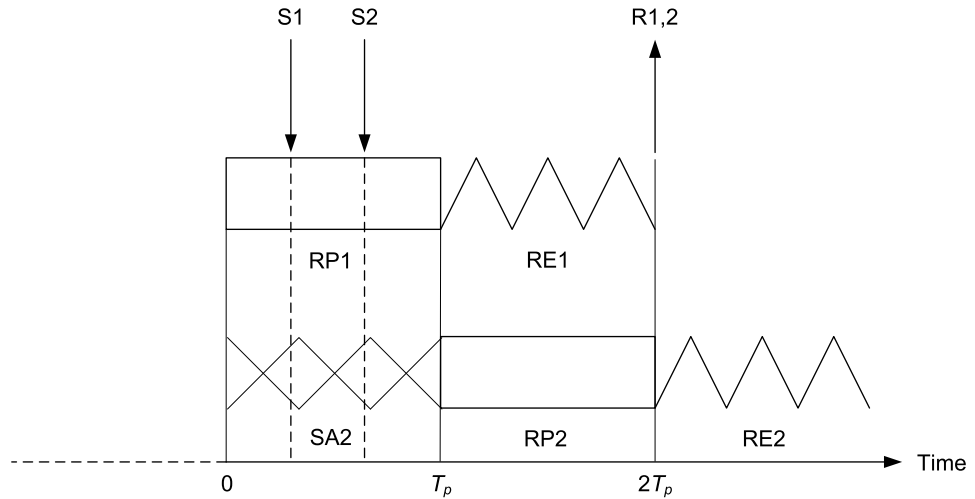


Figure 2.3: Grouping of stimuli. The RP system generates a single response R1,2 to two closely spaced stimuli S1 and S2 presented within one response planning interval, in this case, RP1.



by other investigators of double stimulus reaction time (e.g., Craik, 1948; Gielen, van den Heuvel, & Denier van der Gon, 1984; Kerr & Lockwood, 1995).

### 2.3.7 Serial reaction time experiments

If a subject is required to respond to a series of discrete stimuli, each stimulus will be followed by a PRP. A stimulus arriving during such a PRP will be held in working memory by the SA system until the RP system becomes available. The increase in reaction time will depend on when in the BUMP cycle the stimulus arrives. As an example, Fig. 2.4 shows a third stimulus S3 that arrives after S2 at a time interval  $T_{S3}$  before RP2, where  $T_{S3}$  is greater than the transmission time  $T_t$ . The signal will then have sufficient time to be transmitted before RP2 commences and the RP system will plan a response to S3 instead of, or grouped with, S2 during RP2, giving a reaction time for S3 equal to  $T_r = T_p + T_{S3}$ .

The minimum reaction time for S3 results when S3 arrives exactly  $T_t$  before RP2, such that the signal just has time to be transmitted to the RP system. Fig. 2.5(a) shows the resulting grouped response R2,3, with a reaction time for S3 given by  $T_{r,min} = T_p + T_{S3} = T_p + T_t$ . This minimum reaction time would also occur if S3

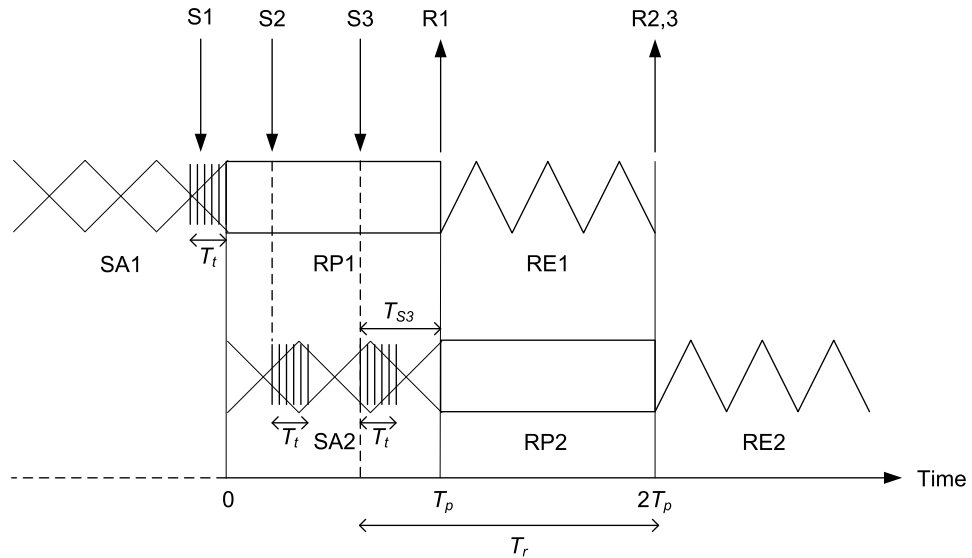
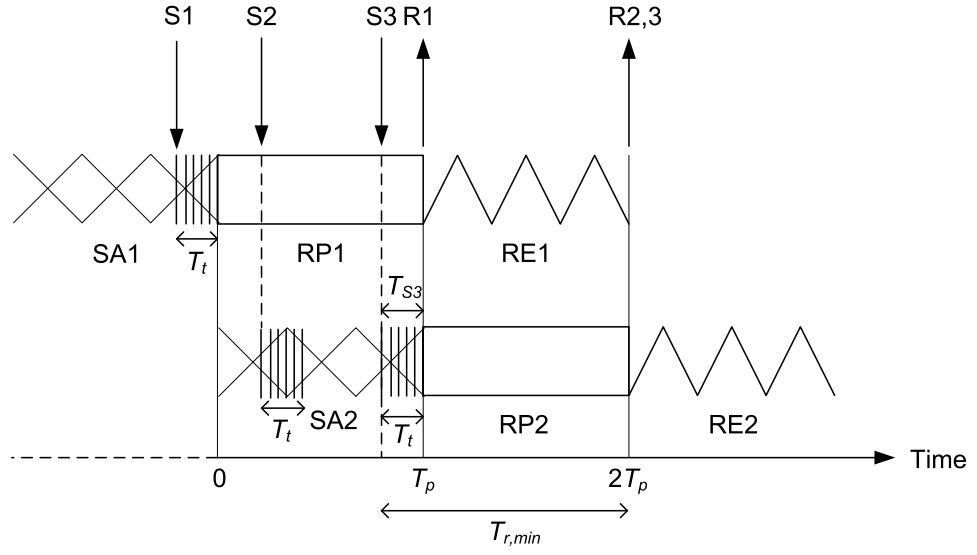
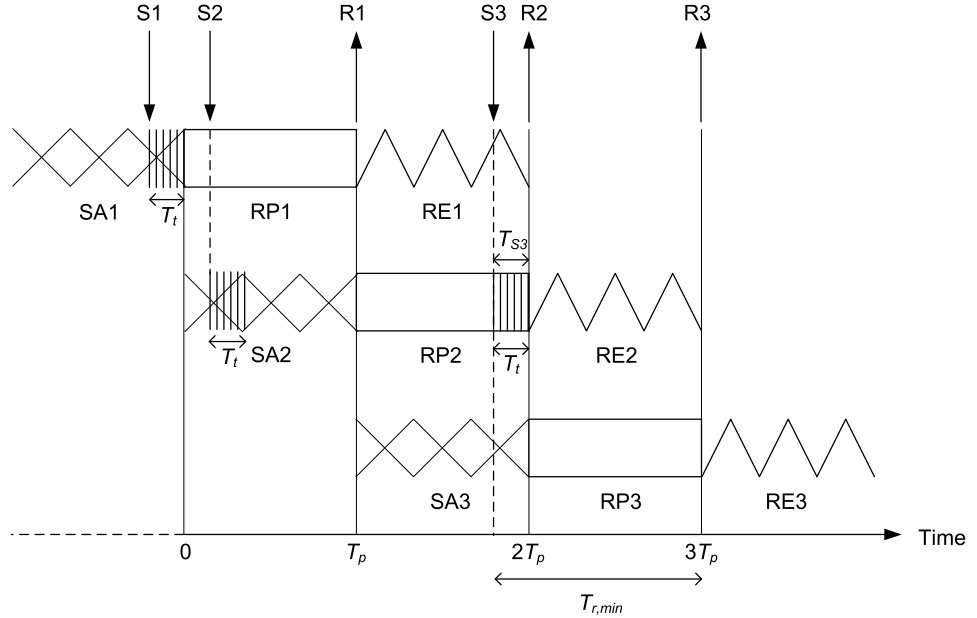


Figure 2.4: Reaction time for the third stimulus S3 in a serial reaction time experiment. S3 arrives a time  $T_{S3} > T_t$  before RP2, thus both S2 and S3 are incorporated by the RP system during RP2 when planning an appropriate grouped response R2,3. The reaction time for S3 is given by  $T_r = T_p + T_{S3}$ .



(a)



(b)

Figure 2.5: Minimum reaction time for the third stimulus  $S_3$  in a serial reaction time experiment.  $S_3$  arrives  $T_{S3} = (T_t)_+$  before  $RP_2$  (a) or  $RP_3$  (b), resulting in a grouped response  $R_{2,3}$  (a) or distinguished responses  $R_2$  and  $R_3$  (b). The minimum reaction time for  $S_3$  in both cases is given by  $T_{r,min} = T_p + T_t$ .

arrives a time interval  $T_t$  before  $RP_3$  has commenced, resulting in two distinguished responses  $R_2$  and  $R_3$  shown in Fig. 2.5(b).

The maximum reaction time for  $S_3$  occurs if  $S_3$  arrives a time interval  $T_{S3}$  just less than the transmission time as illustrated by Fig. 2.6. Because the signal will

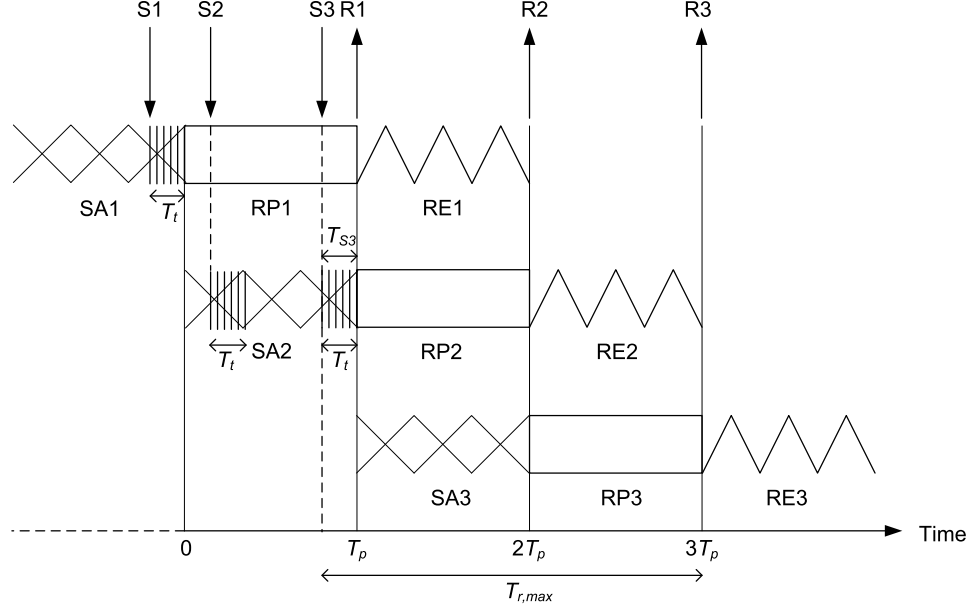


Figure 2.6: Maximum reaction time for the third stimulus S3 in a serial reaction time experiment. S3 arrives  $T_{S3} = (T_t)_-$  before RP2, just too late to be incorporated in the planning of R2,3 (Fig. 2.4). Instead, S3 is being held in memory by the SA system during SA3 and used by the RP system during RP3 for the generation of the response R3. This gives the maximum reaction time  $T_{r,max} = 2T_p + T_t$ .

not be fully transmitted before the RP system commences the RP2 interval, the RP system will plan a response to S2 during RP2, and only afterwards plan a response to S3, which has been held in memory by the SA system during RP3. The consequence is a maximum reaction time for S3 given by  $T_{r,max} = 2T_p + T_{S3} = 2T_p + T_t$ .

From the discussion of minimum and maximum reaction times above, it is clear that the possible range of the reaction time  $T_r$  for S3 is given by  $T_r \in \langle T_p + T_t, 2T_p + T_t \rangle$ . As argued above, realistic planning and transmission times may be given by  $T_p = 100$  ms and  $T_t = 10$  ms, say. The reaction time range for S3 thus becomes  $T_r \in \langle 110, 210 \rangle$  ms.

Finally, if the interstimulus intervals are such that there is an equiprobability of a stimulus arriving at any point during a planning interval, the BUMP model predicts that there should be a rectangular distribution of reaction time intervals. Indeed, such a rectangular distribution has been demonstrated experimentally in serial reaction time studies (Telford, 1931).

### 2.3.8 Continuous-stimulus tracking experiments

The notion that the RP system can respond to a pair of closely spaced stimuli as if they were one provides a theoretical bridge between discrete-stimulus reaction time experiments and continuous-stimulus tracking experiments. Based on the reasoning above, the RP system can generate a single response to a train of closely spaced discrete stimuli as shown in Fig. 2.7. Applying a well-known concept in the signal processing literature, the train of stimuli can be regarded as a continuous-time signal in the limit as the time interval between the stimuli approaches zero. Thus, within a planning time interval, the RP system can generate a response, not to a discrete stimulus, but to a “chunk” of a continuous-time signal. If the continuous-time target signal stretches over several response planning intervals, such as in a visual pursuit tracking task, the response generated can be seen as a concatenated sequence of submovements (cf. the BUMPs of Fig. 2.1), each generated in response to a chunk of continuously changing sensory input. As discussed in the next section, the input-output characteristics derived theoretically from this chunking process exactly match those measured experimentally in human subjects performing visual tracking tasks.

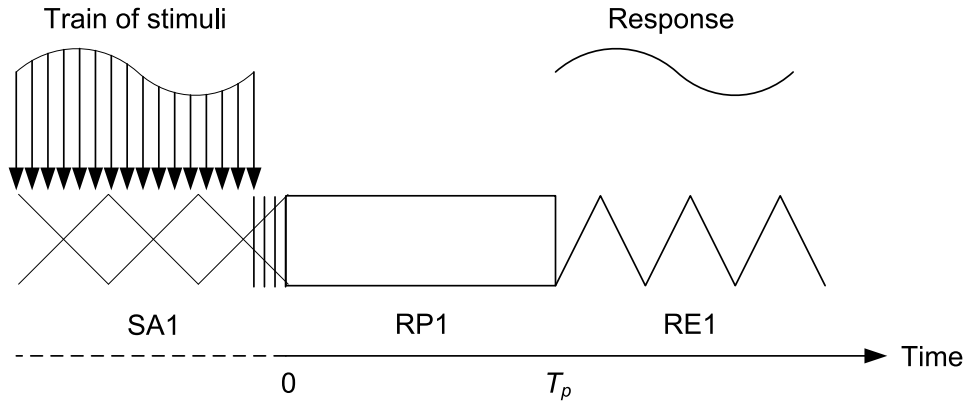


Figure 2.7: Sensory “chunking.” The RP system generates a single response to a train of stimuli. As the interstimulus interval approaches zero, the impulse train can be regarded as a continuous signal. In a tracking task with a continuous target, the RP system plans a single, continuous response to a chunk of continuous sensory input at each RP interval.

### 2.3.9 Input-output characteristics in visual tracking

Regardless of the dynamics of the tracking system, the relationship between tracking error  $e(t)$  and tracking response  $r(t)$  for human subjects can simply be described by a gain  $k$ , a time delay  $T$ , and an integrator (McRuer & Krendel, 1974):

$$r(t) = k \int_0^t e(t - T) dt \quad (2.10)$$

This is a remarkable finding because it shows that the relationship is independent of the input-output characteristics of the tracking system itself<sup>8</sup>. Despite their use of a variety of tracking systems with different transfer functions involving combinations of gain, integrators, and lag filters, McRuer & Krendel (1974) found that the relationship remained as simple as that of Eq. 2.10. Implicitly, this means that the CNS is able to self-organise its input-output characteristics to compensate for those of the tracking system. Although not stated explicitly by McRuer & Krendel, their finding provides compelling evidence that the CNS is able to form internal models of the inverse dynamics of the external systems being controlled. Furthermore, the measured input-output relationship likely corresponds to the residual dynamics in the loop that cannot be compensated because they are associated with processes inherent in the loop itself, such as intermittent response planning.

The relationship between error and response derived theoretically from the intermittent chunking process hypothesised by AMT and demonstrated in computer simulations (Neilson et al., 1988a; Neilson, O'Dwyer, & Neilson, 1988b) is a discrete equivalent of the continuous relationship measured experimentally by McRuer & Krendel (1974). Because the RP system is thought to operate intermittently in the BUMP model, with tracking responses comprised of concatenated sequences of submovements, the response to error relationship is modelled as a time-delay and a discrete-time summer rather than a continuous-time integrator. The measured time-delay is attributed to the time required by the RP system to read sensory

---

<sup>8</sup>The input-output characteristics, or dynamics, of the tracking system relates the motor response, or input (for example the movement of a joystick), to the actual response, or output (for example the movement of a response cursor on a computer screen).

information and to generate a desired response  $\mathbf{R}^*$  in addition to afferent and efferent transmission time-delays. The summer (integrator) action is attributed to the intermittent behaviour of the RP system. At each planning interval the RP system generates an  $\mathbf{R}^*$  to align the response<sup>9</sup> with the target. If the executed response does not reach the target, the RP system simply continues to generate responses at planning time intervals until the error is corrected. Assuming a stationary target such as in a step tracking task, the accumulated effect of such a sequence of error-correcting submovements drives the response into alignment with the target and is responsible for the integral relationship between response and error.

From control theory (e.g., Nise, 2000) it is well-known that integrator, or in this case, summer, action is essential within a feedback loop in order to obtain zero steady state error with a stationary target. Thus, in the BUMP model, the summer (integrator) action introduced by intermittent planning of submovements is vital in assuring steady state accuracy in motor tasks such as tracking and reaching. Furthermore, by slowing down the speed of each submovement, the response takes a longer time to align with the target, thus reducing the accuracy of the tracking performance. Intuitively, then, the faster the preplanned error-correcting submovement, the better the tracking performance, and consequently, best performance should be achieved when the error-correcting submovements are preplanned to be as fast as possible.

### *2.3.10 The isochrony principle*

In a study of the fastest possible voluntary movements of hand and arm muscles, Freund & Büdingen (1978) showed that the duration of the movements remained approximately constant no matter what the amplitude of the movement. This phenomenon is known as the isochrony principle (Viviani & Terzuolo, 1982). Freund & Büdingen (1978) found that the duration of EMG bursts recorded with surface electrodes from agonist and antagonist muscles was 80–90 ms in all fast contractions,

---

<sup>9</sup>The object that tracks a target is typically a cursor in computer-aided tracking tasks. Note, however, that “response” may equally well refer to a tip of a stylus, finger, elbow, or whichever object or body part that is being used to track a target.

regardless of whether they were isotonic or isometric. Similar duration of non-overlapping EMG bursts were recorded in agonist and antagonist muscles during fast alternating movements. The fact that the duration of the EMG burst remains constant while its amplitude varies has been observed in a variety of movements (for example ballistic flexion movements of the elbow (Lestienne, 1979; Hallett, Shahani, & Young, 1975) and the thumb (Hallett & Marsden, 1979) as well as fast step-tracking arm movements (Brown & Cooke, 1981), and forms the basis of the pulse height model (Gottlieb, Corcos, & Agarwal, 1989; Corcos, Gottlieb, & Agarwal, 1989), in which the duration of the EMG burst is held constant while the amount of excitation is controlled only by varying the height of the burst. It may be concluded that the fastest movements are not limited by the mechanical properties of the muscles, otherwise the large amplitude contractions could not be performed many times faster than the small amplitude ones. The amplitude dependent variation of the speed of muscle contractions must therefore be achieved by the neural commands (see Freund, 1983; Berardelli et al., 1996, for reviews).

### *2.3.11 The quantum of motor control*

The EMG burst associated with a fast voluntary muscle contraction results from the activation of many motor neurons firing asynchronously. According to AMT, the duration of the EMG burst during a fast movement may be a reflection of the descending influence from the sensorimotor cortex (Neilson et al., 1992). A similar hypothesis has been proposed by Berardelli et al. (1996), in which it was suggested that the excitatory input to motor neurons has a finite minimum duration of the order of 70 ms, which would explain why EMG bursts also have a minimum duration of 70–80 ms. In effect, such a limit would cause the amount of activation in movements of short duration to be controlled only by varying the height of the pulse. When larger (or longer lasting) force pulses are required, both height and width could be varied. It is the AMT view that the minimum duration of the descending pulse of excitatory activity is a reflection of the bursting activity of neural ensembles, often referred to as cortical columns. As a consequence of

multiple excitatory and inhibitory feedback interconnections between cells in all six layers of the cortex, a common response to a discrete stimulus applied to layer IV is a lightly damped 20 Hz oscillation in a large number of neurons above and below the site of stimulation (von Seelen, Mallot, Krone, & Dinse, 1986). Such oscillations have been demonstrated in post-stimulus histograms of recordings from cortical units in cats and monkeys (von Seelen et al., 1986; Shaw & Silverman, 1988). The activity consists of bursts of 50 ms duration confined to a vertical column of cells with a diameter of roughly 500  $\mu\text{m}$ . Shaw & Silverman (1988) argued that the burst response of 50–100 neurons in each layer of a cortical column defines an appropriate temporal and spatial separation for recording cortical signals. The bursting of cortical columns in the sensory cortex might be the source of the 70–80 ms bursts of lower motor neuron activity recorded during fast voluntary movement.

The change in width of EMG bursts in slower movements (Berardelli, Rothwell, Day, Kachi, & Marsden, 1984; Brown & Cooke, 1984) may be accounted for by a sequence of overlapping bursts of cortical column inputs converging onto the motor neuron pool. Indeed, longer duration EMG bursts recorded during fast movements usually display multiple peaks consistent with such a sequence of descending excitation pulses. According to this view, the minimum duration of the first EMG burst recorded during a fast ballistic movement should be an invariant property of the CNS and not amenable to variation through training. In a study of elbow movements, EMG bursts from elbow muscles were recorded with surface electrodes during fast dart-throwing movements about the elbow (Kelly, 1992). Subjects were challenged to reduce the duration of the initial EMG burst to a minimum by whatever means. Although subjects tried all sorts of tricks, including throwing the arm into a pillow to avoid the need for braking, the minimum duration of EMG bursts was 40–50 ms and was associated with movements of small amplitude (less than 5 degrees rotation). In another study by Wadman, Denier van der Gon, Geuze, & Mol (1979), subjects did fast ballistic movements about the elbow joint but on unpredictable occasions had their arm mechanically constrained. The first agonist



EMG burst occurred exactly the same in both the free and the constrained case. Indeed, half of the second antagonist burst happened exactly the same as well, before a deviation from the usual pattern was detected. Similar observations have been made by Smeets, Erkelens, & Denier van der Gon (1990) in their study of fast elbow movements with unexpected inertial loads, and by Hallett & Marsden (1979), who studied the effect of unexpectedly halting ballistic flexion movements of the top joint of the thumb. Thus, it is argued in AMT that at least the first EMG burst in the agonist muscle is preprogrammed and runs open-loop before any sort of response feedback, either reflex or voluntary, has any influence. This burst is bell-shaped but has been approximated by a rectangular pulse with a duration of 50 ms in the simulation studies of this thesis.

AMT proposes that the first EMG burst in a 100 ms fast ballistic movement is the quantum of control exerted by the cortex over the motor neuron pool. It corresponds to a 50 ms burst of a cortical column dispersed through multiple descending pathways with different transmission times and mixed with continuous afference from the periphery. Thus, the theory argues that descending control of muscle control systems is via a sequence of 50 ms EMG bursts, probably corresponding to bursts of cortical columns, with varying amplitudes. EMG bursts observed experimentally of seemingly longer durations are simply concatenated sequences of 50 ms bursts. Such a quantification was observed by Brown & Cooke (1984), who found that the burst duration in arm movements was not continuously graded but was either 70 or 140 ms, that is, they observed either a 70 ms single burst or two bursts concatenated, each of 70 ms duration. In line with this and as discussed in Chapter 2.3.4, from the organisation of cortical columns (Mountcastle, 1997, 1998), their bursting activity (Shaw & Silverman, 1988; von Seelen et al., 1986; Sardesai et al., 2001), and the nature of cortico-cortical and cortico-subcortical connectivity between cortical columns and subcortical structures (Darian-Smith, Darian-Smith, & Cheema, 1990; Eccles, 1984; Goldman-Rakic, 1987), AMT argues strongly for the applicability and validity of discrete-time models of neural information processing

rather than continuous-time models. Moreover, as is commonly accepted in neurophysiological practice, the output of an ensemble of neurons, such as a pool of alpha motor neurons driving a muscle, can be appropriately measured by counting the total number of impulses that occur during a brief period of time, often set to 50 ms (Jiang et al., 2002). Consequently, in the BUMP model, the activity of an ensemble of neurons is modelled just as it is measured experimentally. That is, a staircase waveform (zero order hold (ZOH) signal) represents the average level of activity over each time window. At periodic intervals (50 ms), the level of activity is adjusted. This is equivalent to approximating the acceleration waveforms associated with EMG bursts as rectangular pulses. AMT appreciates that the actual variation in the instantaneous level of activity is bell-shaped rather than rectangular. Nevertheless, as argued by Neilson & Neilson (2005b), the use of ZOH signals is justified by further experimental parallels. In addition, there is great advantage in the availability and wide acceptance of powerful discrete-time signal processing algorithms developed for analysis of such signals. Finally, it should be emphasised that using discrete-time signal processing theory for constructing a human movement simulator does not contradict the CNS being a continuous-time system using burst code. Afterall, a continuous-time plant driven by ZOH control inputs is still a continuous-time system.

## 2.4 Optimal trajectory generation

Central to the BUMP model is the concept of an optimal trajectory generator (OTG). According to AMT, for each control DOF in the response, there exists in the RP system a separate OTG neural circuit that generates a one-dimensional desired response trajectory, which is optimal in the sense that it minimises acceleration. Operating in parallel, up to  $M$  OTG circuits simultaneously generate an  $M$ -dimensional desired response  $\mathbf{R}^* = [R_1^* \ R_2^* \ \dots \ R_M^*]$  as a vector of coordinates, where each coordinate  $R_i^*$  corresponds to a separate DOF and  $M$  is the number of DOFs in the response. We have limited central processing resources (e.g., Wickens, 1984) and from common experience, our central control capability allows only a

limited number of DOFs to be controlled simultaneously. However, although the maximum number  $N$  of OTG circuits available is unknown, it is certainly at least two, as is well established experimentally, for example from reach and grasp behaviour (e.g., Smeets & Brenner, 1999; Jeannerod, 1999). Furthermore, it has been shown that subjects are able to perform a two DOFs visual pursuit tracking task with no greater central time delay than required to perform a one DOF task, indicating parallel operation of OTG circuits (Navon, Gopher, Chillag, & Spitz, 1984; Oytam, Neilson, & O'Dwyer, 2005). The OTG circuits resemble what is often referred to as “pattern generators” in the literature and are thought to be located in the prefrontal cortex.

By combining information about the most recent response feedback available to the RP system and knowledge of the  $\mathbf{R}^*$  planned during the previous RP interval, the SA system predicts the initial state (position and velocity) of the response at time  $t_i$  at the end of the RP interval. Simultaneously, the SA system predicts the future, or final, state of the target a specified interval of time ahead at time  $t_f$ . This information is passed to a memory buffer and read by the RP system. Given the initial and final states, the OTG generates an optimally smooth, minimum acceleration trajectory that connects the two states, similar to the smooth trajectory resulting from a minimum jerk criterion (Nelson, 1983; Flash & Hogan, 1985). It is hypothesised that at any RP interval, the duration  $T = t_f - t_i$  of the preplanned trajectory can be varied from a minimum of 100 ms, corresponding to the duration of an RP interval, to a few seconds, say. Three examples of minimum acceleration S-shaped response trajectories with different durations preplanned to correct the error between the position of a target and the position of a response cursor in a visual pursuit tracking task are shown in Fig. 2.8. If the response does not align with the target at the next RP interval, the RP system simply generates another  $\mathbf{R}^*$ . This process iterates, thus movement is seen as a concatenated sequence of submovements, or BUMPs, typically of a duration of 100–200 ms.

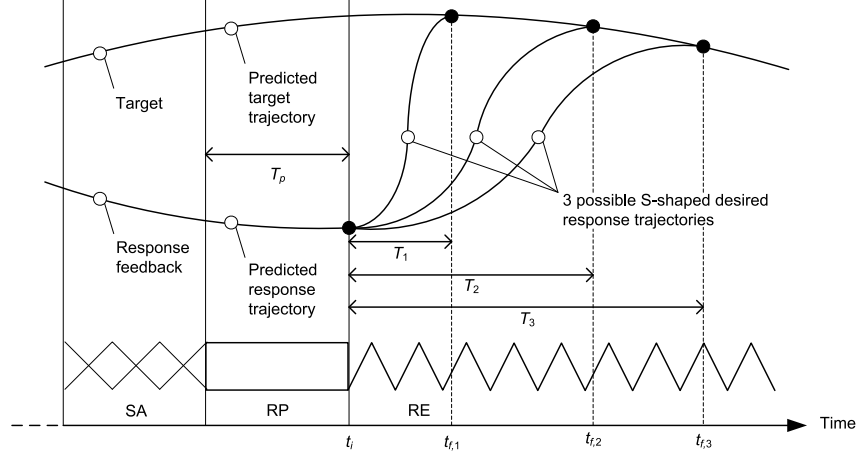


Figure 2.8: Three possible S-shaped desired response trajectories with durations  $T_k = t_{f,k} - t_i$ ,  $k = 1, 2, 3$ .  $T_p = 100$  ms is the response planning time,  $t_i$  is the time for the initial state, and  $t_{f,k}$  is the time for the final state for three possible trajectories.

Researchers who have developed movement-parsing algorithms to detect boundaries of submovements via discontinuities in velocity and acceleration waveforms (e.g., Meyer et al., 1988) commonly report submovement durations of more than 200 ms, however, it should be emphasised that a sequence of BUMPs due to intermittent error correction does not imply the observation of comparable segments of movement in responses, such as peaks and troughs in velocity or acceleration profiles. When an actual response trajectory  $\mathbf{R}$  matches the intended response trajectory  $\mathbf{R}^*$ , the position and velocity at the beginning of a submovement will exactly match that at the end of the previous one. Therefore, the two submovements will be concatenated smoothly with no detectable discontinuities in position, velocity, or acceleration. Discontinuities will only appear when  $\mathbf{R}$  deviates from  $\mathbf{R}^*$  because of lack of skill or uncertainties in response execution. As a consequence, discontinuities in velocity and acceleration profiles are found on average more than 200 ms apart.

Although the duration of  $\mathbf{R}^*$  can be varied, the best possible performance in a visual tracking task is achieved when the positional error between target and response is eliminated as quickly as possible, or when the OTG generates the fastest possible

$\mathbf{R}^*$ . As discussed previously, the fastest possible voluntary movement corresponds to a fast ballistic response limited to a duration of about 100 ms.

#### *2.4.1 Ballistic trajectories*

Research on the isochrony principle has shown that the fastest possible movement of a body segment has a duration of approximately 100 ms regardless of the movement amplitude (Freund & Büdingen, 1978). The duration of such ballistic movements seems to be limited by the duration of the descending bursts of neural activity responsible for the triphasic EMG bursts in agonist and antagonist muscles (Freund, 1983). An agonist burst, AG1, is followed by an antagonist burst, ANT, before a second agonist burst occurs, AG2. The function of AG1 is to accelerate the limb, the function of ANT is to decelerate the limb, and the function of AG2 is to dampen out possible oscillations at the end of the movement (Berardelli et al., 1996). Moreover, muscles act as a low pass filter of EMG activity. According to Berardelli et al. (1996), in the simplest isometric case with a minimum AG1 duration of 70 ms, the peak force produced by the muscle occurs only after 100-150 ms, before another 200 ms are needed for the muscle to relax to its baseline force level. Thus, the total minimum duration for such a phasic voluntary contraction would be of the order of 300 ms.

Because of the influence of force-velocity and length-tension relationships, the force waveform is difficult to determine when muscles are changing their length. The force required for a fast movement must be the resultant of overlapping agonist and antagonist force waveforms. In the case of fast movements with a peak amplitude after only 100 ms, the CNS must start the ANT very shortly after AG1 for its force to exceed the agonist force early in the movement and reverse the direction of the limb after 100 ms, before the force resulting from AG2 is used to stabilize the limb after the reversing movement ends (Berardelli et al., 1996). Despite this complexity, for a step movement, it is known that the triphasic pattern of muscle activity produces a smooth movement with a symmetrical velocity profile, that is, the maximum velocity occurs halfway through the movement. Equivalently, in

100 ms ballistic movements, the limb has a constant acceleration for the first 50 ms and a constant deceleration for the last 50 ms. In the following, each acceleration burst is approximated by a rectangular pulse with a fixed duration of 50 ms. Of course, the actual measured acceleration waveform is more complex and more closely resembles a distorted sinewave than a pair of rectangular pulses (see Meyer et al., 1982, for a discussion). Nevertheless, as long as the waveform of the acceleration remains constant while only its amplitude is varied, the arguments developed here for rectangular acceleration pulses still hold. To some extent, the assumption of a fixed waveform that can be scaled in amplitude is similar to the assumption in the symmetrical impulse-variability model by Meyer et al. (1982) of a prototypical waveform that can be scaled in both amplitude and time.

Let  $x_i = [x_1(t_i) \ \dot{x}_1(t_i)]^T$  and  $x_f = [x_1(t_f) \ \dot{x}_1(t_f)]^T$  denote the initial and final state vector, respectively, where  $x_1(t)$  and  $\dot{x}_1(t)$  denote the position and velocity, respectively. For a fast ballistic movement, the OTG generates a desired response with a duration of 100 ms that connects  $x_i$  and  $x_f$ . In this case, the desired trajectory is unidimensional (one DOF) and therefore denoted by  $R^*$  (instead of boldface notation reserved for multiple DOFs tasks). As already discussed, it is known that ballistic movements have EMG bursts of amplitude modulation only, that is, the duration of the EMG bursts is fixed. The integrated EMG activity in the agonist burst increases almost linearly with the amount of work done by the limb (e.g., Bouisset, Lestienne, & Maton, 1977) while the average duration of the burst is relatively constant (e.g., Lestienne, 1979). Thus, the BUMP model imposes the constraint that the acceleration waveform is comprised of two 50 ms duration rectangular pulses associated with EMG bursts from agonist and antagonist muscles. Fig. 2.9 shows two trajectories that connect an initial state  $x_i$  and a final state  $x_f$  (arbitrary units). In the first case, Fig. 2.9 (a), the limb is assumed to be at stand-still, that is, the initial position and velocity are both zero, or  $x_i = [0 \ 0]^T$ . The final state is at unity position with zero velocity, or  $x_f = [1 \ 0]^T$ . The unique solution to connect  $x_i$  and  $x_f$  is two acceleration pulses with the same magnitude but with

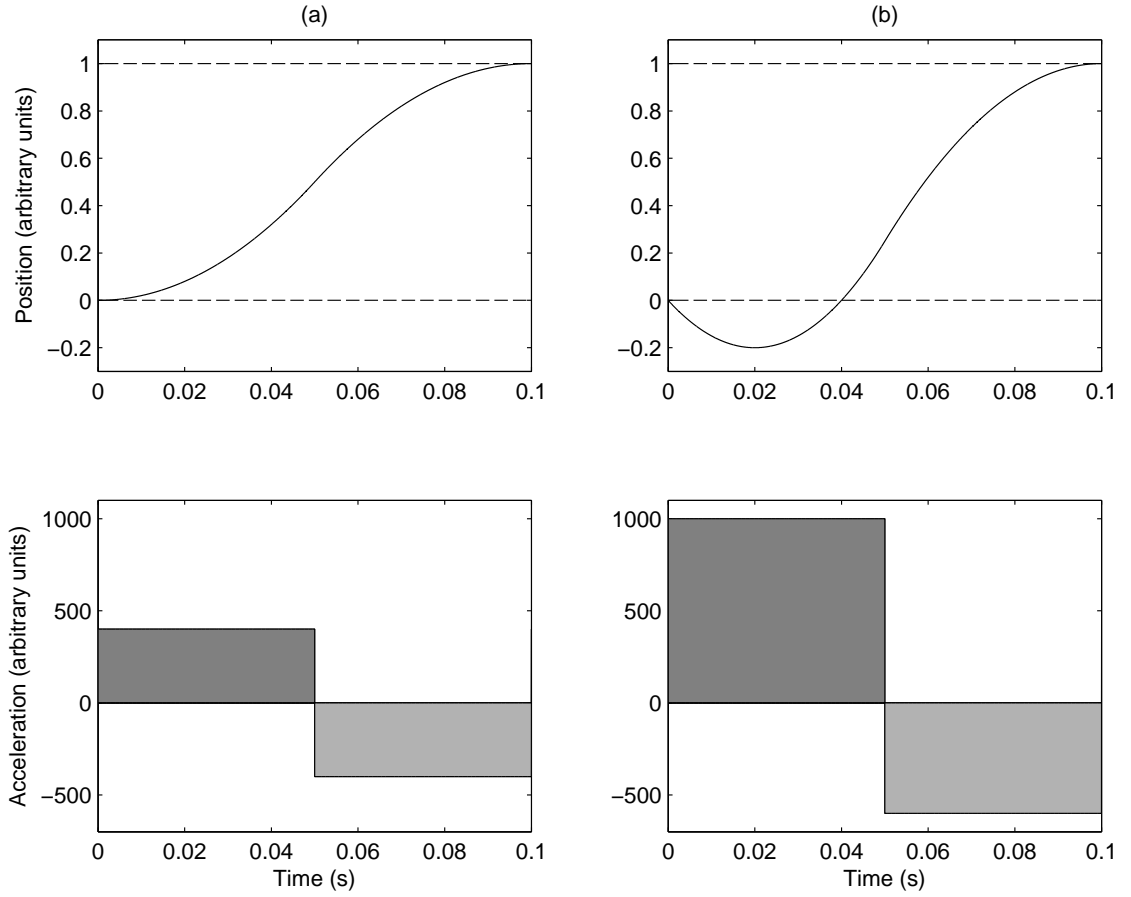


Figure 2.9: Ballistic movement trajectories of 100 ms duration. For two rectangular acceleration pulses with fixed duration of 50 ms, the trajectories connecting initial states (a)  $x_i = [0 \ 0]^T$  and (b)  $x_i = [0 \ -20]^T$  with the final state  $x_f = [1 \ 0]^T$  are unique.

opposite signs, resulting in an S-shaped position trajectory, antisymmetrical about its midpoint. The corresponding velocity profile (not shown) is symmetrical, with the maximum velocity halfway through the movement.

In the second case, Fig. 2.9 (b), the limb is initially moving with a velocity  $\dot{x}_1 = -20$  at zero position, thus  $x_i = [0 \ -20]^T$ . The desired final state is still unity position with zero velocity, or  $x_f = [1 \ 0]^T$ . Again, there is a unique solution, with the first acceleration pulse braking the already moving limb, thus reducing the initially negative velocity to zero, turning it around, and accelerating it back in the positive direction. The second pulse decelerates the movement by just the right amount to achieve the desired final state. In general, there is only one combination of two acceleration pulse amplitudes that will achieve the desired trajectory. In fact,

to move an  $n$ -th order discrete-time dynamic system from an arbitrary initial state to an arbitrary final state requires a minimum of  $n$  ZOH rectangular pulses. If the trajectory cannot be achieved in  $n$  samples then it cannot be achieved at all and the system is said to be uncontrollable (see Ogata, 1995, for proof). This conclusion can be generalised for two fixed duration acceleration pulses with waveforms more complex than the rectangular pulses considered here. Given the assumption that the CNS is constrained to generate acceleration pulses with a minimum duration of 50 ms, there exists only one unique trajectory that can connect a specified initial state and final state in 100 ms.

The proposal that purposive movements are comprised of a sequence of 100 ms duration concatenated submovements planned in advance by OTG circuits and executed open-loop by the RE system has been examined in a study by Lui (1993). Using an electronic pen and whiteboard, the 2D position of the tip of the pen was sampled and recorded for a large number of characters, words, and scribbles drawn by subjects. The  $x$  and  $y$  components of the signals were segmented into 100 ms consecutive intervals and the position and velocity were measured at the beginning and end of each segment. A computer simulation of two OTG circuits operating in parallel (one OTG for each of the DOFs in such a 2D drawing task) was then employed to generate a unique continuous-time S-shaped trajectory connecting the initial state with the final state for each segment. As described above, the computed trajectories were constrained to have an acceleration waveform consisting of two 50 ms duration rectangular pulses, where only the amplitudes of the pulses were modulated. For all recordings, the computer-simulated trajectories matched the actual trajectories extremely well, even around sharp corners. It may be concluded that even in complex purposive movements such as handwriting, the pen-point trajectories produced are not inconsistent with concatenated sequences of 100 ms duration submovements generated independently for each DOF of movement.



### 2.4.2 Non-ballistic trajectories

The simple model presented above for fast ballistic movements can be extended to slower trajectories that are not ballistic and involve more than two acceleration pulses. For example, consider a 150 ms duration movement with an acceleration trajectory consisting of three rectangular pulses with a fixed duration of 50 ms and assume that only the amplitude of the pulses can be controlled. Fig. 2.10 shows two examples of such three-pulse trajectories connecting the same initial and final states as in Fig. 2.9(b), that is,  $x_i = [0 \ -20]^T$  and  $x_f = [1 \ 0]^T$  (arbitrary units). Unlike fast two-pulse ballistic movements such as those illustrated in Fig. 2.9, there exists

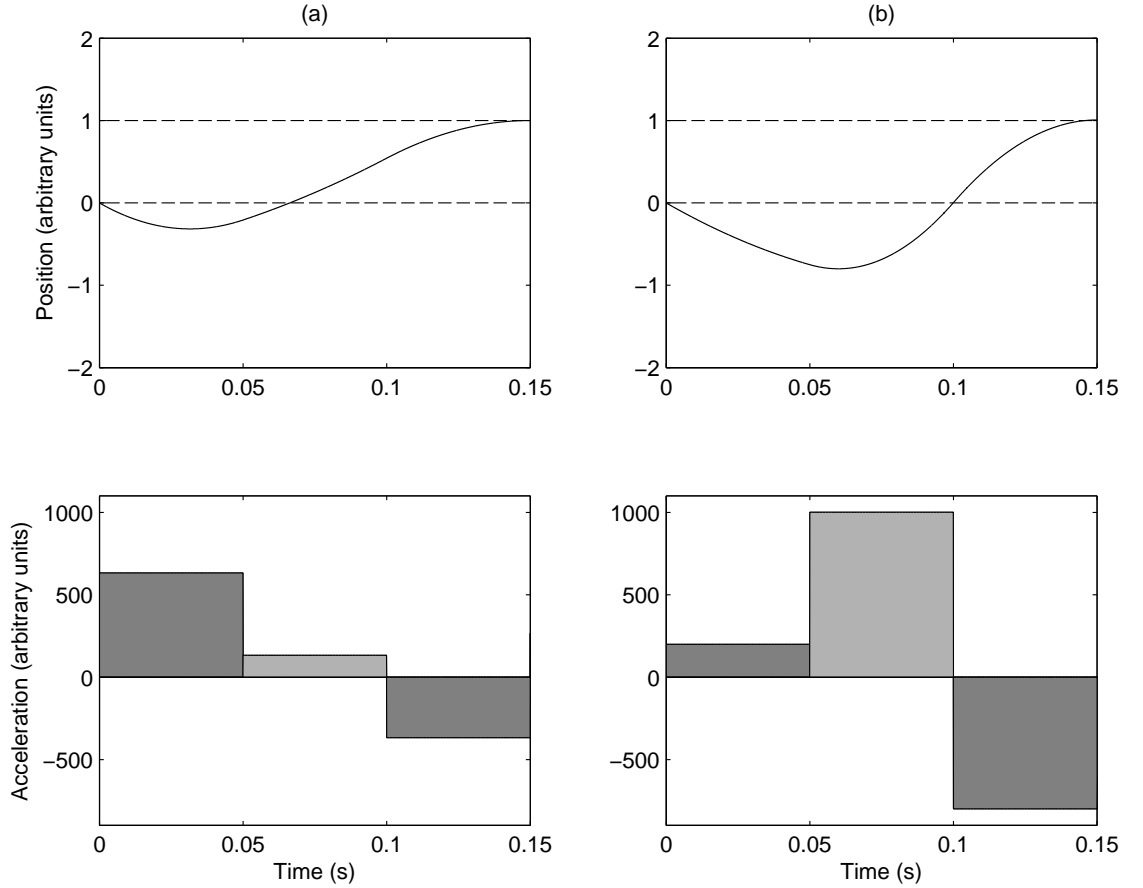


Figure 2.10: Non-ballistic movement trajectories of 150 ms duration. For three rectangular acceleration pulses with fixed duration of 50 ms, (a) and (b) show two possible position and acceleration trajectories connecting the initial state  $x_i = [0 \ -20]^T$  with the final state  $x_f = [1 \ 0]^T$ . In general, for three or more acceleration pulses, there is an infinite number of possible trajectories that can connect an arbitrary initial state  $x_i$  with an arbitrary final state  $x_f$ .

no unique solution to the generation of a three-pulse trajectory. Indeed, there is an infinite number of possible three-pulse trajectories that can connect an arbitrary initial state  $x_i$  with an arbitrary final state  $x_f$ . This problem of redundancy, or trajectory selection, exists for all trajectories involving three or more acceleration pulses.

#### 2.4.3 Solution to the redundancy problem

The AMT solution to the redundancy problem is the application of optimal control theory. By choosing minimum acceleration as a control criterion, there exists a unique solution, or trajectory, that connects an initial and a final state in a specified time. This trajectory minimises the sum of the squares of the acceleration pulse amplitudes.

The solution that drives the state from  $x_i$  to  $x_f$  in  $N$  steps, or samples, with minimum demand on acceleration, has been derived previously (Neilson et al., 1995). The problem can be conceptualised as equivalent to controlling a double integrator system driven by a ZOH sampled input, as illustrated in Fig. 2.11. The corresponding state equation for the continuous-time double integrator system is given

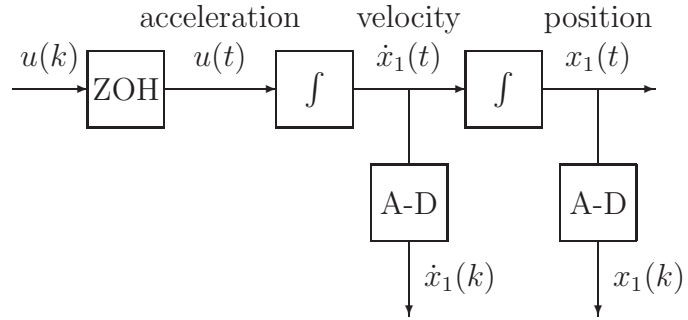


Figure 2.11: Discrete-time equivalent of double integrator system. The discrete-time (sampled) input signal  $u(k)$  is transformed into a ZOH continuous-time signal  $u(t)$  by the ZOH block. The continuous-time velocity  $\dot{x}_1(t)$  and position  $x_1(t)$  signals are transformed into discrete-time signals  $\dot{x}_1(k)$  and  $x_1(k)$  by the analog-to-digital converter (A-D). The vector  $x(k) = [x_1(k) \ \dot{x}_1(k)]^T$  is the state of the system at sample  $k$ .

by Eq. 2.11:

$$\dot{x}(t) = \begin{bmatrix} \dot{x}_1(t) \\ \ddot{x}_1(t) \end{bmatrix} = \begin{bmatrix} 0 & 1 \\ 0 & 0 \end{bmatrix} \begin{bmatrix} x_1(t) \\ \dot{x}_1(t) \end{bmatrix} + \begin{bmatrix} 0 \\ 1 \end{bmatrix} u(t) \quad (2.11)$$

As argued in Chapter 2.3.11, neural activity may be quantified as a staircase waveform (ZOH signal) that represents the average level of activity over each 50 ms time window by the level of each step in the waveform. Accordingly, the ZOH discrete-time equivalent state equation in Eq. 2.12 is obtained by integrating over a 50 ms sample interval:

$$x(k+1) = \mathbf{G}x(k) + \mathbf{H}u(k), \quad (2.12)$$

where

$$x(k) = \begin{bmatrix} x_1(k) \\ \dot{x}_1(k) \end{bmatrix}, \quad \mathbf{G} = \begin{bmatrix} 1 & 0.05 \\ 0 & 1 \end{bmatrix}, \quad \mathbf{H} = \begin{bmatrix} 0.00125 \\ 0.05 \end{bmatrix}, \quad u(k) = \ddot{x}_1(k)$$

By choosing the cost function  $J$  as the mean square acceleration given by Eq. 2.13,

$$J = \frac{1}{N} \sum_{k=0}^{N-1} u^2(k) \quad (2.13)$$

it can be shown by the application of discrete-time optimal control theory (Neilson et al., 1995) that the optimal solution is given by Eq. 2.14:

$$x(k) = \mathbf{G}^k x(0) + \mathbf{\Gamma}(0, k) \mathbf{\Gamma}^{-1}(0, N) (x(N) - \mathbf{G}^N x(0)), \quad (2.14)$$

where  $x(k) = [x_1(k) \ \dot{x}_1(k)]$  is the dynamic state at sample  $k$ ,  $\mathbf{G}$  is the  $2 \times 2$  discrete-time equivalent state matrix,  $\mathbf{H}$  is the  $2 \times 1$  discrete-time equivalent input matrix for a double integrator system, and  $\mathbf{\Gamma}(0, k)$  is the  $2 \times 2$  discrete-time Grammian

matrix at sample  $k$  given by Eq. 2.15:

$$\mathbf{\Gamma}(0, k) = \sum_{j=0}^{k-1} \mathbf{G}^j \mathbf{H} \mathbf{H}^T \mathbf{G}^{T(N-k+j)} \quad (2.15)$$

An example of a unidimensional  $N$ -step optimal desired response trajectory  $R^*$  for  $N = 10$  acceleration pulses is presented in Fig. 2.12. The initial and final states are given by  $x_i = x(0) = [0 \ 0]^T$  and  $x_f = x(N) = [1 \ 0]^T$ , respectively.

The importance of Eq. 2.14 is apparent from the observation that every point in the minimum acceleration discrete-time trajectory can be generated in parallel with every other point by simple  $2 \times 2$  matrix transformations of the initial state

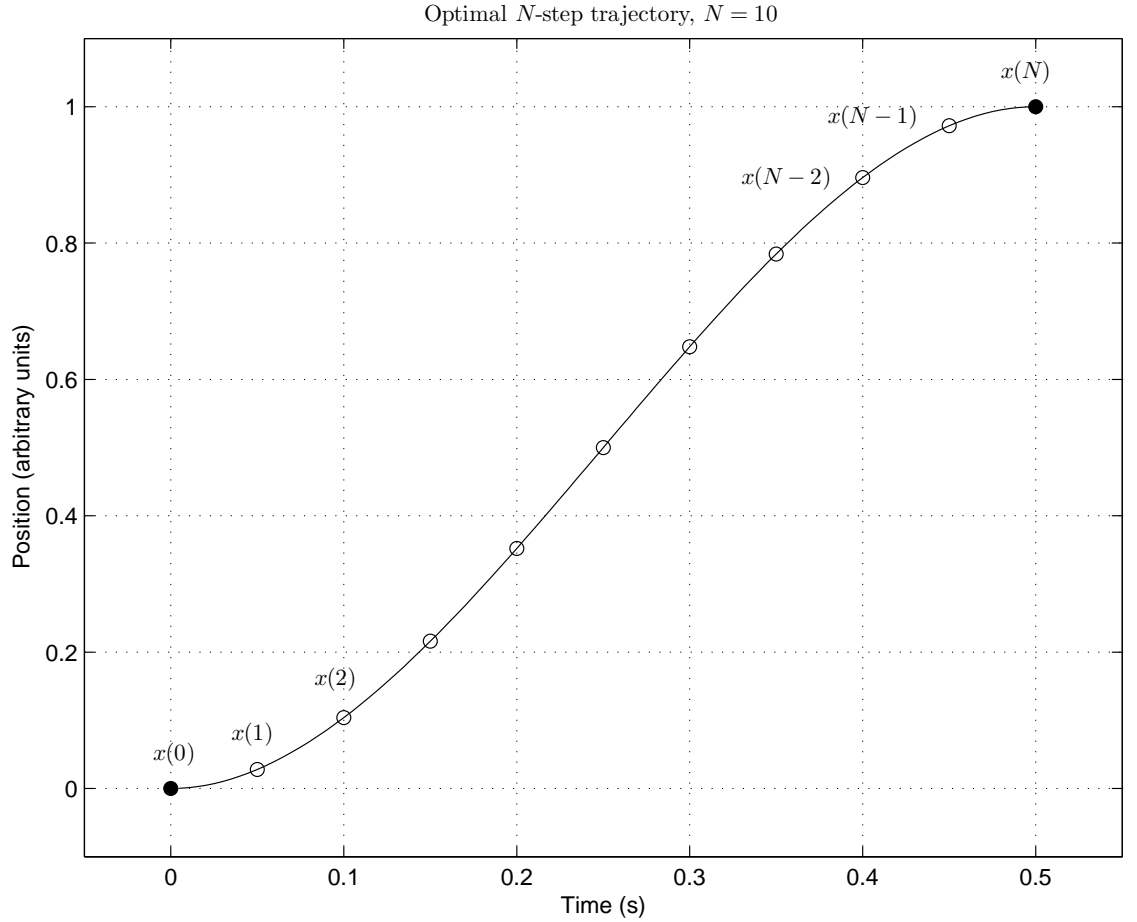


Figure 2.12: Optimal  $N$ -step desired response trajectory  $R^*$  connecting the initial and final states  $x_i = x(0) = [0 \ 0]^T$  and  $x_f = x(N) = [1 \ 0]^T$ . As  $N = 10$ , the movement duration is  $N \times 50 \text{ ms} = 500 \text{ ms}$ . The trajectory is unique in the sense that it minimises the mean square acceleration.

$x(0)$  and final state  $x(N)$ . For example, to calculate  $x(k)$ , there is no need to wait until  $x(k - 1)$  has been calculated. Thus, the entire trajectory can be generated in one operation by an OTG. This can readily be implemented by means of parallel processing circuitry comprised of adaptive neural filters. Hence, the above account of trajectory generation allows all three systems (SA, RP, and RE) to be similar, consisting of parallel repetitions of a basic, physiologically realistic, neural circuit.

A block diagram of an OTG is given in Fig. 2.13. Each block represents a  $2 \times 2$  matrix transformation  $y = \mathbf{M}x$  as illustrated in Fig. 2.14, where

$$x = \begin{bmatrix} x_1 \\ x_2 \end{bmatrix}, \mathbf{M} = \begin{bmatrix} m_{11} & m_{12} \\ m_{21} & m_{22} \end{bmatrix}, \text{ and } y = \begin{bmatrix} y_1 \\ y_2 \end{bmatrix}. \quad (2.16)$$

The solution is given by

$$y_1 = m_{11}x_1 + m_{12}x_2 \quad (2.17)$$

$$y_2 = m_{21}x_1 + m_{22}x_2 \quad (2.18)$$

By applying the initial state  $x(0)$  and the final state  $x(N)$  as inputs, the parallel processing circuit can simultaneously compute all  $N - 1$  samples in between, namely  $x(1), x(2), \dots, x(N - 1)$ , in the discrete-time version of the optimal trajectory  $R^* = [x(0) \ x(1) \ \dots \ x(N - 1) \ x(N)]^T$  in no more time than it takes for the signals to flow through the circuit. The maximum duration of the preplanned trajectory, or equivalently, the maximum number  $N$ , is limited only by the number of parallel processing modules in the OTG circuit. The OTG can only plan a single  $R^*$  at a time, that is, it does not commence planning a second trajectory until it has finished the first. It is this iterative operation of the OTG circuit that introduces intermittency into the control of movement.

#### 2.4.4 Synchronous operation of multiple OTGs

Analogous to the parallel operation within a single OTG circuit, AMT hypothesises that multiple OTG circuits can operate synchronously and in parallel. Con-

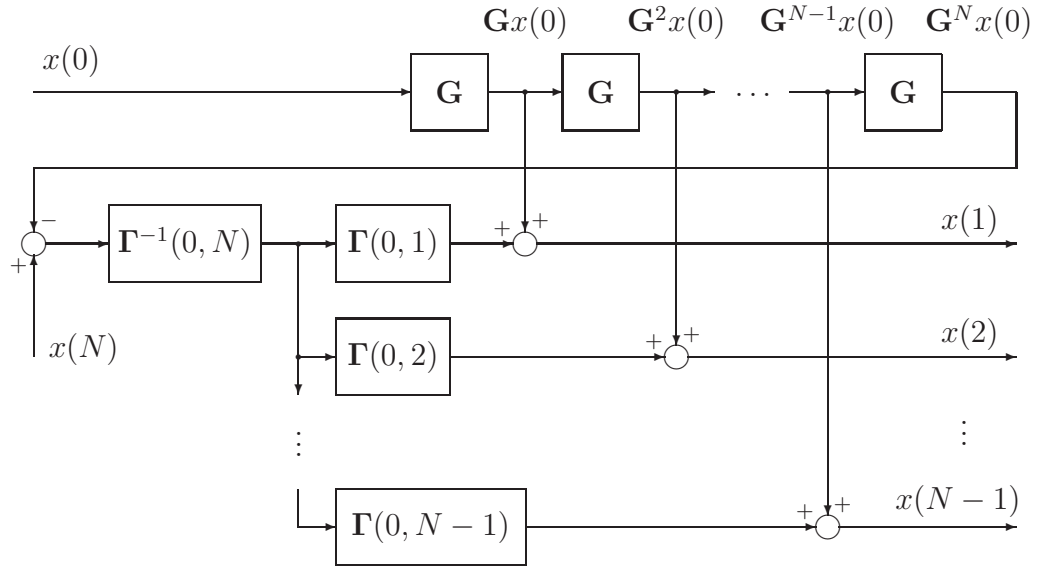


Figure 2.13: The optimal trajectory generator (OTG). Each block represents a  $2 \times 2$  matrix transformation (see Fig. 2.14). Given  $x(0)$  and  $x(N)$  as inputs, the circuit simultaneously computes all  $N - 1$  samples in between to obtain the discrete-time optimal trajectory  $R^* = [x(0) \ x(1) \ \dots \ x(N - 1) \ x(N)]^T$ .

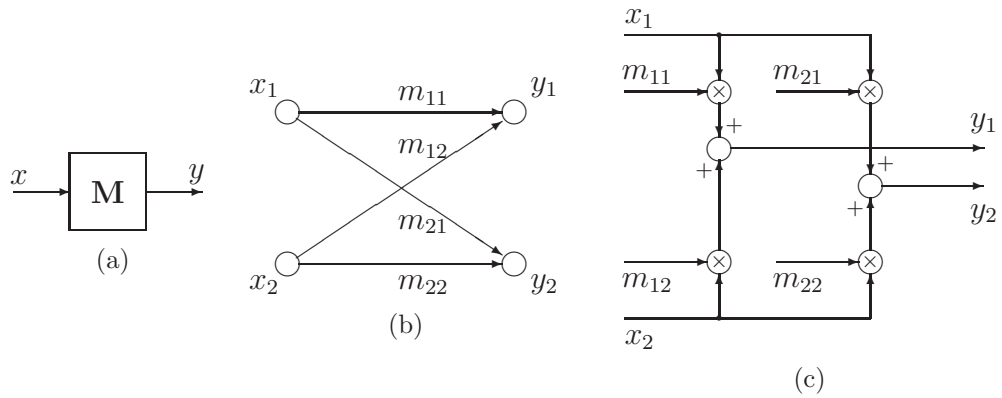


Figure 2.14: Three equivalent representations (a), (b), and (c) of the  $2 \times 2$  matrix transformation  $y = \mathbf{M}x$ .

sequently, a response trajectory  $\mathbf{R}^* = [R_1^* \dots R_M^*]$  with  $M$  control DOFs can be generated in no more time than is required for a single OTG to generate a single trajectory with only one DOF, as long as there exists at least one OTG circuit for every DOF in the response, that is, at least  $M$  OTG circuits must be available. The proposal that the time required to generate a multidimensional response trajectory is no greater than the time required for a unidimensional trajectory does not contradict the wealth of evidence of increased reaction time with increased complexity of the planned response. In AMT, the OTG circuits are thought to operate at the lowest level in a hierarchical structure of cognitive processes involved in response planning. Whereas the time required for higher cognitive processes may increase or decrease depending on a number of factors, thereby changing the reaction time, it is only the lowest levels of the RP system, namely the OTG circuits, that normally participate in the perceptual-motor loop. Performance of any feedback loop, including the perceptual-motor loop, is limited by the time delay within the loop. Therefore, performance can be no better than the ability of the system to compensate for the time delay by predicting future inputs. Thus, it would be biologically advantageous for the CNS to have evolved an RP system capable of generating error-correcting responses in the shortest possible time, regardless of their complexity. Experimentally, many results support this view. Pashler (1992) showed that subjects can generate assemblages of responses to a stimulus with no greater a reaction time than required for a single response. Similarly, in a variety of visual tracking experiments (e.g., Oytam, Neilson, & O'Dwyer, 1998; Oytam et al., 2005; Navon et al., 1984; Wickens, 1984), it has been shown that the time delay between the target and response signals, as measured by phase lag, is the same for both one DOF and two DOFs tracking tests. In other words, subject can perform two independent visual tracking tasks simultaneously without increasing the response time delay beyond that measured when performing either task separately. The multiple trajectories generated by multiple OTGs may be regarded as a vector trajectory  $\mathbf{R}^*$  in a multidimensional vector space, or a single response associated with a single

BUMP but involving multiple DOFs. For example, in a reaching movement to a target in 3D space of duration  $N \times 50$  ms, separate trajectories  $R_x^*$ ,  $R_y^*$ , and  $R_z^*$  for the  $x$ ,  $y$ , and  $z$  components of the movement would be generated simultaneously by three OTG circuits within one RP interval to form the desired response trajectory  $\mathbf{R}^*$  given by

$$\mathbf{R}^* = \begin{bmatrix} R_x^* & R_y^* & R_z^* \end{bmatrix} = \begin{bmatrix} x(0) & y(0) & z(0) \\ \vdots & \vdots & \vdots \\ x(N) & y(N) & z(N) \end{bmatrix} \quad (2.19)$$

Equivalently, if the spherical coordinates  $\rho$ ,  $\phi$ , and  $\theta$  were more appropriate, such as in a rotating task, trajectories  $R_\rho^*$ ,  $R_\phi^*$ , and  $R_\theta^*$  would be generated simultaneously.

## 2.5 Variable horizon predictive control

The output of the OTG circuits is the preplanned response trajectory  $\mathbf{R}^*$ . The duration of  $\mathbf{R}^*$  may be termed the prediction horizon  $T_h$ . To provide continuity of movement in any task, the RP system must predict the initial state of the movement at the end of the RP interval and the target state  $T_h = N \times 50$  ms ahead in time of the initial state (e.g., initial state  $x(0)$ , final state  $x(N)$ , and  $N = 10$  in Fig. 2.12–2.13). The ability to vary the prediction horizon gives rise to the concept of variable horizon predictive control. Moreover, the ability of the RP system to plan an  $\mathbf{R}^*$  of duration much longer than the RP interval (100 ms), say  $T_h = 1\text{--}2$  s, is referred to as planning in accelerated time. After an RP interval, only the first 100 ms of  $\mathbf{R}^*$  is executed by the RE system. At the same time, the RP system plans another  $\mathbf{R}^*$  while the first one is being executed. The new  $\mathbf{R}^*$  replaces the previous one in working memory before the RE system again only executes the first 100 ms. This process iterates as a series of BUMPs (Fig. 2.1). Thus, although such response planning is inherently intermittent it will produce optimally smooth trajectories provided that the prediction is accurate.



### 2.5.1 Receding and fixed horizon control

Variable horizon control leads to two main control strategies, receding horizon control and fixed horizon control. Receding horizon control, also known as model predictive control, is currently one of the most popular control algorithms employed in computer-controlled systems, predominantly in the petrochemical industry, but also increasingly so in electromechanical control problems (Goodwin, Graebe, & Salgado, 2001). It can be shown that receding horizon controllers can be designed with guaranteed asymptotic closed-loop stability (Goodwin et al., 2001) and this remarkable property is perhaps the most important reason for its popularity. Receding horizon control is implemented in the BUMP model by having the RP system plan a new  $\mathbf{R}^*$  that is predicted a fixed time ahead at every RP interval, that is,  $T_h$  remains constant during the entire movement. Consequently, the prediction horizon, like the earth's horizon, recedes as it is approached (see Fig. 2.15 for an example).

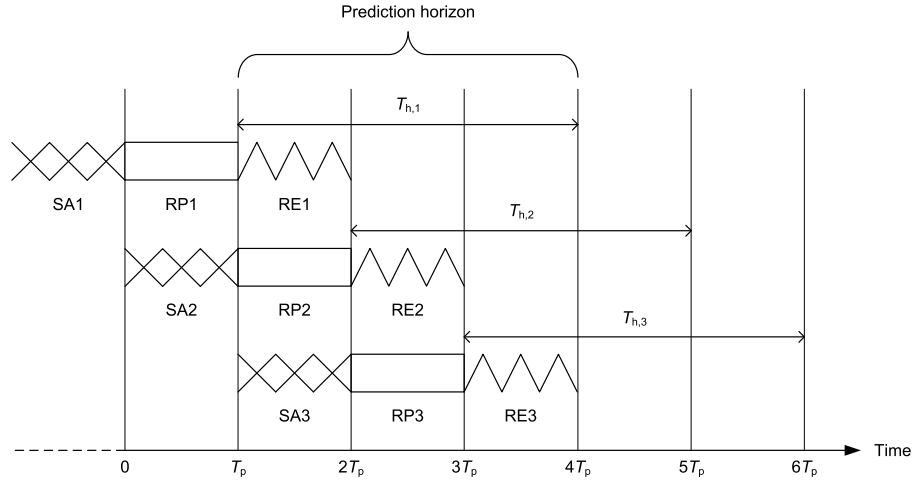


Figure 2.15: Example of receding horizon control. At every RP interval, OTG circuits generate a new  $\mathbf{R}^*$  of a fixed duration  $T_{h,i}$ . In this particular example, the duration is equal to three RP intervals. During RP1, the OTG circuits generate an optimal  $\mathbf{R1}^*$  of duration  $T_{h,1} = 3T_p = 300$  ms. While  $\mathbf{R1}^*$  is being executed during RE1, a new trajectory  $\mathbf{R2}^*$  of the same duration  $T_{h,2} = 3T_p = 300$  ms is being planned during RP2 and then replaces  $\mathbf{R1}^*$  in working memory. Thus, after executing only the first  $T_p = 100$  ms of  $\mathbf{R1}^*$ , the RE system commences execution of  $\mathbf{R2}^*$  during RE2. The process repeats, with trajectories planned  $T_{h,i} = 300$  ms ahead in time but only the first 100 ms executed, until the target is reached. Effectively, the prediction horizon recedes as it is approached.

In contrast, if a fixed horizon control strategy is implemented, the prediction horizon decreases as the movement approaches its target. At every RP interval, the RP system plans a new  $\mathbf{R}^*$  connecting the current position and velocity, or initial state, with a final (target) state at a fixed point ahead in both time and space. Thus, with the horizon fixed in this way, the prediction horizon must decrease as the fixed horizon is approached (see Fig. 2.16 for an example).

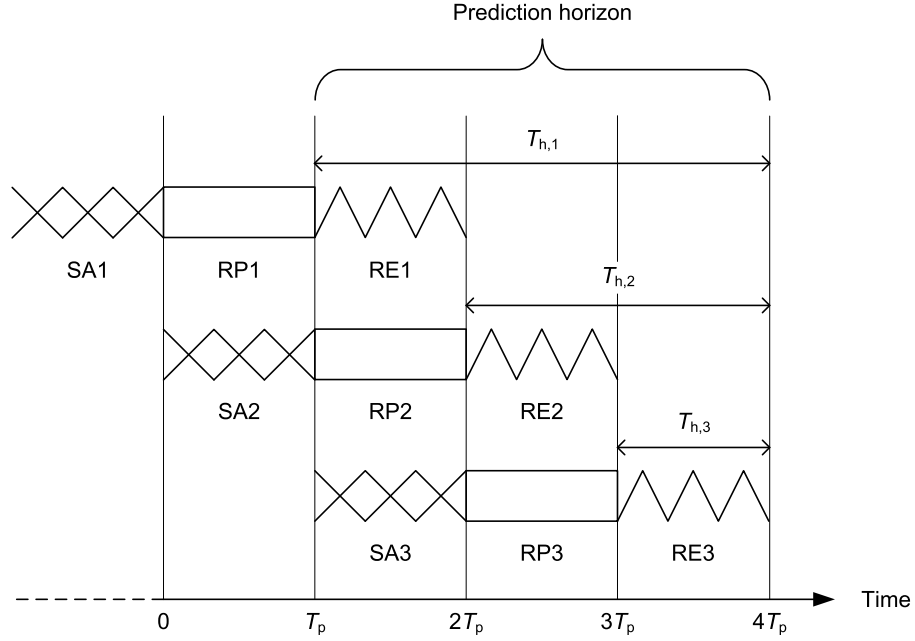


Figure 2.16: Example of fixed horizon control. At every RP interval, OTG circuits generate a new  $\mathbf{R}^*$  connecting the current state with a fixed final state, or target. In this particular example, the initial trajectory  $\mathbf{R1}^*$  has a duration of  $T_{h,1} = 3T_p = 300$  ms. While  $\mathbf{R1}^*$  is being executed during RE1, a new trajectory  $\mathbf{R2}^*$  is being planned during RP2 to a fixed horizon ahead and replaces  $\mathbf{R1}^*$  in working memory. As the RP system spent  $T_p = 100$  ms to preplan  $\mathbf{R2}^*$ , the duration of  $\mathbf{R2}^*$  is given by  $T_{h,2} = T_{h,1} - T_p = 200$  ms. The process repeats, with only the first 100 ms executed of every trajectory, which each has a duration planned 100 ms shorter ahead in time than the previous one, until the target is reached. Effectively, the prediction horizon stays fixed as it is approached.

It is proposed that whenever the task allows, a subject is likely to adopt a receding horizon control strategy in aimed movement, since this has the great advantage of stability. On the other hand, fixed horizon control is exactly the strategy a subject needs if the goal is to reach the target at a fixed point in time. It makes sense that a fixed horizon strategy is adopted in time-matching tasks because then both

the spatial and temporal component of the target is incorporated into the planning of each submovement. It is therefore proposed that in tasks in which subjects are required to control the timing as well as the spatial accuracy of the response, they are likely to adopt a fixed horizon strategy rather than a receding horizon one.

## 2.6 Noise in the motor system

According to the BUMP model, trajectory planning proceeds smoothly provided prediction is accurate. However, accurate prediction depends on ability to model the target trajectory accurately (in the case of a moving target) as well as ability to model the RE system that gives rise to the actual response. And apart from uncertainties of this nature, the activation of an accurate response is inevitably affected by disturbances, even when the planned trajectory is accurate. Noise is ubiquitous in the CNS. A number of authors have proposed that inaccuracies in reaching movements can be attributed to the influence of stochastic noise in the motor system (e.g., Fitts, 1954; Schmidt, 1976; Meyer et al., 1988; Chan & Childress, 1990; Harris & Wolpert, 1998; van Beers, Baraduc, & Wolpert, 2002; van Beers et al., 2004; Hamilton, Jones, & Wolpert, 2004). Some have argued that the amount of noise is related to the velocity of the movement, while others maintain that it is related to the level of force. In studies of speech in normal and athetoid cerebral palsy adult subjects (Neilson & O'Dwyer, 1984; O'Dwyer & Neilson, 1988), EMG activity from six speech muscles was recorded and quantified during repetitions of a test sentence. By measuring the variation about the mean integrated EMG waveform for each syllable, it was found that the standard deviation increased with the average level of integrated EMG activity in each muscle in both normal and cerebral palsy subjects. In another study, O'Dwyer & Neilson (1998) examined isometric force responses generated about the elbow joint to control the deflection of a response cursor on a computer monitor in a visual pursuit tracking task. Subjects were required to track a target that was moving in a slow sinusoidal fashion at 0.3 Hz under two different experimental conditions. In one condition, the required range of isometric force was 10–20% of maximum, while it was 40–50% of

maximum in the other condition. Consistent with impulse-variability theory and findings of Carlton & Newell (1993), tracking performance deteriorated when the average level of force or muscle activation was increased. All these results support the view that the nervous system injects stochastic noise into the movement control signals. Consistent with the proposal of Harris & Wolpert (1998), AMT suggests that broadband stochastic noise is probably introduced at the level of motor commands to individual muscles and that its standard deviation increases with the size of the motor command. Accordingly, such noise is introduced in the simulation experiments that follow.

---

## CHAPTER 3

### Study I: Speed-accuracy tradeoffs and velocity profiles

---

#### 3.1 Literature review

One of the most fundamental relationships observed in aimed movements is the speed-accuracy tradeoff: As the movement speed increases, the spatial accuracy decreases. Conversely, as the spatial accuracy increases, the movement speed decreases. Historically, research on speed-accuracy tradeoffs in human movements can be traced back to the end of the 19th century. Often credited as the founder of research on speed-accuracy tradeoffs is one of the pioneers in the behavioural study of aimed movements, namely Woodworth (1899). He systematically investigated how accuracy changed with movement speed when certain spatial (distance) and temporal (duration) goals were attained. Proposing several interesting hypotheses to interpret results obtained from his experiments, his ideas anticipated subsequent research on human motor performance (Keele, 1968). According to the review of Meyer et al. (1990), the seminal work of Woodworth (1899) was followed by a “dormant period” for nearly 50 years, where only sporadic research on speed-accuracy tradeoff occurred. However, with World War II and the need for good tracking performance in a number of military applications, development of tracking control theory was triggered, stimulating considerable scientific interest in the relationship between movement speed and accuracy. Researchers started to play with the idea of modelling sensory-motor mechanisms using a systems orientation, viewing the CNS as the controller of a plant (Craig, 1947, 1948). Based on such ideas, Baron & Kleinman (1969); Baron et al. (1970); Kleinman et al. (1970, 1971) would later

hypothesise that the well-trained human operator behaves in an optimal manner subject to inherent limitations, or in other words, suggesting that the CNS acts as an optimal controller involving continuous error corrections. However, following up the influential research of Craik (1947, 1948), experiments showed that tracking behaviour often consists of small discrete movements. This led to a closer investigation of such movements, extending the study of speed-accuracy tradeoff initiated by Woodworth (1899). An often-cited worker is Vince (1948), who had her subjects track discrete step changes as well as continuous targets. Confirming many of the findings of Woodworth (1899), her results substantiated the importance of feedback for movement accuracy. Furthermore, Vince (1948) concluded that the human operator responds intermittently in a tracking task. She suggested that there exists a psychological refractory period (PRP) during which the CNS is occupied and cannot respond to incoming stimulus.

The BUMP model can be thought of as a discrete equivalent of the optimal control model hypothesised by Baron & Kleinman (1969); Kleinman et al. (1970), however, AMT addresses several of its limitations (Neilson & Neilson, 1999), with perhaps the greatest difference being the use of intermittent error corrections hypothesised in AMT. Complementing the research of Vince (1948) and others who had focused on performance in time-matching tasks, researchers began to investigate speed-accuracy tradeoff in time-minimisation tasks, resulting in the discovery by Fitts (1954) that such movements obey a logarithmic tradeoff between movement speed and endpoint accuracy. Indeed, this relationship, which is known as Fitts' law, has been shown to hold for a vast variety of movement tasks. However, despite the robustness of Fitts' law, it fails in time-matched movements. In fact, Schmidt et al. (1979) showed that the mathematical form of the speed-accuracy tradeoff depends on the inclusion of a temporal goal or not in the movement task. While movements that are spatially constrained typically yield a logarithmic speed-accuracy tradeoff, movements that are temporally constrained, that is, timed movements, typically result in a linear speed-accuracy tradeoff (Meyer et al., 1982; Wright & Meyer,

1983). Whereas the logarithmic and the linear speed-accuracy tradeoffs are the two most important tradeoffs reported in the literature, several other relationships have been hypothesised, including other logarithmic and linear functions, power laws, quadratic laws, and the delta-lognormal law (see Plamondon & Alimi, 1997, for a review). In the following sections, the logarithmic and linear tradeoffs will be discussed more thoroughly.

### 3.1.1 *Logarithmic speed-accuracy tradeoff*

The logarithmic speed-accuracy tradeoff results during spatially constrained movements, that is, tasks in which subjects must end their movements inside a pre-defined target region while attempting to minimise their average movement time (Meyer et al., 1988). The first formalisation of this logarithmic relationship came with the reciprocal tapping experiments of Fitts (1954). He had his subjects move a hand-held stylus rapidly back and forth between two target regions, tapping the targets at the end of each movement. The subjects were required to have at least 95% of their movements end inside the target regions while minimising their average movement times. By systematically varying two independent variables, namely the target distance  $D$  and the target width  $W$ , Fitts (1954) showed that the mean movement time  $T$  closely matched the following equation, which is also known as Fitts' law:

$$T = a + b \log_2 \frac{2D}{W}, \quad (3.1)$$

where  $a$  and  $b$  are constants. The logarithmic term of Equation 3.1 is referred to as the index of difficulty  $I_d$ :

$$I_d = \log_2 \frac{2D}{W} \quad (3.2)$$

Substituting  $I_d$  into the expression, a linear relationship arises between the index of movement difficulty and average movement time:

$$T = a + bI_d \quad (3.3)$$

Inspired by the advances in information theory at the time of his experiment, Fitts (1954) explained the speed-accuracy tradeoff as a result of the channel capacity of the motor system for transfer of information being independent of the motor task. Thus, when reducing the target width for the same target distance, the subject must either accept a greater error rate or reduce the speed of the movement in order for the channel capacity not to change. Specifically, Fitts (1954) defined an index of performance  $I_p$  as the ratio of the index of difficulty  $I_d$  and the mean movement time  $T$ :

$$I_p = \frac{I_d}{T} \quad (3.4)$$

For all combinations of target distance and target width in the experiment of Fitts (1954), the index of performance stayed nearly constant with values between 10.3 and 11.5 bits/s, indicating constant channel capacity.<sup>1</sup>

Whereas the experiment of Fitts (1954) involved repetitive self-paced movement tasks, Fitts & Peterson (1964) examined the generality of Fitts' law when applied to discrete movements. Again, a strong linear relationship between the index of difficulty and the mean movement time was found. Indeed, Fitts' law has been shown to hold for an extraordinary amount of movement paradigms, including several kinds of movement (e.g., tapping, throwing, rotating, and other finger-, leg-, head-, or wrist movements), manipulators (e.g., using a joystick, computer mouse, rotary handle, keyboard, or foot pedal), environments (e.g., on land, under water, during aircraft flights, viewing through a microscope, or under deprivation of visual feedback), and subjects (e.g., children, young adults, elderly adults, mentally challenged people, patients with Parkinson's disease, or drugged people) (Meyer et al., 1988, 1990; Zelaznik, 1993; Plamondon & Alimi, 1997). It should be emphasised, however, that the logarithmic tradeoff is generally limited to spatially constrained movements. In contrast, when subjects are instructed to make movements with a

---

<sup>1</sup>Information theory was also the reason behind Fitts (1954) using a logarithm with base 2 for the index of difficulty to obtain units of bits. As pointed out by Meyer et al. (1990), other bases can be used instead without changing the linearity of the function. Changing the base simply corresponds to changing the slope of the function.



particular movement duration, that is, temporally constrained movements, a linear speed-accuracy tradeoff occurs.

### 3.1.2 Linear speed-accuracy tradeoff

Schmidt et al. (1979) discovered that temporally constrained movements result in a linear speed-accuracy tradeoff. Extending the discrete tapping task of Fitts & Peterson (1964), subjects made single aimed tapping movements not only with pre-specified distances (10, 20, and 30 cm) but also with pre-specified durations (140, 170, and 200 ms). Schmidt et al. (1979) found that the standard deviation  $S$  of the movement endpoints increased linearly with the average velocity  $V_{av}$ :

$$S = a + bV_{av} = a + b\frac{D}{T}, \quad (3.5)$$

where  $a$  and  $b$  are constants,  $D$  is the mean movement distance, and  $T$  is the mean movement duration. The standard deviation of the endpoint  $S$  is also referred to as the effective target width  $W_e$  analogous to the target width  $W$  in Fitts' law, because it may correspond to an implicit well-defined region around the target point within which the subjects try to end their movements (Schmidt et al., 1979). Substituting  $W_e$  for  $S$  and rearranging Eq. 3.5 for comparison with Fitts' law (Eq. 3.1), the following non-logarithmic relationship emerges:

$$T = b\frac{D}{W_e - a} \quad (3.6)$$

Letting  $a$  be sufficiently small and comparing the linear tradeoff in Equation 3.6 with the logarithmic tradeoff in Eq. 3.1, one can observe that both are monotonically increasing functions of the ratio of movement distance and target width.

Because Schmidt et al. (1979) found a strong linear tradeoff only for movements with a duration of 200 ms or less, the linear tradeoff was initially explained as being due to the lack of feedback, culminating in the movement-brevity and feedback-deprivation hypotheses (Wright & Meyer, 1983). The movement-brevity hypothesis predicts a linear tradeoff only for fast, ballistic movements without any

corrective submovements. Certainly this assumption would explain the lack of a logarithmic tradeoff when considering the great success with which corrective submovement models have explained Fitts' law (e.g., Crossman & Goodeve, 1983; Keele, 1968). The feedback-deprivation hypothesis states that the linear tradeoff is due to the lack of peripheral feedback. Therefore, different from the movement-brevity hypothesis, the feedback-deprivation hypothesis can account for a linear tradeoff also for movements with durations greater than 200 ms. Accordingly, Schmidt et al. (1979) suggested that the movement-brevity hypothesis is simply a special case of the feedback-deprivation hypothesis. In contrast, Meyer et al. (1982) proposed the temporal-precision hypothesis, which suggests that a linear tradeoff occurs when subjects have to make precisely timed movements. Just like the feedback-deprivation hypothesis, the temporal-precision hypothesis can account for linear tradeoffs observed for movements with long duration, however, it states that the linearity is not a result of deprivation of visual feedback but rather the subjects performing time-matching movement tasks. Although some empirical evidence exists for the movement-brevity hypothesis and the feedback-deprivation hypothesis (Schmidt et al., 1979; Zelaznik, Shapiro, & McColsky, 1981), the behavioural evidence largely supports the temporal-precision hypothesis. In particular, the experiments by Zelaznik, Mone, McCabe, & Thaman (1988) provide strong support for the temporal-precision hypothesis and against the movement-brevity and feedback-deprivation hypotheses. Further evidence has been found not only in single tapping tasks (e.g., Zelaznik et al., 1981), but also in saccadic eye movements (Abrams, Meyer, & Kornblum, 1989), wrist rotations (Wright & Meyer, 1983; Meyer et al., 1988), and other time-matching aiming tasks (see Zelaznik, 1993, for a review).

### *3.1.3 Velocity profiles in aimed movements*

An important feature, or invariant, of human aimed movements is the shape of the velocity profile. It has been shown repeatedly that the velocity profile of simple arm movements is bell-shaped (e.g., Georgopoulos, Kalaska, & Massey, 1981; Soechting & Lacquaniti, 1981; Morasso, 1981; Abend, Bizzi, & Morasso, 1982; Atkeson &

Hollerbach, 1985; Nagasaki, 1989; Uno et al., 1989). Virtually all rapid point-to-point limb movements have a bell-shaped velocity profile regardless of whether single-joint or multiple-joint movements are under examination (Berardelli et al., 1996). Moreover, movements with different kinematic and kinetic features show a similar bell-shaped velocity profile after transformation of amplitude, duration, or inertial load (Brown & Cooke, 1990; Berardelli et al., 1996).

For spatially constrained movements, the fastest possible ballistic movements, with a duration of only 100 ms, have a symmetrical velocity profile (Berardelli et al., 1996) whereas slower movements have a positively skewed (left-skewed) asymmetrical bell-shape (e.g., Plamondon & Alimi, 1997). Beggs & Howarth (1972) observed that the amount of this skewness increases as movements are slowed. For some very high-speed movements, the asymmetry has been observed to be inverted, or right-skewed (Zelaznik, Schmidt, & Gielen, 1986).

For movements that include both spatial and temporal constraints, that is, time-matching movements with endpoint spatial error requirements, the velocity profile stays symmetrical no matter the speed of the movement (Shapiro & Walter, 1986; Cooke & Brown, 1994; Schmidt & Lee, 1999). Furthermore, symmetrical velocity profiles have also been shown for movements of different speeds when no spatial or temporal accuracy requirements were imposed on the subjects (Atkeson & Hollerbach, 1985) or when subjects were instructed to move at their preferred speed (Flanagan & Ostry, 1990).

Plamondon (see Plamondon & Alimi, 1997, for a review) has written extensively about the asymmetry of the bell-shaped velocity profile and its relationship to movement speed. He has proposed a kinematic theory to explain this phenomenon in which it is suggested that synergies of agonist and antagonist muscles have a log-normal velocity impulse resulting from the limiting behaviour of a large number of interdependent neuromuscular networks as predicted by the central limit theorem. With this log-normal velocity function, termed the delta-lognormal law, the kinematic theory can almost perfectly reproduce the asymmetrical velocity profiles

as well as the invariance and rescalability of these patterns observed under a variety of experimental conditions (e.g., Plamondon & Alimi, 1997; Plamondon, 1998; Plamondon & Djoua, 2006). Bullock & Grossberg (1988) have pointed out that the asymmetry, its degree, and its changes in direction are of major theoretical importance. They argue, for example, that the minimum jerk model (Hogan, 1984; Flash & Hogan, 1985) predicts symmetrical profiles and that superimposability of velocity profiles after time rescaling is a defining characteristic of generalised motor program models. Therefore, as Bullock & Grossberg point out, these models cannot explain how the velocity profile asymmetry varies with movement speed.

The BUMP model hypothesises that receding and fixed horizon control in the motor system predict asymmetrical and symmetrical velocity profiles, respectively. Arguments for this hypothesis will be developed below.

## 3.2 Predictions of the BUMP model

### 3.2.1 *Logarithmic speed-accuracy tradeoff*

As outlined previously, the BUMP model sees movement as being comprised of a concatenated sequence of 100 ms duration submovements. The acceleration and deceleration waveforms associated with agonist and antagonist EMG bursts are approximated as two rectangular pulses with a fixed duration  $T = 50$  ms. For fast ballistic movements, the two acceleration pulses will have equal and opposite amplitudes, yielding a symmetrical S-shaped position trajectory (desired response) such as that of Fig. 3.1(a). This is equivalent to receding horizon control with a prediction horizon  $T_h$  equal to the duration of an RP interval, that is,  $T_h = T_p = 100$  ms.

Letting the amplitudes of the positive and negative acceleration pulses equal  $a$  and  $-a$ , respectively, the acceleration waveform  $A(t)$  depicted in Fig. 3.1(a) is given by Eq. 3.7 with  $a = 400$  (arbitrary units). The corresponding functions describing the velocity  $V(t)$  and position  $P(t)$  are obtained by integration and

given by Eq. 3.8–3.9:

$$A(t) = \begin{cases} a & , 0 < t \leq T \\ -a & , T < t \leq 2T \end{cases} \quad (3.7)$$

$$V(t) = \begin{cases} at & , 0 < t \leq T \\ -a(t - T) + aT & , T < t \leq 2T \end{cases} \quad (3.8)$$

$$P(t) = \begin{cases} \frac{1}{2}at^2 & , 0 < t \leq T \\ -\frac{1}{2}a(t - T)^2 + aT(t - T) + \frac{1}{2}aT^2 & , T < t \leq 2T \end{cases} \quad (3.9)$$

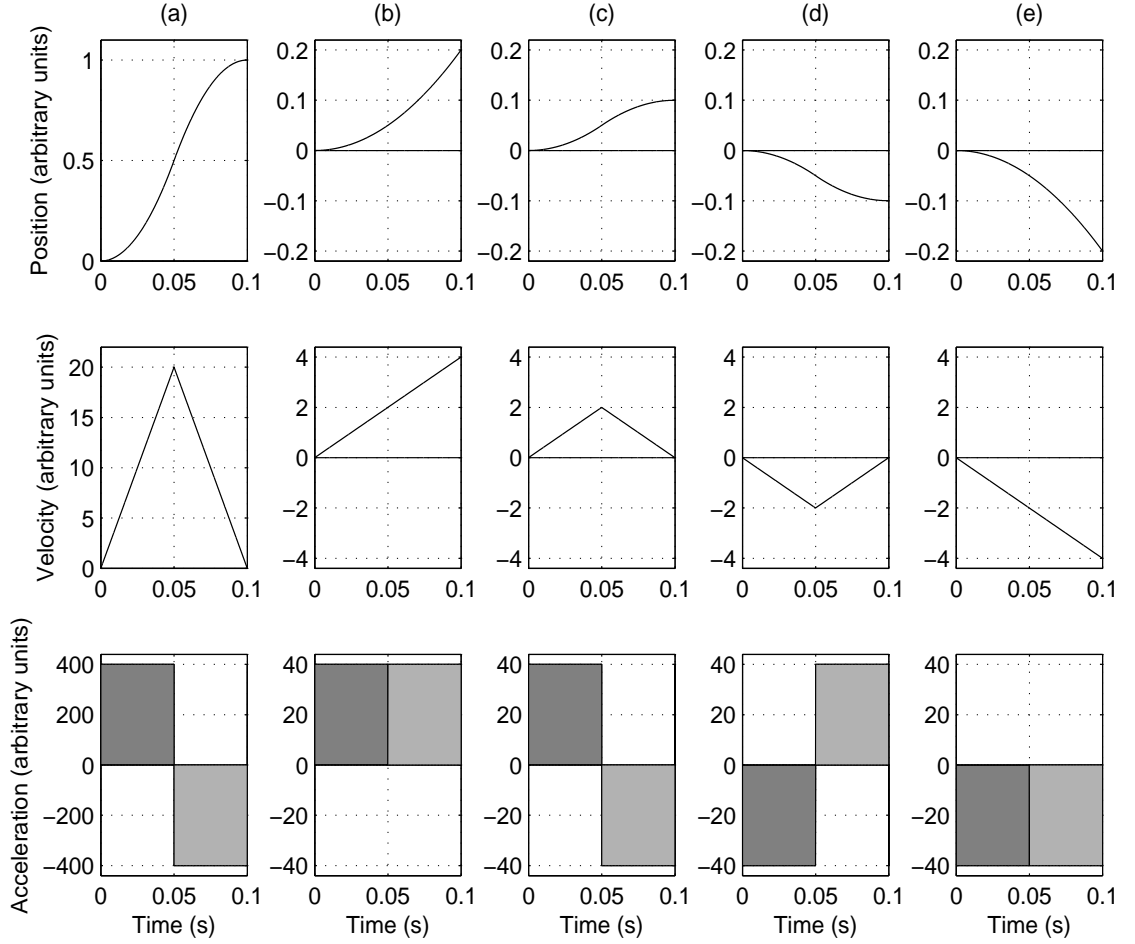


Figure 3.1: Position (top) and velocity (middle) waveforms resulting from two rectangular acceleration pulses (bottom) of fixed duration  $T = 50$  ms and opposite amplitudes (arbitrary units). (a) Ideal acceleration pulses with amplitudes  $\pm a = 400$  for a desired response. (b)–(e) Acceleration pulses due to additive stochastic noise with amplitudes  $\pm \Delta a = 40$ .

Thus, the total displacement  $D$  resulting from two rectangular acceleration pulses, each of duration  $T$  and with amplitudes  $a$  and  $-a$ , is given by

$$D = P(2T) = -\frac{1}{2}aT^2 + aT^2 + \frac{1}{2}aT^2 = aT^2 \quad (3.10)$$

In the example shown in Fig. 3.1(a), the total displacement resulting from the two acceleration pulses is given by  $D = 400 \times 0.05^2 = 1$ . It may be observed from Eq. 3.10 that the displacement  $D$  is proportional to the magnitude  $a$  of the acceleration pulses, or vice versa,  $a \propto D$ . Furthermore, according to AMT, additive stochastic noise in the motor system introduces statistical variation,  $\Delta a$ , into the height of the acceleration pulses. As hypothesised in Chapter 2.6, this noise is signal-dependent and varies with the size of the motor command. Specifically, on average, the amplitude of each acceleration pulse will either increase or decrease by an amount  $\Delta a$  proportional to the magnitude  $a$  of the pulse, or  $\Delta a \propto a$ . However, as  $a$  is proportional to the displacement  $D$ ,  $\Delta a$  is also proportional to  $D$ , or  $\Delta a \propto D$ .

Because this motor noise is hypothesised to be stochastic, the variation  $\Delta a$  occurs independently for each acceleration pulse. Consequently, for the two acceleration pulses depicted in Fig. 3.1(a), there exist four possible combinations of additive stochastic noise: (i) Both acceleration pulses might be increased by  $\Delta a$  as in Fig. 3.1(b); (ii) the first might be increased by  $\Delta a$  and the second decreased by  $\Delta a$  as in Fig. 3.1(c); (iii) the first might be decreased by  $\Delta a$  and the second increased by  $\Delta a$  as in Fig. 3.1(d); or (iv) both might be decreased by  $\Delta a$  as in Fig. 3.1(e). For the example in Fig. 3.1,  $\Delta a$  has been chosen as 10% of  $a$ , or  $\Delta a = 40$ .

The position trajectories in Figs. 3.1(b)–(e) show the displacement error  $E$  for all four combinations of additive noise. It is apparent that the unity endpoint of the unidimensional desired position trajectory  $R^*$  depicted in Fig. 3.1(a) will either be overshoot by an amount of 0.2 (Fig. 3.1(b)) or 0.1 (Fig. 3.1(c)), or undershoot by an amount of 0.1 (Fig. 3.1(d)) or 0.2 (Fig. 3.1(e)) due to motor noise. In other words, the error  $E$  in either the positive (overshoot) or negative (undershoot) direction is proportional in each case to  $D$ , or  $E \propto D$ .

Consider the task of reaching towards a target as illustrated in Fig. 3.2. At the beginning of each RP interval, the SA system has sensory feedback information about the current state of the response based on afferent input acquired during the previous RP interval. In addition, the  $R^*$  trajectory preplanned during the previous RP interval and about to be executed in real-time by the RE system is available from working memory. By combining these two pieces of information passed from the SA

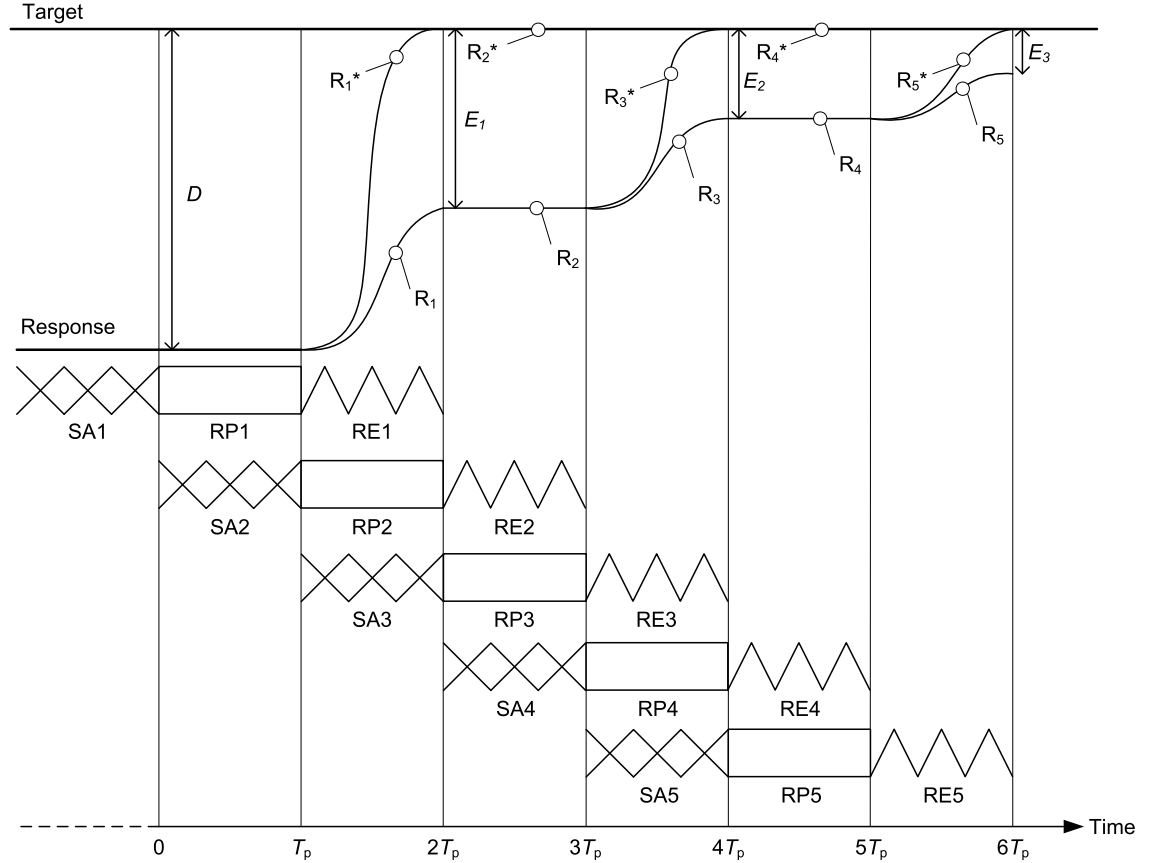


Figure 3.2: Reaching task using receding horizon control. The receding prediction horizon is fixed at  $T_h = T_p = 100$  ms. During RP1, a desired response  $R_1^*$  is generated. However, during the execution interval RE1, the actual response  $R_1$  deviates from the desired response  $R_1^*$  by an error  $E_1$  due to additive noise. During SA2 there is no sensory information available about this future error about to occur and the RP system therefore assumes that the actual response will match that of the desired response at the end of RE1. Thus, during RP2, no correcting trajectory is generated, and during RE2, no correcting trajectory is executed. During RP3, however, an error-correcting submovement  $R_3^*$  is planned based on information about the error  $E_1$  collected during SA3. Again, the actual response  $R_3$  deviates from the desired response  $R_3^*$  by an error  $E_2$ . This process iterates and reduces the error in a logarithmic fashion.

system, and assuming that the actual response  $R$  will match the desired response  $R^*$ , the RP system can generate a prediction of the response position and velocity 100 ms ahead at the end of the current RP interval, that is, the initial state for the trajectory about to be planned. As the target in this case is stationary, it is a simple task for the RP system to project its future position (depicted as the top horizontal line in Fig. 3.2). The RP system then generates an  $R^*$  trajectory connecting the predicted position and velocity of the response at the end of the RP interval (the initial state) with the predicted position and velocity of the target one RP interval,  $T_p = 100$  ms, ahead in time (the final state). However, due to stochastic noise in the motor system, the actual response  $R$  will deviate from the desired response  $R^*$ . As mentioned, the standard deviation of the stochastic noise is assumed to be proportional to the size of the motor command, which in turn, for a pure inertial load, is proportional to acceleration. The time required to correct these execution errors is independent of whether the actual response overshoots or undershoots the desired response. Thus, for the sake of simplicity, only undershooting errors are illustrated in Fig. 3.2. Furthermore, for the purpose of clarity, the execution errors have been vastly exaggerated.

In the example of Fig. 3.2 the target is located a distance  $D$  away from the limb about to be moved. The RP system plans a desired trajectory  $R_1^*$  to align the response with the target within 100 ms, that is, the fastest possible ballistic movement. However, the first submovement  $R_1$  undershoots the desired response  $R_1^*$  by an error  $E_1$  due to stochastic variation  $\Delta a$  added to the desired acceleration waveform of  $R_1^*$ . As noted above, the average error  $E_1$  is proportional to the displacement  $D$ , thus  $E_1 = \alpha D$ . Because no sensory information about  $E_1$  is gathered during SA2, there is no correction for  $E_1$  incorporated in  $R_2^*$ . The desired response  $R_1^*$  is used as a prediction of the actual response  $R_1$ , and consequently,  $R_2^*$  is planned on the assumption that  $R_1$  matches  $R_1^*$ . During RP3, however, sensory information about  $E_1$  has been gathered during SA3 and an error-correcting desired response  $R_3^*$  is planned. Again, due to stochastic noise, the actual response  $R_3$  deviates from



the desired response  $R_3^*$  with an average amount of  $E_2$ . This error is proportional to the remaining distance  $E_1$  to the target, or  $E_2 = \alpha E_1 = \alpha^2 D$ . This process iterates, and in general, the error for the  $k$ -th correction is given by

$$E_k = \alpha^k D \quad , 0 \leq \alpha \leq 1 \quad (3.11)$$

By exactly the same argument used previously to derive the logarithmic speed-accuracy tradeoff for the deterministic iterative-corrections model (Chapter 2.2.1), the total movement time  $T_k$  after  $k$  corrections, each of duration  $2T_p$  (only every second submovement reduces the error in this example), is given by  $T_k = k \times 2T_p$ . Then  $k = \frac{T_k}{2T_p}$  and Eq. 3.11 becomes

$$E_k = \alpha^{\frac{T_k}{2T_p}} D \quad (3.12)$$

Taking logarithms on both sides of Eq. 3.12 and rearranging, the total movement time  $T_k$  after  $k$  corrections ( $2k$  submovements) is given by

$$T_k = 2T_p \log_{\alpha} \left( \frac{E_k}{D} \right) \quad (3.13)$$

For direct correspondence with Fitts' law (Eq. 3.1, p. 62), substitute  $2T_p = b$  and  $\alpha = 0.5$ , and let the error  $E_k$  after  $k$  corrections equal half the target width  $W$  (equivalent to the target being reached), or  $E_k = \frac{W}{2}$ . Eq. 3.13 then becomes

$$T_k = b \log_{0.5} \left( \frac{W/2}{D} \right) = b \log_2 \left( \frac{2D}{W} \right) \quad (3.14)$$

In addition, it is a reasonable assumption that the initial submovement differs from the other corrective submovements by a constant  $a$ , because the planning time for the first submovement is not part of the movement time. Hence, Eq. 3.14 can be

rewritten as

$$T_k = (k - 1)2T_p + (2T_p + a) = k2T_p + a = b \log_2 \left( \frac{2D}{W} \right) + a, \quad (3.15)$$

which is identical to Fitts' law. In other words, receding horizon control with a prediction horizon duration  $T_h$  equal to the duration of one RP interval,  $T_h = T_p = 100$  ms, predicts a logarithmic tradeoff between the speed of a reaching movement and its accuracy, consistent with Fitts' law.

For the general case of receding horizon control, with a prediction horizon kept constant at a duration greater than  $T_p = 100$  ms, the RP system will generate S-shaped minimum acceleration desired trajectories with a duration  $T_h$  greater than that of one RP interval used in the example above. Of course, as outlined previously, only the first 100 ms of an  $R^*$  trajectory will be executed before it is replaced by an updated version during every RP interval. This implies that the first two acceleration pulses of  $R^*$  generally will not have equal but opposite amplitudes such as those in Fig. 3.1(a). Let  $a$  and  $b$  denote the amplitudes of the first and the second rectangular acceleration pulses, respectively. The acceleration, velocity, and position waveforms are then given by

$$A(t) = \begin{cases} a & , 0 < t \leq T \\ b & , T < t \leq 2T \end{cases} \quad (3.16)$$

$$V(t) = \begin{cases} at & , 0 < t \leq T \\ b(t - T) + aT & , T < t \leq 2T \end{cases} \quad (3.17)$$

$$P(t) = \begin{cases} \frac{1}{2}at^2 & , 0 < t \leq T \\ \frac{1}{2}b(t - T)^2 + aT(t - T) + \frac{1}{2}aT^2 & , T < t \leq 2T \end{cases} \quad (3.18)$$

It may be observed that the special case of Eq. 3.7–3.9 is obtained by substituting  $b = -a$  in the general case of Eq. 3.16–3.18. The total displacement due to both pulses is

$$D = P(2T) = \frac{1}{2}bT^2 + aT^2 + \frac{1}{2}aT^2 = \frac{1}{2}(3a + b)T^2 \quad (3.19)$$

Thus, the displacement  $D$  is proportional to a linear combination of  $a$  and  $b$ , namely  $3a + b$ , and by the same argument as above, with the stochastic variations  $\Delta a$  proportional to  $a$  and  $\Delta b$  proportional to  $b$ , the stochastic variation  $3\Delta a + \Delta b$  will be proportional to  $3a + b$ , and therefore also to  $D$ . Hence, as before, the displacement error  $E$  is proportional to the displacement  $D$  resulting from two rectangular acceleration pulses of amplitudes  $a$  and  $b$ .

For prediction horizons greater than  $T_p$ , only the first 100 ms of  $R^*$  is executed before  $R^*$  is being updated, that is, for the  $k$ -th submovement, the response moves only a distance  $d_k$  towards the target, where  $d_k$  is smaller than the remaining distance to the target. As before, the error  $E_k$  is certainly proportional to the distance  $d_k$  moved during the  $k$ -th submovement, however, contrary to the example of fast ballistic movements above, where the prediction horizon was 100 ms,  $d_k$  is no longer equal to the remaining distance to the target before the  $k$ -th submovement. Let  $E_0 = D$ , then

$$\begin{aligned}
d_1 &= \beta_1 D \Rightarrow \\
E_1 &= \alpha d_1 = \alpha \beta_1 D, \\
d_2 &= \beta_2 E_1 = \alpha \beta_2 \beta_1 D \Rightarrow \\
E_2 &= \alpha d_2 = \alpha^2 \beta_2 \beta_1 D, \\
&\vdots \\
E_k &= \alpha^k \beta_k \dots \beta_1 D
\end{aligned} \tag{3.20}$$

where  $\beta_i$  for  $i = 1, \dots, k$  is some fraction of the remaining distance. Thus, unless the movement is ballistic, and  $\beta_i = 1$  for all  $i$ ,  $\beta_i$  will vary. Therefore, although  $E_k = \alpha d_k$ , there is no such simple relationship as  $E_k = \alpha E_{k-1} = \alpha^k D$  as before, because  $d_k \neq E_{k-1}$ . Instead,  $d_k$  will be equal to some fraction  $\beta_k$  of the remaining distance. This fraction will be dependent on the initial and final state used during the  $k$ -th RP interval.

Consider for example a unit step movement with receding horizon control and  $T_h = 200$  ms. The optimal trajectory planned during RP1 will move the response from zero to unity in two submovements that minimise acceleration. This implies a first submovement from zero to 0.5 and a second submovement from 0.5 to unity, hence  $\beta_1 = 0.5$ . However, only the first portion is executed. During RP2, another optimal trajectory is planned to bring the response from 0.5 to unity but because of the velocity at the initial state (at position 0.5), the response trajectory will be planned to overshoot the target before returning in order to minimise acceleration. Moreover, the trajectory will have to move some fraction  $\beta_2$  of the remaining distance that is smaller than  $\beta_1$ . An analytic expression for  $\prod_{i=1}^k (\beta_i)$  is difficult to obtain. Decomposing  $\beta_i$  into a constant term  $\gamma$  and some residual function  $\phi(i)$  results in

$$\beta_i = \gamma + \phi(i), \quad 0 < \gamma < 1 \quad (3.21)$$

Thus, if  $\phi(i)$  is sufficiently negligible for all  $i$ , the endpoint error for the  $k$ -th submovement can be approximated by

$$E_k = \alpha^k \gamma^k D \quad (3.22)$$

and a logarithmic speed-accuracy relationship can be derived. The simulation study presented in this chapter shows that the logarithmic relationship gradually shifts towards a linear one when increasing the prediction horizon  $T_h$  for receding horizon control simulations. This indicates that as  $T_h$  increases,  $\prod_{i=1}^k (\beta_i)$  gradually takes the form

$$\prod_{i=1}^k (\beta_i) = \alpha^{-k} (1 - kc) \quad (3.23)$$

where  $c$  is some constant. Substituting Eq. 3.23 into Eq. 3.20 shows that the endpoint error will then be reduced linearly as movement speed is slowed (and the number of submovements  $k$  is increased):

$$E_k = (1 - kc)D \quad (3.24)$$

### 3.2.2 *Asymmetrical velocity profiles*

The BUMP model hypothesises that receding horizon control predicts asymmetrical velocity profiles, where the level of asymmetry increases as movement is slowed, or conversely, the velocity profile becomes increasingly symmetrical for faster movements, with the fastest possible ballistic movement of 100 ms duration yielding a symmetrical velocity profile. The asymmetry occurs as a consequence of the slowed responses being comprised of a sequence of overlapping submovements, with each submovement preplanned to a receding prediction horizon a fixed interval of time ahead. This gives rise to a movement strategy of moving quickly to get within the ballpark of the target before finetuning the movement endpoint with slower submovements. As a result, the acceleration phase of the movement becomes shorter relative to the deceleration phase as the number of submovements, or movement duration, increases. Consequently, the velocity profile becomes asymmetrical, or left-skewed, and the level of asymmetry increases with movement duration. The velocity profile resulting from the superposition of submovements can be approximated by a log-normal function similar to that described by Plamondon & Alimi (1997), who showed that the log-normal function accounts for the invariance and rescalability of velocity profiles as well as for observations concerning the change in maximum and mean velocities and time to maximum velocity under different experimental conditions.

### 3.2.3 *Linear speed-accuracy tradeoff*

The BUMP model predicts a linear speed-accuracy tradeoff when movements are made with a fixed horizon control strategy. Consider the unidimensional task of reaching to a stationary target as illustrated in Fig. 3.3. Initially, the limb about to be moved is at a distance  $D$  away from the target. Employing fixed horizon control, every desired response trajectory  $R^*$  is planned to a fixed point ahead in time and space. In this example, the prediction horizon is set to  $T_h = 5T_p = 500$  ms initially and is then reduced by  $T_p = 100$  ms at every RP interval. During RP1, a desired response  $R_1^*$  of duration  $T_h = 5T_p = 500$  ms is generated, of which only the first

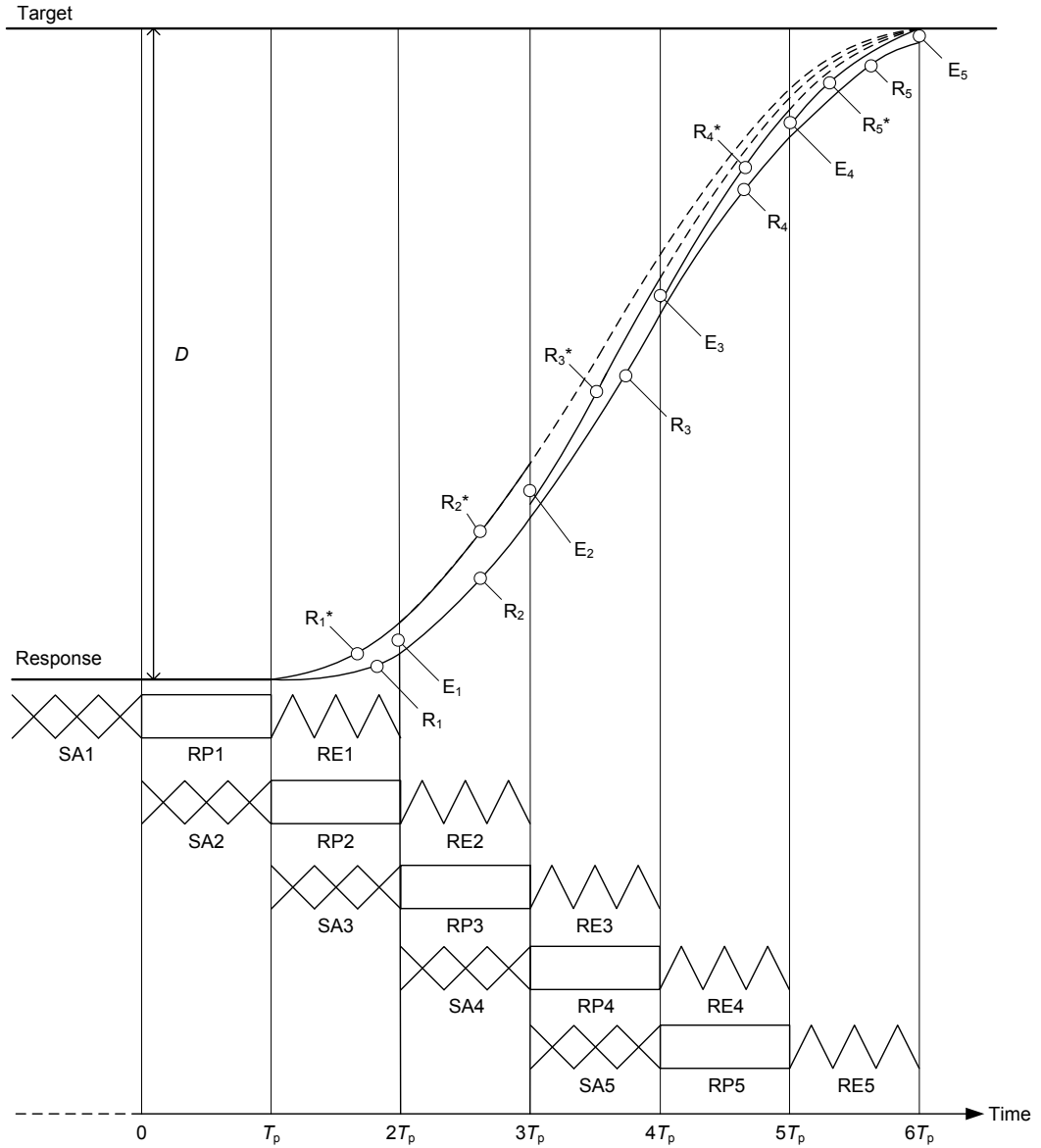


Figure 3.3: Reaching task using fixed horizon control. Each desired response  $R_i^*$  is being planned to a fixed point ahead in time and space, in this case,  $T_h = 500$  ms ahead in time. However, only the first 100 ms of each desired response, corresponding to the duration  $T_p$  of an RP interval, is being executed. The remaining part of each desired response  $R_i^*$  is therefore shown with a stapled line to emphasise that it is not being executed. As the target is approached, the duration of the desired response decreases by  $T_p = 100$  ms at every RP interval. For clarity, all errors  $E_i$  between desired responses  $R_i^*$  and actual responses  $R_i$  are shown as undershoot errors. The only errors not incorporated in the desired response  $R_i^*$  are the errors that occur during execution of  $R_i^*$  and  $R_{i-1}^*$ . Thus, the error at the end of any submovement is always determined solely by the execution errors occurring during the previous 200 ms during which the submovement is being planned and executed open-loop and the RP system is refractory to sensory feedback. The predicted endpoint error of the movement is proportional to the average speed of the movement.

100 ms will be executed. During the execution interval RE1, the actual response  $R_1$  deviates from the desired response  $R_1^*$  by an error  $E_1$  due to stochastic noise. During SA2 there is no sensory information available about this future error about to occur, therefore, the RP system assumes that the actual response matches that of the desired response. Hence, the desired trajectory  $R_2^*$  of duration  $T_h = 4T_p = 400$  ms is generated without taking  $E_1$  into account. As always, only the first 100 ms of the desired trajectory  $R_2^*$  is executed during RE2, and again, an execution error occurs. Therefore, the error  $E_2$  is a result of the execution errors that occurred during RE1 and RE2 combined. During RP3, an error-correcting submovement  $R_3^*$  of duration  $T_h = 3T_p = 300$  ms is planned based on information about the error  $E_1$  collected during SA3. The execution error that happens simultaneously during RE2 is not taken into account until RP4, during which the only errors not taken into account are those that occur during RE3 and RE4. The process iterates. Despite intermittent error correction at planning time rates, at the end of any submovement, the only errors not taken into account are those that occurred during that particular submovement and the submovement immediately preceding it, that is, during the previous 200 ms.

A movement trajectory generated using fixed horizon control has a symmetrical velocity profile (see Chapter 3.2.4 below) and a position trajectory that is antisymmetrical about its midpoint. This implies that the trajectory can be scaled in time and space. For example, if the endpoint error  $E$  of a movement is equal to some fraction of the movement distance  $D$  for a movement time  $T$ , scaling  $D$  by some factor while keeping  $T$  constant will scale  $E$  by the same factor. Likewise, scaling  $T$  by some factor while keeping  $D$  constant will scale  $E$  by the inverse of the scaling factor. As a result, a fixed horizon control strategy causes a linear speed-accuracy tradeoff since the error at the end of the overall movement is proportional to the average speed of the movement  $\frac{D}{T}$ . In statistical terms, the mean trajectory is the ideal trajectory that has zero endpoint error and consequently,  $E$  corresponds to the standard deviation of the linear law (Eq. 3.5, p. 64) of Schmidt et al. (1979).

### 3.2.4 Symmetrical velocity profiles

Contrary to receding horizon control, fixed horizon control predicts symmetrical velocity profiles not just for the fastest possible movements, but for movements of any duration. The reason for this is the strategy of planning every submovement to the same point ahead fixed in time and space. Consider the optimal  $N$ -step desired response  $R^*$  in Fig. 2.12 discussed previously (Chapter 2.4, p. 51). The position trajectory minimises acceleration and is perfectly antisymmetrical about its midpoint. The underlying velocity profile is also symmetrical, with the peak velocity occurring midway through the movement. At every RP interval, the RP system generates an updated  $R^*$  that smoothly connects the current state and the final state with minimum demand on acceleration. Assuming zero noise, which is equivalent to the average case because the additive noise is stochastic with zero mean, the updated  $R^*$  will trace the initial S-shaped trajectory generated at the very first RP interval at every consecutive RP interval until the target is reached. Consequently, when subjects adopt a fixed horizon strategy, the velocity profile is symmetrical and independent of the movement speed.

## 3.3 Method

The theoretical mathematics used previously to describe the BUMP model can appear overwhelming, even to those with a high level of mathematical expertise. Moreover, testing the theory numerically quickly becomes a tedious task due to the number of factors to consider, such as choice of variable horizon control strategy, duration of the prediction horizon, and noise level. Finally, results obtained from a theoretical model should be compared with human experimental data in order to examine the validity of the model. For these reasons a computer-simulated environment of the theory is required. MATLAB and Simulink are software packages developed by The MathWorks (see [www.mathworks.com](http://www.mathworks.com)) and have become the *de facto* standard for modelling and simulation. MATLAB is a programming language for technical computing. It offers an array of tools for simulation and modelling



through its capabilities of mathematical computation and data analysis. Simulink is built on MATLAB and is capable of representing dynamical, possibly time-varying, systems graphically as engineering block diagrams that implement mathematical rules and equations. It provides an interactive graphical environment in which a large collection of library building blocks can be connected to form a desired system, or model. For particular needs, custom blocks can be developed with the aid of MATLAB code. Through batch processing scripts, the overall system can be simulated with a number of combinations of settings and parameter values to produce a large set of real-time response waveforms for comparison with data from human experiments.

This thesis hypothesises that the BUMP model of response planning accounts for both the logarithmic and the linear speed-accuracy tradeoffs in aimed movement as well as for the accompanying asymmetrical and symmetrical velocity profiles and the way these change with movement speed. This hypothesis is tested by means of a computational simulation of the intermittently operating optimal trajectory generator described in the model. Trajectories for aimed step movements are implemented with variable horizon predictive control along with signal-dependent noise. As outlined in Chapter 3.2, the BUMP model predicts that receding horizon control corresponds to spatially constrained movements with logarithmic speed-accuracy tradeoffs and asymmetrical velocity profiles, whereas fixed horizon control corresponds to time-matched movements with linear speed-accuracy tradeoffs and asymmetrical velocity profiles.

### *3.3.1 Description of simulator*

A comprehensive simulator of human movement planning and control has been developed within the AMT framework utilising MATLAB and Simulink software (see Appendix B.1 for a Simulink block diagram and explanation). The simulator implements the SA, RP, and RE systems and the detailed model description presented in Chapter 2 and elsewhere (Neilson & Neilson, 2005b). Extending the work of Olsen (2001), particular attention has been given to the development of the RP system

and the OTG described in Chapter 2.4. Provided with position and velocity feedback of the actual response as well as the predicted future state of the target from the SA system, the RP system calculates an optimal trajectory  $R^*$  to reach the predicted future state of the target and to compensate for executional error. Operating intermittently, the RP system passes  $R^*$  to the RE system at 100 ms intervals. Because the present study was focussed on response planning, the RE system was simplified by pre-tuning the inverse model to exactly compensate for the dynamics of the plant (i.e., wired-in synergy generator, the musculoskeletal system, and the external world). Thus, the response at the output of the plant matches the required response trajectory  $R^*$  generated by the RP system regardless of plant dynamics. Consequently, error in response execution is only related to stochastic noise, which is added to the motor commands and whose standard deviation is proportional to their magnitude.

### 3.3.2 *Simulator settings*

The simulator was programmed to implement a fixed horizon strategy and a receding horizon strategy for simulated aimed movement in order to investigate the corresponding speed-accuracy tradeoffs and velocity profiles. Aimed movement was simulated by specifying planned step movements, that is, to move from one fixed spatial position to another fixed position some distance away. For receding horizon control, 10 cm step movements with 10 different prediction horizons  $T_h$  were simulated. The test cases consisted of trials with  $T_h = 100, 200, \dots, 1000$  ms. The prediction horizon remained constant during each movement. For fixed horizon control, step movements of amplitudes 10, 20, and 30 cm with 20 different initial prediction horizons  $T_h = 100, 150, \dots, 1000$  ms were simulated. At every planning time interval  $T_p = 100$  ms, the prediction horizon was reduced by 100 ms until a minimum of  $T_h = 100$  ms was reached, after which  $T_h$  remained constant at a value of 100 ms. The only exception to the rule of subtracting 100 ms from the prediction horizon occurred if the prediction horizon was  $T_h = 150$  ms during an

Setting	Receding strategy	Fixed strategy
$T_p$ (ms)	100	100
$T_h$ (ms)	$\{100, 200, \dots, 1000\}$	$\{100, 150, \dots, 1000\}$
$D$ (cm)	10	$\{10, 20, 30\}$
$T_s$ (s)	5	5
$n_c$	$\{0.5\}$	$\{0.5\}$
$S$	$\{5, 10, \dots, 5000\}$	$\{5, 10, \dots, 5000\}$
$N_s$	1000	1000
$N_{total}$	10,000	60,000

Table 3.1: Settings for simulations of speed-accuracy tradeoffs in human aimed movements.  $T_p$  is the RP interval;  $T_h$  is the constant or initial prediction horizon for receding or fixed horizon control, respectively;  $D$  is step movement amplitude;  $T_s$  is simulation duration;  $n_c$  is the noise constant;  $S$  are the seeds used in MATLAB to generate sequences of zero mean Gaussian numbers;  $N_s$  is the number of simulations for each test case, which is equal to the number of different seeds; and  $N_{total}$  is the total number of simulations for each control strategy.

RP interval, which resulted in the next prediction horizon being  $T_h = 100$  ms, that is, a reduction of only 50 ms occurred in this particular case.

To investigate speed-accuracy tradeoffs, stochastic noise was added to the motor commands and was proportional to them by a factor, or noise constant,  $n_c = 0.5$ . Each test case was simulated  $N_s = 1000$  times with 1000 different “seeds”  $S = \{5, 10, \dots, 5000\}$ , or sequences of random numbers, generated by the noise module to signify stochastic noise. The same seeds were used for each test case. The first  $T_s = 5$  s of each simulated movement were recorded for subsequent analysis. Table 3.1 summarises the experimental setup for the speed-accuracy tradeoff simulations.

To investigate velocity profiles, stochastic noise was set to zero for ten test cases with  $T_h = 100, 200, \dots, 1000$  ms for both receding or fixed horizon control. In addition, to simulate two typical velocity profiles observed in handwritten strokes,  $T_h$  was set to 150 and 200 ms, also with noise turned off.

## 3.4 Results and conclusions

### 3.4.1 Logarithmic speed-accuracy tradeoff

Fig. 3.4(a) and (b) show the endpoint mean absolute error  $W$  versus time (top) and the movement time  $T$  versus the index of difficulty  $I_d = \log_2 \frac{2D}{W}$  (bottom) for simulations of 10 cm step movements using receding horizon control. Throughout each movement the prediction horizon is kept constant at either  $T_h = 100$  ms (Fig. 3.4(a)) or  $T_h = 500$  ms (Fig. 3.4(b)). In both figures, the error appears to be reduced exponentially with time. Employing unconstrained nonlinear minimisation through the Nelder-Mead direct search method, the best fit exponential function  $W = D \times 2^{-\lambda t}$  is found and superimposed as a solid line for the top plots. For the bottom plots, a linear function  $T = aI_d + b$  that is the best fit in the least-squares sense is superimposed as a solid line. Both the movement time and the index of difficulty are in correspondence with those reported in the literature (e.g., Fitts, 1954; Fitts & Peterson, 1964). Movement time ranges from 100 to 700 ms ( $T_h = 100$  ms) and from 500 to 1100 ms ( $T_h = 500$  ms), while the index of difficulty ranges from 1.5 to 4.1 ( $T_h = 100$  ms) and from 2.2 to 3.8 ( $T_h = 500$  ms).

For each test case (only  $T_h = 100$  ms and  $T_h = 500$  ms presented graphically here), Table 3.2 shows the goodness of fit given by the coefficient of determination  $R^2$ , which is the proportion of variability in a data set that is accounted for by a statistical model and is equal to the square of Pearson's product-moment correlation coefficient. As is evident from Table 3.2, an exponential function is able to explain 99.39% or more of the variability of the endpoint mean absolute error, except for the cases of  $T_h = 100$  ms and  $T_h = 200$  ms, where it explains 97.21% and 95.56%, respectively. Table 3.2 also shows that a linear function is able to explain 98.04% or more of the variability of the index of difficulty. Consequently, it may be concluded that the error decreases exponentially with movement time, or equivalently, as the movement amplitude is constant (10 cm), the error increases exponentially with movement speed. Furthermore, it may be concluded that movement time increases linearly as a function of the index of difficulty, a finding equivalent to Fitts' law.

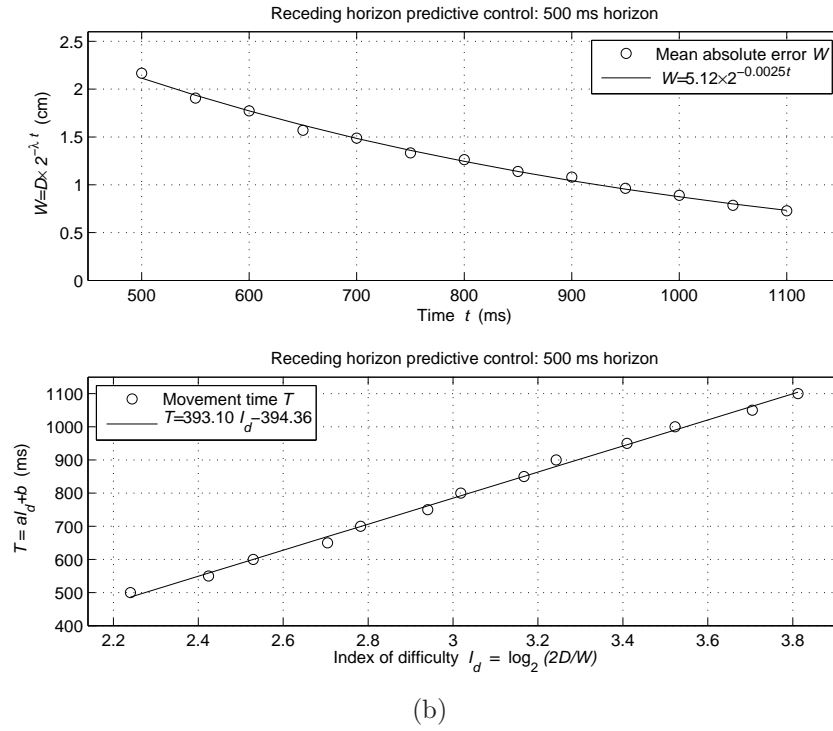
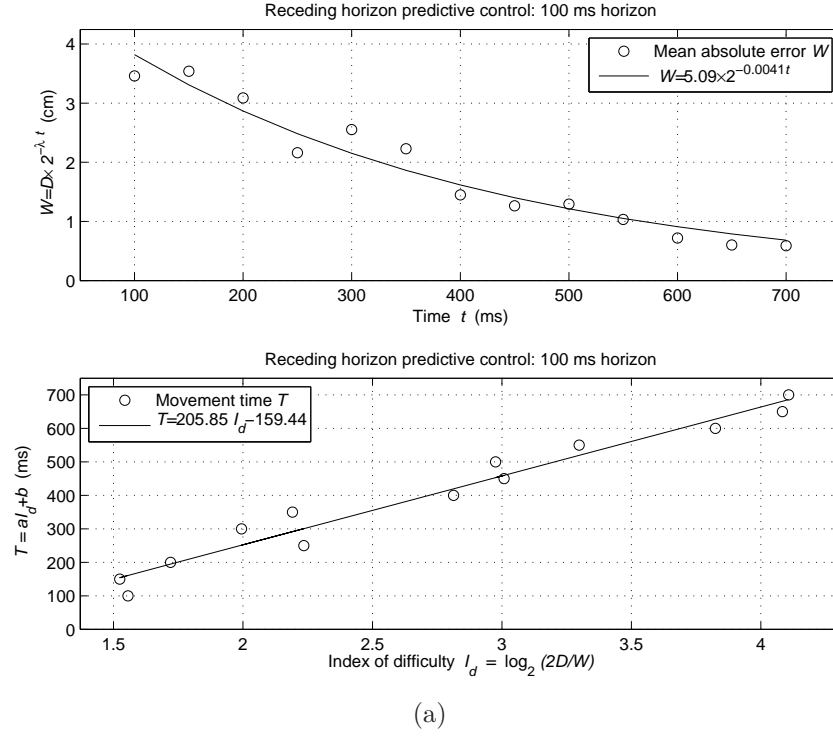


Figure 3.4: Endpoint mean absolute error for simulations of a 10 cm step movement using receding horizon control. A best fit exponential function of the form  $W = D \times 2^{-\lambda t}$  (top) as well as a best fit linear function  $T = aI_d + b$  (bottom) is superimposed as a solid line for (a)  $T_h = 100$  ms and (b)  $T_h = 500$  ms.

Prediction horizon $T_h$ (ms)	Exponential fit $R^2$	Linear fit $R^2$
100	0.9721	0.9804
200	0.9556	0.9805
300	0.9985	0.9982
400	0.9982	0.9985
500	0.9981	0.9984
600	0.9968	0.9978
700	0.9972	0.9982
800	0.9970	0.9970
900	0.9945	0.9946
1000	0.9939	0.9947

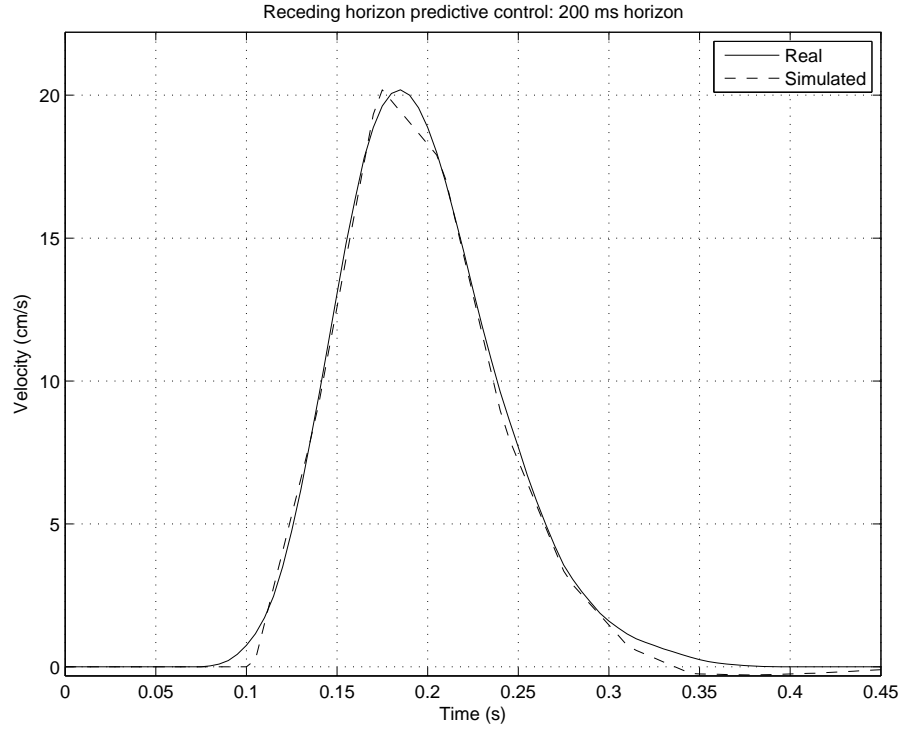
Table 3.2: Coefficient of determination  $R^2$  as a measure of goodness of fit for the best fit exponential and linear functions  $W = D \times 2^{-\lambda t}$  and  $T = aI_d + b$ , respectively, for 10 cm step movements employing receding horizon control and prediction horizons  $T_h = \{100, 200, \dots, 1000\}$  ms.

#### 3.4.2 Asymmetrical velocity profiles

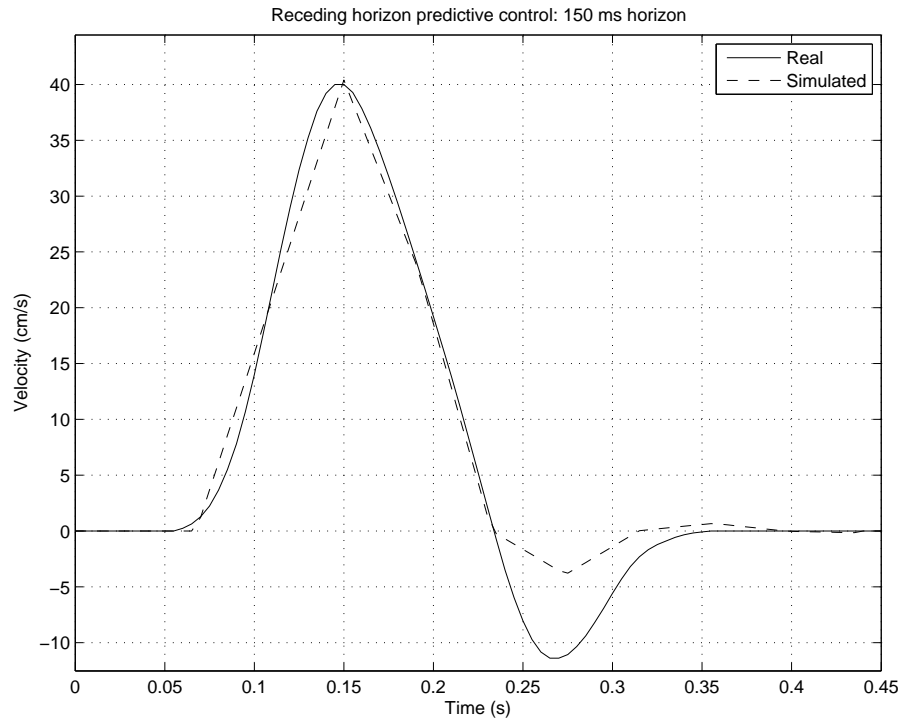
Fig. 3.5(a) shows the velocity profile of a real 2-cm rapid handwritten stroke (adapted from Fig. 4b, Plamondon, 1998) and its reproduced counterpart, simulated using a receding horizon strategy with  $T_p$  and  $T_h$  time-scaled to 70 ms and 140 ms, respectively. The corresponding position trajectory (Fig. 4a, Plamondon, 1998, not shown) is S-shaped with no overshoot. The goodness of fit is given by a coefficient of determination  $R^2 = 0.9990$ .

Fig. 3.5(b) shows the velocity profile of a real 3-cm rapid handwritten stroke (adapted from Fig. 4e, Plamondon, 1998). Its reproduced counterpart was simulated using a receding horizon strategy with  $T_p$  and  $T_h$  time-scaled to 83 ms and 124 ms, respectively. The goodness of fit is given by a coefficient of determination  $R^2 = 0.9879$ . The corresponding position trajectory (Fig. 4d, Plamondon, 1998, not shown) is S-shaped with more than 20% overshoot, which causes the second negative peak in the velocity profile.

The correspondence between real and simulated data in Fig. 3.5 is remarkable given that the simulated profile has straight-line segments (due to the approximation of EMG bursts as rectangular pulses).



(a)



(b)

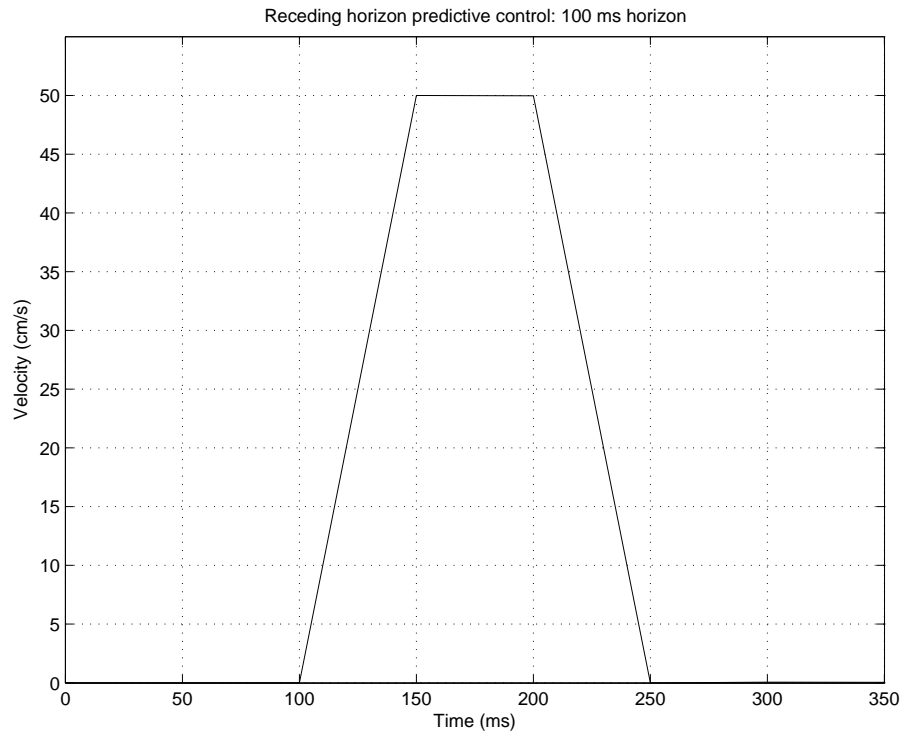
Figure 3.5: Comparison between typical velocity profiles (solid lines) observed in handwritten strokes (adapted from Plamondon, 1998) and simulated velocity profiles (stapled lines) obtained using receding horizon control with (a)  $T_h = 200$  ms and (b)  $T_h = 150$  ms.

Prediction horizon $T_h$ (ms)	Acceleration time $T_a$ (ms)	Deceleration time $T_d$ (ms)	Asymmetry ratio $\frac{T_a}{T_d}$
100	75	75	1.0000
200	100	250	0.4000
300	150	400	0.3750
400	200	550	0.3636
500	250	700	0.3571
600	250	900	0.2778
700	300	1150	0.2609
800	350	1350	0.2593
900	400	1550	0.2581
1000	450	1750	0.2571

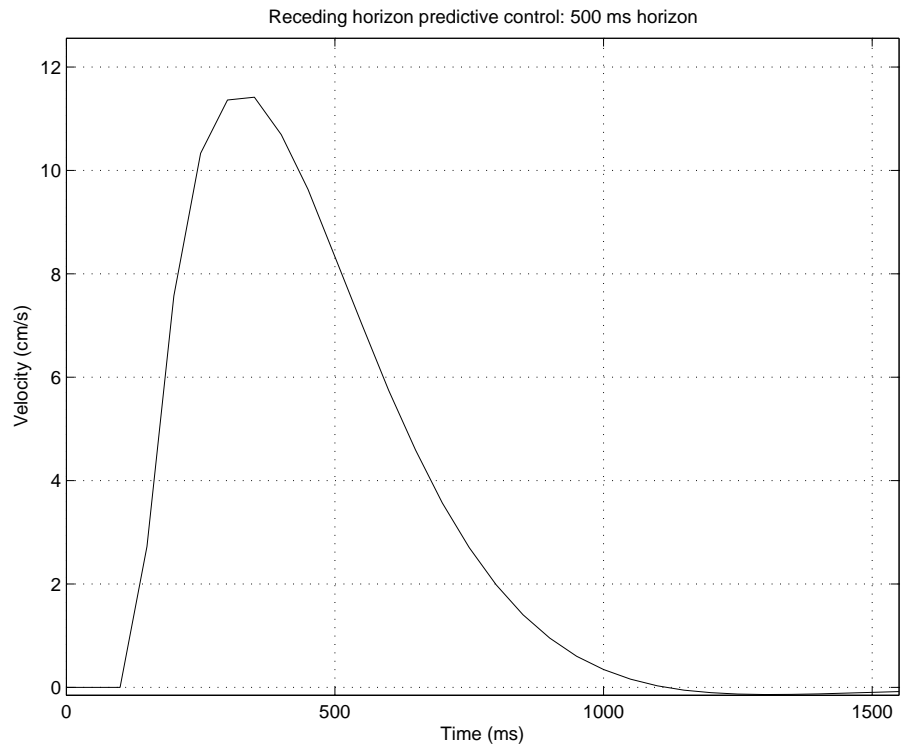
Table 3.3: Level of asymmetry in velocity profiles for 10 cm step movements using receding horizon control given by the ratio of duration of positive and negative acceleration.

Fig. 3.6(a) and (b) shows the velocity profiles for simulations of 10 cm step movements using receding horizon control where the prediction horizon is kept constant at either (a)  $T_h = 100$  ms, or (b)  $T_h = 500$  ms. The sharp corners of the profiles are due to the approximation of EMG bursts as rectangular pulses. In the case of Fig. 3.6(a), the maximum velocity occurs midway through the movement and thus, the velocity profile is symmetrical. However, in the case of Fig. 3.6(b), the maximum velocity occurs early in the movement and thus, the velocity profile is left-skewed, or asymmetrical. Both velocity profiles are comparable to ones observed experimentally (e.g., Berardelli et al., 1996; Plamondon & Alimi, 1997). Examination of the velocity profiles of all 10 test cases ranging from  $T_h = 100$  ms to  $T_h = 1000$  ms (only  $T_h = 100$  ms and  $T_h = 500$  ms presented graphically here) shows that the velocity profile becomes increasingly asymmetrical, that is, left-skewed, as the prediction horizon  $T_h$  is increased, just as observed experimentally by Beggs & Howarth (1972). Numerically, Table 3.3 shows the level of asymmetry given by the ratio between the duration of positive and negative acceleration for each test case.





(a)



(b)

Figure 3.6: Velocity profiles for simulations of a 10 cm step movement using receding horizon control. (a) Movement with prediction horizon  $T_h = 100$  ms. The profile is perfectly symmetrical. (b) Movement with prediction horizon  $T_h = 500$  ms. The profile is left-skewed, or asymmetrical.

These findings are consistent with the proposal that when performing spatially constrained aimed movements without timing constraints, the CNS selects a receding horizon control strategy, and as a direct consequence, the resulting movements obey Fitts' law and display asymmetrical velocity profiles, as observed experimentally.

### 3.4.3 *Linear speed-accuracy tradeoff*

To obtain comparisons of speed versus accuracy for movements employing fixed horizon control, movements with different speeds, where the speed depends on the initial prediction horizon (desired movement duration) and the movement distance, are grouped together. In all, there are 60 test cases where the initial prediction horizon varies from  $T_h = 100$  ms to  $T_h = 1000$  ms in 50 ms intervals and the movement distance is either 10, 20, or 30 cm. Fig. 3.7 shows the endpoint standard deviation  $W_e$  versus average velocity  $v_{av}$  for one such group of movements with durations of 100, 150, and 200 ms made to a target 10, 20, or 30 cm away.

The standard deviation appears to increase linearly as the movement speed increases. The linear function  $W_e = av_{av} + b = a\frac{D}{T} + b$  that fits the data best in the least-squares sense is superimposed as a solid line. Both the standard deviation and the average velocity are directly comparable to those reported by Schmidt et al. (1979). The standard deviation ranges from 2 to 9 mm while the average velocity ranges from 70 to 300 cm/s.

Table 3.4 summarises the correlation coefficients between the best fit linear function and the data for movement groups A–F. It shows that a linear function is able to explain 99.16% or more of the variability of the endpoint standard deviation, except for the case of group B, where it explains 98.57% of the data. This implies that the standard deviation increases linearly with the average velocity of the movement.

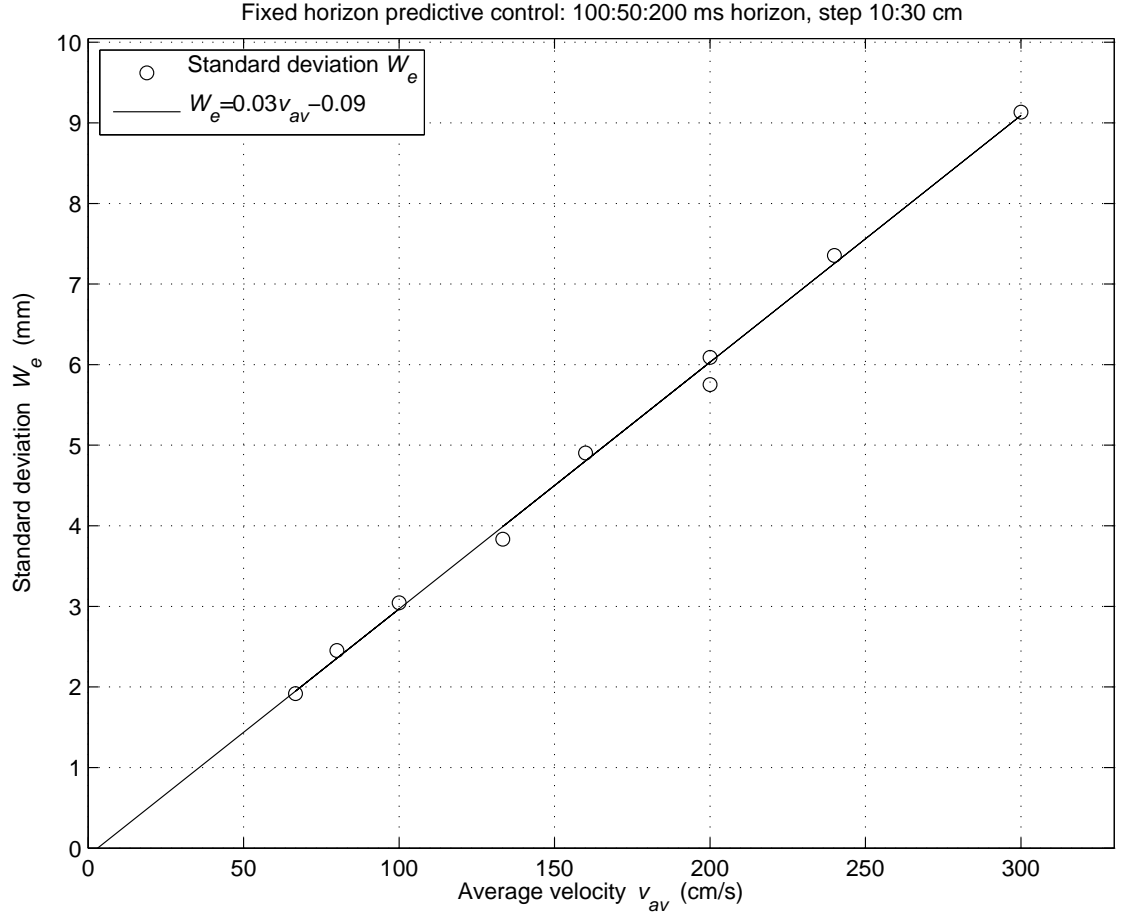


Figure 3.7: Endpoint standard deviation  $W_e$  versus average velocity  $v_{av}$  using fixed horizon control for step movements with 10, 20, and 30 cm amplitudes and initial prediction horizons  $T_h$  of 100, 150, and 200 ms. A best fit linear function of the form  $W_e = av_{av} + b = a\frac{D}{T} + b$  is superimposed as a solid line.

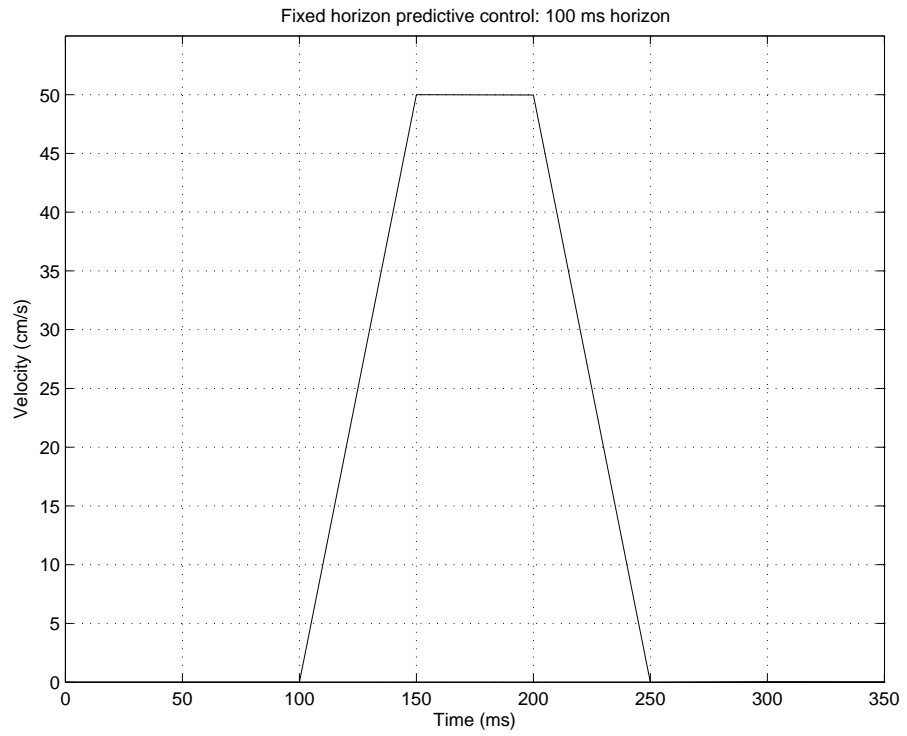
Group	Initial prediction horizons $T_h$ (ms)	Movement distance $D$ (cm)	Linear fit $R^2$
A	{100, 150, 200}	{10, 20, 30}	0.9968
B	{150, 200, 250}	{10, 20, 30}	0.9940
C	{100, 150, ..., 500}	{10, 20, 30}	0.9920
D	{200, 400, ..., 1000}	{10, 20, 30}	0.9916
E	{100, 150, ..., 500}	10	0.9857
F	{100, 200, ..., 1000}	10	0.9942

Table 3.4: Groups of fixed horizon control step movements of varying initial prediction horizons and movement distances and their corresponding correlation coefficient  $R^2$  as a measure of goodness of fit for the best linear function  $W_e = av_{av} + b = a\frac{D}{T} + b$ .  $T_h$  is the initial prediction horizon;  $D$  is the movement distance; and  $R^2$  is the correlation coefficient.

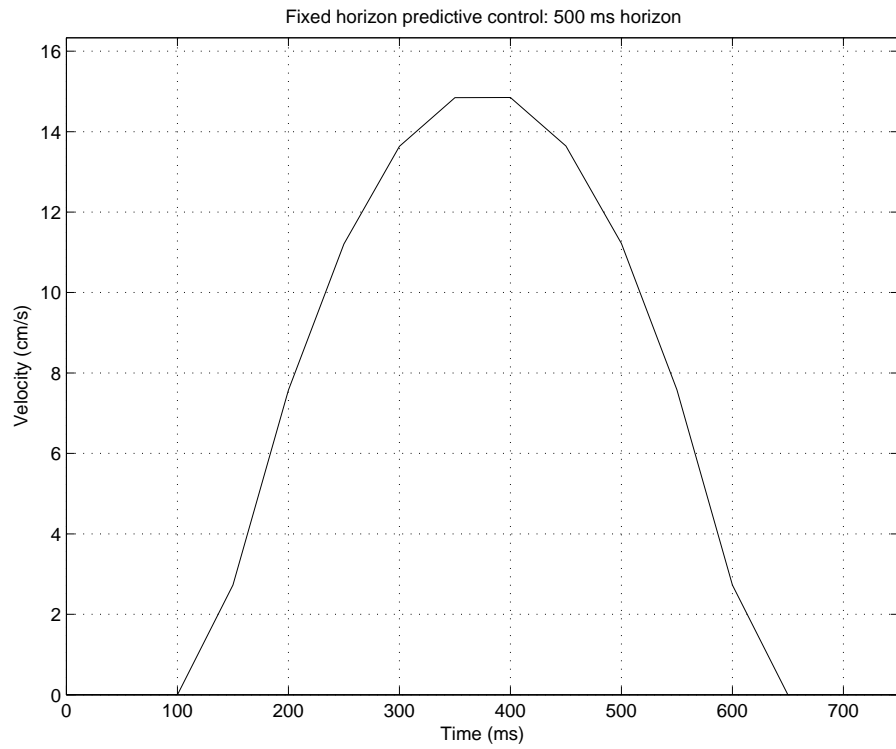
#### 3.4.4 Symmetrical velocity profiles

Fig. 3.8(a) and (b) show the velocity profiles for simulations of 10 cm step movements using fixed horizon control where the initial prediction horizon is either (a)  $T_h = 100$  ms, or (b)  $T_h = 500$  ms. Both velocity profiles have their maximum velocity halfway through the movement, that is, the profiles are perfectly symmetrical. Indeed, examination of the velocity profiles of all 10 test cases ranging from  $T_h = 100$  ms to  $T_h = 1000$  ms (only  $T_h = 100$  ms and  $T_h = 500$  ms presented graphically here) shows that the velocity profile is perfectly symmetrical in all cases, or equivalently, the ratio of asymmetry is equal to one. These velocity profiles match those reported experimentally (e.g., Novak, Miller, & Houk, 2000; Atkeson & Hollerbach, 1985).

The findings are consistent with the proposal that when performing movements that minimise endpoint error with a prespecified duration, the CNS selects a fixed horizon control strategy, resulting in a linear speed-accuracy tradeoff and with symmetrical velocity profiles, as observed experimentally.



(a)



(b)

Figure 3.8: Velocity profiles for a 10 cm step movement using fixed horizon control. Movements with prediction horizons (a)  $T_h = 100$  ms; and (b)  $T_h = 500$  ms. The velocity profile is perfectly symmetrical in both cases.

## 3.5 Discussion

### 3.5.1 *Logarithmic speed-accuracy tradeoff*

The simulation results exemplified by Fig. 3.4(a) and (b) and summarised in Table 3.2 show how the endpoint mean absolute error is reduced logarithmically with time for 10 cm step movements employing a receding horizon control strategy. The top graph in each figure shows a best fit exponential function of the same form as Eq. 3.1 (Fitts' law, p. 62) whereas the bottom graph shows a best fit linear function of the same form as Eq. 3.3 (Fitts' law as a function of the index of difficulty, p. 62). Using a receding horizon control strategy, the duration of the preplanned optimal trajectory  $R^*$  generated at every RP interval is held constant. This duration is referred to as the prediction horizon  $T_h$ . As the prediction horizon is increased for each test case, the exponential fit becomes gradually more linear as the decay rate decreases. The simulations suggest that when subjects are told to make a point-to-point movement with emphasis on spatial accuracy but in their own time of choice, they adopt a receding horizon control strategy. By making slower than ballistic movements they can reduce energy demands on muscles. It would also appear that this is the strategy adopted when subjects are instructed explicitly to make slow movements, or movements with durations within a broad time range. In such movements where there is no or very little temporal accuracy involved, the simulations show a fast initial movement followed by one or more correcting movements, just as observed experimentally. Such movements have consistently been reported to abide by Fitts' law. However, it should be emphasised that experimental paradigms that confirm Fitts' law usually involve time-minimisation tasks where the subjects are instructed to move as fast as possible while keeping within the maximally allowed error range. This is equivalent to keeping the prediction horizon as small as possible, that is, the prediction horizon is  $T_h = 100$  ms, resulting in the logarithmic tradeoff in Fig. 3.4(a). When Fitts (1954) proposed his logarithmic law, he did not do any line fitting of his findings, however, in their discrete movement experiments equivalent to the step movements examined here, Fitts & Peterson (1964) report

strong correlation coefficients of 0.994 and 0.995 between the index of difficulty and the movement time. Corresponding to the simulation test case of  $T_h = 100$  ms, the comparable correlation coefficient  $R^2$  is slightly lower at 0.9804 for the best fit linear function. In addition, Fitts' law does hold for slower movements too, and in the case of the simulations presented here, all the other test cases ( $T_h > 100$  ms) also have strong correlation coefficients with values above 0.9556 and 0.9805 for their exponential and linear functions, respectively.

### 3.5.2 *Linear speed-accuracy tradeoff*

The simulation results exemplified by Fig. 3.7 and summarised in Table 3.4 show how the endpoint standard deviation increases linearly with the average movement velocity for movements employing fixed horizon control. Each figure shows a best fit linear function of the same form as Eq. 3.5 (p. 64) found by Schmidt et al. (1979). Using a fixed horizon control strategy, the duration, or prediction horizon  $T_h$ , of the preplanned optimal trajectory  $R^*$  is reduced at every RP interval by an amount equal to the time it takes for the RP system to generate a new  $R^*$ , namely 100 ms. Therefore, the initial prediction horizon corresponds to the desired total movement duration. The simulations include movements to a step target located at a distance of 10, 20, or 30 cm. The initial prediction horizon ranges from 100 to 1000 ms. Particularly interesting are groups A and B in Table 3.4, where group A is also depicted graphically in Fig. 3.7. Group A consists of step movements of amplitudes 10, 20, and 30 cm, with durations of 100, 150, and 200 ms. Therefore, this simulation is analogous to the experiment by Schmidt et al. (1979), where subjects made single aimed tapping movements with the same amplitudes and 140, 170, and 200 ms durations. Schmidt et al. (1979) report a correlation of 0.97 between the endpoint standard deviation and average velocity, whereas the simulations yield a correlation coefficient of  $R^2 = 0.9968$ . Group B, on the other hand, consists of step movements of amplitudes 10, 20, and 30 cm and durations of 150, 200, and 250 ms. This simulation is analogous to the experiment by Zelaznik et al. (1986), who had subjects perform exactly the same group of movements. Zelaznik et al.

(1986) report a correlation of 0.96 while the simulation results show a correlation coefficient of  $R^2 = 0.9940$ . Although the linear relationships of both Schmidt et al. (1979) and Zelaznik et al. (1986) are very strong, it is perhaps not surprising that the correlations in the simulations are even stronger. After all, experiments with human beings are inherently prone to noise factors, for example lack of concentration, whereas the simulator personifies someone who is highly skilled and does not get distracted by external factors.

### 3.5.3 *Velocity profiles*

As previously discussed, acceleration waveforms associated with EMG bursts of the agonist and antagonist muscle activity are approximated in the simulations by rectangular pulses. Consequently, the velocity profiles produced by the simulator (Figs. 3.5, 3.6, and 3.8) include sharp corners instead of being smooth. The distortion introduced by this simplification becomes less important as the duration of the movement is increased.

Applying a receding horizon control strategy, the simulator reproduces exactly the left-skewed asymmetrical velocity profiles observed experimentally that occur in spatially constrained movements. As can be seen in Fig. 3.6(a), the velocity profile is perfectly symmetrical for a ballistic movement, just as reported experimentally (e.g., Berardelli et al., 1996). However, the profile becomes gradually more asymmetrical as the prediction horizon is increased (Fig. 3.6(b), Table 3.3). This is in line with experimental data (e.g., Beggs & Howarth, 1972). When subjects are instructed to emphasise spatial accuracy only, the velocity profile becomes increasingly asymmetrical as movement speed is reduced, with the peak velocity occurring relatively early in the movement. This corresponds to a strategy of making a fast initial movement to move into the ballpark of the target before zooming in on the target with one or several correcting movements.

Furthermore, applying a fixed horizon control strategy, the simulator reproduces the symmetrical velocity profiles that occur in movements that are both spatially and temporally constrained. As can be seen in Fig. 3.8(a), the velocity profile



is symmetrical for a ballistic movement, however, examination of all test cases show that it remains symmetrical even as the initial prediction horizon is increased, with an example given by Fig. 3.8(b). The symmetrical velocity profiles are in line with experimental findings in time-matching tasks (Shapiro & Walter, 1986; Cooke & Brown, 1994; Schmidt & Lee, 1999). When subjects make movements that emphasise both spatial and temporal accuracy, that is, time-matching tasks, the maximum velocity occurs approximately midway, and the velocity profile is symmetrical for a range of movement durations.

---

## CHAPTER 4

### Study II: Physiological tremor

---

#### 4.1 Literature review

##### *4.1.1 Introduction*

Tremor in relation to human motor control may be defined as unintentional back-and-forth movements of a body part. Normal, or physiological, tremor is exhibited by any healthy person. When it is exacerbated by stress, ageing, fatigue, anxiety, the influence of some medications, or medical conditions such as hyperthyroidism, it is termed enhanced physiological tremor (Bain, 2002; McAuley & Marsden, 2000). In contrast, pathological tremors occur as a manifestation of movement disorders. Common pathological tremors include essential, parkinsonian, cerebellar, psychogenic, orthostatic, rubral, Holmes', and neuropathic tremor (Deuschl, Raethjen, Lindemann, & Krack, 2001). According to Louis, Ottman, & Hauser (1998), essential tremor is the most common adult movement disorder, being more than 20 times more prevalent than Parkinson's disease. Thus, it is not surprising that research into pathological tremor has received much interest. Physiological tremor, on the other hand, is a normal phenomenon unknown to most people as its small amplitude oscillations are barely visible and generally do not impair everyday motor tasks. Perhaps as a result, physiological tremor has traditionally been considered simply as unwanted biological "noise" in the motor system (e.g., see Fox & Randall, 1970; Goodman & Kelso, 1983; Lakie & Combes, 1999) and a purposeless feature of motor control (Brumlik, 1962; Stiles & Randall, 1967). According to Morrison & Keogh (2001), this view is still held, which is somewhat surprising,

given that oscillatory behavior is considered an intrinsic property of a normally functioning motor system. Nevertheless, researchers have attempted to disclose the origin of physiological tremor and its potential function for more than 120 years (e.g., Horsley & Schäfer, 1886). Indeed, the view that physiological tremor may be a manifestation in the periphery of functional central oscillatory activity has gained interest in recent years (see McAuley & Marsden, 2000, for a review).

Tremor may be divided into categories depending on the conditions under which it occurs. For the purpose of identification of pathological tremor, clinicians usually consider tremors that occur during rest, posture, or goal-directed movements (Deuschl et al., 2001). According to Bain (2007), tremor can be defined as either rest tremor or action tremor. Rest tremor is tremor that occurs when a body part is not voluntarily activated and is completely supported against gravity. On the contrary, action tremor is any tremor that occurs during voluntary muscle contractions. Action tremor may be further subdivided into postural tremor (tremor during the voluntary maintenance of posture against gravity), kinetic tremor (tremor during any voluntary movement), intention tremor (tremor occurring towards the end of a target-directed movement), task-specific tremor (tremor during specific activities, e.g., primary writing tremor), and isometric tremor (tremor during muscle contraction against a rigid stationary object) (Bain, 2007). Other categories include higher amplitude tremors and tremor during compliant contractions (McAuley & Marsden, 2000).

#### *4.1.2 Mechanisms of physiological tremor*

According to the review by Elble (1996), physiological tremor consists of two distinct components, namely mechanical-reflex oscillations and 8–12 Hz central-neurogenic oscillations. Mechanical properties such as the inertia, viscosity, and elasticity of a body part cause damped oscillations to occur in response to pulsatile perturbations (Elble, 2003). In addition, under the influence of mechanical load, drugs, or fatigue, the spinal reflex arc may also contribute (Stiles, 1976; Hagbarth & Young, 1979),

therefore this component is commonly termed mechanical-reflex tremor (Mayston, Harrison, Stephens, & Farmer, 2001).

In contrast, the central-neurogenic tremor is always associated with modulation of motor unit activity (Elble, 2003). Whereas the mechanical-reflex tremor may be seen as a passive response to perturbations originating externally or internally (Mayston et al., 2001), the central-neurogenic component is an active component, where rhythmic motor unit activity, likely originating from an oscillating neural network in the CNS (Elble, 1996), drives the tremor observed in a body part (Elble, 2003).

Both components are superimposed on a background of irregular fluctuations in muscle force and limb displacement (Elble & Randall, 1976, 1978). These oscillations have a frequency of 0–15 Hz and are produced by motor units that fire near their threshold (Allum, Dietz, & Freund, 1978; Christakos & Lal, 1980; Dietz, Bischofberger, Wita, & Freund, 1976; Freund, 1983; Marshall & Walsh, 1956). However, skeletal muscles act as a low-pass filter, thus attenuating frequency components above 3–5 Hz (Partridge, 1966).

It is certainly possible to view the components of physiological tremor differently than Elble (1996). For example, Deuschl et al. (2001) postulate three causes of physiological tremor: Mechanical tremor, reflexes of the CNS, and central oscillations. McAuley & Marsden (2000) extend this view and lists five factors contributing to physiological tremor, all of which contribute to varying degrees depending on the conditions under which the tremor occurs: Mechanical resonances, feedback resonances, motor unit firing properties, synchronised motor unit oscillations, and central oscillations.

#### *Mechanical resonances*

Mechanical properties of bone, muscle, and soft tissue of a body part imply a system possessing properties such as inertia, viscosity, and elasticity. This allows for a body part to be modeled as a second-order mass-spring system. Based on this idea, investigation of muscle-load tremor of the rat and of the human hand and finger led to

the mechanical resonance hypothesis (Rietz & Stiles, 1974; Stiles & Randall, 1967), which assumes that broadband stochastic frequency forcing, i.e., asynchronous muscle fiber contraction, within an underdamped viscoelastic-mass system accounts for physiological tremor (Stiles, 1976, 1980). By systematically varying the moment of inertia through the addition of loads, Rietz & Stiles (1974) found that tremor frequency varied in the same manner as that predicted by a mass-spring model. Similar results were obtained by Joyce & Rack (1974) from examination of mechanically loaded elbow flexion movements against a spring. Varying both the stiffness and load, Joyce & Rack were able to adjust the tremor frequency between 2 and 12 Hz. In general, it is agreed that the mechanical fundamental, or resonant, frequency  $\omega_0$  of a body limb approximates

$$\omega_0 = 2\pi f_0 = \sqrt{\frac{K}{I}}, \quad (4.1)$$

where  $K$  is the stiffness or forces exerted on the limb and  $I$  is the moment of inertia (e.g., Elble, 1996; Deuschl et al., 2001; McAuley & Marsden, 2000).

For the unloaded finger, the resonant frequency is in the range of 25 Hz (Stiles & Randall, 1967) to 27 Hz (Halliday & Redfearn, 1956). The resonant frequency of the wrist has been reported as 9 Hz (Marsden, 1984) or more broadly as 8–12 Hz (Elble & Randall, 1978; Lakie, Walsh, & Wright, 1986), whereas the elbow has been found to have a resonant frequency of 2 Hz (Marsden, 1984) or 3–5 Hz (Fox & Randall, 1970).

If loaded or under force exertion, new fundamental frequencies can be found by sharply perturbing the body part. Similar to tapping a tuning fork, the perturbation results in die-away oscillations of the new load and force dependent frequency (Halliday & Redfearn, 1956).

From the above, mechanical resonance may only account for physiological tremor of the wrist, which has a fundamental frequency in the same range as physiological tremor. To account for more proximal limbs, their fundamental frequencies must be increased by increasing muscle tension and stiffening the limbs. Still, mechanical

resonance can play a passive but important role in tremor generation through its filtering properties. Tremor of a frequency widely different from the fundamental frequency needs to be of great power to exert a noticeable modulation (McAuley & Marsden, 2000). Consequently, the likelihood of detecting higher peak frequencies decreases from including mechanical loads and increases from using elastic forces.

#### *Reflex loop resonances*

Many have proposed reflex loop resonances to be a major contributor to physiological tremor (e.g., Halliday & Redfearn, 1958; Joyce & Rack, 1974; Joyce, Rack, & Ross, 1974; Lippold, Redfearn, & Vučo, 1957; Lippold, 1970; Mori, 1975; Perkins, 1945). This view is based upon the fact that the peripheral stretch reflex can be considered a negative feedback loop. Such a servo-mechanism may cause synchronised EMG activity and tremor with a period of double the loop delay (McAuley & Marsden, 2000). In other words, if the loop delay is half the period of a muscle oscillation, the negative feedback signal will become positive due to phase reversal in the loop and a self-maintained oscillation may occur (Halliday & Redfearn, 1956). According to Marsden (1978), the loop time for the spinal stretch reflex in the finger is approximately 50 ms. Therefore, a muscle oscillation with a period of 100 ms, or a frequency of 10 Hz, could be enhanced by reflex loop resonance. Similarly, oscillations due to the long latency stretch reflex would occur at 7 Hz (Marsden, 1978). As pointed out by McAuley & Marsden (2000), even in cases where short or long latency reflex loop times do not correspond exactly with experimentally observed tremor frequencies, they may still be influential, as co-existing loops may interact together or with other modulations, thus causing other tremor peak frequencies to occur (Matthews, 1993).

Early examinations of finger tremor in tabetic patients provided support for the servo-loop hypothesis because of an absence of a 10 Hz peak for the most severely deafferented patients (Halliday & Redfearn, 1958), however, others have been unable to reproduce this finding (Marsden, Meadows, Lange, & Watson, 1967b).

The relative size of a physiological tremor power peak generally increases with the tremor amplitude (Marsden, Meadows, Lange, & Watson, 1969c). One possible explanation is that muscle spindles receive increased stimuli from the mechanical oscillations, which in turn increases the synchronisation of motor neuron discharge around the peak frequency (Marsden, Meadows, & Lange, 1970).

As for mechanical resonances, mechanical loading decreases the reflex loop tremor frequencies (Berthoz & Metral, 1970). The greater inertia due to the load increases the delay from movement production to detection by afferent receptors (McAuley & Marsden, 2000), thus lowering the frequency of the tremor component due to reflex loop resonance.

Together with mechanical resonances, reflex resonances may be seen as passive contributors to physiological tremor. For example, as suggested by Joyce & Rack (1974), a tremor may have its principal frequencies determined by the mechanical system in the limb as well as the stretch reflex timing, whereas the driving mechanism may be an irregular disturbance signal due to the irregularity of motor neuron discharge (Taylor, 1962), cardiac factors such as the pulsatile ejection of blood and its movements through vessels (Yap & Boshes, 1967), chest movements due to respiration (Padsha & Stein, 1973), or other mechanically coupled movements in the body.

#### *Motor unit firing properties*

Individual motor units do not fire over a continuous frequency range but start firing at a minimum frequency of about 8–10 Hz (Henneman, 1979), possibly in part due to spinal mechanisms such as Renshaw inhibition (Granit & Renkin, 1961). According to McAuley & Marsden (2000), frequency spectra from surface EMG recordings of multiple motor units during steady isometric contractions generally have a peak in the 8–12 Hz range, suggesting summated activity of a number of motor units. Therefore, summation of motor unit forces at a muscle tendon resulting in active tremor could reflect such motor unit firing properties (Marshall & Walsh, 1956; Hömberg, Reiners, Hefter, & Freund, 1986).

Change in mean motor unit firing rates or varying contraction lengths do not shift the active tremor frequency from its 10 Hz peak, which seems to oppose the above hypothesis. McAuley & Marsden (2000) explain this invariance on the basis that newly recruited motor units firing in the minimum 8–12 Hz range will be larger and dominate the other faster firing units. The phenomenon of fusion means that force fluctuations due to faster firing units are relatively more attenuated by mechanical properties of the muscle (Marsden, 1978). Hence, newly recruited units, which contribute a proportionately large amount to the force output (Allum et al., 1978), will cause unfused twitches at 8–12 Hz. Examining submaximal isometric knee contractions, Ebenbichler et al. (2000) observed a 10 Hz tremor that was probably due to the recruitment of units and fatigue-related properties of high threshold motor units of muscles.

#### *Synchronised motor unit oscillations*

It is known from studies on isometric contraction that under some experimental conditions, the 8–12 Hz peak frequency results from synchronisation of motor units that tend to fire together in a pervasive 8–12 Hz rhythm rather than at random (Fox & Randall, 1970; Mori, 1975; Elble & Randall, 1976; Elble, 1986). For example, Elble & Randall (1976) found that the majority of individual finger muscle units were firing in the range 13–22 Hz, whereas surface EMG showed a 8–12 Hz rhythm related to whole populations of units. Examination of individual motor unit spike trains displayed transient sequences of double discharges with interspike intervals (ISIs) of approximately 8–30 ms alternated with ISIs of 60–90 ms. As a result, the frequency spectra of these motor units showed distinct 8–12 Hz peaks in addition to peaks in the higher mean firing range. Coherency analysis demonstrated that the 8–12 Hz peak was correlated to the 8–12 Hz finger tremor and surface EMG modulation.

Based on the shape of cross-correlation histograms (cross-correlograms) of pairs of intercostal motor units in the anaesthetised cat, Kirkwood, Sears, Tuck, & Westgaard (1982) defined three forms of synchronisation, namely short-term synchroni-



sation, broad-peak synchronisation, and high-frequency oscillation synchronisation. Short-term synchronisation is the result of branching, or divergence, of immediate motor unit inputs and the corresponding cross-correlogram contains a very narrow peak ( $\pm 3$  ms) that occurs independent of any synchronisation between discharges of individual presynaptic axons (Sears & Stagg, 1976). Broad-peak synchronisation, on the other hand, results from a common input many synapses distant from the motor units; the synapses introduce temporal “jitter” in signal transmission, and hence, a “looser” synchronisation and a broader cross-correlogram peak occur (McAuley & Marsden, 2000). Finally, as for short-term synchronisation, high-frequency oscillation synchronisation occurs due to branching of motor unit inputs, but in addition, these inputs are themselves driven by a common driving oscillation, such as that of the medullary respiratory centre at 60–120 Hz (Cohen, 1979).

A central cross-correlation peak between the EMG activity of two muscles in the same limb does not imply a common CNS oscillatory modulation of motor unit inputs (McAuley & Brown, 1995). Indeed, Dietz et al. (1976) suggested that physiological tremor could be non-specifically augmented by short-term synchronisation due to the divergence of descending spinal inputs to several motor units in a limb. To confirm a common central driving oscillation, it is necessary to examine the coherence between motor units rather than their cross-correlation. Such a common rhythmic modulation of motor unit inputs was found by Elble & Randall (1976), who performed coherence analyses of simultaneously recorded motor units.

#### *Central oscillations*

As noted by McAuley & Marsden (2000), by inference, evidence against synchronisation by peripheral mechanisms strengthens arguments for synchronisation by central oscillations. In a deafferented patient, Marsden et al. (1967b) found a well-defined 9 Hz physiological tremor peak both in the normal left arm and in a totally deafferented right arm, thus providing evidence that the tremor peak arises independently of sensory feedback and is not due solely to the stretch reflex mechanism. Furthermore, contrary to Halliday & Redfearn (1958), their examination of finger

tremor in patients with severe tabes dorsalis consistently confirmed the presence of this peak. Finally, Marsden et al. (1967b) reported that patients with notable slowing of conduction in peripheral nerves still had a tremor peak of about 9 Hz rather than at lower frequencies as predicted by the servo-loop hypothesis.

Related results obtained by Proudlock & Scott (2003) demonstrated that a 8–10 Hz tremor was present in both position holding and in slow finger movements even after complete ulnar nerve transection and subsequent reinnervation of intrinsic hand muscles. Their observations are corroborated by the findings of Wessberg & Vallbo (1995b), who showed that spindle output during slow movements is insufficient to generate the 8–10 Hz oscillations.

Examinations of slow voluntary finger movements have shown a motion tremor consisting of regular pulses fixed at 8–10 Hz (Vallbo & Wessberg, 1993). The pulses have large amplitudes, are unaffected by varying the finger velocity or mechanical load, and display a timing inconsistent with the timing of reafferent impulses (Wessberg & Vallbo, 1995a). Analysing the effect of stretch perturbations during such movements, Wessberg & Vallbo (1996) found that stretch reflexes are too delayed and too weak to fit a reflex loop hypothesis.

Freund, Büdingen, & Dietz (1975) reported that newly recruited motor units, which are the strongest, discharge at 6–10 Hz and could therefore provide an explanation to finger movement discontinuities<sup>1</sup>. However, in a study by Wessberg & Kakuda (1999), no units were able to exhibit a sustained 8–10 Hz firing pattern. Instead, units consistently fired at higher frequencies but were frequency modulated at *circa* 8–12 Hz, implying a common modulatory input to a high proportion of the active motor neurons. This matches well with results obtained by Wessberg (1996), who demonstrated significant intermittent left-right synchronisation during a bi-manual finger movement task, a result that implies supraspinal, possibly cortical, control.

---

<sup>1</sup>Whereas the term “discontinuities” in its strict mathematical sense denotes points where a signal is not continuous, the term is commonly abused in the tremor literature to denote (sharp) oscillations.

In studies of compliant finger muscle contractions, McAuley, Rothwell, & Marsden (1997) found that mechanical loading, stiffness, or anaesthesia did not shift the frequency of synchronised 10 Hz motor unit activity and therefore attributed the tremor to central neural oscillators.

Studies of patients with X-linked Kallmann’s syndrome (XKS) and pathological mirror movements have shown that shared voluntary motor commands are conducted through bilateral corticospinal pathways, with abnormal synchronisation of motor unit firing between homologous left and right muscles as a result (Farmer, Ingram, & Stephens, 1990; Mayston, Harrison, Quinton, Stephens, Krams, & Bouloux, 1997). Unilateral magnetic brain stimulation of patients with XKS resulted in significant coherence for all combinations of left and right tremor and EMG, with load-independent coherent frequencies in the range of 7–12 Hz (Mayston et al., 2001). This is in contrast to recordings of finger tremor and EMG in healthy subjects, which only show significant coherence unilaterally (Marsden, Meadows, Lange, & Watson, 1969a; Köster et al., 1998).

Similarly, it has been demonstrated that subjects with bilateral projections of the corticospinal tract and corresponding congenital mirror movements have an 8–12 Hz component that is coherent in both arms (Köster et al., 1998), whereas normal subjects do not (Lauk, Köster, Timmer, Guschlbauer, Deuschl, & Lücking, 1999; Raethjen et al., 2000).

All of the evidence presented above suggest that the 8–12 Hz tremor is central in origin. Indeed, this evidence is so strong that some authors matter-of-factly refer to the 8–12 Hz power peak as the central-neurogenic component of physiological tremor (e.g., Mayston et al., 2001).

#### *4.1.3 The degree of contribution depends on the condition*

The previous section presented a variety of mechanisms contributing to physiological tremor. Much evidence point to central oscillators being responsible for 8–12 Hz oscillations in movement, yet, hypotheses related to intrinsic mechanical properties,

individual motor unit firing, and synchronisation by mechanical or reflex loop resonances have also received considerable support. The apparent contradictions in the tremor literature are related to the fact that the degree to which a mechanism contributes to tremor is dependent on the conditions under which the tremor occurs.

It is commonly accepted that physiological tremor may be separated into a mechanical-reflex component and an 8–12 Hz central-neurogenic component (e.g., Deuschl et al., 2001; Elble, 1996; Mayston et al., 2001). Many conflicting views have probably arisen due to both tremor peaks overlapping at the same frequency band, thus appearing as a single frequency peak. Although both peaks are often indistinguishable around 10–12 Hz (Timmer, Lauk, Pflieger, & Deuschl, 1998), it is usually possible to identify the mechanical-reflex component by shifting its peak through the addition of load (bias towards lower frequencies) or using an elastic force (bias towards higher frequencies). The following sections attempt to resolve some of the confusion by investigating the relative contribution of peripheral and central mechanisms under various experimental conditions.

#### *Rest tremor*

A body part is at rest if no voluntary neuromuscular activity is required for support against gravity (Bain, 2007). Therefore, by definition, the small-amplitude rest tremor that occurs is unlikely to be central-neurogenic in origin (McAuley & Marsden, 2000). Instead, ballistocardiogram (BCG) recordings suggest that rest tremor is related to cardioballistic effects (Yap & Boshes, 1967), respiratory chest movements (Padsha & Stein, 1973), or other movements in the body that are mechanically coupled to the trembling limb.

#### *Postural tremor*

Postural tremor occurs during the voluntary maintenance of posture against gravity. The 10 Hz tremor that occurs when trying to keep an outstretched limb at standstill has been attributed to mechanical resonances (Lakie et al., 1986; Amjad et al., 1994) because the tremor frequency can be varied by mechanical loading or

as a peripheral stretch reflex loop resonance (e.g., Halliday & Redfearn, 1956; Hagbarth & Young, 1979; Sakamoto et al., 1992). On the other hand, postural tremor has been shown to persist, albeit with a less sharply “tuned” 10 Hz frequency component, in deafferented patients without reflex loop contributions (Marsden et al., 1967b). Moreover, postural tremor at the extremities may in part be due to the transfer, mechanical or otherwise, of oscillations from a more “active” tremor of proximal muscles maintaining the posture (Marsden, Meadows, Lange, & Watson, 1969b). Postural tremor therefore appears to be multifactorial in origin, with both mechanical and reflex loop components as well as a central component.

#### *Tremor during isometric contractions*

As noted by McAuley & Marsden (2000), tremor at around 10 Hz during isometric contraction is associated with EMG activity and, when of low amplitude, may be a result of single motor unit activity (Freund & Dietz, 1978). Historically, centrally generated oscillations in the 10 Hz range have not been found to manifest peripherally in many studies dominated by isometric paradigms, which is probably due to the strong dampening effect on tremor from muscle contractions against a stationary object (McAuley & Marsden, 2000). For example, Joyce & Rack (1974) had subjects perform compliant contractions against a spring, however, as the spring stiffness was progressively increased, the experimental paradigm gradually approached an isometric one, with the result that the tremor amplitude diminished and became irregular and the corresponding power spectra had a variety of frequency components.

Durbaba, Taylor, Manu, & Buonajuti (2005) argue that under true isometric conditions with the body limb attached to a rigid transducer, tremor is abolished. Addressing this, Sowman & Türker (2005) examined physiological tremor in the jaw by attaching the mandible via the teeth to a rigid transducer, thus obtaining an almost direct coupling to the bone and minimising the contribution from the stretch reflex. Sowman & Türker were able to consistently observe a 7 Hz tremor independent of bite force and concluded from coherence and phase analyses of the tremor

and EMG that this tremor is centrally generated, with reflex loop contributions being modulatory at the most.

Introducing ischaemic sensory deafferentation in the upper limb during isometric contractions, Pohja & Salenius (2003) found that the frequency of coherence between whole-scalp magnetoencephalogram (MEG) and EMG did not change significantly during ischaemia, although the strength of the coherence was reduced. As for the experiments of Sowman & Türker (2005), this implies that a reflex loop may be seen as a passive element modulating centrally driven oscillations.

In a study of coherence between MEG and EMG during isometric contractions, Salenius, Portin, Kajola, Salmelin, & Hari (1997) demonstrated significant coherence in the frequency range of 15–33 Hz between MEG from the primary sensorimotor cortex (S1–M1) and the rectified EMG of the contralateral hand or foot muscles. A similar result was obtained by Ohara et al. (2000), who found significant coherence between hand muscle EMG and the electroencephalogram (EEG) of the primary motor area (M1), the supplementary motor area proper (SMA proper), and the primary somatosensory area (S1) at peak frequencies in the range 12–15 Hz. Both results are highly indicative of cortical rhythms being responsible for peripheral tremor, although in both cases, the frequency range of coherence was higher than the 10 Hz range of physiological tremor. A possible reason was given by Gross et al. (2000), who found strong 10 Hz components in the power spectra of EMG and MEG of M1, but significant coherence was restricted to the 20 Hz range. This result is in accord with the hypothesis that the 10 and 20 Hz components may have different functional roles (Salmelin & Hari, 1994). Furthermore, Gross et al. (2000) speculated that the 20 Hz motor cortex oscillations may arise under stationary conditions such as those of isometric contractions where no encoding of the dynamics of motor control is needed, and the motor cortex might be sending the same motor commands repeatedly at a constant rate of 20 Hz. In a similar vein, Baker, Kilner, Pinches, & Lemon (1999) suggested that when little information needs to be trans-

ferred, sending oscillatory motor commands yields an efficient recruitment of motor units (see also Hari & Salenius, 1999).

From the above, it is clear that the experimental condition often being isometric has contributed significantly to much confusion in the literature. The strong dampening effect have probably rendered tremor unobservable, or at least irregular, in many studies, leading to the rejection of centrally generated oscillations hypotheses and the support of stretch reflex hypotheses, even very recently (Durbaba et al., 2005). Furthermore, the fact that the limb is not moving may mean that the mechanism being studied is different to the one causing tremor during movement, which may explain the high coherence frequencies (12–33 Hz) reported for isometric contractions. Overall, it may be concluded that tremor during isometric contractions likely is central in origin, but reflex loop resonances may contribute as a modulatory factor.

#### *Tremor during compliant contractions*

Studies of compliant, or elastic, contractions avoid the problem of the strong dampening effect during isometric contractions. Observing compliant finger muscle contractions, McAuley et al. (1997) found that frequency peaks of tremor and EMG were coherent at 10, 20, and 40 Hz and had a fixed phase difference. Thorough analyses excluded the possibility that the three frequency peaks simply represented harmonics. Because amplitudes were too great to have been generated by single motor units and because polyphasic activity at the peak frequencies was seen in both surface and needle EMG records, the authors concluded that tremor during compliant contractions is due to synchronised firing of motor units. Moreover, because the tremor frequency was insensitive to anaesthesia and inertial or elastic loading, the results suggest that the synchronisation was centrally generated.

Different results were obtained by Joyce & Rack (1974) for compliant elbow contractions against a spring, where the tremor and EMG frequency peaks were reduced by adding weight to the wrist or increased by stiffening the spring. Similar

findings have been reported by Matthews & Muir (1980) and suggest a mechanical-reflex mechanism causing the tremor. Both studies were slightly different from the finger study of McAuley et al. (1997) in their experimental setup. In the studies of Joyce & Rack (1974) and Matthews & Muir (1980), the elbow was fairly stabilised and the forearm raised vertically in a balancing position, while the finger in the study of McAuley et al. (1997) had no support against gravity and contractions were made in the horizontal plane.

The literature suffers from most studies examining isometric contractions rather than elastic ones, but the studies mentioned here may indicate that tremor observed in compliant contractions is multifactorial, where the contribution depends on the experimental conditions (McAuley & Marsden, 2000)

#### *Higher amplitude tremor*

According to Deuschl et al. (2001), the distinction between physiological and enhanced physiological tremor is purely clinical and they share common mechanisms. Enhanced physiological tremor has higher amplitudes, can occur during posture or active contractions, and is likely due to unit synchronisation from an external source (McAuley & Marsden, 2000). Compared with physiological tremor, the general view is that reflexes are the tremor component that is being enhanced and causes higher amplitude tremor (Deuschl et al., 2001).

In a study on strong contractions and fatigue, Ebenbichler et al. (2000) concluded that load-dependent, fatigue-related high amplitude tremor during submaximal voluntary contractions was the result of recruitment of motor units and the fatigue-related properties of high threshold units.

It has been shown in studies of thyroid hormones (Hefter, Hömberg, Reiners, & Freund, 1987; Hömberg, Hefter, Reiners, & Freund, 1987; Marsden et al., 1970) and stress and  $\beta$ -adrenergic agents (Foley, Marsden, & Owen, 1967; Marsden, Foley, Owen, & McAllister, 1967a; Marsden & Meadows, 1968, 1970) that the gain of muscle receptors and spinal reflex loops increases with hyperthyroidism, stress, and



adrenaline. The enhancement of afferent feedback results in increased synchronisation of units and increased tremor amplitude (Hagbarth & Young, 1979).

Recently, however, a drug-induced enhancement of the central rather than the reflex component of physiological tremor was obtained. After amitriptyline intake, patients had an increase in tremor amplitude as well as a synchronisation of motor units between different muscles in the range of 7–15 Hz (Raethjen et al., 2001). Moreover, Decima (1996) found that tremor activity induced by the drug oxotremorine continued even after deafferentation of the cat, and concluded that the synchronising mechanism was central, probably located in the ventral horn.

Studying visually enhanced goal-directed pointing, Morrison & Keogh (2001) showed that tremor amplitude of the digits increased with higher accuracy requirements and enhanced visual feedback, whereas it decreased for the hand. The authors suggested that the participants, upon receiving augmented visual information about their tremor, stiffened their joint muscles in an attempt to reduce this tremor, however, this resulted in a reduced coupling between hand and finger, and enhanced tremor at the periphery. In general, even without visual enhancement, motion tremor is characterised by 8–10 Hz pulses of large amplitudes (Vallbo & Wessberg, 1993; Wessberg & Vallbo, 1995a). Motion tremor is discussed more thoroughly in the next section.

Together, these studies of higher amplitude tremor confirm the view that physiological tremor can be divided into mechanical-reflex and central-neurogenic components, where the contribution of each depends on the external source.

#### *Motion tremor*

It has been shown that slow finger movements we conceive as continuous are not smooth but have discontinuities at approximately 8–10 Hz (Vallbo & Wessberg, 1993). Effects from varying the velocity or mechanical load as well as timing properties and the effect of stretch perturbations have been inconsistent with reflex resonance hypotheses (Wessberg & Vallbo, 1995a, 1996). Furthermore, the hypothesis that newly recruited units give rise to this tremor has also been rejected (Wessberg

& Kakuda, 1999; Wessberg, 1996). Instead, these studies consistently show that 8–10 Hz motion tremor is a centrally generated phenomenon.

In visual pursuit tracking tasks, McAuley, Farmer, Rothwell, & Marsden (1999) found synchronised 3 and 10 Hz oscillations between hand and eye, and between the two hands, when tracking the same target. In a related study, Evans & Baker (2003) observed task-dependent intermanual coupling of 8 Hz discontinuities during slow finger movements. Both studies indicate that a central oscillator may modulate anatomically distinct structures. Moreover, that coupling is task-dependent suggest that such a mechanism may play a functional role in eye-hand coordination (McAuley et al., 1999).

Pulsatile control (Vallbo & Wessberg, 1993; Farmer, 1999) has also been demonstrated in slow movements of other limbs than the finger, such as jaw or wrist movements. The control system for masticatory muscles differ from that of the fingers because jaw-opening muscles hardly contain muscle spindles and lack reciprocal stretch reflexes (Luschei & Goldberg, 1981). Jaberzadeh et al. (2003) showed that 8 Hz physiological tremor of the jaw muscles during slow movements is the result of centrally generated alternating bursts of activity analogous to that of finger muscles (Vallbo & Wessberg, 1993). Examining motor unit pairs during slow movements as well as position holding of the wrist, Kakuda, Nagaoka, & Wessberg (1999) found significant coherence at 6–12 Hz between unit pairs and between single units and acceleration records. These workers concluded that a 6–12 Hz common modulation of agonist motor units is a distinguishing feature of slow wrist movements but is very small or absent during postural control.

A neural basis for intermittent motor control of continuous movements was recently demonstrated by Gross et al. (2002). Combining whole-head MEG recordings, dynamic imaging of coherent sources (DICS), and finger muscle EMG, these authors were able to pin-point synchronised oscillatory activity around 8 Hz in the cerebello-thalamo-cortical loop as being responsible for the corresponding pulsatile

velocity changes of slow finger movements. Possible functions of such a central oscillating network is presented next.

#### *4.1.4 Functional significance of central oscillations*

Tremor has traditionally been viewed as a source of unwanted noise in the motor system; something to be dampened out or controlled (Goodman & Kelso, 1983). For example, theories based on a closed-loop servomechanism that focus on setpoints and error correction processes consider such oscillations as an unwanted source of variability (e.g., Adams, 1971). Nevertheless, the idea that tremor exists for a reason is not new and potential functional significance of central oscillations is presented below.

#### *Function at the peripheral level*

McAuley & Marsden (2000) suggest that motor commands consisting of synchronised pulses may cause motor neurons to uniformly approach firing thresholds simultaneously, which in turn results in a more linear and uniform motor neuron output. Moreover, from mechanics, a continuously oscillating system with a forcing function that is appropriately phased requires less energy to move than a system in static equilibrium (Goodman & Kelso, 1983). Finally, a pulsatile output could be helpful for achieving sudden velocity changes when substantial inertial resistance is involved (Greene, 1972). These views are in accord with the proposition that the motor control system is sensitive to its own physical dynamics and is capable of taking advantage of them (e.g., Kelso, 1981; Kelso et al., 1981; Kugler et al., 1982).

#### *Synchronisation and binding*

According to McAuley & Marsden (2000), groups of inferior olive units in rats can become temporarily linked by oscillatory modulation of their firing during various phases of a licking task. Such linking might represent a functional coordination of combinations of muscle actions, where movement consists of a concatenated sequence of discrete ballistic movements (Llinás, 1991; Welsh, Lang, Sugihara, & Llinás, 1995).

From studies of 40 Hz oscillations in the visual cortex it has been proposed that synchronisation may serve as a function for feature linking or binding when processing sensory information (Eckhorn et al., 1988; Gray, König, Engel, & Singer, 1989). Thus, although parallel processing may occur in different cortical areas and have variable durations, sensory information can still be identified and associated with a particular visual feature (McAuley & Marsden, 2000). Analogously, binding of motor signals can form discrete muscle collectives, where different tasks make use of different combinations of such functional groups and thereby avoiding a “combinatorial explosion” (Farmer, 1998; Welsh & Llinás, 1997).

Central oscillations manifest in the periphery provide a means to investigate a possible binding mechanism, however, many studies have been unable to demonstrate linking between peripheral rhythms. For example, Marsden et al. (1969a) found that left and right hand tremors are independent of each other during posture. Similarly, recordings of EMG of the hands during simultaneous pinch-gripping (Conway et al., 1995) and EMG of the bicepses during dual-hand weightlifting (Bruce & Ackerson, 1986) have failed to show a left-right linking. Furthermore, examining different muscles of the same hand, McAuley & Brown (1995) did not find significant coherence during simultaneous contractions. One possible explanation may be that the tasks in these studies did not sufficiently require functional linking resulting in a common modulation of the motor commands (McAuley & Marsden, 2000).

On the contrary, animal studies involving direct cortical measurements have shown linking between 25 Hz oscillations in cortical areas (Murthy & Fetz, 1992, 1996; Nicolelis, Baccala, Lin, & Chapin, 1995). The linking appeared to be task-dependent, as it only occurred during complex motor activity and not during simple over-learned movements (Murthy & Fetz, 1992, 1996).

Different but closely related muscles may reveal coherence between single motor units, for example in a grip task such as that of Farmer, Bremner, Halliday, Rosenberg, & Stephens (1993). However, this coherence may be due to so-called

“hard-wired” branching of single corticospinal axons rather than linking of cortical oscillations (McAuley & Marsden, 2000). To reduce the risk of mistaking hard-wired branching for functional binding, McAuley et al. (1999) studied eye and finger movements, which involve dissimilar and spatially separate motor systems. The authors observed linking between eye and finger oscillations at 3 and 10 Hz when the eye and finger simultaneously tracked a visual target but never when they moved independently. However, such functional binding was not always present and McAuley et al. (1999) suggested three possible reasons for this: First, the oscillations may simply be an epiphenomenon superimposed on related motor signals. Second, central binding might exist but only manifest irregularly at the periphery. Third, competing mechanisms for eye-hand coordination may exist and are sometimes preferred to central oscillatory motor control.

#### *Frequency and phase coding*

Studying finger movements, McAuley et al. (1997) found multiple coexisting central oscillations at 10, 20, and 40 Hz and postulated that these rhythms may reflect central “timing” mechanisms that assist in coding of motor commands. The different frequencies may represent separate muscle collectives and aid in identifying different classes of a task (McAuley & Marsden, 2000). 10 Hz oscillations are usually associated with slow movements (cf. Vallbo & Wessberg, 1993) and has recently been shown to be correlated with MEG activity (Gross et al., 2002). 20 Hz oscillations, on the other hand, tend to occur during the hold phase (e.g., Kilner et al., 1999) of humans and pinch-grip tasks of monkeys (Baker, Olivier, & Lemon, 1997). Coherence between MEG and EMG in the 20 Hz range have been shown in many studies (e.g., Conway et al., 1995; Salenius et al., 1997; Halliday, Conway, Farmer, & Rosenberg, 1998; Baker et al., 1997). In light of this, the study of McAuley et al. (1997) may provide an example of frequency coding, where central 10 and 20 Hz oscillations cause closely related muscle collectives of a single peripheral structure to simultaneously achieve fine motion control (10 Hz frequency coding) and maintenance of posture (20 Hz frequency coding).

Further indications of frequency coding are found from studies of parkinsonian patients, where both 10 Hz and 40 Hz tremors exist during movement when patients are on medication, but vanish when medication is withheld (Brown & Corcos, 1997; McAuley, Corcos, Rothwell, Quinn, & Marsden, 2001). That the 40 Hz Piper rhythm (Piper, 1907) also vanishes suggests that the Piper rhythm is a mechanism of motor control that is disrupted in parkinsonian patients (McAuley & Marsden, 2000).

As noted by McAuley & Marsden (2000), phase shifts between oscillations of a particular frequency in different structures provide a mechanism for coding of motor signals. Such phase coding seems to occur in hippocampal spatial memory cells of the rat, where spatial locations are mapped to specific phase shifts (O'Keefe & Recce, 1993). A similar consistent mapping between postures and phase shifts are observed in primary orthostatic tremor (McAuley, Britton, Rothwell, Findley, & Marsden, 2000).

#### *Pulsatile CNS motor output*

Studies have shown a timing relationship between movement and the phase of physiological tremor, where upward movements are initiated during the ascending phase of tremor and vice versa for downward movements (Goodman & Kelso, 1983; Travis, 1929). However, in a more recent study by Lakie & Combes (2000), no such relationship was found. Nevertheless, it has been hypothesised that the computational demand associated with motor actions can be reduced by a discontinuous timing of motor output (Welsh & Llinás, 1997). For example, movement trajectories could be computed at 100 ms intervals corresponding to 10 Hz oscillations rather than continuously. In fact, such a scheme is reminiscent of the biphasic pulse generator proposed by Vallbo & Wessberg (1993). They suggest that a central generator produces a biphasic pulse pattern consisting of an agonist burst followed by an antagonist burst, and that slow movements consist of several such patterns concatenated at 8–10 Hz, with a pulse height regulator controlling the overall speed of the movement. A 8–10 Hz tremor would then manifest itself in the moving limb

although the movement would still be adequately smooth for most purposes (Vallbo & Wessberg, 1993).

The views of Vallbo & Wessberg (1993) and Welsh & Llinás (1997) are corroborated by Gross et al. (2002). They showed that a cerebello-thalamo-cortical loop is the neural basis for intermittent motor control, where the cerebellum is responsible for optimisation and intermittent error correction of ongoing movements by using sensory information. As a result, movement is composed of successive “micromovements” that have a fixed duration inversely related to the 6–9 Hz oscillations of the loop. Two afferent channels separately coding acceleration and deceleration (Wessberg & Vallbo, 1995b) allow the cerebellum to make accurate adjustments of the relative amplitude and timing of the agonist and antagonist bursts (MacKinnon & Rothwell, 2000; Topka et al., 1999) when planning each micromovement.

The cerebellum may be the origin of a 10 Hz clock involved in motor timing (Welsh et al., 1995). Considering the similar frequency of synchronisation at 6–9 Hz by the cerebello-thalamo-cortical loop, it is possible that the motor system is synchronising oscillations of spatially separate areas at a fundamental frequency around 10 Hz (Gross et al., 2002), similar to the function of gamma band synchronisation in perceptual binding (Singer, 1999).

The findings by Gross et al. (2002) imply a discrete mode of motor control, where the cerebellum plans micromovements of constant duration intermittently at a rate corresponding to the frequency of oscillations in the cerebello-thalamo-cortical system. Such a *modus operandi* may be favourable, or even necessary, in order to reduce computational workload and obtain a sensorimotor control loop that is stable and robust, even in the presence of loop delays (Gross et al., 2002).

## 4.2 Method

This thesis hypothesises that intermittent optimal control through sequential operation of BUMPs is a fundamental mechanism of 10 Hz physiological tremor in movement. As outlined in Chapter 2 and elaborated in Chapter 3.2, the optimal response trajectory  $R^*$  planned during an RP interval minimises acceleration and

will therefore be S-shaped. When tracking a ramp target, the RP system incorporates the future state of the target as well as available sensory information about execution error. Consequently, a sequence of error-correcting minimum acceleration trajectories are executed at 100 ms intervals. These submovements will not be perfectly antisymmetrical about the midpoint due to execution error but will still approximate an S-shape and have a single-peaked velocity profile. Therefore, the response will contain a tremor component at 10 Hz, inversely related to the 100 ms duration of the submovements. This hypothesis is tested by means of a computational simulation of the intermittently operating optimal trajectory generator described in Chapter 2.4. Trajectories for constant velocity tracking movements are simulated with receding horizon control along with signal-dependent noise. The simulation results are compared with results from the slow finger movement experiments by Vallbo & Wessberg (1993).

#### *4.2.1 Description of simulator*

The simulator developed and used for the simulation study in Chapter 3 has been further developed to allow for a simulation study of physiological tremor in movement (see Appendix B.2 for a Simulink block diagram and explanation). Extending the work of Master (2003), attention has been given to the development of the RP system and the OTG described in Chapter 2.4. In addition, the simulator has been extended to enable simulation of movements without visual feedback, adaptation of internal models, and continuous-time movement trajectories. The latter enables frequency analysis of 10 Hz physiological tremor in simulated trajectories because data points can be obtained at any desirable sample rate.

In this study, the sample rate is set to 100 Hz, more than sufficient to capture the frequency content of interest. Provided with position and velocity feedback of the actual response as well as the predicted future state of the target from the SA system, the RP system calculates an optimal trajectory  $R^*$  to reach the predicted future state of the target and to compensate for executional error. For simulations of movements without visual feedback, the RP system assumes that the actual



response is executed without executional error and matches the desired response planned during the previous RP interval. Operating intermittently, the RP system passes  $R^*$  to the RE system at 100 ms intervals.

To simulate a highly skilled human subject, the RE system was simplified by pre-tuning the inverse model to exactly compensate for the dynamics of the plant (i.e., wired-in synergy generator, the musculoskeletal system, and the external world). Thus, the response at the output of the plant matches the required response trajectory  $R^*$  generated by the RP system regardless of plant dynamics. Consequently, error in response execution is only related to stochastic noise, which is added to the motor commands and whose standard deviation is proportional to their magnitude.

To simulate a less skilled human subject, the inverse model was pre-tuned through adaptive tuning, in which an initial arbitrary inverse model is allowed to converge (adapt) over time while tracking a training signal. The level of convergence corresponds to the skill level of a simulated human subject. Early interruption of the adaptation process yields a highly detuned inverse model corresponding to a poorly skilled subject, while a completely converged model yields an inverse model close to ideal corresponding to a highly skilled subject. The adaptation process is heuristic and dependent on many factors such as choice of initial inverse model, level of noise, adaptation gain, and the complexity of the training signal. With a non-ideal inverse model, error in response execution is related both to stochastic noise and less than ideal motor commands.

The following sections describe the simulation experiments and corresponding simulator settings.

#### *4.2.2 Experiment 1*

Experiment 1 is devoted to the results presented in Fig. 1 of Vallbo & Wessberg (1993). The top two plots of Fig. 4.1 (p. 124) depict two selected sequences of ramp and hold movements, one with visual feedback and one without (adapted from Fig. 1A, Vallbo & Wessberg, 1993). Both sequences consist of one extension (downward) movement and one flexion (upward) movement. The remaining six

plots of Fig. 4.1 show the joint angle (position), angular velocity and acceleration records from another sequence of ramp and hold movements performed with visual feedback (adapted from Fig. 1B, Vallbo & Wessberg, 1993).

To simulate the ramp and hold movements of Fig. 4.1, the simulator was set up with an ideal inverse model, thus simulating a highly skilled subject. The noise constant was set to 0.2. Simulations were performed both with and without visual feedback.

### 4.2.3 *Experiment 2*

Experiment 2 is devoted to the results presented in Fig. 2 and 3 of Vallbo & Wessberg (1993). Fig. 4.4 (p. 128) shows characteristics of ramp and hold movements of two subjects M.S. and A.P. of different skill level (adapted from Fig. 2, Vallbo & Wessberg, 1993). The top and middle plots show the position and velocity records, respectively, of M.S., whereas the bottom plots show the velocity records of A.P. Fig. 4.5 (p. 128) shows the power spectra of acceleration records from ramp movements of eight subjects, including subjects M.S. and A.P. (adapted from Fig. 3, Vallbo & Wessberg, 1993). From observation, Fig. 4.4–4.5 show that M.S. performed ramp movements with a very distinguished 10 Hz power peak, whereas A.P. had a broader 10 Hz peak with less power as well as a secondary frequency component at 2–3 Hz. As argued in detail in Chapter 4.4, it may be inferred from Fig. 4.4–4.5 that M.S., being a semi-professional cellist, likely is a highly skilled subject, whereas subject A.P., together with subject K.G. (see Experiment 4), is the subject with the poorest skill out of all eight subjects.

To simulate the two extremes, a highly skilled subject (M.S.) and a poorly skilled subject (A.P.), there are two factors to consider: The level of signal-dependent noise in the motor system, and the accuracy of the internal models. When subjects are poorly trained, they often co-contract and stiffen, which increases the amount of signal-dependent noise. Moreover, less trained subjects have not developed an accurate internal model of the external system to be controlled, that is, the inverse

model of the plant is detuned. Out of the two factors, an inaccurate internal model is probably the biggest difference between the two subjects.

Consequently, the simulated subject M.S. was assigned a noise constant of 0.2 and an ideal inverse model. The simulated subject A.P. was assigned a noise constant of 0.4 and a highly detuned inverse model corresponding to a short period of adaptation. Visual feedback was turned on for both subjects. Whereas the power spectra in Fig. 4.5 are averages of 42–204 ramp movements, likely of duration 2–3 seconds, the simulator produced a single ramp movement of 10 seconds duration for each simulated subject.

#### *4.2.4 Experiment 3*

Experiment 3 is devoted to the results presented in Fig. 4 of Vallbo & Wessberg (1993). Fig. 4.11 (p. 135) shows the position records of ramp movements with velocities 4, 10, 25, and 62 deg/s, whereas Fig. 4.12 (p. 135) shows the corresponding velocity records (both figures adapted from Fig. 4A, Vallbo & Wessberg, 1993).

The simulator was set up with an ideal inverse model, thus simulating a highly skilled subject. The noise constant was set to 0.2. Ramp speeds were set to 4, 10, 25, 50, and 62 deg/s. Visual feedback was turned on.

#### *4.2.5 Experiment 4*

Experiment 4 is devoted to the results presented in Fig. 5 of Vallbo & Wessberg (1993). Fig. 4.15 (p. 139) shows ramp movements performed with and without visual feedback by the poorly skilled subject K.G. (adapted from Fig. 5A, Vallbo & Wessberg, 1993). Fig. 4.16 (p. 139) shows power spectra for the same movements (adapted from Fig. 5B, Vallbo & Wessberg, 1993).

The simulated subject K.G. was assigned a noise constant of 0.4 and a highly detuned inverse model similar to the one used for the poorly skilled subject A.P. in Experiment 2. Simulations were performed both with and without visual feedback.

Setting	Exp. 1	Exp. 2	Exp. 3	Exp. 4
$T_p$ (ms)	100	100	100	100
$T_h$ (ms)	100	100	100	100
$S$ (deg/s)	10	10	{4, 10, 25, 50, 62}	10
$T_s$ (s)	10	10	7	10
$n_c$	0.2	{0, 0.2, 0.4}	0.2	0.4
Ideal model	Yes	{Yes, No}	Yes	No
Visual feedback	{Yes, No}	Yes	Yes	{Yes, No}

Table 4.1: Settings for simulations of human ramp movements.  $T_p$  is the RP interval;  $T_h$  is the constant prediction horizon for receding horizon control;  $S$  is ramp speed;  $T_s$  is simulation duration; and  $n_c$  is the noise constant. When an ideal inverse model was not used, a highly detuned model was used instead. Visual feedback was employed as indicated.

#### 4.2.6 Summary of simulator settings

All simulation experiments were performed with a fixed duration planning interval of  $T_p = 100$  ms and a receding horizon control strategy with a prediction horizon  $T_h = 100$  ms. Stochastic noise was added to the motor commands and was proportional to them by a factor, or noise constant,  $n_c$  dependent on the particular experiment. Other experiment-specific settings include tracking speed  $S$ , simulation time  $T_s$ , use of visual feedback or not, and employing an ideal inverse model or not. When an ideal inverse model was not used, a highly detuned inverse model signifying an unskilled subject was used instead. The simulator settings are summarised in Table 4.1.

### 4.3 Results

#### 4.3.1 Experiment 1

Fig. 4.2–4.3 show simulations of the human experiment depicted in Fig. 4.1 (adapted from Fig. 1, Vallbo & Wessberg, 1993). Both figures show a tracking task consisting of ramp and hold movements, one extension (downward) and one flexion (upward) movement. When movement is simulated with visual feedback (Fig. 4.2), the response ramps to a distance of -20, holds, returns to zero, and holds again. When

movement is simulated in the absence of visual feedback (Fig. 4.3), the hold phases are at inaccurate distances due to the lack of feedback assisting in error correction.

It is evident from the velocity and acceleration profiles in Fig. 4.2–4.3 that there are cyclic discontinuities at intervals of 100 ms, corresponding to a tremor frequency of 10 Hz. This matches the human experiment in Fig. 4.1, where inspection of the waveforms, particularly velocity and acceleration, shows that discontinuities occur at a rate of approximately 8–10 Hz.

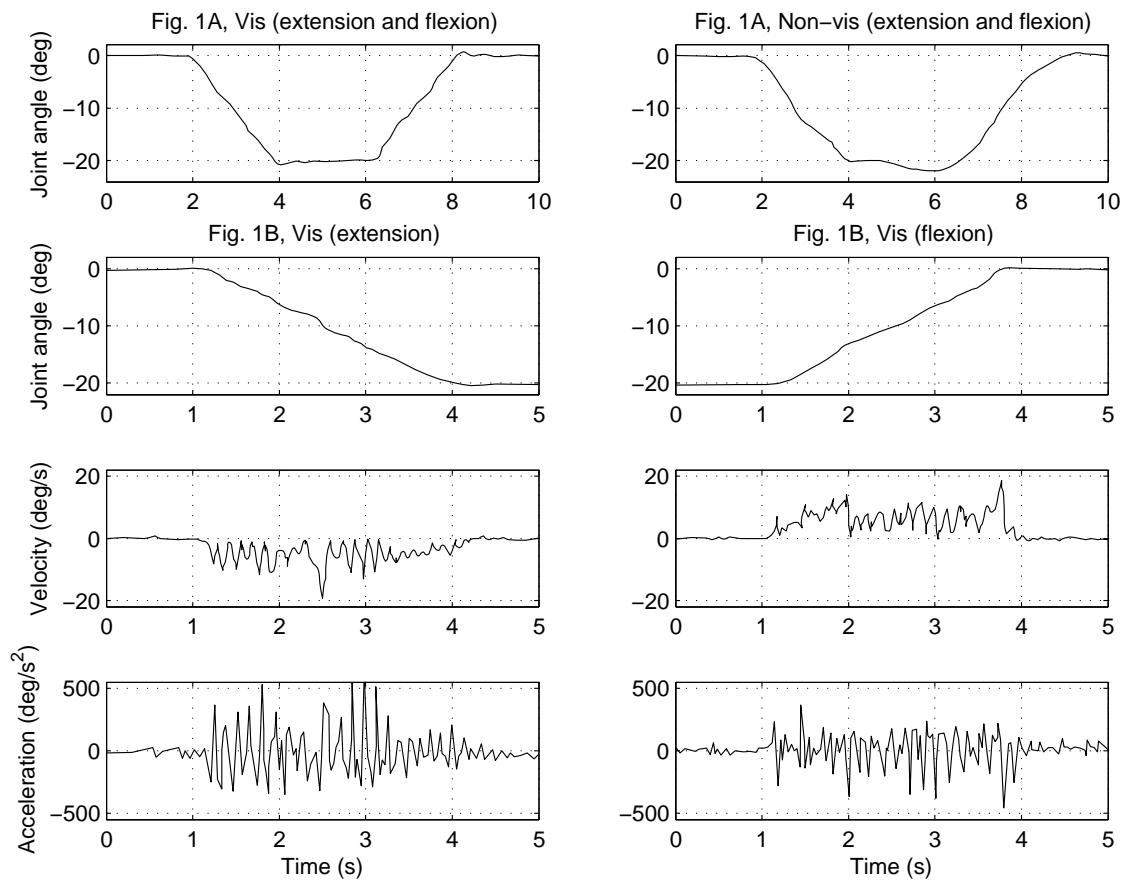


Figure 4.1: Human ramp and hold movements. The top two plots show position records with (left) and without (right) visual feedback (adapted from Fig. 1A, Vallbo & Wessberg, 1993). The remaining six plots show position, velocity, and acceleration records with visual feedback (adapted from Fig. 1B, Vallbo & Wessberg, 1993).

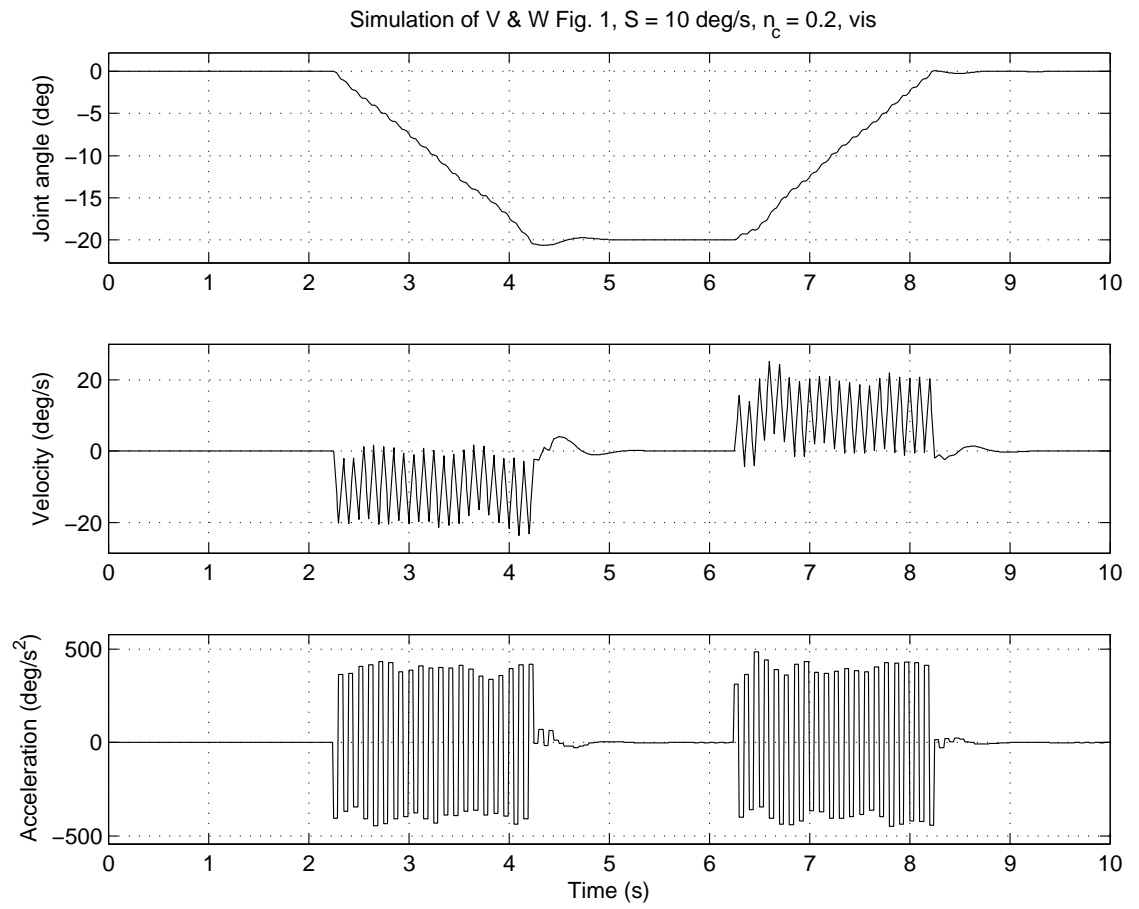


Figure 4.2: Simulated ramp and hold movements with visual feedback.

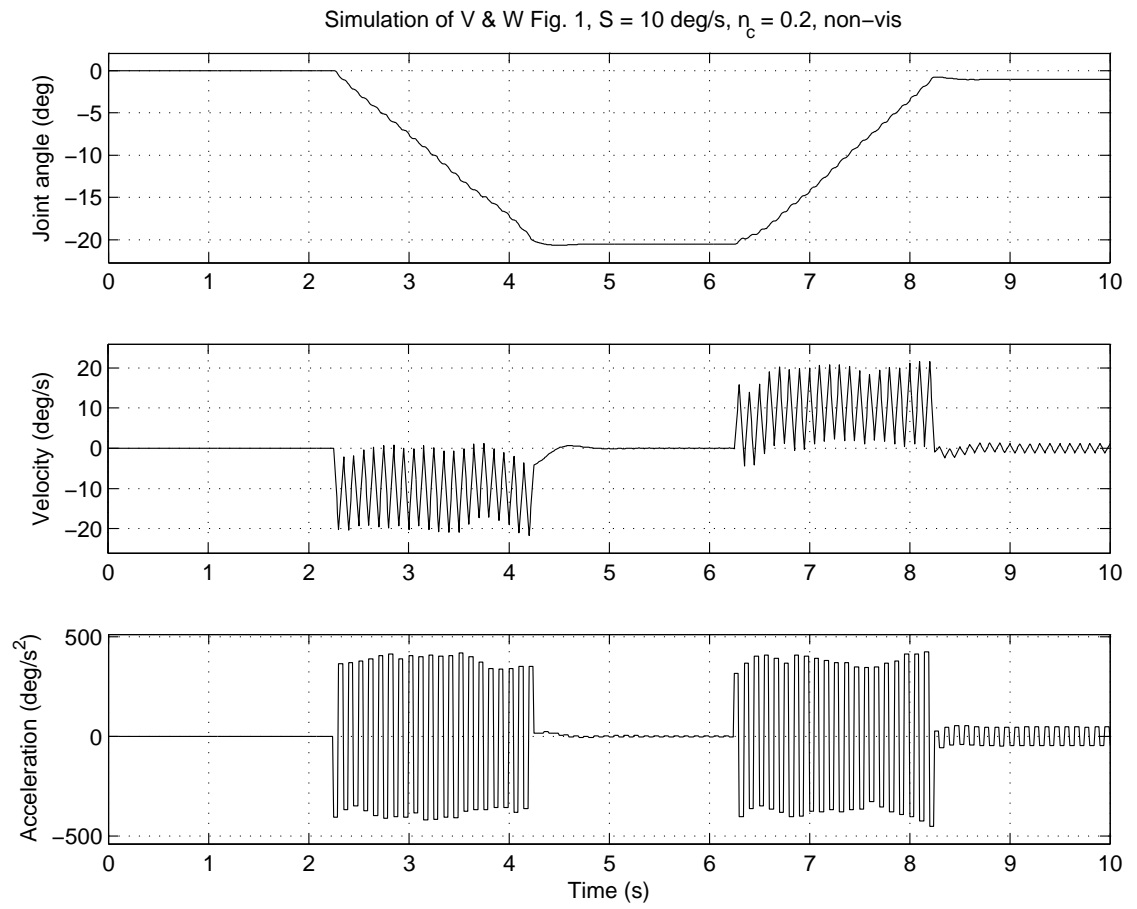


Figure 4.3: Simulated ramp and hold movements without visual feedback.

#### 4.3.2 *Experiment 2*

Fig. 4.6–4.10 show the simulated position, velocity, acceleration, power of acceleration, and power of velocity of ramp movements performed by human subjects M.S. and A.P. as illustrated by Fig. 4.4–4.5 (adapted from Fig. 2–3, Vallbo & Wessberg, 1993). From inspection, the position (Fig. 4.6), velocity (Fig. 4.7), and acceleration (Fig. 4.8) records for the ramp movement signifying the poorly skilled subject A.P. have a low frequency component in addition to the 10 Hz component. However, the power spectrum of acceleration for A.P. (Fig. 4.9) only shows the 10 Hz component. This is due to the acceleration waveform being rectangular at 50 ms intervals. By low-pass filtering the acceleration waveform using a simple 100-tap finite impulse response (FIR) filter before calculating the spectrum, the low frequency component does indeed show up (not shown graphically here). A simpler remedy, however, is to take the power spectrum of the velocity record instead. The power spectra of velocity for the M.S. and A.P. simulations (Fig. 4.10) show that the simulation of a highly skilled subject (M.S.) depicts a very distinguished 10 Hz power peak, while the poorly skilled subject (A.P.) has a low frequency power peak at approximately 2 Hz in addition to the 10 Hz peak. These results match those of Vallbo & Wessberg (1993) shown in Fig. 4.4–4.5.

It is possible to simulate subject A.P. with a range of detuned inverse models that are closer to the ideal, that is, more accurate inverse models. The observed effect of detuning the inverse model is the emergence of the low frequency peak around 2 Hz with gradually increasing power as the model is increasingly detuned. Conversely, gradually increasing the accuracy for the inverse model has the effect that the power of the low frequency peak gradually decreases while the power of the 10 Hz peak gradually increases. Hence, it is possible to obtain a similar range of power spectra (not shown graphically here) as in Fig. 4.5.



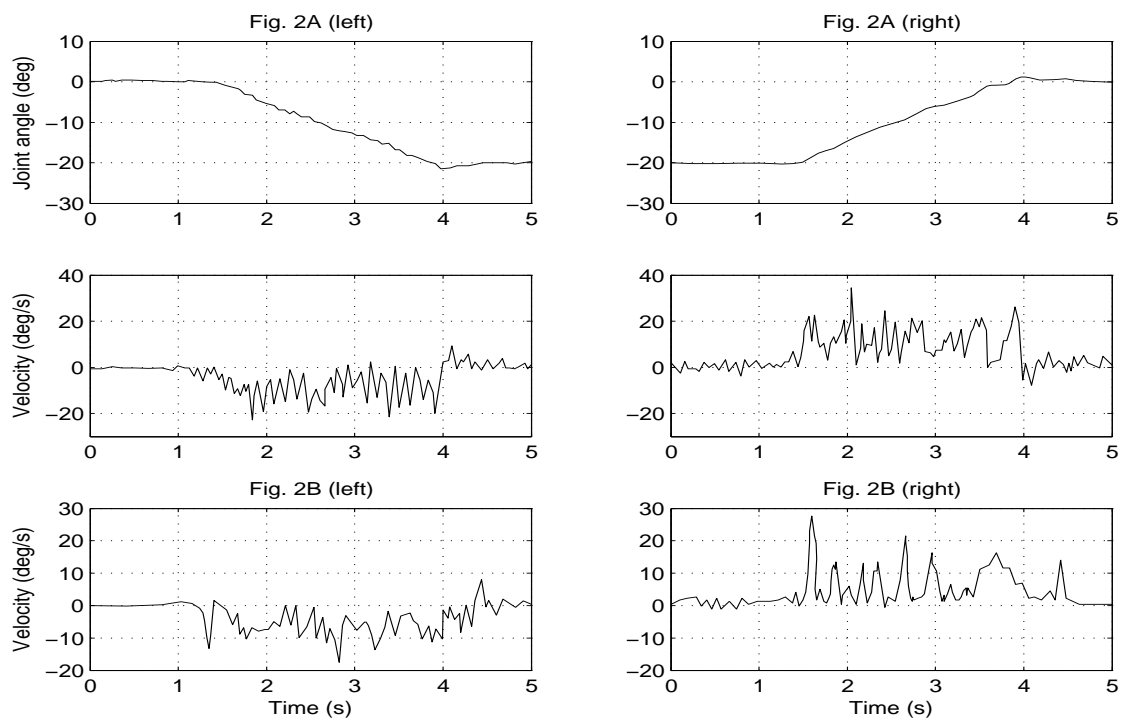


Figure 4.4: Human ramp and hold movements. Position (top) and velocity (middle) records of subject M.S. and velocity records (bottom) of subject A.P. (adapted from Fig. 2, Vallbo & Wessberg, 1993).

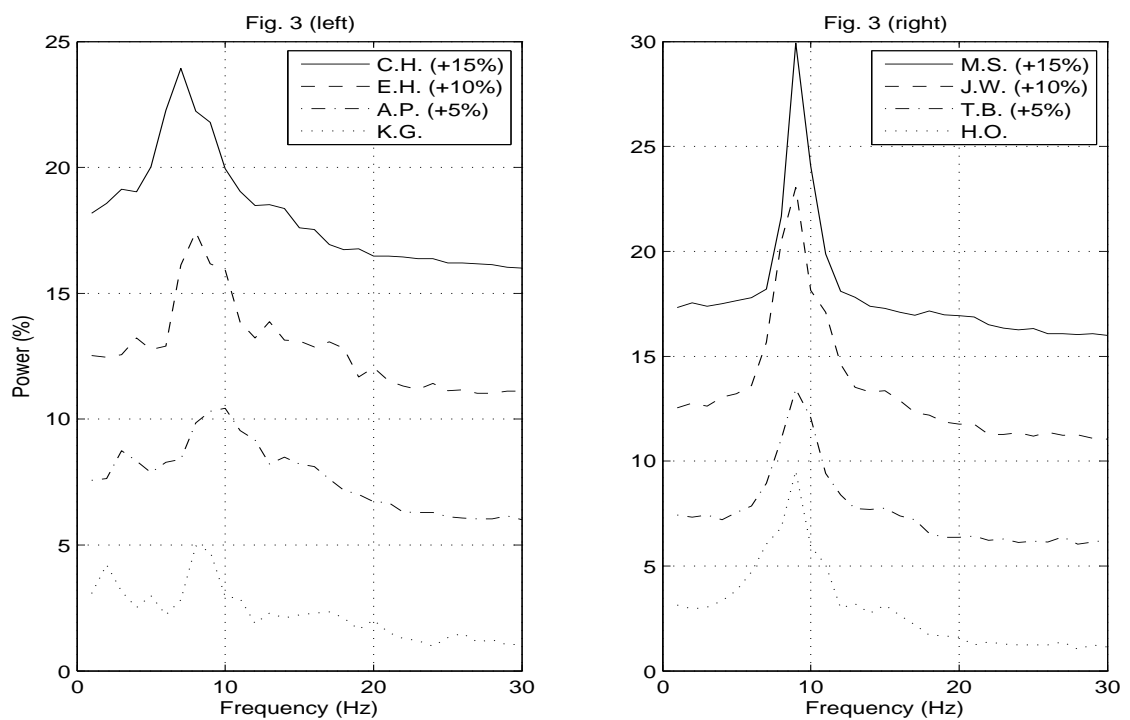
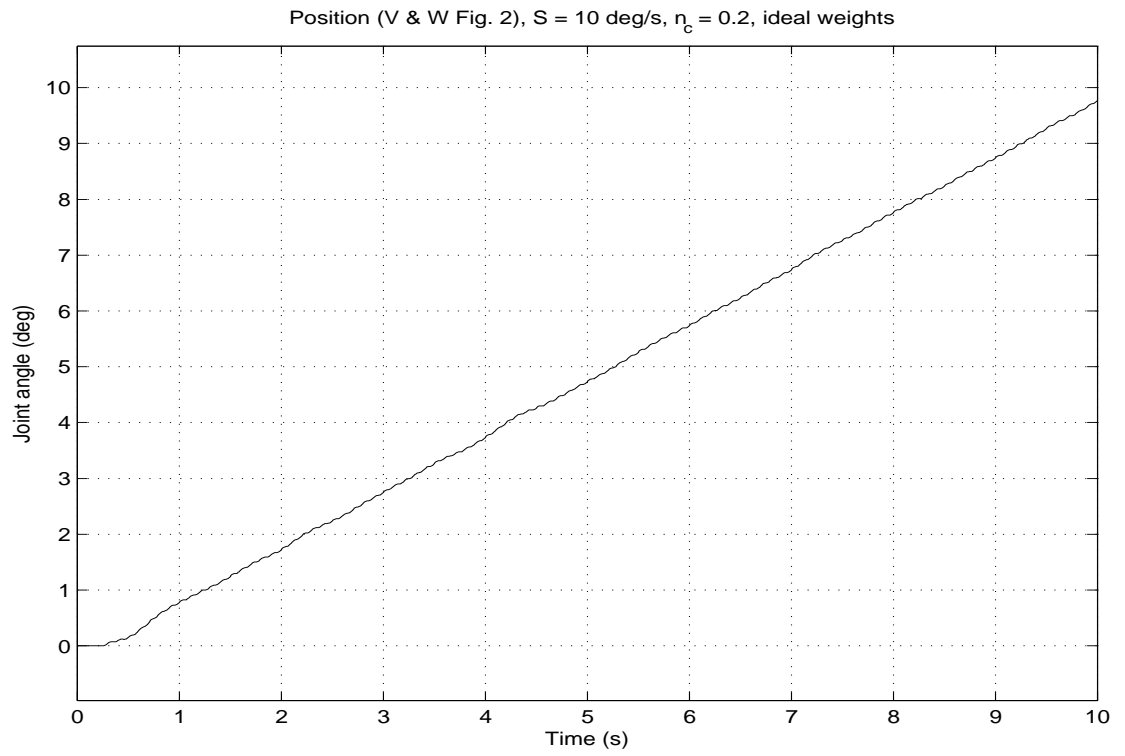
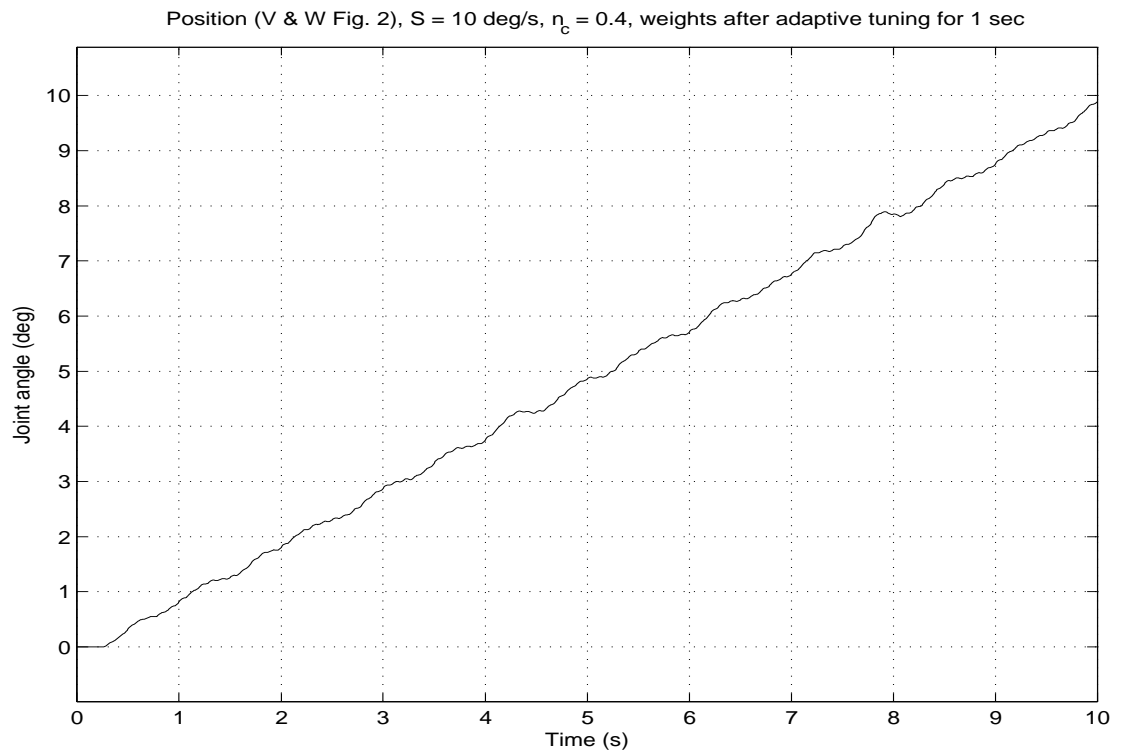


Figure 4.5: Power spectra of acceleration records of eight human subjects. Plots are offset from each other by 5%. Adapted from Fig. 3 of Vallbo & Wessberg (1993).

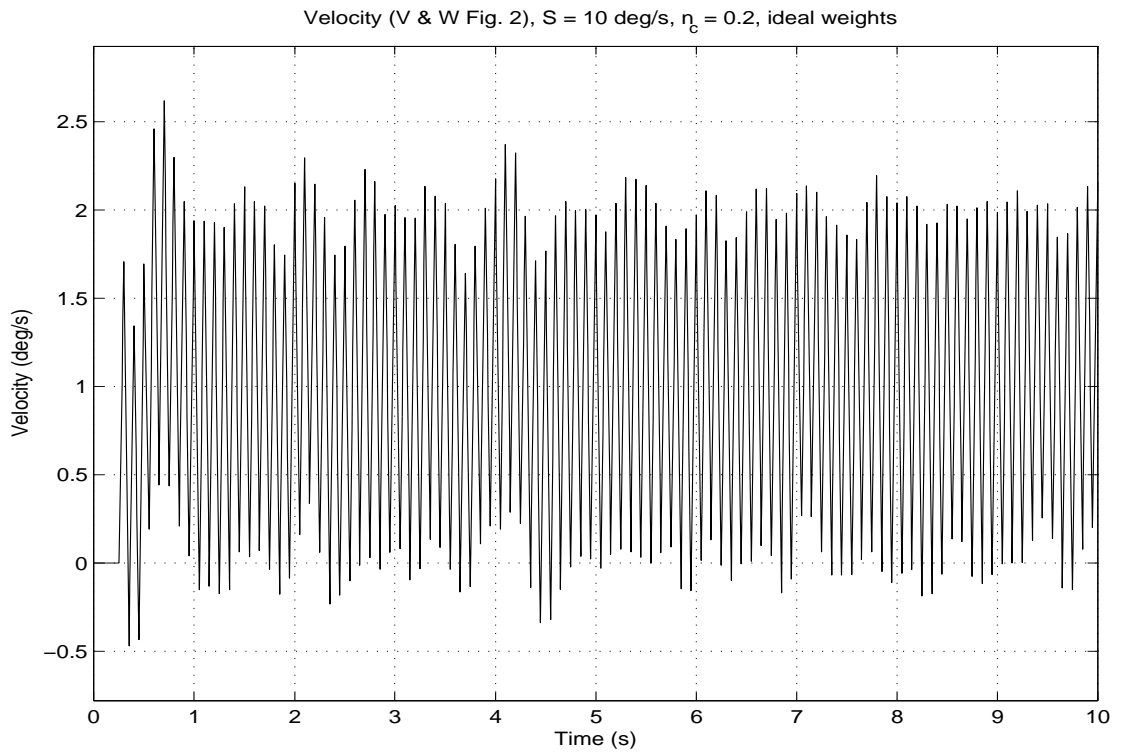


(a) Position (M.S.)

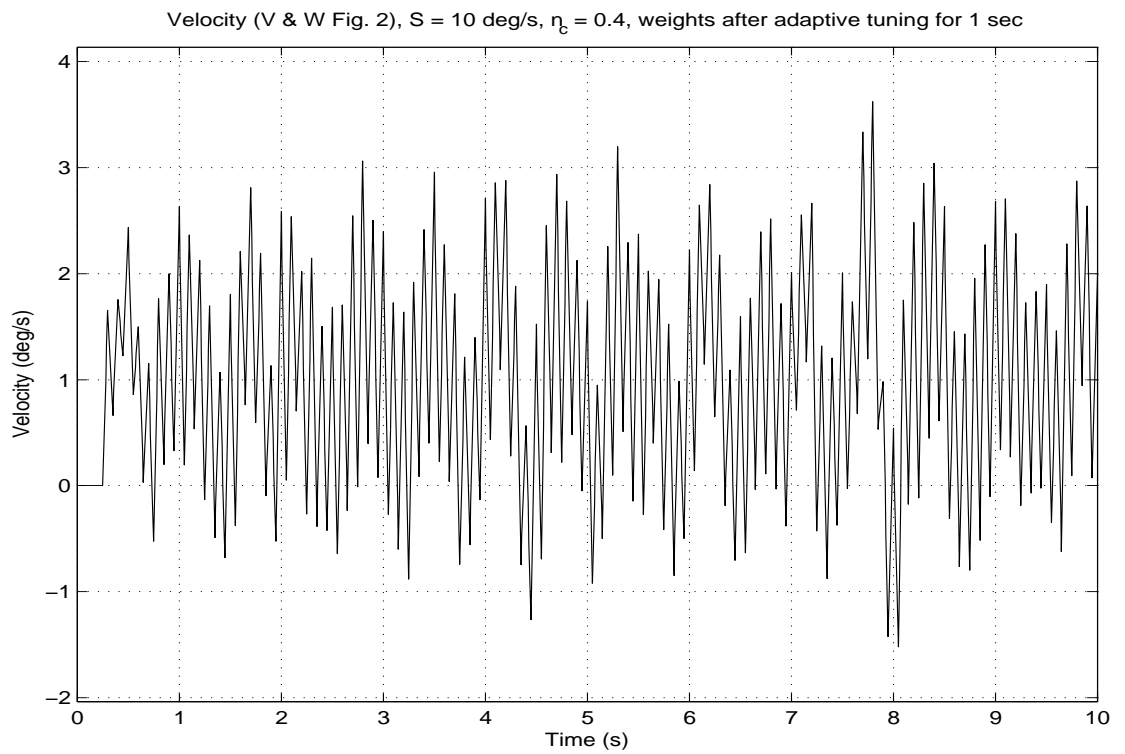


(b) Position (A.P.)

Figure 4.6: Simulated ramp movements performed by subjects (a) M.S. and (b) A.P., position.

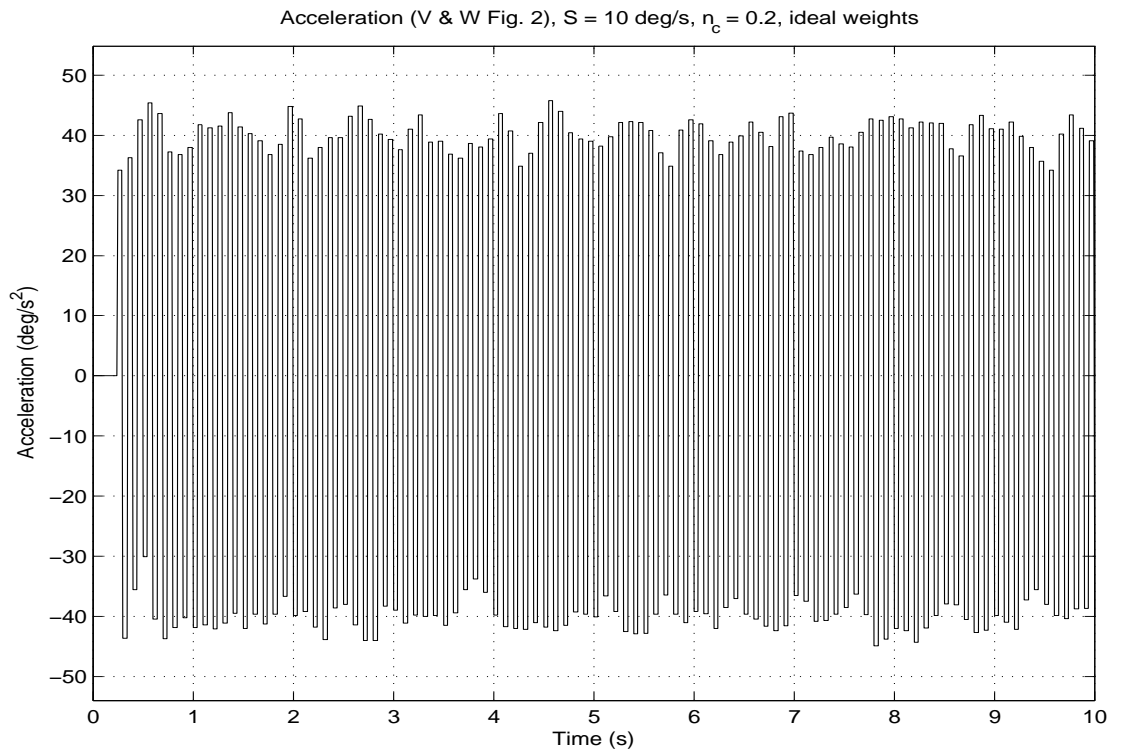


(a) Velocity (M.S.)

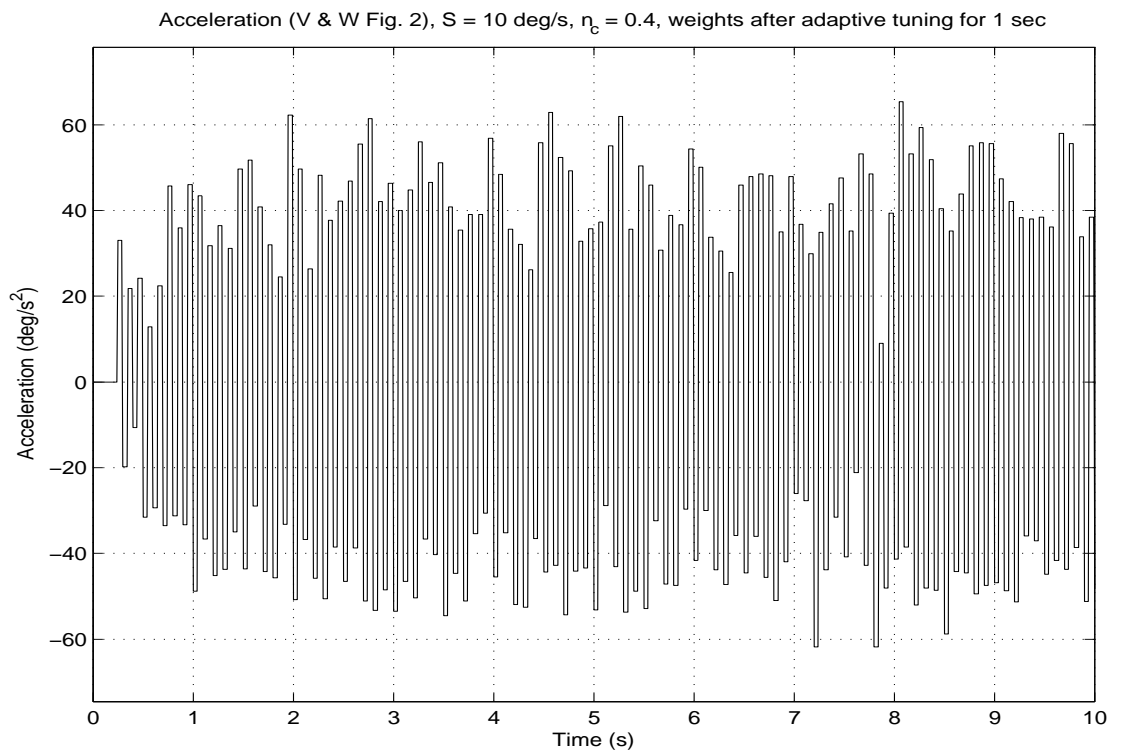


(b) Velocity (A.P.)

Figure 4.7: Simulated ramp movements performed by subjects (a) M.S. and (b) A.P., velocity.

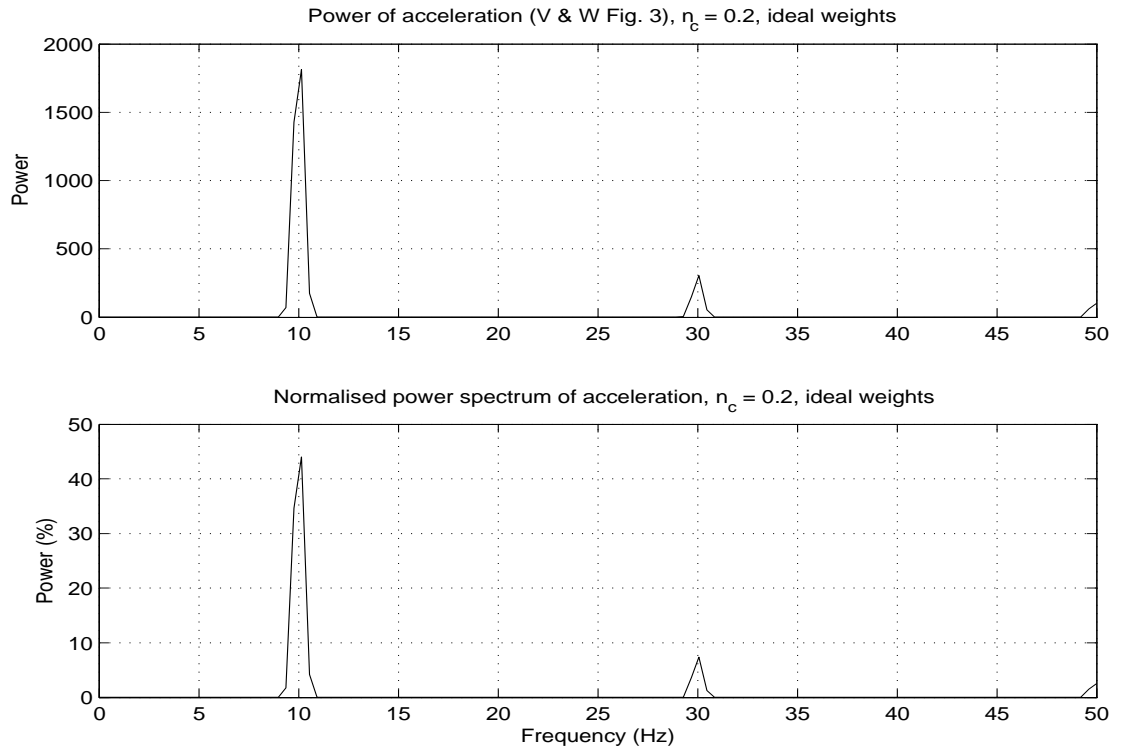


(a) Acceleration (M.S.)

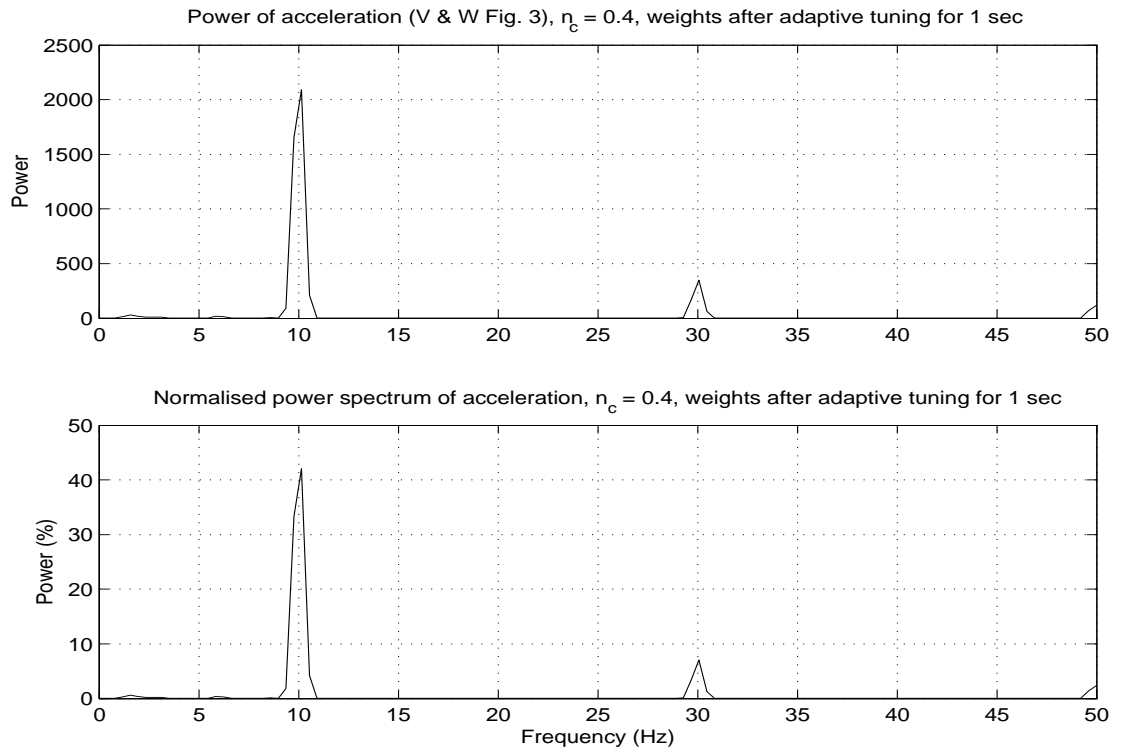


(b) Acceleration (A.P.)

Figure 4.8: Simulated ramp movements performed by subjects (a) M.S. and (b) A.P., acceleration.



(a) Power of acceleration (M.S.)



(b) Power of acceleration (A.P.)

Figure 4.9: Simulated ramp movements performed by subjects (a) M.S. and (b) A.P., power of acceleration.

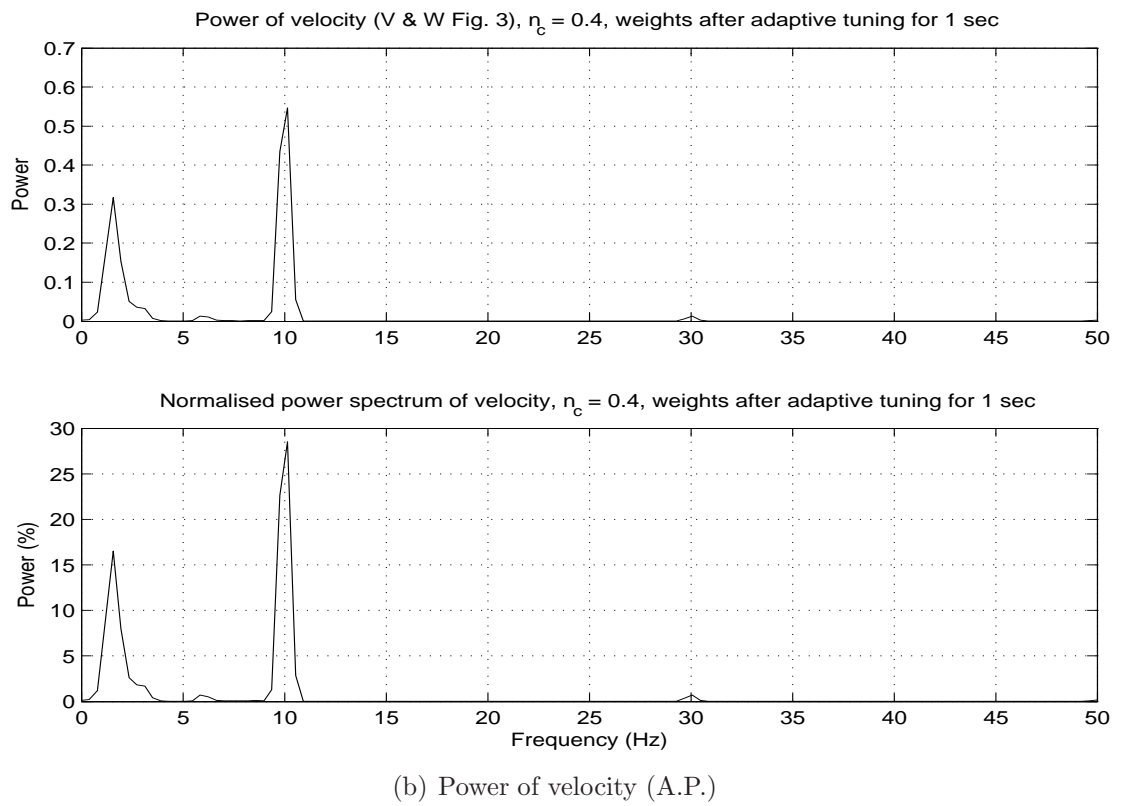
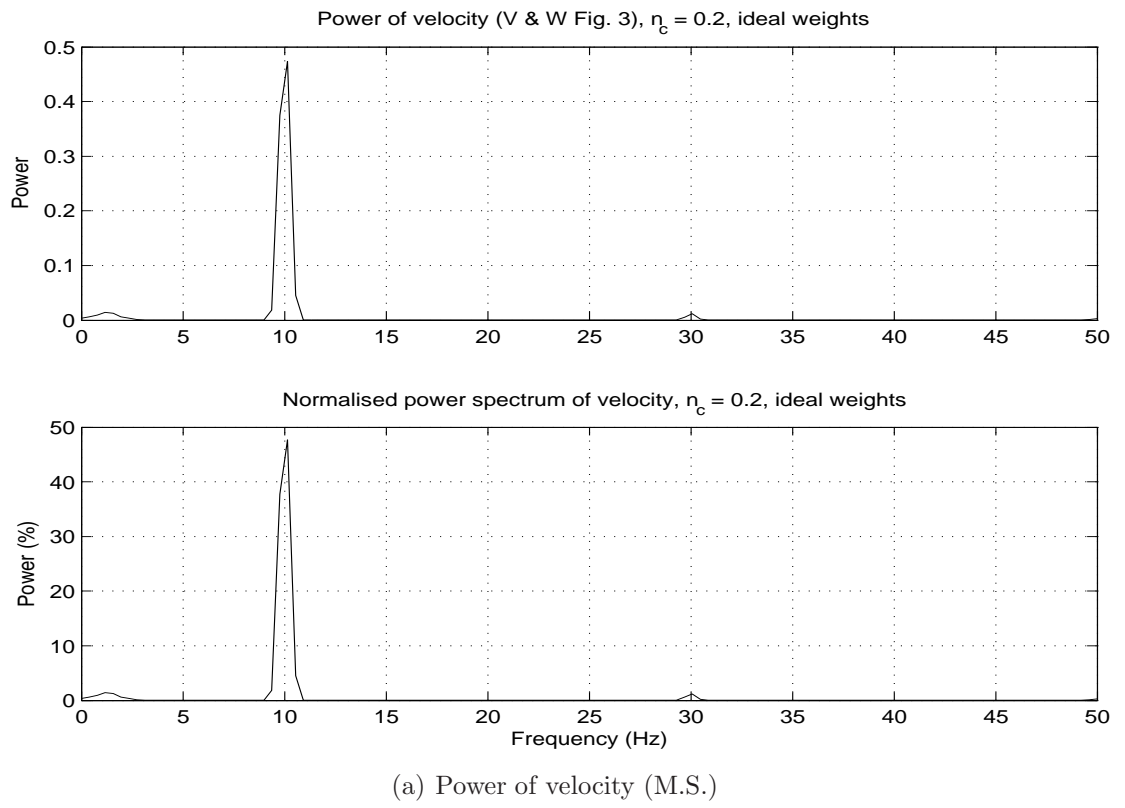


Figure 4.10: Simulated ramp movements performed by subjects (a) M.S. and (b) A.P., power of velocity.

### 4.3.3 Experiment 3

Fig. 4.13 shows the simulated position and velocity records of the four human ramp movements depicted in Fig. 4.11–4.12 (adapted from Fig. 4A of Vallbo & Wessberg (1993)). From inspection, it appears that the amplitude of the simulated position and velocity oscillations increases with the ramp velocity. This impression is verified by Fig. 4.14(a), which shows the position records in Fig. 4.13(a) zoomed-in to a time interval from  $t = 1.25$  to  $t = 1.50$  s and then detrended. It shows that faster ramps have bigger oscillations perpendicular to the direction of movement, which also seems to be the case for the human ramp movements shown in Fig. 4.11–4.12.

Vallbo & Wessberg (1993) mention that “the amplitude [of the individual movement cycle] clustered around 0.4 deg in the slowest movements (track speed 4 deg/s) to about 6 deg in the fastest movements (track speed 62 deg/s).” This is a different kind of amplitude to the one in Fig. 4.14(a). With this statement, Vallbo & Wessberg are referring to the amount by which the joint angle changes for each submovement. Examination of Fig. 4.13 shows that the slowest movement (ramp speed 4 deg/s) moves from zero to 20 deg in 5 s and has approximately 50 submovements. Thus, each submovement constitutes on average a joint angle change of  $20/50 = 0.4$  deg, corresponding to  $1/10$  of the movement made with that ramp speed for one second. The same relationship seems to appear for the other ramp speeds. Indeed, this relationship is verified by the simulation of four ideal (zero noise and ideal inverse model) ramp movements with speeds 4, 10, 25, and 50 deg/s (using 50 deg/s to get an integer number of submovements when moving through 20 degrees) as depicted in Fig. 4.14(b). For any ramp speed, dividing the angular displacement by the number of submovements during a time interval shows that each submovement contributes a joint angle change equal to  $1/10$  of a one-second movement with the corresponding ramp speed, exactly replicating the finding of Vallbo & Wessberg (1993).

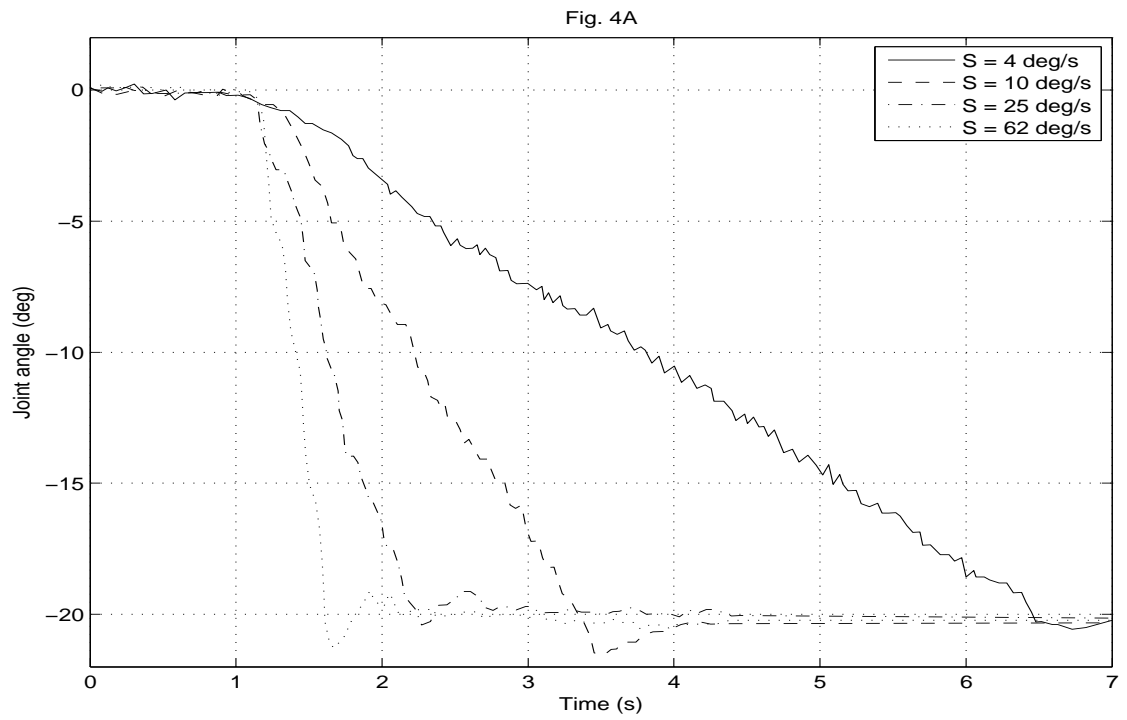


Figure 4.11: Position records for human ramp movements with speeds 4, 10, 25, and 62 deg/s (adapted from Fig. 4A, Vallbo & Wessberg, 1993).

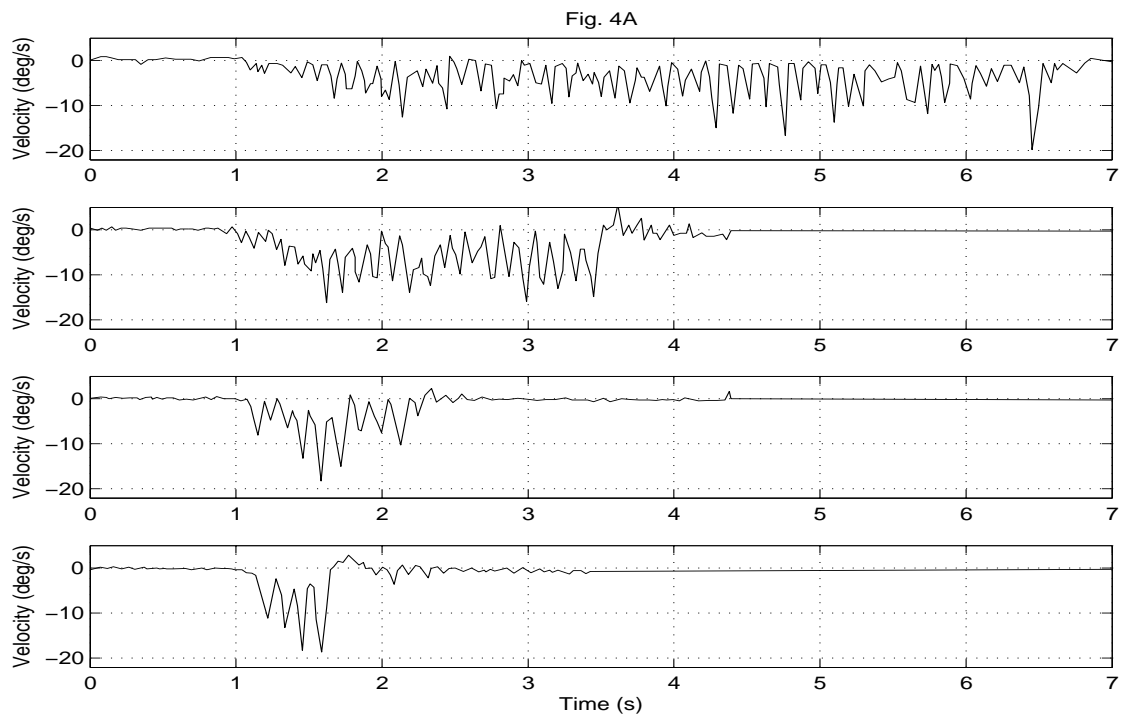


Figure 4.12: Velocity records for human ramp movements with speeds 4, 10, 25, and 62 deg/s (adapted from Fig. 4A, Vallbo & Wessberg, 1993).



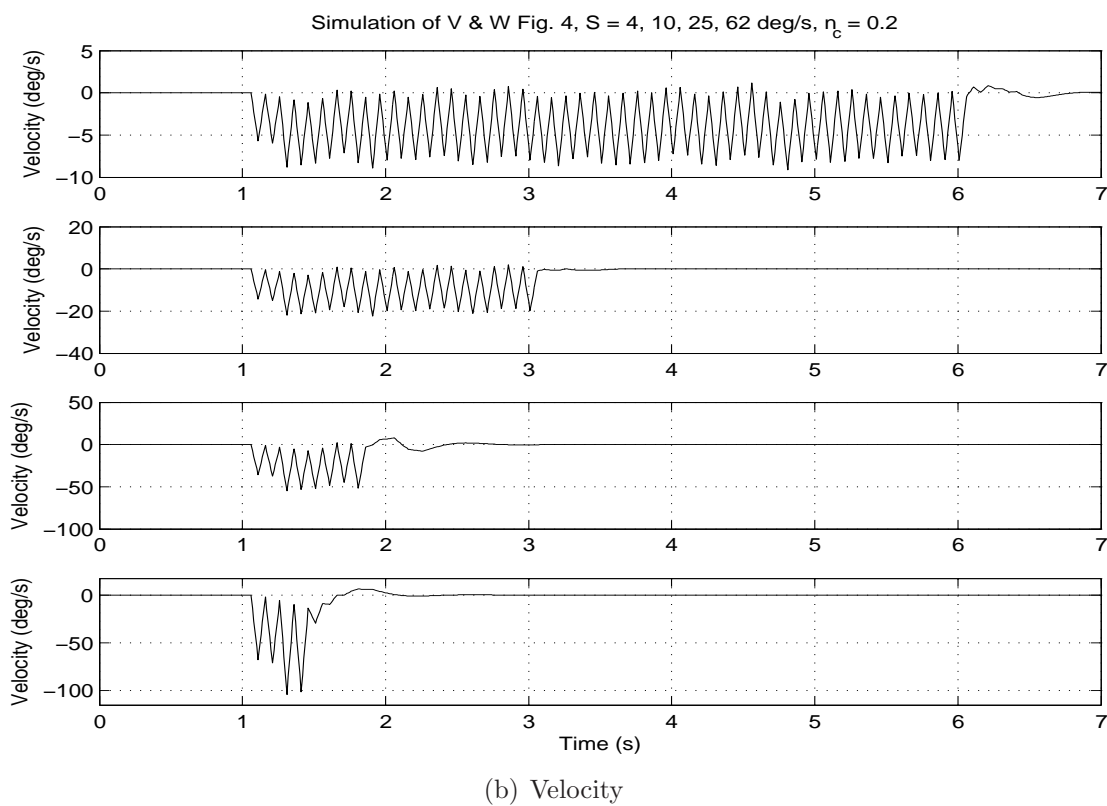
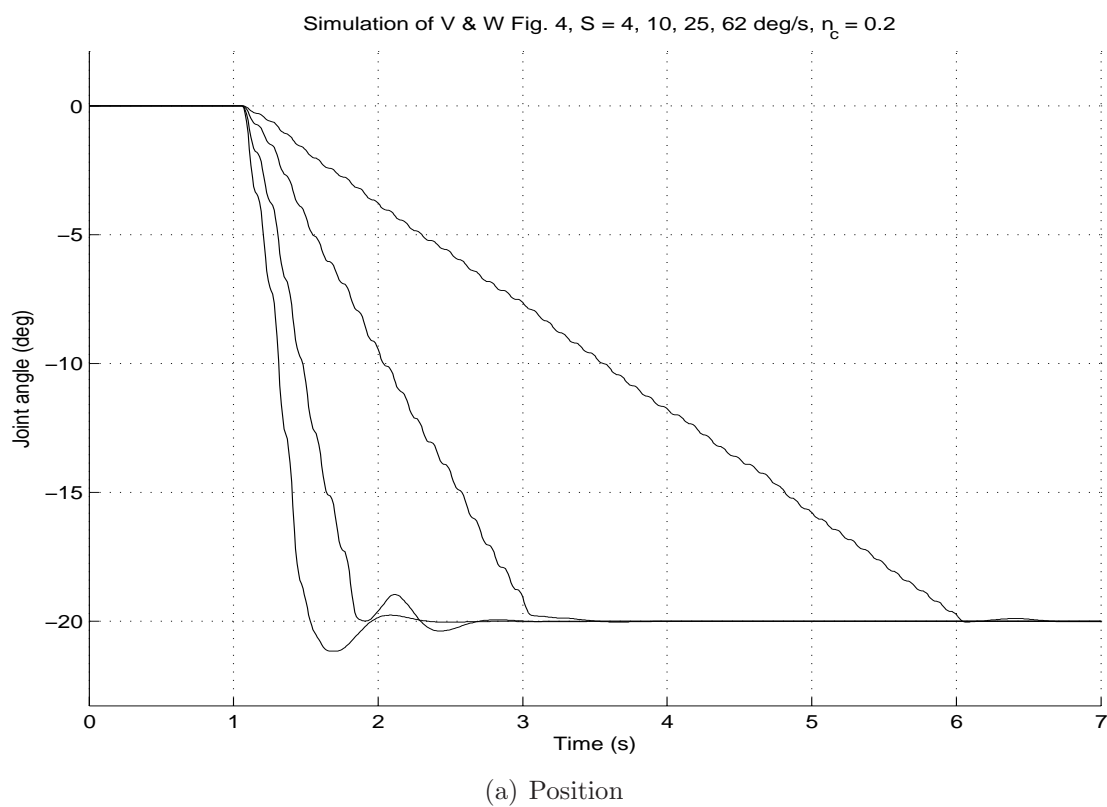
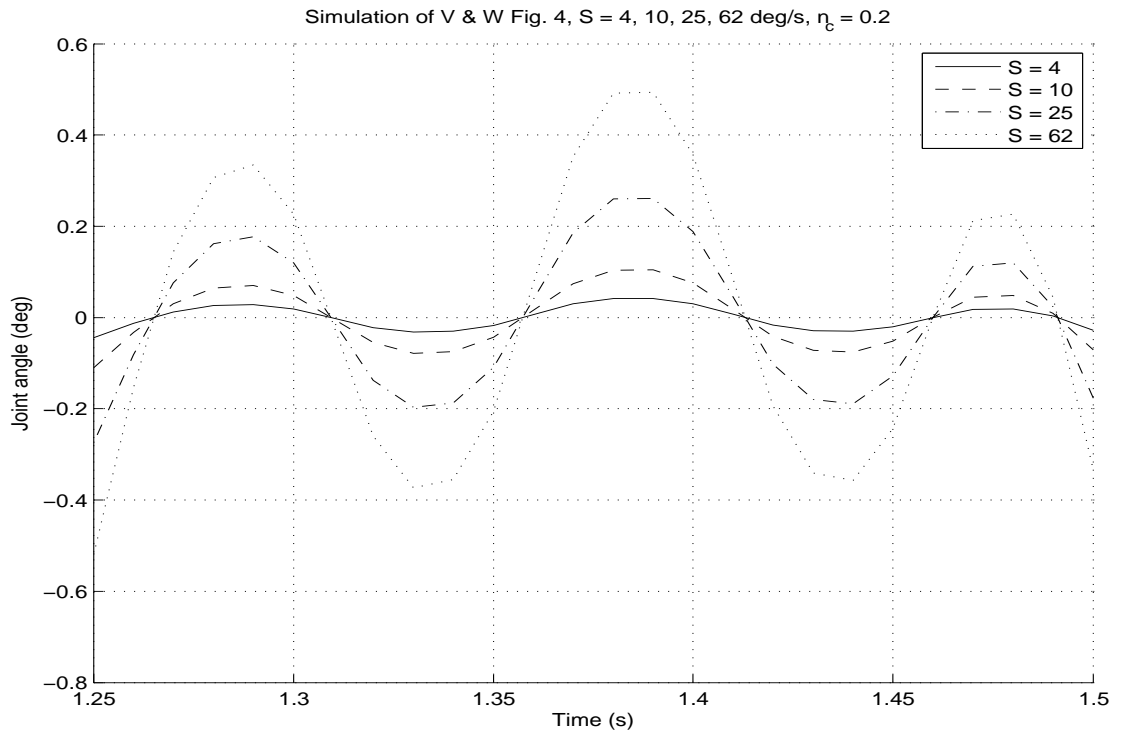
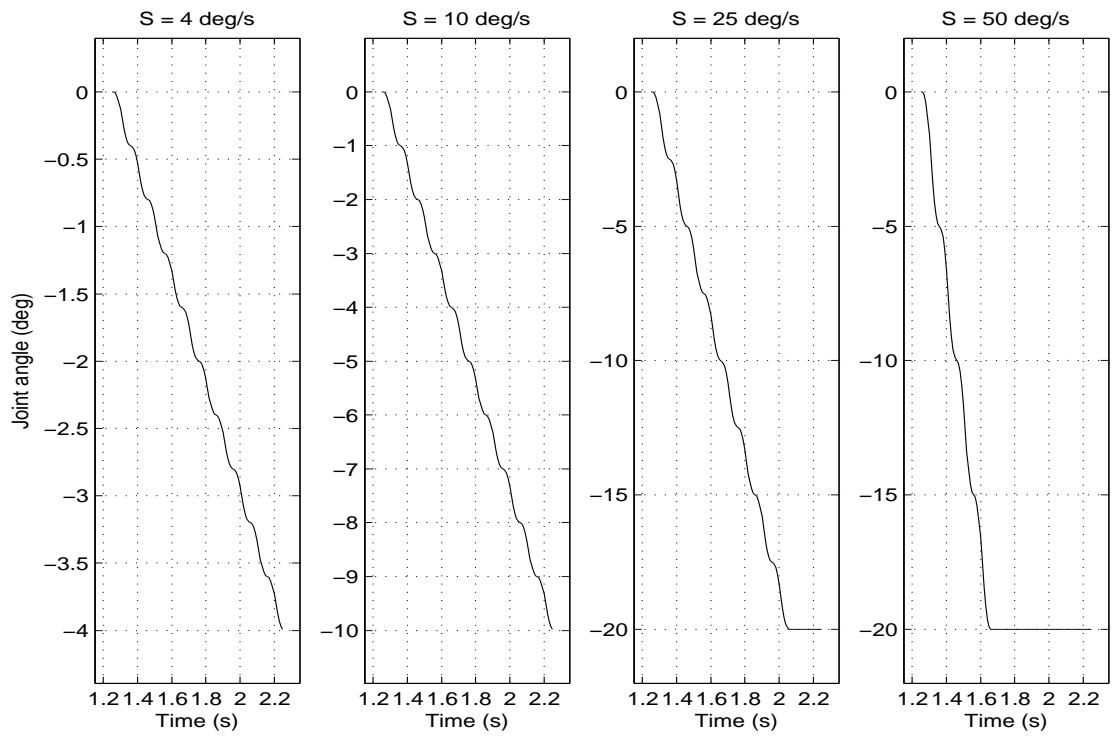


Figure 4.13: Simulated ramp movements with speeds 4, 10, 25, 62 deg/s.



(a)



(b)

Figure 4.14: Amplitude of submovements increases with ramp speed. (a) Position records of Figure 4.13(a) zoomed-in and detrended. (b) Position records of ideal ramp movements ( $n_c = 0$ ) with speeds 4, 10, 25, 50 deg/s, zoomed-in.

#### 4.3.4 *Experiment 4*

Fig. 4.17–4.19 show the simulated position, velocity, and power of velocity records for ramp movements with and without visual feedback performed by human subject K.G. as depicted in Fig. 4.15–4.16 (adapted from Fig. 5, Vallbo & Wessberg, 1993). Fig. 4.17–4.18 show that the simulated ramp movement performed without visual feedback is much smoother than the one performed with visual feedback. The same finding is observed for the human ramp movements in Fig. 4.15. Moreover, Fig. 4.19 shows that the low frequency component at  $\sim 2$  Hz has halved, from about 16% to 8% (normalised power), due to the inclusion of visual feedback. This is a reduction of exactly the same magnitude as that of the human subject in Fig. 4.16, where normalised power was reduced from 8% to 4% when allowing visual feedback.

#### 4.3.5 *Conclusions*

The results presented above show that the simulator consistently reproduced the human experiments of Vallbo & Wessberg (1993). All simulated ramp movements had a dominant 10 Hz peak in their velocity profiles. In addition, detuning the inverse model, thus simulating a less skilled subject, led to the emergence of a low frequency component around 2 Hz. The normalised power of this component was approximately doubled by the inclusion of visual feedback. The step size, or angular displacement, of each submovement increased linearly with ramp speed. Varying ramp speed, each submovement consistently contributed a joint angle change equal to 1/10 of a one-second movement, reflecting a 10 Hz tremor independent of ramp speed. The simulator's ability to reproduce human ramp movements performed both with and without visual feedback, at different speeds, and by subjects with different skill levels provides strong support to the BUMP model of response planning and the corresponding hypotheses presented in this thesis.

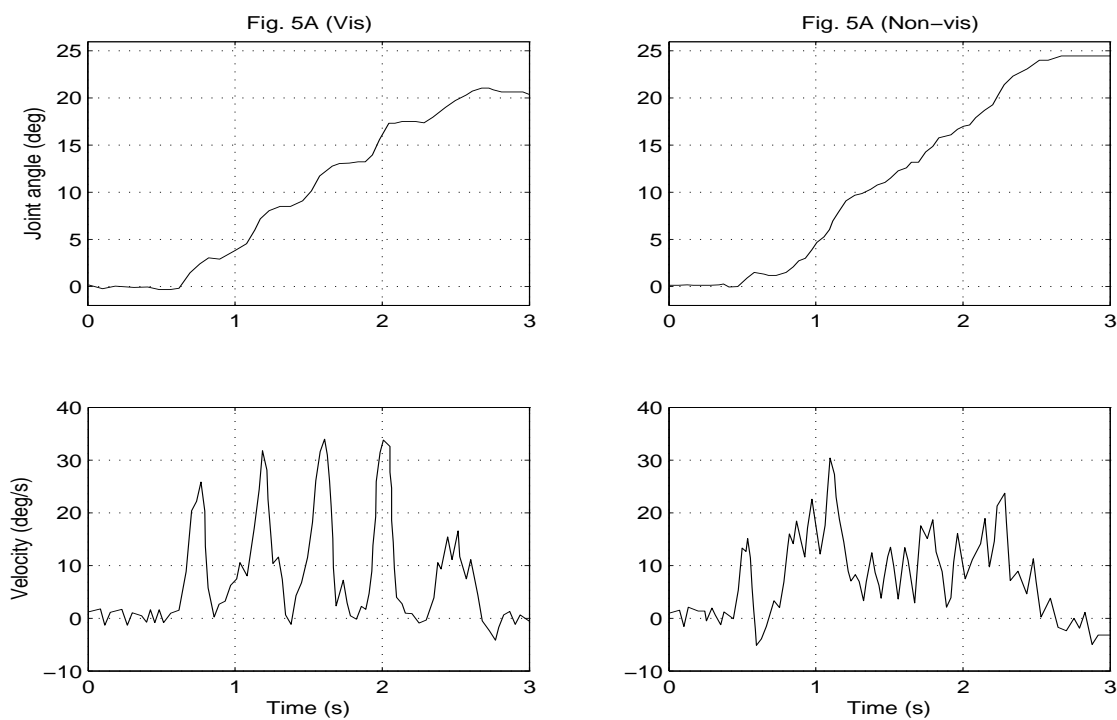


Figure 4.15: Position and velocity records from human ramp movements performed by K.G. with and without visual feedback (adapted from Fig. 5A, Vallbo & Wessberg, 1993).

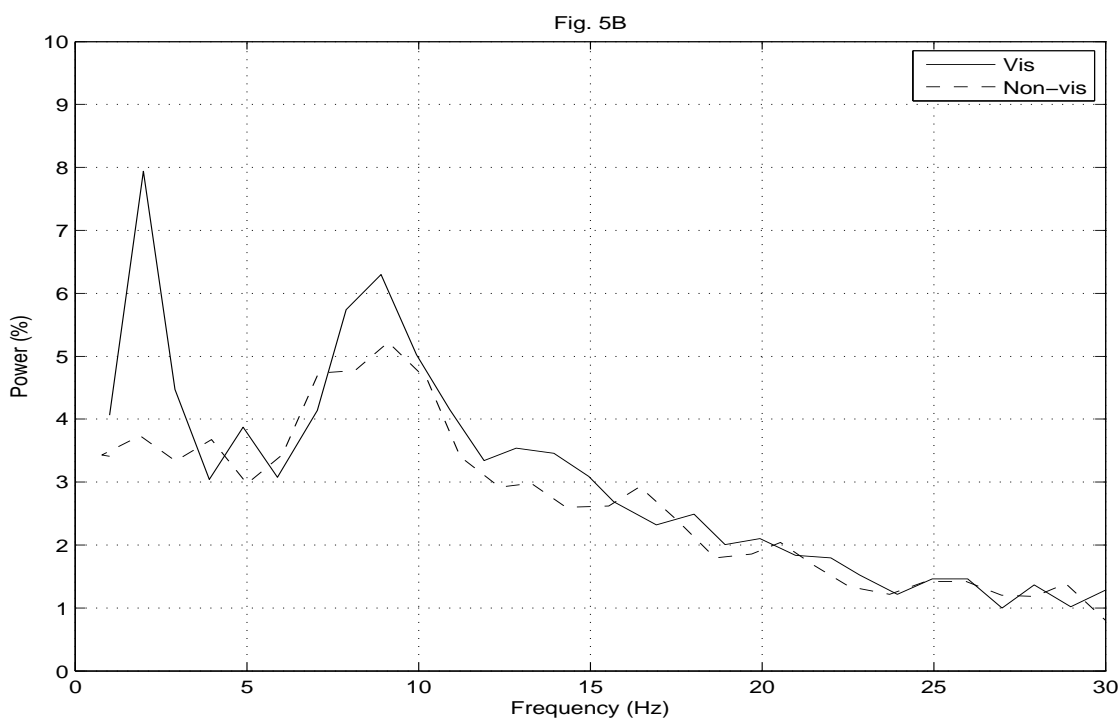
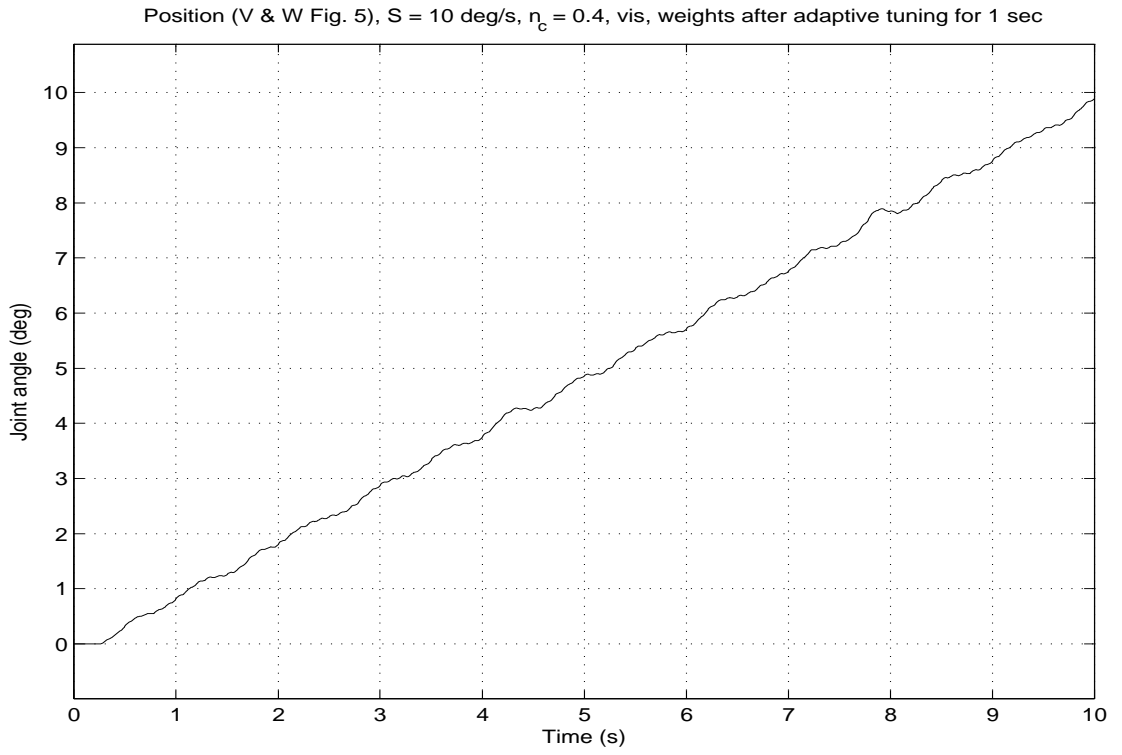
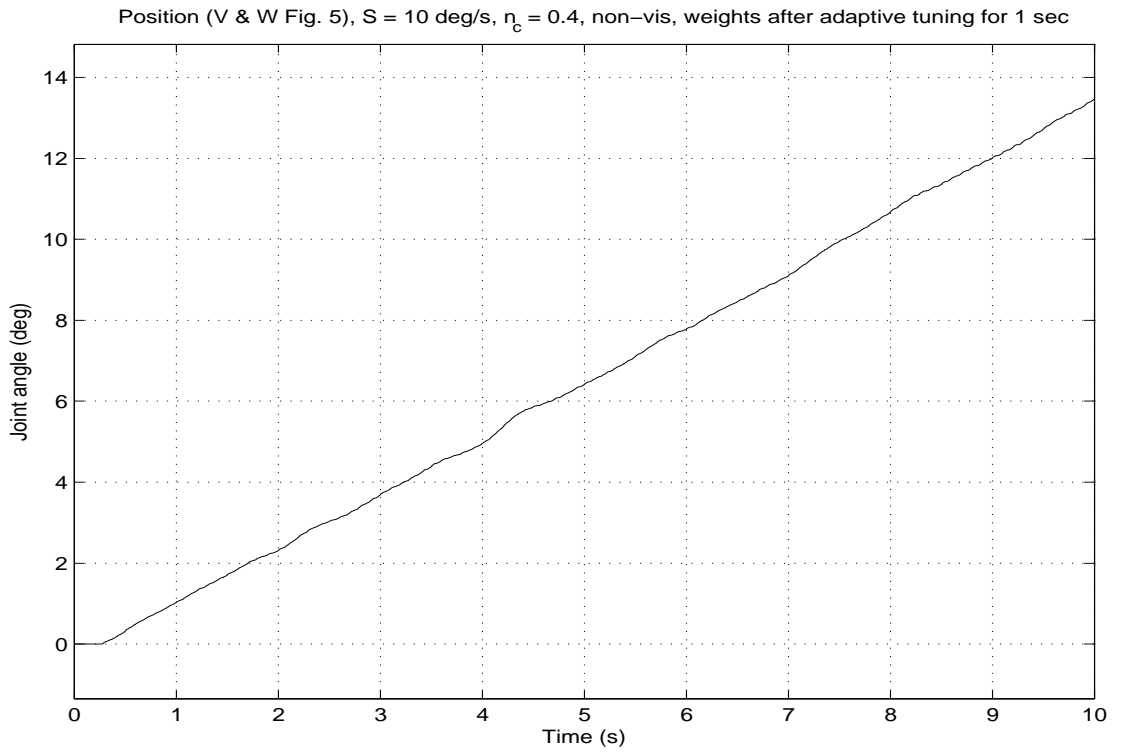


Figure 4.16: Power spectra from human ramp movements performed by K.G. with and without visual feedback (adapted from Fig. 5B, Vallbo & Wessberg, 1993).

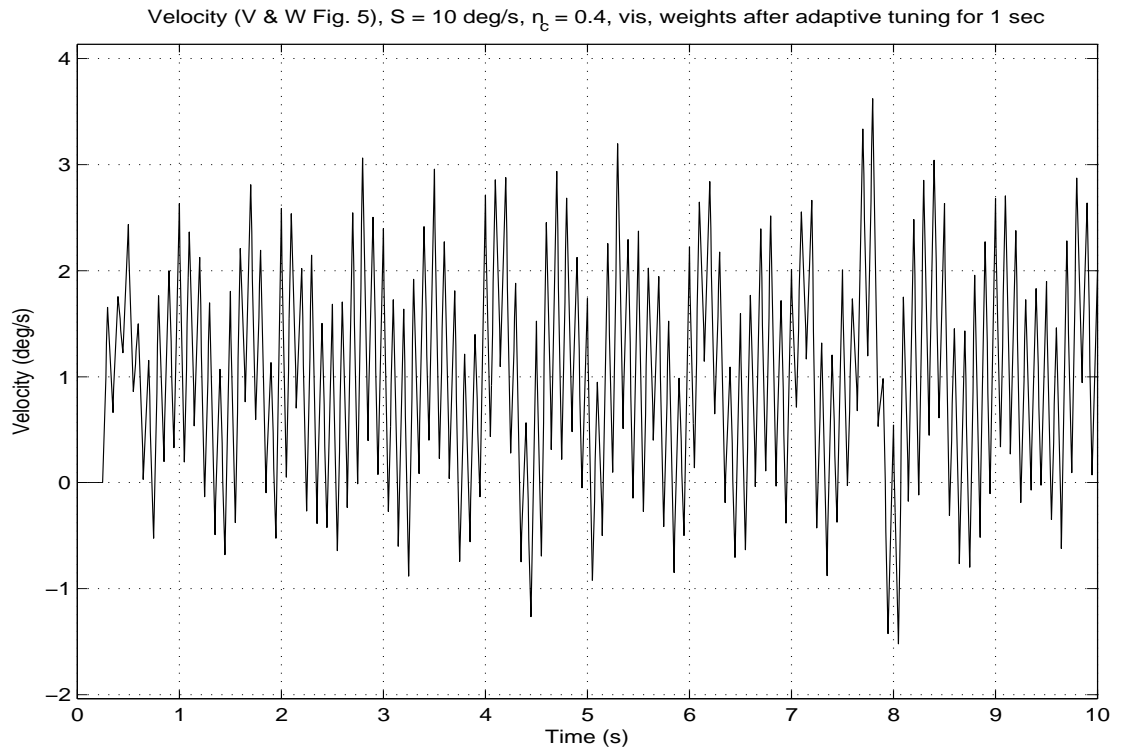


(a) Position (visual)

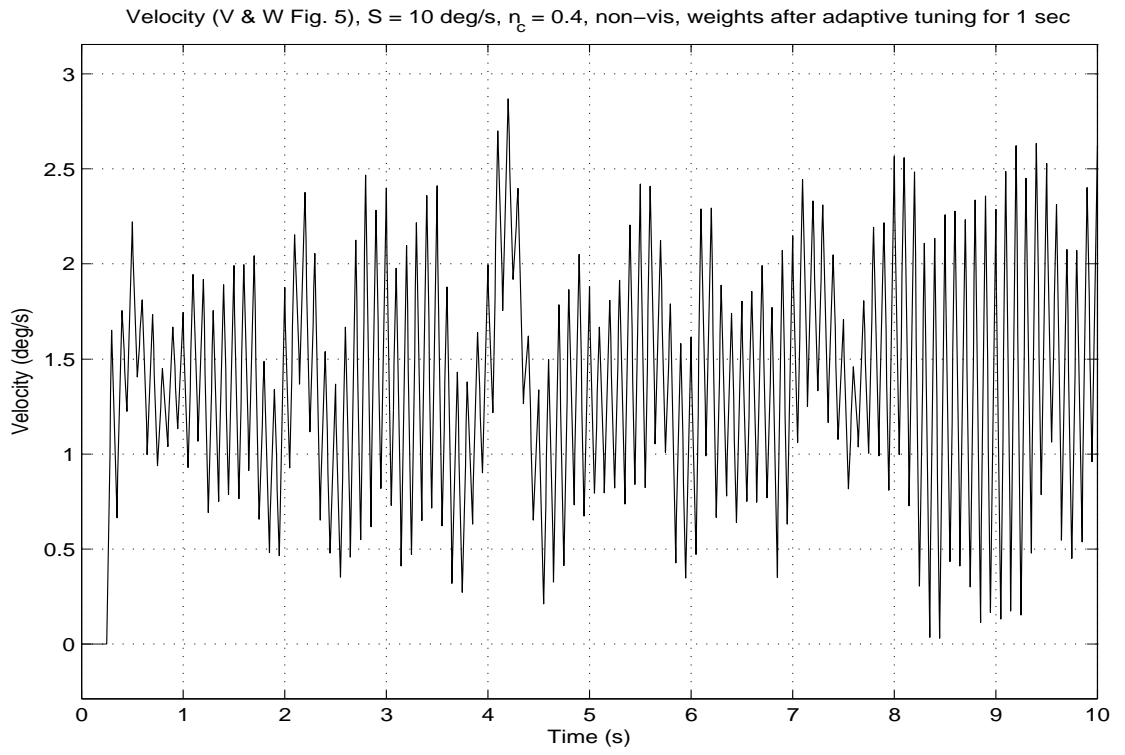


(b) Position (non-visual)

Figure 4.17: Simulated ramp movements performed by subject K.G., position.



(a) Velocity (visual)



(b) Velocity (non-visual)

Figure 4.18: Simulated ramp movements performed by subject K.G., velocity.

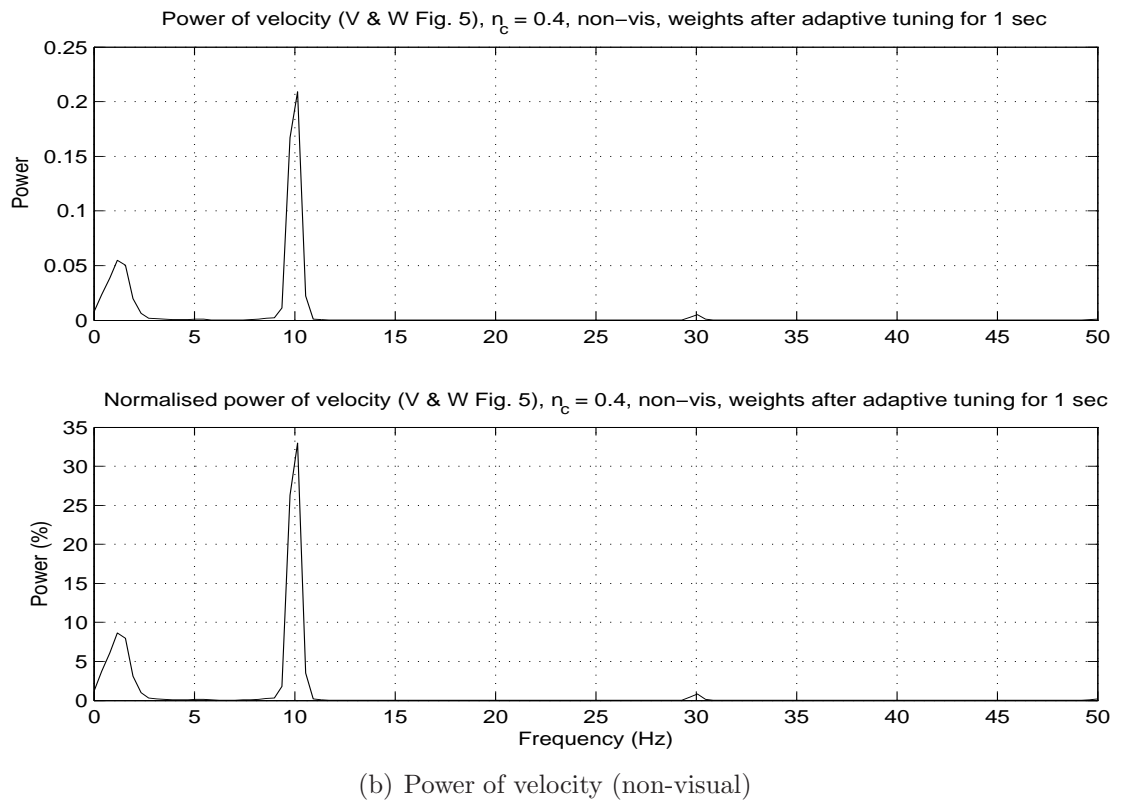
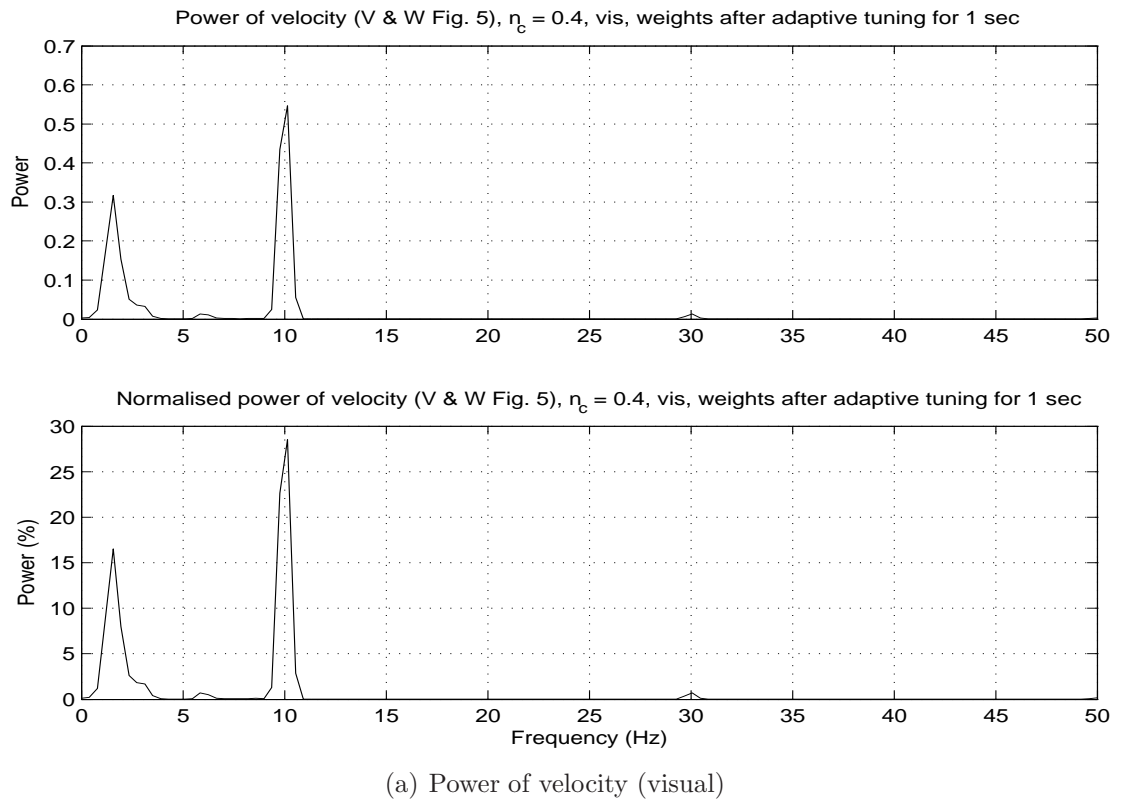


Figure 4.19: Simulated ramp movements performed by subject K.G., power of velocity.

## 4.4 Discussion

The results of the simulation experiments in Chapter 4.3 show that the simulated implementation of the BUMP model reproduces the experimental results of Vallbo & Wessberg (1993). Using a receding horizon control strategy, the duration of the preplanned optimal trajectory  $R^*$  generated at every RP interval is kept constant. This duration is referred to as the prediction horizon  $T_h$  and is set to 100 ms for all simulations. The duration of the planning interval is referred to as  $T_p$  and is fixed at 100 ms. Because each optimal response is generated to minimise acceleration it will have an S-shaped position trajectory. The resulting overall movement will be non-smooth, consisting of a concatenated sequence of S-shaped submovements, or BUMPs, dispersed at 100 ms intervals. These oscillations are observed in the overall movement trajectory at a rate inversely related to  $T_p$ , namely 10 Hz. The simulation results suggest that such an intermittent optimal control scheme through sequential operation of BUMPs is a fundamental mechanism of 10 Hz physiological tremor in movement.

### 4.4.1 *Velocity of movements*

Vallbo & Wessberg (1993) found that the 8–10 Hz frequency of discontinuities in ramp movements were independent of ramp speed. Moreover, Vallbo & Wessberg showed that the amplitude, or step size, of each movement cycle increased linearly with ramp speed. For example, with a ramp speed of 4 deg/s, each cycle contributed approximately 0.4 deg, while with a ramp speed of 10 deg/s, each cycle contributed approximately 1 deg. These findings of Vallbo & Wessberg are illustrated in Fig. 4.11–4.12 and are reproduced by the simulator. The simulated results, depicted in Fig. 4.13–4.14, show that ramp movements of varying speed are composed of submovements with a fixed duration of 100 ms, corresponding to a tremor rate of 10 Hz. Moreover, the step size of each submovement varies linearly with ramp speed. Just like the human experiment, small variations of the step size may occur due to motor noise and an inaccurate inverse model. However, on average, each submovement moves through the same angle as did the human



subjects of Vallbo & Wessberg, namely 1/10 of a one-second ramp movement. In fact, Fig. 4.14(b) shows that by switching off motor noise and using an ideal inverse model, the simulator reproduces this relationship between angular displacement of submovements and ramp speed exactly.

#### *4.4.2 Visual feedback and skill level*

The study of Vallbo & Wessberg (1993) found that visual feedback in some cases promoted 2–3 Hz discontinuities, particularly for subject K.G. Fig. 4.15–4.16 shows the joint angle and velocity records as well as power spectra from ramp movements performed by K.G. with and without visual feedback. With visual feedback, a low frequency component is clearly visible as steps in the movement trajectory, whereas the trajectory is considerably smoother without visual feedback. The power spectra quantify this observation and show that a distinct 2–3 Hz peak with even more power than the 10 Hz peak dominate the power spectrum for records with visual feedback, whereas without visual feedback, the magnitude of the 2–3 Hz peak is halved.

Vallbo & Wessberg (1993) reported that the occurrence of 2–3 Hz cycles was inconsistent across subjects and varied considerably. This is reflected in Fig. 4.5, which shows the power spectra of eight subjects, ranging from subject K.G. to M.S. Whereas M.S. has a narrow and distinct 10 Hz peak, K.G. has a 10 Hz peak that has less power and is wider than that of M.S. In addition, K.G. has a significant low frequency peak at 2–3 Hz. In between these two subjects, the power spectra for the other subjects all have a 10 Hz peak that is wider and of less power than M.S. but more distinct and with more power than K.G. Moreover, the 2–3 Hz component is also clearly visible for subject A.P. but decreases or vanishes for subjects whose 10 Hz peak is narrower and of more power than that of K.G.

Vallbo & Wessberg (1993) did not provide much information about the skill-level or preferred hand of their subjects. Their main concern was with demonstrating that 8–10 Hz discontinuities occur independent of factors such as visual feedback, skill level, or handedness, not with the potential dependence of the 2–3 Hz low

frequency component on such factors. Nevertheless, it is possible to speculate on the latter given the information available. M.S. was a semi-professional cellist and used her preferred hand for the experiments, whereas C.H. used her non-preferred hand and claimed poor manual skill. Examination of Fig. 4.5 shows that the power spectra of C.H. is “mid-range” compared with the power spectra of the other seven subjects, with a 10 Hz peak broader and of less magnitude than four other subjects, and a 2–3 Hz component smaller than three other subjects. As mentioned above, M.S. represents one end of the power spectrum range, while K.G. represents the other. It may be inferred that high skill level and using the preferred hand (e.g., M.S.) enhances the 10 Hz power peak while repressing the 2–3 Hz peak. It may also be inferred, although slightly more speculatively, since no information about skill level and handedness is given for K.G., that low skill level enhances the 2–3 Hz peak while reducing the power of 10 Hz peak.

Moreover, although not stated explicitly by Vallbo & Wessberg (1993), it appears that Fig. 4.5 displays the average spectra of ramp movements both with and without visual feedback. This can be deduced from a comparison of the power spectrum of K.G. in Fig. 4.5 with her two power spectra (with and without visual feedback) in Fig. 4.16. As a result, a potential 2–3 Hz component promoted by unskilled subjects with visual feedback will be camouflaged in Fig. 4.16 from the averaging effect of including spectra without visual feedback.

Simulations of subjects M.S., A.P., and K.G. requires an adaptation paradigm (see Neilson & Neilson, 2005b, for further details on adaptation). Replacing the ideal inverse model with a highly inaccurate one, the model is allowed to converge while the simulator tracks a training signal. Interrupting the training process before the model has fully converged results in an inaccurate, or detuned, model. Early interruption yields a highly detuned model corresponding to an unskilled subject with little practice, while late interruption yields a more accurate model corresponding to a more skilled subject that has practiced more. Here, M.S. is simulated with an ideal inverse model (no adaptation process needed), whereas A.P. and K.G.

are assigned a highly detuned inverse model obtained from an adaptation process. The results from Experiment 2 (Fig. 4.6–4.10) and Experiment 4 (Fig. 4.17–4.19) show that the BUMP model simulator is able to closely reproduce the actual ramp movements and power spectra of M.S., A.P., and K.G. shown in Fig. 4.4–4.5 and Fig. 4.15–4.16. Like the experiments by Vallbo & Wessberg (1993), the results suggest that 10 Hz discontinuities occur in movements independent of visual feedback or skill level. In addition, but with more speculative support from the experiments by Vallbo & Wessberg, the simulated results indicate that unskilled subjects will also display a low frequency power peak at 2–3 Hz. This peak is promoted by visual feedback and is halved in power from removing visual feedback.

#### *4.4.3 Bandwidth of tremor*

By turning off the noise generator during simulation of ramp movements, the simulator produces a sequence of perfectly symmetrical S-shaped submovements and a very distinguished 10 Hz peak is observed in its power spectrum. Turning on the noise generator will cause execution errors in the response, therefore each submovement will overshoot or undershoot its planned endpoint. Combined with detuned inverse models, the effect of noise is the occurrence of a low frequency peak in addition to the strong 10 Hz peak broadening and decreasing in amplitude. Still, the bandwidths of the power peaks found by Vallbo & Wessberg (1993) are broader than those of the simulator. Comparing with the power spectrum analysis performed on the simulation results, Vallbo & Wessberg (1993) used a much lower frequency resolution of only 1 Hz. The power spectra from 5-s time series were averaged and the frequency content was split into bands of 1 Hz bandwidth. In the simulator, power spectra were obtained from single ramp movements of durations of 10 s and had a much higher spectral resolution. It is possible that running a large set of simulations with shorter duration ramp movements and averaging the power spectra using the same frequency resolution would have produced power peaks of broader bandwidths that more resembled the figures of Vallbo & Wessberg (1993).

#### 4.4.4 *Handedness and flexion versus extension movements*

According to Vallbo & Wessberg (1993), 8–10 Hz discontinuities were present in preferred as well as in non-preferred hands. As discussed in Chapter 2, an inverse model must compensate for the dynamics of the plant to be controlled, namely wired-in synergy generator, the musculoskeletal system, and the external world. Therefore, differences in control of the two hands correspond to differences in the accuracy of the internal inverse models representing them. In the current simulated version of the BUMP model, a distinction between left and right hand can be made by using different inverse models and different noise levels. For example, to simulate the non-preferred hand, the inverse model could be slightly more detuned than for the preferred hand. Also, a higher noise constant could be employed. The simulated result would be the same as for simulating an unskilled subject, with 8–10 Hz discontinuities consistently present. In addition, if the inverse model were sufficiently detuned, the 2–3 Hz component would also emerge as discussed above.

In terms of flexion versus extension movements, Vallbo & Wessberg (1993) found that the 8–10 Hz discontinuities were slightly more pronounced during extension than during flexion for all subjects. The simulated results presented here does not show such a difference because the simulator does not distinguish between extension and flexion movements. However, from the same argument as above, one could simulate the two by assigning slightly different inverse models to each of them. Accordingly, the finding by Vallbo & Wessberg indicates that the inverse model for the extension movement is slightly more accurate than the inverse model for the flexion movement, and therefore results in more pronounced discontinuities.

#### 4.4.5 *Oscillations during position holding*

The study of Vallbo & Wessberg (1993) was focused on 8–10 Hz discontinuities during movement, however, oscillations of the same frequency were occasionally observed during the hold phase. When present, the oscillations were most prominent at the beginning of the hold phase, successively decreasing in amplitude. Co-contractions or large constant-torque loads promoted the tremor, which was gen-

erally of much lower amplitude than the 8–10 Hz discontinuities during voluntary ramps.

Fig. 4.2 shows that the simulator produces no such tremor during hold phases when visual feedback is turned on. However, as depicted in Fig. 4.3, the simulator does produce oscillations of low amplitude for ramp and hold movements without visual feedback. Thus, the lack of feedback assisting in error correction seems to be the reason for tremor in the simulated hold phases.

Vallbo & Wessberg (1993) do not refer to such a distinction between ramp and hold tasks with and without visual feedback. On the other hand, they do suggest that the phenomenon of 10 Hz discontinuities during movements may be of a different nature than physiological finger tremor and enhanced physiological tremor in postural tasks. For example, physiological tremor during posture is an order of magnitude smaller than physiological tremor during movement (e.g., Halliday & Redfearn, 1956; Lippold, 1970; Hagbarth & Young, 1979; Marsden, 1984). Moreover, postural tremor consists of back and forth movements about a neutral position, whereas the discontinuities during movement are consistently unidirectional and imply periodic speed variations in the direction of movement (Vallbo & Wessberg, 1993). Based on these findings, Vallbo & Wessberg (1993) suggest that physiological tremor during motion may be of a different nature than physiological tremor during posture.

The AMT view of motion tremor versus posture tremor is not in disagreement with the findings listed above. As this simulation study shows, 10 Hz oscillations of significant magnitude during movement can be the result of an intermittently operating optimal controller that generates BUMPs at intervals of 100 ms. During posture, however, the simulator does not produce this tremor. Nevertheless, although not incorporated into the current version of the simulator, it is possible that external influences such as heartbeats or breathing can provide perturbations that cause the limb to deviate from its desired neutral position. As a result, the central intermittent controller would try to correct such small errors at a rate of 10 Hz.

Reinforced by mechanical resonances and stretch reflexes, the limb would experience small amplitude oscillations around its desired neutral point, a condition known as postural tremor. Thus, in terms of the mechanical-reflex and central-neurogenic components discussed in Chapter 4.1, AMT sees 10 Hz physiological tremor during motion as a phenomenon dominated by the central-neurogenic component but weakly modulated by mechanical-reflex resonances, whereas physiological tremor during posture is seen as a phenomenon dominated by the mechanical-reflex component but weakly modulated by the central-neurogenic component.

#### 4.4.6 *Pulsatile motor output*

Based on their findings, Vallbo & Wessberg (1993) suggested that slow finger movements are implemented by a series of biphasic force pulses that reflect the organisation of the descending motor commands. They hypothesised that a central generator produces the biphasic pattern, characterised by an agonist burst followed by an antagonist burst “a few tens of milliseconds” later. Indeed, their EMG records (Fig. 8, Vallbo & Wessberg, 1993) as well as findings by Gross et al. (2002) show that alternating acceleration and deceleration phases during ramp movements correspond with alternating extensor and flexor EMG bursts, each with a bell-shaped envelope and a duration of approximately 50 ms. Furthermore, Vallbo & Wessberg postulated a pulse height regulator to set the overall speed of the voluntary movement.

The above description of an intermittent regulator controlling only the height of fixed duration EMG pulses resembles that of the BUMP model. As discussed in Chapter 2.3.11, AMT hypothesises that at least the first 50 ms EMG burst in a 100 ms fast ballistic movement constitute the quantum of control exerted by the cortex over the motor neuron pool. Longer duration movements are seen as a concatenated sequence of 100 ms submovements, or BUMPs. Each BUMP corresponds to a pair of agonist and antagonist bell-shaped EMG bursts, each of 50 ms duration, where the height of each pulse determines movement speed.

---

## CHAPTER 5

### General discussion

---

#### 5.1 Comparison with other models

##### *5.1.1 Speed-accuracy tradeoff*

The BUMP model of response planning has elements in common with the deterministic iterative-corrections model (Crossman & Goodeve, 1983) as well as the impulse-variability model (Schmidt et al., 1979) and the stochastic optimised-submovement model (Meyer et al., 1988), however, it differs in some key aspects. The Crossman and Goodeve model successfully accounts for the logarithmic speed-accuracy tradeoff by suggesting that submovements have a fixed duration and move a constant proportion of the remaining distance. Comparing with the BUMP proposal, both models are based on submovements that have a fixed duration. However, in the BUMP account the required response trajectory  $\mathbf{R}^*$  is always planned to hit the target predicted ahead in time, and the whole trajectory is updated at the end of each fixed duration planning interval, thereby introducing intermittency and the opportunity for error correction. As a consequence, the actual response is comprised of a concatenated sequence of fixed duration submovements similar to the Crossman and Goodeve account.

Unlike the Crossman and Goodeve model, the BUMP model incorporates prediction. This allows a variety of movement control strategies to be implemented, ranging from receding horizon control, producing the logarithmic tradeoff, to fixed horizon control, producing the linear tradeoff. The linear speed-accuracy tradeoff was accounted for by Schmidt et al. (1979) with their impulse-variability model.

But whereas that model applies only to fast movements preprogrammed and executed open loop, the BUMP proposal produces linear tradeoffs for both ballistic movements and for slower movements that require temporal precision. While slower movements can incorporate error-correcting submovements based on feedback, in the case of time constraint the final submovement will necessarily be ballistic and therefore subject to all the noise-induced error that underpins the linear tradeoff in the fast movements of the more restricted impulse-variability model.

For their open-loop movements, Schmidt and colleagues postulated the variability of their force impulse to be proportional to the average movement velocity. In the BUMP model simulator the standard deviation of the introduced noise is proportional to the signal that represents the motor command that generates each BUMP. Effectively, for inertial loads, this is equivalent to setting the variability of the noise proportional to the average velocity of the generated *submovement*. A similar arrangement of noise proportionality to submovement velocity was used in the proposal of Meyer et al. (1988), however, they discarded the Crossman & Goodeve notion of fixed duration submovements to which the BUMP model adheres. Their stochastic optimised-submovement model incorporates submovements of variable duration, a decision based on experimental findings using movement-parsing algorithms that detect peaks and troughs in velocity and acceleration profiles. However, their movement-parsing findings do not invalidate the hypothesis that submovements have a fixed duration of 100 ms. In the BUMP model, fixed duration submovements are planned to connect smoothly at RP intervals, and consequently, peaks and troughs in velocity and acceleration waveforms will only be observed when the actual response differs from the intended response due to noise in the nervous system, lack of skill, and/or other uncertainties in response execution (Neilson & Neilson, 2005b). This is consistent with early observations of Vince (1948) that peaks and troughs in velocity and acceleration waveforms are particularly visible in untrained subjects. Thus, it is not surprising that durations between discontinuities in velocity and acceleration vary, as argued by Meyer and colleagues,



and on average are observed more than 200 ms apart. Moreover, in contrast with the BUMP model, the stochastic optimised-submovement model does not give any account of the time required by central processes to detect execution errors and to program and initiate corrective responses that incorporate prediction of future errors. Finally, the stochastic optimised-submovement model does not address the problem of redundancy in trajectory generation, as an infinite number of possible response trajectories would satisfy its specifications. AMT provides a solution to the redundancy problem, suggesting that the CNS uses task-dependent synergies to overcome this difficulty (see Neilson & Neilson, 2005b).

Nevertheless, the Meyer et al. (1988) model presented a possible way to account theoretically for the logarithmic tradeoff and for the linear tradeoff, at least for rapid movements in the case of the latter. The need for a unified account that applies to the complete range of movement generation was strongly argued by Hancock & Newell (1985). In their influential contribution they emphasised that both spatial and temporal components of movement should be considered in the same framework (i.e., space-time). Certainly, as realised by Zelaznik et al. (1988), the required spatial precision and the required temporal precision for a task dually affect the nature of the speed-accuracy relation by virtue of the control structure imposed. In allowing for differing space-time constraints by means of variable horizon predictive control, the BUMP model succeeds in accounting for both logarithmic and linear tradeoffs (and indeed for other intermediate tradeoffs, although that has not been simulated here). It also succeeds in accounting for movement velocity profiles.

### 5.1.2 *Velocity profiles*

As mentioned in Chapter 3.1.3, the kinematic theory of Plamondon (see Plamondon & Alimi, 1997, for a review) accounts for asymmetrical velocity profiles by suggesting that synergies of agonist and antagonist muscles have a log-normal velocity impulse response function. This is attributed to the limiting behaviour of a large number of neuromuscular networks involved in generating a movement whose averaged behaviour tends towards a log-normal impulse response function in the

manner of the central limit theorem. In a sense, the BUMP model of response planning is not inconsistent with this. As described in Chapter 2.4, AMT proposes that within response planning there exist parallel neural circuits, the OTGs, that require a fixed interval of time (100 ms), to read in sensory information, generate a required response trajectory  $\mathbf{R}^*$ , and write  $\mathbf{R}^*$  into working memory ready for response execution. The OTGs generate an optimally smooth  $\mathbf{R}^*$  (i.e., minimum second or third derivative consistent with minimum acceleration or minimum jerk) to move the selected sensory feature of the intended response from its initial state  $x_i$ , detected by sensory feedback, to a required final state  $x_f$  predicted ahead in time. The required response  $\mathbf{R}^*$  is then transformed in real-time into appropriate motor commands by an adaptive, optimal feedforward/feedback control system (the RE system). This repeating process introduces intermittency into movement control, creating a response comprised of a sequence of 100 ms duration submovements. At the level of response feedback, each submovement can be thought of as analogous to an impulse response function of the type proposed by Plamondon. Each BUMP consists potentially of a family of possible  $\mathbf{R}^*$  trajectories, so a particular response  $\mathbf{R}$  is comprised of a sequence of  $\mathbf{R}^*$  trajectories (actually the first 100 ms of each  $\mathbf{R}^*$  trajectory) drawn from this family. Statistically, the result is a response  $\mathbf{R}$  generated by a summation (i.e., a convolution) of impulse response functions, each drawn from a family of possible impulse response functions. This creates a statistical picture not dissimilar to that proposed by Plamondon and colleagues. Hence, the BUMP model provides a possible computational mechanism that can account for the log-normal impulse response function proposed by Plamondon.

## 5.2 Challenges from experiment

### 5.2.1 *Glitches in rapid movements*

A commonly observed phenomenon in movements such as handwriting strokes or reaching and grasping is reversals in the direction of motion in the beginning and/or end of the trajectory. According to Plamondon & Djoua (2006), there may be up to

two such glitches at the end of the trajectory, or one at the beginning and one at the end. The simulation experiments presented in this thesis have focused exclusively on one-dimensional straight rapid movements, however, in a previous two-dimensional simulation study on reaching and grasping movements (Jiang et al., 2002), the BUMP model successfully reproduced curved trajectories of the finger and thumb as well as glitches and the resulting multiple peaks in velocity profiles, similar to those presented by Plamondon & Djuioua.

### 5.2.2 *Fitts' law in unsighted movements*

While the simulation experiments of this thesis have implicitly assumed the availability of vision during movements, Wallace & Newell (1983) showed that unsighted movements also obey Fitts' law. This finding does not contradict the BUMP model. According to AMT, responses can be planned in terms of desired sensory (perceptual) consequences in any sensory mode, including kinaesthetic. It is merely for the sake of simplicity that simulated trajectories have been related to visual targets. Furthermore, even with visual feedback removed, there will still be proprioceptive feedback assisting in response planning.

## 5.3 Modelling issues

### 5.3.1 *Continuous-time versus discrete-time modelling*

It may be tempting to dismiss a minimum acceleration approach on the rationale that it implies discontinuities in acceleration at the start and end of a movement. Such discontinuities are not observed in human aimed movements. This thesis argues that acceleration waveforms related to EMG (force) bursts can be approximated in the simulator by rectangular pulses. Introducing smoothness in the EMG pulses by rounding the corners of rectangular pulses does not imply moving towards a continuous-time domain. In line with AMT, it is argued that descending control of muscles is achieved through a sequence of discrete units of bell-shaped EMG bursts with a fixed duration but with varying amplitudes. In the BUMP model these bell-shaped EMG bursts are approximated by a sequence of 50 ms duration

rectangular pulses with varying amplitudes. Discrete-time control theory is perfectly applicable whether the discrete control signal is a ZOH signal (rectangular pulse), a first order hold (FOH) signal (linear slope), or a bell-shaped pulse.

### 5.3.2 *Model parameters*

An important question that model developers are interested in is the total number of parameters that is required by a model to produce the simulated data and which ones are the most critical. For an  $N$ -step optimal trajectory, the OTG performs  $2N$  matrix multiplications in parallel involving the state matrix  $\mathbf{G}$  and the Grammian matrix  $\mathbf{\Gamma}(0, k)$ . As observed from Eq. 2.15 (p. 51), the Grammian matrix will have four elements dependent on the state matrix  $\mathbf{G}$  and the input matrix  $\mathbf{H}$ . Therefore, there are six parameters involved in calculating any point in the trajectory, four for the state matrix  $\mathbf{G}$ , and two for the input matrix  $\mathbf{H}$ .

### 5.3.3 *Choice of response planning interval*

Simulation studies based on AMT have previously been using an RP interval  $T_p$  in the range of 100–200 ms. Results have yielded good agreement with studies of human visual tracking. This is a strength of AMT and underlines the robustness of the theory. In terms of the fixed duration RP interval, AMT argues that this interval is fixed for any single person but may vary across individuals. In fact, from an AMT point of view, this difference in planning time is likely the main source of difference in motor skill between one person and another. Changes in planning time between 100 to 200 ms from one individual to another should, according to AMT, change the frequency of physiological tremor between 5 and 10 Hz. These figures are consistent with the tremor literature, in which physiological tremor is typically reported with a frequency of 7–12 Hz, which corresponds to a planning time of approximately 80 to 140 ms. In this thesis,  $T_p$  was set to 100 ms, corresponding to 10 Hz physiological tremor.

#### 5.3.4 *Genuine results or consequences of system design?*

It might be asked whether the phenomena observed in these simulations are genuine results or inevitable consequences of the system design. Specifically, one may ask if the well-known discrete-time control phenomenon of oscillations at half the sample frequency combined with a quantum of control consisting of 50 ms EMG bursts could provide an alternative explanation of physiological tremor.

The answer would be yes if one were considering a discrete-time sampled data system as used in digital signal theory. However, the nervous system is *not* such a system. In AMT, it is hypothesised that the nervous system requires a fixed interval of time to read in sensory information, plan an appropriate response trajectory, and write it into working memory ready for execution. This introduces intermittency into response planning and breaks control of movement into a concatenated sequence of submovements. It is proposed that it is this intermittency in response planning within the nervous system that underlies physiological tremor. It is not an artifact of the simulation, but a fundamental proposal within BUMP theory.

Furthermore, consider the well-known phenomenon of colour blending when flashing different colours at a subject. When increasing the flash frequency, the temporal order of the flashes will not be perceivable at some frequency and the colours will blend in an additive manner. Moreover, consider presenting a very short auditory signal of 5 ms, say, to a subject. The nervous system will not miss the signal as if it fell between 50 ms samples. The nervous system detects brief stimuli but it cannot determine temporal order within about 50 ms. It is as if the nervous system continuously integrates sensory inputs over time and resets at about 50 ms intervals. In conclusion, the alternative explanation does not apply.

#### 5.3.5 *Analytical proofs*

It is prudent to ask whether analytical proofs could be used instead of, or in addition to, selected simulation cases. Clearly, analytical proofs are stronger than simply providing simulation examples. In Chapter 3.2, one such analytical proof is provided to show that the BUMP model predicts a logarithmic speed-accuracy

tradeoff when employing receding horizon control. In addition, graphical figures and the theory of the BUMP model laid out previously are used to explain how the linear speed-accuracy tradeoff and both asymmetrical and symmetrical velocity profiles are predicted by the BUMP model. Thus, whilst not as strong as a full list of analytical proofs, this section sufficiently serves the purpose of explaining how the BUMP model predicts a set of human movement phenomena *without* resorting simply to particular simulation cases.

Furthermore, one must also consider that the targeted readership of this thesis, many of which with backgrounds from experimental psychology, physiology, neurology, and motor behaviour, more often than not will lack the necessary mathematical skills to appreciate analytical proofs. To such a readership, this amount of mathematical detail may rather obfuscate than clarify.

#### 5.3.6 *Choice of sampling rates*

In this study, the sampling rate is set to 100 Hz, which corresponds to five times oversampling. Real-world signals are not perfectly filtered and will often contain frequency components greater than the Nyquist frequency, which is equal to half the sampling frequency. One reason for oversampling is to increase the foldover frequency to ensure that unwanted frequency components are not aliased into the passband. Another reason relates to the capturing of fast edges or transients.

In its simplest form, the BUMP simulator requires a continuous-time plant with continuous-time sampling of position and velocity, which is then sampled and fed back to the discrete-time controller. The implementation constructs velocity and position signals through the integration of rectangular acceleration pulses. The sampling rate of these pulses can be set to any desired frequency. Thus, there is complete knowledge of the shape of the signals dealt with, which are rectangular (acceleration), triangular or piecewise linear (velocity), and symmetrically S-shaped (position). In light of this, and in accord with the simulation results, it appears that a sampling frequency of 100 Hz is be more than sufficient to capture the frequency content of interest, namely a 10 Hz bandwidth.

### 5.3.7 *Choice of noise constants*

It may be noted that a noise constant  $n_c = 0.5$  was used for simulations of speed-accuracy tradeoffs, whereas  $n_c = 0.2$  and  $n_c = 0.4$  were used for simulations of physiological tremor. Thus, the curious reader may question the rationale behind the choice of  $n_c$ .

In the BUMP model simulator, variability in the descending motor commands is set to vary with the size of the commands. Specifically, and in line with experimental results (for example, see the much-quoted paper by Harris & Wolpert, 1998), the standard deviation of noise is determined by the level of descending drive to the alpha motor neurons. The exact relationship between the level of alpha drive and the standard deviation of the noise, equivalent to the noise constant  $n_c$ , is uncertain and probably dependent on many factors.

In terms of simulating human movements, setting the noise levels too high will lead to responses being dominated by noise. In the study of speed-accuracy tradeoffs, the human operator was simulated with a perfect inverse model of the plant, thus, noise was the only contributor to error. Due to the very high performance of this simulated operator, the noise constant had to be set very high ( $n_c = 0.5$ ) in order for the endpoint error to be within similar range as in human experiments. An alternative could have been to detune the inverse model as was done in the study on physiological tremor. In that study, the noise constant was set to  $n_c = 0.2$  for the skilled subject and to  $n_c = 0.4$  for the less skilled subject in order to best mimic actual human behaviour observed by Vallbo & Wessberg (1993). The exact relationship between standard deviation of noise and alpha drive employed in the simulations should probably not be given much importance. Of greater importance, however, is the fact that noise is modelled as being signal-dependent, in line with the suggestion by Harris & Wolpert (1998).

## 5.4 Implications of the BUMP model

### 5.4.1 *Predictive control*

It is known from human tracking experiments that regardless of the dynamics of the tracking system, open-loop tracking characteristics always converge with practice to a gain, a time delay, and a first-order lag filter (McRuer & Krendel, 1974). This finding has been reproduced in AMT simulations of tracking and equates to the formation of accurate internal models of the neuromusculoskeletal system in interaction with the external system (Neilson et al., 1988a). AMT hypothesises that such internal models are formed by adaptive neural filters. These filter networks can also be used to generate predictions of future values of stochastic signals (Neilson & Neilson, 2005b). The proposition that human subjects employ stochastic prediction of target and response signals has been strongly substantiated in a simulation study of human tracking (Neilson et al., 1988b).

In line with the above, Gawthrop, Lakie, & Loram (2008) note in a recent paper that Fitts' law is exactly consistent with the closed-loop step response of a time-delayed, first order system. Moreover, assuming the existence of closed-loop feedback, be it continuous or intermittent, Gawthrop et al. demonstrate using known control theory that the controller must be predictive in order to be consistent with Fitts' law. The authors suggest that this new insight implies that prediction is an inherent part of speed-accuracy tradeoffs.

AMT agrees that predictive control is fundamental to speed-accuracy tradeoffs, thus matching the conclusions of Gawthrop et al. (2008). This thesis demonstrates that variable horizon predictive control with some similarity to the intermittent predictive control reported in the engineering literature (e.g., Gawthrop & Wang, 2006) is able to reproduce both the logarithmic and the linear speed-accuracy tradeoffs. Moreover, Gawthrop et al. (2008) points to the cerebellum as a potential location associated with prediction. The neuroanatomy of the intermittent optimal controller of the BUMP model is described in terms of cortico-cerebellar-cortical loops and is discussed further below.



#### 5.4.2 *Optimal control and strategy selection*

In a pursuit tracking task, the RP system can function as an optimal controller that can vary the tradeoff between variance of the error and the demand on muscular energy by varying the prediction horizon for planning of  $\mathbf{R}^*$  (Neilson et al., 1995). AMT suggests that varying the prediction horizon corresponds to adjusting the weights, typically denoted  $Q$  and  $R$ , of a linear quadratic cost function. If  $Q$  is large relative to  $R$ , low error variance is emphasised, whereas if  $R$  is large relative to  $Q$ , low input (muscular) energy is emphasised. Not only does this ability explain (i) speed-accuracy tradeoffs, it also accounts for (ii) an accuracy-energy tradeoff, (iii) a mechanism for tuning of stability margins and stability robustness, (iv) the strategy of unskilled subjects to slow and stiffen, and (v) differences in performance between subjects. When tracking a stationary target (e.g., reaching to a target at a fixed position), reducing the prediction horizon causes a faster movement at the expense of increasing the endpoint error. When tracking a moving target, reducing the prediction horizon will reduce the variance of the error between the target and tracking response waveforms at the expense of increasing the input energy, whereas increasing the prediction horizon effectively introduces a low-pass filter between target and response that limits high-speed tracking (Neilson et al., 1988a,b). Moreover, unskilled subjects or subjects with a damaged CNS such as that of cerebral palsy patients lack accurate internal models of their musculoskeletal system and slow and stiffen in movement tasks. This corresponds to an optimal control strategy that involves increasing the prediction horizon and detuning the inverse model (Neilson & Neilson, 1999). The resulting reduction in gain and bandwidth in the perceptual-motor loop improves stability margins and stability robustness. Furthermore, the strategy of slowing responses may be seen as a means of reducing the variance of neural noise, which in turn improves the accuracy of the movement. Finally, AMT argues that differences in performance between subjects are accounted for, partly at least, by differences in prediction horizon settings. Subjects with different skill levels will choose different optimal control strategies.

#### 5.4.3 *Neuroanatomy of the intermittent optimal controller*

The findings of Llinás (1991) suggest that a clock device responsible for the pulsatile control of motor output may be located in the olivocerebellar system. Furthermore, it was recently shown by Gross et al. (2002) that synchronised oscillatory activity in the cerebello-thalamo-cortical loop is responsible for pulsatile motor control observed in slow finger movements. These workers demonstrated 8 Hz coupling between MEG recordings of central brain areas, EMG activity, and tremor during slow finger movements. Gross et al. propose that the cerebellum is responsible for optimisation and ongoing error correction based on available sensory information reflected in their finding of coupling from muscle to cerebellum. Moreover, they suggest that coupling from the motor cortex (M1) to cerebellum represents an efference copy needed to predict the consequence of motor output.

Neural adaptive processing in AMT is described in terms of cortico-cerebellar-cortical loops. As described in detail by Neilson & Neilson (2005b), AMT hypothesises that neuroanatomical connections involving the cerebellum, thalamus, and cortex form a circuit implementing the least mean squares (LMS) algorithm. This LMS module is repeated hundreds of thousands of times within the cerebellar structure, with each module operating more or less independently in parallel with each other. If this circuit is actually implemented in the CNS, its parallel operation synchronised at a frequency of 10 Hz should be detected in MEG recordings coupled with EMG bursts and intermittency in movement of the same frequency. Indeed, such coupling is reported by Gross et al. (2002), albeit at a slightly lower frequency, and provides strong support to this fundamental hypothesis of AMT.

#### 5.4.4 *Synchronisation and binding*

From studies of 40 Hz oscillations in the visual cortex it has been proposed that synchronisation may serve as a function for feature linking or binding in sensory information processing (Eckhorn et al., 1988; Gray et al., 1989). Moreover, it has been suggested that binding of motor signals can form discrete muscle synergies, where different tasks make use of different combinations of such functional groups

(Farmer, 1998; Welsh & Llinás, 1997). However, many studies have been unable to demonstrate linking between peripheral rhythms such as tremors in the two hands (e.g., Marsden et al., 1969a; Conway et al., 1995; Bruce & Ackerson, 1986). Even different muscles of the same hand have failed to display coherence during simultaneous contractions (McAuley & Brown, 1995). One possible explanation may be that the tasks in these studies did not sufficiently require functional linking resulting in a common modulation of motor commands (McAuley & Marsden, 2000).

AMT agrees with this explanation. In AMT, each desired optimal trajectory  $\mathbf{R}^*$  generated centrally by the RP system corresponds to a functional (synergistic) linking of functional muscles, elemental movements, forces, and other reafferent signals. Thus, muscles which are linked within a synergy will have coherent EMG bursts during a task requiring coordinated muscle contractions. On the other hand, in a task with multiple degrees of freedom, individual functional muscles can be involved in multiple overlapping synergies, receiving bursts from multiple cortical ensembles. This might break up the coherence between EMG in different muscles. Furthermore, local feedback (reflex) loops contribute to EMG, which in turn will weaken coherence between central bursts as observed in EMG recordings.

#### 5.4.5 *Phase coding*

Phase shifts between oscillations of a particular frequency in different structures provide a mechanism for coding of motor signals (McAuley & Marsden, 2000). Spatial locations have been shown to be mapped to specific phase shifts in the hippocampal spatial memory cells of the rat (O’Keefe & Recce, 1993). Similarly, consistent mapping between postures and phase shifts have been observed in primary orthostatic tremor (McAuley et al., 2000)

An appropriate analogy to the bursting of a cortical ensemble of neurons is the underdamped swing of a pendulum. The contribution of another ensemble of neurons driving the cortical column will be determined from its phase. If the driving ensemble is in phase with the receiving ensemble, it will act as a positive input. If the driving ensemble is out of phase with the receiving ensemble, it will act as a

negative input. Phase shifts less than 90 degrees, which could be caused by neural transmission time delays of up to about 10 ms between one part of the nervous system and another, would be like gain change and could be easily compensated. Thus, a burst code might allow neural processing to be relatively insensitive to transmission time delays within the brain.

## 5.5 Concluding remarks

The success of the BUMP model of response planning in reproducing speed-accuracy tradeoffs and accompanying velocity profiles as well as 10 Hz physiological tremor as demonstrated by this thesis strengthens the foundation for a unified theory of motor control and planning. This success is of particular theoretical importance in light of the fact, mentioned earlier, and pointed out by Bullock & Grossberg (1988), that other models of response planning, such as the minimum-jerk model and the generalized motor programs model, cannot explain the experimentally observed variation of velocity profile with movement speed and distance.

The aim of this thesis was to test the BUMP model by establishing whether or not it reproduces (i) both the logarithmic and the linear speed-accuracy tradeoffs in aimed movement as well as the accompanying asymmetrical and symmetrical velocity profiles, and (ii) the 10 Hz physiological tremor in ramp movements. Indeed, the simulations show that intermittent adaptive optimal control employing the two extremes of variable horizon predictive control, combined with the addition of noise, yields results in accord with the experimental findings. On the one extreme, a receding horizon strategy results in a logarithmic speed-accuracy tradeoff as well as asymmetrical velocity profiles. On the other extreme, a fixed horizon strategy results in a linear speed-accuracy as well as symmetrical velocity profiles. In addition, the intermittent behaviour of the controller causes a tremor of 10 Hz to occur during ramp movements.

While it is certainly the case that variable horizon strategies are not necessary to explain speed-accuracy tradeoffs or velocity profiles, they are nonetheless sufficient. Moreover, it is now well established that physiological tremor during movement is

driven by centrally generated oscillations, thus implying an intermittent mode of control. This thesis shows that the BUMP model of response planning provides one possible account of the sensory-motor processes that generate these phenomena.

Importantly, all the components of the BUMP model simulator embody precise proposals from AMT about the nature of information processing within the CNS, based on its actual structure and function. This fact adds to the credibility of the correspondence between the data computed from theory and that from observation. With these simulation results, speed-accuracy tradeoffs, velocity profiles, and physiological tremor are added to a variety of other movement phenomena that have been found consistent with the AMT account of sensory-motor control and its disorders (Neilson 1999; Neilson & Neilson, 1987; Neilson et al., 1988, 1992, 1993, 1995). With the recent development of biologically-feasible nonlinear adaptive filters (Neilson & Neilson, 2005b), AMT now offers a complete framework for simulation of human movement planning and control.

---

## References

---

- Abend, W., Bizzi, E., & Morasso, P. (1982). Human arm trajectory formation. *Brain*, *105*, 331–348.
- Abernethy, B., & Sparrow, W. A. (1992). The rise and fall of dominant paradigms in motor behaviour research. In J. J. Summers (Ed.) *Approaches to the study of motor control and learning*. Amsterdam: Elsevier Science.
- Abrams, R. A., Meyer, D. E., & Kornblum, S. (1989). Speed and accuracy of saccadic eye movements: Characteristics of impulse variability in the oculomotor system. *Journal of Experimental Psychology: Human Perception and Performance*, *15*(3), 529–543.
- Adams, J. A. (1968). Response feedback and learning. *Psychological Bulletin*, *70*(6), 486–504.
- Adams, J. A. (1971). A closed-loop theory of motor learning. *Journal of Motor Behavior*, *3*(2), 111–149.
- Allum, J. H. J., Dietz, V., & Freund, H.-J. (1978). Neuronal mechanisms underlying physiological tremor. *Journal of Neurophysiology*, *41*(3), 557–571.
- Amjad, A. M., Conway, B. A., Farmer, S. F., O’Leary, C., Halliday, D. M., & Rosenberg, J. R. (1994). A load-independent 30–40 Hz component of physiological tremor in man. *Journal of Physiology*, *476*, 21P.
- Atkeson, C. G., & Hollerbach, J. M. (1985). Kinematic features of unrestrained vertical arm movements. *Journal of Neuroscience*, *5*(9), 2318–2330.
- Bain, P. G. (2002). The management of tremor. *Journal of Neurology, Neurosurgery, and Psychiatry*, *72*, i3–i9.
- Bain, P. G. (2007). Tremor. *Parkinsonism and Related Disorders*, *13*, S369–S374.

- Baker, S. N., Kilner, J. M., Pinches, E. M., & Lemon, R. N. (1999). The role of synchrony and oscillations in the motor output. *Experimental Brain Research*, 128, 109–117.
- Baker, S. N., Olivier, E., & Lemon, R. N. (1997). Coherent oscillations in monkey motor cortex and hand muscle EMG show task-dependent modulation. *Journal of Physiology*, 501, 225–241.
- Baron, S., & Kleinman, D. L. (1969). The human as an optimal controller and information processor. *IEEE Transactions on Man-Machine Systems*, 10(1), 9–17.
- Baron, S., Kleinman, D. L., & Levison, W. H. (1970). An optimal control model of human response. Part II: Prediction of human performance in a complex task. *Automatica*, 6, 371–383.
- Beggs, W. D. A., & Howarth, C. I. (1972). The movement of the hand towards a target. *Quarterly Journal of Experimental Psychology*, 24, 448–453.
- Berardelli, A., Hallett, M., Rothwell, J. C., Agostino, R., Manfredi, M., Thompson, P. D., & Marsden, C. D. (1996). Single-joint rapid arm movements in normal subjects and in patients with motor disorders. *Brain*, 119, 661–674.
- Berardelli, A., Rothwell, J. C., Day, B. L., Kachi, T., & Marsden, C. D. (1984). Duration of the first agonist EMG burst in ballistic arm movements. *Brain Research*, 304, 183–187.
- Bernstein, N. (1967). *The co-ordination and regulation of movements*. Oxford: Pergamon.
- Berthoz, A., & Metral, S. (1970). Behavior of a muscular group subjected to a sinusoidal and trapezoidal variation of force. *Journal of Applied Physiology*, 29, 378–384.
- Bouisset, S., Lestienne, F., & Maton, B. (1977). The stability of synergy in agonists during the execution of a simple voluntary movement. *Electroencephalography and Clinical Neurophysiology*, 42(4), 543–551.

- Brown, P., & Corcos, J. C., D. M. Rothwell (1997). Does parkinsonian action tremor contribute to muscle weakness in Parkinson's disease? *Brain*, 120, 401–408.
- Brown, S. H., & Cooke, J. D. (1981). Amplitude- and instruction-dependent modulation of movement-related electromyogram activity in humans. *Journal of Physiology*, 316, 97–107.
- Brown, S. H., & Cooke, J. D. (1984). Initial agonist burst duration depends on movement amplitude. *Experimental Brain Research*, 55, 523–527.
- Brown, S. H., & Cooke, J. D. (1990). Movement-related phasic muscle activation. I. Relations with temporal profile of movement. *Journal of Neurophysiology*, 63(3), 455–464.
- Bruce, E. N., & Ackerson, L. M. (1986). High-frequency oscillations in human respiratory electromyograms during voluntary contractions. *Journal of Neurophysiology*, 56, 542–553.
- Brumlik, J. (1962). On the nature of normal tremor. *Neurology*, 12, 159–179.
- Bullock, D., & Grossberg, S. (1988). Neural dynamics of planned arm movements: Emergent invariants and speed-accuracy properties during trajectory formation. *Psychological Review*, 95(1), 49–90.
- Bye, R. T., & Neilson, P. D. (2008). The BUMP model of response planning: Variable horizon predictive control accounts for the speed-accuracy tradeoffs and velocity profiles of aimed movement. *Human Movement Science*, 27(5), 771–798.
- Carlton, L. G., & Newell, K. M. (1993). Force variability and characteristics of force production. In K. M. Newell, & D. M. Corcos (Eds.) *Variability and motor control*, (pp. 15–36). Champagne, IL: Human Kinetics.
- Cathers, I., O'Dwyer, N., & Neilson, P. (1996). Tracking performance with sinusoidal and irregular targets under different conditions of peripheral feedback. *Experimental Brain Research*, 111, 437–446.
- Chan, R. B., & Childress, D. S. (1990). On a unifying noise-velocity relationship and information transmission in human-machine systems. *IEEE Transactions on Systems, Man, and Cybernetics*, 20(5), 1125–1135.



- Christakos, C. N., & Lal, S. (1980). Lumped and population stochastic models of skeletal muscle: Implications and predictions. *Biological Cybernetics*, *36*, 73–85.
- Cohen, M. I. (1979). Neurogenesis of respiratory rhythm in the mammal. *Physiological Reviews*, *59*, 1105–1173.
- Conway, B. A., Halliday, D. M., Farmer, S. F., Shahani, U., Maas, P., Weir, A. I., & Rosenberg, J. R. (1995). Synchronization between motor cortex and spinal motoneuronal pool during the performance of a maintained motor task in man. *Journal of Physiology*, *489*, 917–924.
- Cooke, J. D., & Brown, S. H. (1994). Movement-related phasic muscle activation. *Experimental Brain Research*, *99*, 473–482.
- Corcos, D. M., Gottlieb, G. L., & Agarwal, G. C. (1989). Organizing principles for single-joint movements: II. A speed-sensitive strategy. *Journal of Neurophysiology*, *62*(2), 358–368.
- Craik, K. J. W. (1947). Theory of the human operator in control systems: I. The operator as an engineering system. *British Journal of Psychology*, *38*, 56–61.
- Craik, K. J. W. (1948). Theory of the human operator in control systems: II. Man as an element in a control system. *British Journal of Psychology*, *38*, 142–148.
- Crossman, E. R. F. W., & Goodeve, P. J. (1983). Feedback control of hand-movement and Fitts' law. *Quarterly Journal of Experimental Psychology*, *35A*, 251–278. Reprint of Communication to the Experimental Society (1963).
- Darian-Smith, C., Darian-Smith, I., & Cheema, S. S. (1990). Thalamic projections to sensorimotor cortex in the newborn macaque. *Journal of Comparative Neurology*, *299*, 47–63.
- Davidson, P. R., Jones, R. D., Sirisena, H. R., & Andreae, J. H. (2000). Detection of adaptive inverse models in the human motor system. *Human Movement Science*, *19*, 761–795.
- Decima, E. E. (1996). Role of the stretch reflex in oxotremorine tremor. *Life Sciences*, *58*(22), 2041–2047.

- Deuschl, G., Raethjen, J., Lindemann, M., & Krack, P. (2001). The pathophysiology of tremor. *Muscle Nerve*, 24(6), 716–735.
- Dietz, V., Bischofberger, E., Wita, C., & Freund, H.-J. (1976). Correlation between the discharges of two simultaneously recorded motor units and physiological tremor. *Electroencephalography and Clinical Neurophysiology*, 40, 97–105.
- Durbaba, R., Taylor, A., Manu, C. A., & Buonajuti, M. (2005). Stretch reflex instability compared in three different human muscles. *Experimental Brain Research*, 163(3), 295–305.
- Ebenbichler, G. R., Kollmitzer, J., Erim, Z., Löscher, W. N., Kersch, K., Posch, M., Nowotny, T., Kranzl, A., Wöber, C., & Bochsansky, T. (2000). Load-dependence of fatigue related changes in tremor around 10 Hz. *Clinical Neurophysiology*, 111, 106–111.
- Eccles, J. C. (1984). The cerebral neocortex: A theory of its operation. In E. G. Jones, & A. Peters (Eds.) *Cerebral cortex: Functional properties of cortical cells*, vol. 2, (pp. 1–36). New York: Plenum.
- Eckhorn, R., Bauer, R., Jordan, W., Brosch, M., Kruse, W., Munk, M., & Reitboeck, H. J. (1988). Coherent oscillations: A mechanism of feature linking in the visual cortex? Multiple electrode and correlation analyses in the cat. *Biological Cybernetics*, 60, 121–130.
- Elble, R. J. (1986). Physiologic and essential tremor. *Neurology*, 36, 225–231.
- Elble, R. J. (1996). Central mechanisms of tremor. *Journal of Clinical Neurophysiology*, 13(2), 133–144.
- Elble, R. J. (2003). Characteristics of physiologic tremor in young and elderly adults. *Clinical Neurophysiology*, 114, 624–635.
- Elble, R. J., & Randall, J. E. (1976). Motor-unit activity responsible for the 8- to 12-Hz component of human physiological finger tremor. *Journal of Neurophysiology*, 39(2), 370–383.
- Elble, R. J., & Randall, J. E. (1978). Mechanistic components of normal hand tremor. *Electroencephalography and Clinical Neurophysiology*, 44, 72–82.

- Evans, C. M. B., & Baker, S. N. (2003). Task-dependent intermanual coupling of 8-Hz discontinuities during slow finger movements. *European Journal of Neuroscience*, *18*, 453–456.
- Farmer, S. F. (1998). Rhythmicity, synchronization and binding in human and primate motor systems. *Journal of Physiology*, *509*, 3–14.
- Farmer, S. F. (1999). Pulsatile central nervous control of human movement. *Journal of Physiology*, *517*, 3P.
- Farmer, S. F., Bremner, F. D., Halliday, D. M., Rosenberg, J. R., & Stephens, J. A. (1993). The frequency content of common synaptic inputs to motoneurons studied during voluntary isometric contraction in man. *Journal of Physiology*, *470*, 127–155.
- Farmer, S. F., Ingram, D. A., & Stephens, J. A. (1990). Mirror movements studied in a patient with Klippel-Feil syndrome. *Journal of Physiology*, *428*, 467–484.
- Fitts, P. M. (1954). The information capacity of the human motor system in controlling the amplitude of movement. *Journal of Experimental Psychology*, *47*, 381–391.
- Fitts, P. M., & Peterson, J. R. (1964). Information capacity of discrete motor responses. *Journal of Experimental Psychology*, *67*(2), 103–112.
- Flanagan, J. R., & Ostry, D. J. (1990). Trajectories of human multi-joint arm movements: Evidence of joint level planning. In V. Hayward, & O. Khatib (Eds.) *Experimental robotics I: Lecture notes in control and information sciences*, (pp. 594–613). London: Springer.
- Flash, T., & Hogan, N. (1985). The coordination of arm movements: An experimentally confirmed mathematical model. *Journal of Neuroscience*, *5*(7), 1688–1703.
- Foley, T. H., Marsden, C. D., & Owen, D. A. (1967). Evidence for a direct peripheral effect of adrenaline on physiological tremor in man. *Journal of Physiology*, *189*, 65P–66P.
- Fox, J. R., & Randall, J. E. (1970). Relationship between forearm tremor and the biceps electromyogram. *Journal of Applied Physiology*, *29*, 103–108.

- Freund, H.-J. (1983). Motor unit and muscle activity in voluntary motor control. *Physiological Reviews*, 63(2), 387–436.
- Freund, H.-J., & Büdingen, H. J. (1978). The relationship between speed and amplitude of the fastest voluntary contractions of human arm muscles. *Experimental Brain Research*, 31(1), 1–12.
- Freund, H.-J., Büdingen, H. J., & Dietz, V. (1975). Activity of single motor units from human forearm muscles during voluntary isometric contractions. *Journal of Neurophysiology*, 38, 933–946.
- Freund, H.-J., & Dietz, V. (1978). The relationship between physiological and pathological tremor. In J. E. Desmedt (Ed.) *Physiological tremor, pathological tremors and clonus. Progress in clinical neurophysiology*, vol. 5, (pp. 66–89). Basel: Karger.
- Gawthrop, P. J., Lakie, M., & Loram, I. (2008). Predictive feedback control and Fitts' law. *Biological Cybernetics*, 98(3), 229–238.
- Gawthrop, P. J., & Wang, L. (2006). Intermittent predictive control of an inverted pendulum. *Control Engineering Practice*, 14(11), 1347–1356.
- Georgopoulos, A. P., Kalaska, J. F., & Massey, J. T. (1981). Spatial trajectories and reaction times of aimed movements: Effects of practice, uncertainty, and change in target location. *Journal of Neurophysiology*, 46(4), 725–743.
- Ghous, A., & Neilson, P. D. (2002). Evidence for internal representation of a static nonlinearity in a visual tracking task. *Human Movement Science*, 21, 847–879.
- Gibson, M. B., & Neilson, P. D. (1999). Optimal trajectory generation in reaching and tracking: Minimum acceleration versus minimum jerk. In P. Treffner, & S. Morrison (Eds.) *Abstracts of the 5th biennial motor control and human skill research workshop, Surfers Paradise, QLD, Jan. 2000*, (p. 60). Goldcoast, QLD: School of Physiotherapy and Exercise Science, Griffith University.
- Gielen, C. C. A. M., van den Heuvel, P. J. M., & Denier van der Gon, J. J. (1984). Modification of muscle activation patterns during fast goal-directed arm movements. *Journal of Motor Behavior*, 16(1), 2–19.

- Goldman-Rakic, P. S. (1987). Circuitry of primate prefrontal cortex and regulation of behavior by representational memory. In F. Plum (Ed.) *Handbook of physiology: Sec. 1. The nervous system: Vol. V. Higher functions of the brain, Part 1*, (pp. 373–417). Bethesda, MD: American Physiological Society.
- Goodman, D., & Kelso, J. A. S. (1983). Exploring the functional significance of physiological tremor: A biospectroscopic approach. *Experimental Brain Research*, 49, 419–431.
- Goodwin, G. C., Graebe, S. F., & Salgado, M. E. (2001). *Control system design*. New Jersey: Prentice Hall.
- Gottlieb, G. L., Corcos, D. M., & Agarwal, G. C. (1989). Organizing principles for single-joint movements: I. A speed-insensitive strategy. *Journal of Neurophysiology*, 62(2), 342–357.
- Granit, R., & Renkin, B. (1961). Net depolarization and discharge rate of motoneurons, as measured by recurrent inhibition. *Journal of Physiology*, 158, 461–475.
- Gray, C. M., König, P., Engel, A. K., & Singer, W. (1989). Oscillatory responses in cat visual cortex exhibit inter-columnar synchronization which reflects global stimulus properties. *Nature*, 338, 334–337.
- Greene, P. H. (1972). Problems of organization of motor systems. In R. Rosen, & F. M. Snell (Eds.) *Progress in theoretical biology*, vol. 2, (pp. 303–338). New York: Academic Press.
- Gross, J., Tass, P. A., Salenius, S., Hari, R., Freund, H.-J., & Schnitzler, A. (2000). Cortico-muscular synchronization during isometric muscle contraction in humans as revealed by magnetoencephalography. *Journal of Physiology*, 527, 623–631.
- Gross, J., Timmermann, L., Kujala, J., Dirks, M., Schmitz, F., Salmelin, R., & Schnitzler, A. (2002). The neural basis of intermittent motor control in humans. *Proceedings of the National Academy of Sciences of the USA*, 99(4), 2299–2302.
- Hagbarth, K.-E., & Young, R. R. (1979). Participation of the stretch reflex in human physiological tremor. *Brain*, 102, 509–526.

- Hallett, M., & Marsden, C. D. (1979). Ballistic flexion movements of the human thumb. *Journal of Physiology*, *294*, 33–50.
- Hallett, M., Shahani, B. T., & Young, R. R. (1975). EMG analysis of stereotyped voluntary movements in man. *Journal of Neurology, Neurosurgery, and Psychiatry*, *38*, 1154–1162.
- Halliday, A. M., & Redfearn, J. W. T. (1956). An analysis of the frequencies of finger tremor in healthy subjects. *Journal of Physiology*, *134*, 600–611.
- Halliday, A. M., & Redfearn, J. W. T. (1958). Finger tremor in tabetic patients and its bearing on the mechanism producing the rhythm of physiological tremor. *Journal of Neurology, Neurosurgery, and Psychiatry*, *21*, 101–108.
- Halliday, D. M., Conway, B. A., Farmer, S. F., & Rosenberg, J. R. (1998). Using electroencephalography to study functional coupling between cortical activity and electromyograms during voluntary contractions in humans. *Neuroscience Letters*, *241*, 5–8.
- Hamilton, A., Jones, K. E., & Wolpert, D. M. (2004). The scaling of motor noise with muscle strength and motor unit numbers in humans. *Experimental Brain Research*, *157*, 417–430.
- Hancock, P. A., & Newell, K. M. (1985). The movement speed-accuracy relationship in space-time. In H. Heuer, U. Kleinbeck, & K.-H. Schmidt (Eds.) *Motor behavior: Programming, control and acquisition*, (pp. 153–188). Berlin: Springer.
- Hari, R., & Salenius, S. (1999). Rhythmical corticomotor communication. *Neuroreport*, *10*, R1–R10.
- Harris, C. M., & Wolpert, D. M. (1998). Signal-dependent noise determines motor planning. *Nature*, *394*, 780–784.
- Haykin, S. (2002). *Adaptive filter theory*. Upper Saddle River, NJ: Prentice Hall, 4th ed.
- Hefter, H., Hömberg, V., Reiners, K., & Freund, H.-J. (1987). Stability of frequency during long-term recordings of hand tremor. *Electroencephalography and Clinical Neurophysiology*, *67*, 439–446.

- Henneman, E. (1979). Functional organization of motoneuron pools: The size-principle. In H. Asanuma, & V. J. Wilson (Eds.) *Integration in the nervous system*, (pp. 13–25). Tokyo: Igaku-Shoin.
- Henry, F. M., & Rogers, D. E. (1960). Increased response latency for complicated movements and a “memory drum” theory of neuromotor reaction. *Research Quarterly*, 31(3), 448–458.
- Hogan, N. (1984). An organizing principle for a class of voluntary movements. *Journal of Neuroscience*, 4(11), 2745–2754.
- Hömborg, V., Hefter, H., Reiners, K., & Freund, H.-J. (1987). Differential effects of changes in mechanical limb properties on physiological and pathological tremor. *Journal of Neurology, Neurosurgery, and Psychiatry*, 50, 568–579.
- Hömborg, V., Reiners, K., Hefter, H., & Freund, H.-J. (1986). The muscle activity spectrum: Spectral analysis of muscle force as an estimator of overall motor unit activity. *Electroencephalography and Clinical Neurophysiology*, 63, 209–222.
- Horsley, V., & Schäfer, E. A. (1886). Experiments on the character of the muscular contractions which are evoked by excitation of the various parts of the motor tract. *Journal of Physiology*, 7, 96–110.
- Jaberzadeh, S., Brodin, P., Flavel, S. C., O’Dwyer, N. J., Nordstrom, M. A., & Miles, T. S. (2003). Pulsatile control of the human masticatory muscles. *Journal of Physiology*, 547, 613–620.
- Jeannerod, M. (1999). Visuomotor channels: Their integration in goal-directed prehension. *Human Movement Science*, 18, 201–218.
- Jiang, J., Shen, Y., & Neilson, P. D. (2002). A simulation study of the degrees of freedom of movement in reaching and grasping. *Human Movement Science*, 21, 881–904.
- Joyce, G. C., & Rack, P. M. H. (1974). The effects of load and force on tremor at the normal human elbow joint. *Journal of Physiology*, 240, 375–396.

- Joyce, G. C., Rack, P. M. H., & Ross, H. F. (1974). The forces generated at the human elbow joint in response to imposed sinusoidal movements of the forearm. *Journal of Physiology*, *240*, 351–374.
- Kakuda, N., Nagaoka, M., & Wessberg, J. (1999). Common modulation of motor unit pairs during slow wrist movement in man. *Journal of Physiology*, *520*, 929–940.
- Kantowitz, B. H. (1974). Double stimulation. In B. H. Kantowitz (Ed.) *Human information processing: Tutorials in performance and cognition*. Hillsdale: Erlbaum.
- Karlin, L., & Kestenbaum, R. (1968). Effects of number of alternatives on the psychological refractory period. *Quarterly Journal of Experimental Psychology*, *20*, 167–178.
- Keele, S. W. (1968). Movement control in skilled motor performance. *Psychological Bulletin*, *70*(6 Part I), 387–403.
- Kelly, D. (1992). Analysis of muscle activity during fast ballistic movement. Undergraduate thesis, School of Electrical Engineering & Telecommunications, The University of New South Wales, Australia.
- Kelso, J. A. S. (1981). Contrasting perspectives on order and regulation in movement. In J. Long, & A. Baddeley (Eds.) *Attention and performance IX*, (pp. 437–457). Hillsdale, NJ: Erlbaum.
- Kelso, J. A. S., Holt, K. G., Rubin, P., & Kugler, P. N. (1981). Patterns of human interlimb coordination emerge from the properties of non-linear, limit cycle oscillatory processes: Theory and data. *Journal of Motor Behavior*, *13*(4), 226–261.
- Kerr, G. K., & Lockwood, R. J. (1995). Amplitude scaling compensates for serial delays in correcting eye and arm movements. *Journal of Motor Behavior*, *27*(4), 349–365.
- Kilner, J. M., Baker, S. N., Salenius, S., Jousmäki, V., Hari, R., & Lemon, R. N. (1999). Task-dependent modulation of 15-30 Hz coherence between rectified



- EMGs from human hand and forearm muscles. *Journal of Physiology*, 516, 559–570.
- Kirkwood, P. A., Sears, T. A., Tuck, D. L., & Westgaard, R. H. (1982). Variations in the time course of the synchronization of intercostal motoneurons in the cat. *Journal of Physiology*, 327, 105–135.
- Kleinman, D. L., Baron, S., & Levison, W. H. (1970). An optimal control model of human response. Part I: Theory and validation. *Automatica*, 6, 357–369.
- Kleinman, D. L., Baron, S., & Levison, W. H. (1971). A control theoretic approach to manned-vehicle systems analysis. *IEEE Transactions on Automatic Control*, 16(6), 824–832.
- Köster, B., Lauk, M., Timmer, J., Winter, T., Guschlbauer, B., Glocker, F. X., Danek, A., Deuschl, G., & Lucking, C. H. (1998). Central mechanisms in human enhanced physiological tremor. *Neuroscience Letters*, 241, 135–138.
- Kugler, P. N. (1986). A morphological perspective on the origin and evolution of movement patterns. In M. G. Wade, & H. T. A. Whiting (Eds.) *Motor development in children: Aspects of coordination and control*, (pp. 459–525). Dordrecht: Martinus Nijhoff.
- Kugler, P. N., Kelso, J. A. S., & Turvey, M. T. (1982). On the control and coordination of naturally developing systems. In J. A. S. Kelso, & J. E. Clark (Eds.) *The development of movement control and co-ordination*, (pp. 5–78). New York: John Wiley.
- Kugler, P. N., & Turvey, M. T. (1987). *Information, natural law, and the self-assembly of rhythmic movement*. Hillsdale, NJ: Lawrence Erlbaum.
- Kvålseth, T. O. (1980). An alternative to Fitts' law. *Bulletin of the Psychonomic Society*, 16, 371–373.
- Lakie, M., & Combes, N. (1999). The phase of postural hand tremor is not influenced by repetitive photic brain stimulation. *Clinical Neurophysiology*, 110, 2020–2025.

- Lakie, M., & Combes, N. (2000). There is no simple temporal relationship between the initiation of rapid reactive hand movements and the phase of an enhanced physiological tremor in man. *Journal of Physiology*, 523, 515–522.
- Lakie, M., Walsh, E. G., & Wright, G. W. (1986). Passive mechanical properties of the wrist and physiological tremor. *Journal of Neurology, Neurosurgery, and Psychiatry*, 49, 669–676.
- Lauk, M., Köster, B., Timmer, J., Guschlbauer, B., Deuschl, G., & Lücking, C. H. (1999). Side-to-side correlation of muscle activity in physiological and pathological human tremors. *Clinical Neurophysiology*, 110, 1774–1783.
- Lestienne, F. (1979). Effects of inertial load and velocity on the braking process of voluntary limb movements. *Experimental Brain Research*, 35, 407–418.
- Lippold, O. C. J. (1970). Oscillation in the stretch reflex arc and the origin of the rhythmical, 8–12 c/s component of physiological tremor. *Journal of Physiology*, 206, 359–382.
- Lippold, O. C. J., Redfearn, J. W. T., & Vučo, J. (1957). The rhythmical activity of groups of motor units in the voluntary contraction of muscle. *Journal of Physiology*, 137, 473–487.
- Llinás, R. R. (1991). The noncontinuous nature of movement execution. In D. R. Humphrey, & H.-J. Freund (Eds.) *Motor control: Concepts and issues*, (pp. 223–242). Chichester, UK: John Wiley.
- Louis, E. D., Ottman, R., & Hauser, W. A. (1998). How common is the most common adult movement disorder? Estimates of the prevalence of essential tremor throughout the world. *Movement Disorders*, 13(1), 5–10.
- Lui, B. K. (1993). Computer analysis of hand-writing movements. Undergraduate thesis, School of Electrical Engineering & Telecommunications, The University of New South Wales, Australia.
- Luschei, E. S., & Goldberg, G. M. (1981). Neural mechanisms of mandibular control: Mastication and biting. In J. M. Brookhart, & V. B. Mountcastle (Eds.) *Handbook*

- of physiology: The nervous system*, vol. 2, (pp. 1237–1274). Bethesda: American Physiological Society.
- MacKinnon, C. D., & Rothwell, J. C. (2000). Time-varying changes in corticospinal excitability accompanying the triphasic EMG pattern in humans. *Journal of Physiology*, 528, 633–645.
- Marsden, C. D. (1978). The mechanisms of physiological tremor and their significance for pathological tremors. In J. E. Desmedt (Ed.) *Physiological tremor, pathological tremors and clonus. Progress in clinical neurophysiology*, vol. 5, (pp. 1–16). Basel: Karger.
- Marsden, C. D. (1984). Origins of normal and pathological tremor. In L. J. Findley, & R. Capildeo (Eds.) *Movement disorders: Tremor*, (pp. 37–84). London: MacMillan.
- Marsden, C. D., Foley, T. H., Owen, D. A., & McAllister, R. G. (1967a). Peripheral  $\beta$ -adrenergic receptors concerned with tremor. *Clinical Science*, 33, 53–65.
- Marsden, C. D., & Meadows, J. C. (1968). The effect of adrenaline on the contraction of human muscle — one mechanism whereby adrenaline increases the amplitude of physiological tremor. *Journal of Physiology*, 194, 70P–71P.
- Marsden, C. D., & Meadows, J. C. (1970). The effect of adrenaline on the contraction of human muscle. *Journal of Physiology*, 207, 429–448.
- Marsden, C. D., Meadows, J. C., & Lange, G. W. (1970). Effect of speed of muscle contraction on physiological tremor in normal subjects and in patients with thyrotoxicosis and myxoedema. *Journal of Neurology, Neurosurgery, and Psychiatry*, 33, 776–782.
- Marsden, C. D., Meadows, J. C., Lange, G. W., & Watson, R. S. (1967b). Effect of deafferentation on human physiological tremor. *Lancet*, 2, 700–702.
- Marsden, C. D., Meadows, J. C., Lange, G. W., & Watson, R. S. (1969a). The relation between the physiological tremor of the two hands in healthy subjects. *Electroencephalography and Clinical Neurophysiology*, 27, 179–185.

- Marsden, C. D., Meadows, J. C., Lange, G. W., & Watson, R. S. (1969b). The role of the ballistocardiac impulse in the genesis of physiological tremor. *Brain*, *92*, 647–662.
- Marsden, C. D., Meadows, J. C., Lange, G. W., & Watson, R. S. (1969c). Variations in human physiological finger tremor, with particular reference to changes with age. *Electroencephalography and Clinical Neurophysiology*, *27*, 169–178.
- Marshall, J., & Walsh, E. G. (1956). Physiological tremor. *Journal of Neurology, Neurosurgery, and Psychiatry*, *19*, 260–267.
- Master, J. (2003). The influence of motor noise on optimal trajectory planning and physiological tremor. Master of Biomedical Engineering thesis, Graduate School of Biomedical Engineering, The University of New South Wales, Australia.
- Mathew, A., & Cook, M. (1990). The control of reaching movements by young infants. *Child Development*, *61*(4), 1238–1257.
- Matthews, P. B. (1993). Interaction between short- and long-latency components of the human stretch reflex during sinusoidal stretching. *Journal of Physiology*, *462*, 503–527.
- Matthews, P. B., & Muir, R. B. (1980). Comparison of electromyogram spectra with force spectra during human elbow tremor. *Journal of Physiology*, *302*, 427–441.
- Mayston, M. J., Harrison, L. M., Quinton, R., Stephens, J. A., Krams, M., & Bouloux, P. M. (1997). Mirror movements in X-linked Kallmann’s syndrome. I. A neurophysiological study. *Brain*, *120*, 1199–1216.
- Mayston, M. J., Harrison, L. M., Stephens, J. A., & Farmer, S. F. (2001). Physiological tremor in human subjects with X-linked Kallmann’s syndrome and mirror movements. *Journal of Physiology*, *530*(3), 551–563.
- McAuley, J. H., Britton, T. C., Rothwell, J. C., Findley, L. J., & Marsden, C. D. (2000). The timing of primary orthostatic tremor bursts has a task-specific plasticity. *Brain*, *123*, 254–266.

- McAuley, J. H., & Brown, P. (1995). Absence of coherence between frequency peaks of surface electromyogram recorded in humans from different muscles of the same hand. *Journal of Physiology*, *487*, 70P.
- McAuley, J. H., Corcos, D. M., Rothwell, J. C., Quinn, N. P., & Marsden, C. D. (2001). Levodopa reversible loss of the Piper frequency oscillation component in Parkinson's disease. *Journal of Neurology, Neurosurgery, and Psychiatry*, *70*, 471–476.
- McAuley, J. H., Farmer, S. F., Rothwell, J. C., & Marsden, C. D. (1999). Common 3 and 10 Hz oscillations modulate human eye and finger movements while they simultaneously track a visual target. *Journal of Physiology*, *515*, 905–917.
- McAuley, J. H., & Marsden, C. D. (2000). Physiological and pathological tremors and rhythmic central motor control. *Brain*, *123*, 1545–1567.
- McAuley, J. H., Rothwell, J. C., & Marsden, C. D. (1997). Frequency peaks of tremor, muscle vibration and electromyographic activity at 10 Hz, 20 Hz and 40 Hz during human finger muscle contraction may reflect rhythmicities of central neural firing. *Experimental Brain Research*, *114*, 525–541.
- McLeod, P. (1977). Parallel processing and the psychological refractory period. *Acta Psychologica*, *41*, 381–391.
- McRuer, D. T., & Krendel, E. S. (1974). Mathematical models of human pilot behaviour. In *AGARDograph No. 188*. Neuilly sur Seine, France: Advisory Group for Aerospace Research and Development, North Atlantic Treaty Organization.
- Meyer, D. E., Abrams, R. A., Kornblum, S., Wright, C. E., & Smith, J. E. K. (1988). Optimality in human motor performance: Ideal control of rapid aimed movements. *Psychological Review*, *95*(3), 340–370.
- Meyer, D. E., Smith, J. E. K., Kornblum, S., Abrams, R. A., & Wright, C. E. (1990). Speed-accuracy tradeoffs in aimed movements: Toward a theory of rapid voluntary action. In M. Jeannerod (Ed.) *Attention and performance XIII: Motor representation and control*, (pp. 173–226). Hillsdale, NJ: Lawrence Erlbaum.

- Meyer, D. E., Smith, J. E. K., & Wright, C. E. (1982). Models for the speed and accuracy of aimed movements. *Psychological Review*, 89(5), 449–482.
- Morasso, P. (1981). Spatial control of arm movements. *Experimental Brain Research*, 42(2), 223–227.
- Mori, S. (1975). Entrainment of motor-unit discharges as a neuronal mechanism of synchronization. *Journal of Neurophysiology*, 38, 859–870.
- Morrison, S., & Keogh, J. (2001). Changes in the dynamics of tremor during goal-directed pointing. *Human Movement Science*, 20, 675–693.
- Mountcastle, V. B. (1997). The columnar organization of the neocortex. *Brain*, 120, 701–722.
- Mountcastle, V. B. (1998). *Perceptual neuroscience: The cerebral cortex*. Cambridge, MA: Harvard.
- Murthy, V. N., & Fetz, E. E. (1992). Coherent 25- to 35-Hz oscillations in the sensorimotor cortex of awake behaving monkeys. *Proceedings of the National Academy of Sciences of the USA*, 89, 5670–5674.
- Murthy, V. N., & Fetz, E. E. (1996). Synchronization of neurons during local field potential oscillations in sensorimotor cortex of awake monkeys. *Journal of Neurophysiology*, 76, 3968–3982.
- Nagasaki, H. (1989). Asymmetric velocity and acceleration profiles of human arm movements. *Experimental Brain Research*, 74(2), 319–326.
- Navon, D., Gopher, D., Chillag, N., & Spitz, G. (1984). On separability of and interference between tracking dimensions in dual-axis tracking. *Journal of Motor Behavior*, 16(4), 364–391.
- Neilson, M. D., & Neilson, P. D. (1987). Speech motor control and stuttering: A computational model of adaptive sensory-motor processing. *Speech Communications*, 6, 325–333.
- Neilson, P. D. (1993). The problem of redundancy in movement control: The adaptive model theory approach. *Psychological Research*, 55, 99–106.

- Neilson, P. D. (1999). Influence of intermittency and synergy on grasping. *Motor Control*, 3, 280–284.
- Neilson, P. D. (2000). A theoretical model of response planning within the perceptual-motor loop. Unpublished manuscript.
- Neilson, P. D., & Neilson, M. D. (1999). A neuroengineering solution to the optimal tracking problem. *Human Movement Science*, 18, 155–183.
- Neilson, P. D., & Neilson, M. D. (2001). Neural mechanisms for control of multivariable, redundant, nonlinear musculoskeletal systems. In *Proceedings of the 40th IEEE conference on decision and control, Orlando, FL, Dec. 2001*, (pp. 13–14). Piscataway, NJ: IEEE Control Systems Society.
- Neilson, P. D., & Neilson, M. D. (2005a). Motor maps and synergies. *Human Movement Science*, 24, 774–797.
- Neilson, P. D., & Neilson, M. D. (2005b). An overview of adaptive model theory: Solving the problems of redundancy, resources, and nonlinear interactions in human movement control. *Journal of Neural Engineering*, 2(3), S279–S312.
- Neilson, P. D., Neilson, M. D., & O’Dwyer, N. (1992). Adaptive model theory: Application to disorders of motor control. In J. J. Summers (Ed.) *Approaches to the study of motor control and learning*, (pp. 495–548). Amsterdam: Elsevier.
- Neilson, P. D., Neilson, M. D., & O’Dwyer, N. (1998). Evidence for rapid switching of sensory-motor models. In J. P. Piek (Ed.) *Motor control and human skill: A multidisciplinary approach*, (pp. 105–126). Champaign, IL: Human Kinetics.
- Neilson, P. D., Neilson, M. D., & O’Dwyer, N. J. (1988a). Internal models and intermittency: A theoretical account of human tracking behavior. *Biological Cybernetics*, 58, 101–112.
- Neilson, P. D., Neilson, M. D., & O’Dwyer, N. J. (1993). What limits high speed tracking performance? *Human Movement Science*, 12, 85–109.
- Neilson, P. D., Neilson, M. D., & O’Dwyer, N. J. (1995). Adaptive optimal control of human tracking. In D. J. Glencross, & J. P. Piek (Eds.) *Motor control*

- and sensory-motor integration: Issues and directions*, (pp. 97–140). Amsterdam: Elsevier.
- Neilson, P. D., Neilson, M. D., & O'Dwyer, N. J. (1997). Adaptive model theory: Central processing in acquisition of skill. In K. J. Connolly, & H. Forssberg (Eds.) *Neurophysiology and psychology of motor development. Clinics in developmental medicine*, (pp. 346–370). London: MacKeith.
- Neilson, P. D., & O'Dwyer, N. J. (1984). Reproducibility and variability of speech muscle activity in athetoid dysarthria of cerebral palsy. *Journal of Speech and Hearing Research*, *27*, 502–517.
- Neilson, P. D., O'Dwyer, N. J., & Neilson, M. D. (1988b). Stochastic prediction in pursuit tracking: An experimental test of adaptive model theory. *Biological Cybernetics*, *58*, 113–122.
- Nelson, W. L. (1983). Physical principles for economies of skilled movements. *Biological Cybernetics*, *46*, 135–147.
- Nicolelis, M. A., Baccala, L. A., Lin, R. C., & Chapin, J. K. (1995). Sensorimotor encoding by synchronous neural ensemble activity at multiple levels of the somatosensory system. *Science*, *268*, 1353–1358.
- Nise, N. S. (2000). *Control systems engineering*. New York: Wiley, 3rd ed.
- Novak, K. E., Miller, L. E., & Houk, J. C. (2000). Kinematic properties of rapid hand movements in a knob turning task. *Experimental Brain Research*, *132*, 419–433.
- O'Dwyer, N. J., & Neilson, P. D. (1988). Voluntary muscle control in normal and athetoid dysarthric speakers. *Brain*, *111*, 877–899.
- O'Dwyer, N. J., & Neilson, P. D. (1998). Motor output variability: Variation with average level and range of force. *Australian Journal of Psychology*, *50*(Suppl. 8).
- O'Dwyer, N. J., & Neilson, P. D. (2000). Metabolic energy expenditure and accuracy in movement: Relations to levels of muscle and cardiorespiratory activation and the sense of effort. In W. A. Sparrow (Ed.) *Energetics of human activity*, (pp. 1–43). Champaign, IL: Human Kinetics.



- Ogata, K. (1995). *Discrete-time control systems*. Upper Saddle River, NJ: Prentice Hall, 2nd ed.
- Ohara, S., Nagamine, T., Ikeda, A., Kunieda, T., Matsumoto, R., Taki, W., Hashimoto, N., Baba, K., Mihara, T., Salenius, S., & Shibasaki, H. (2000). Electrocorticogram–electromyogram coherence during isometric contraction of hand muscle in human. *Clinical Neurophysiology*, *111*, 2014–2024.
- O’Keefe, J., & Recce, M. L. (1993). Phase relationship between hippocampal place units and the EEG theta rhythm. *Hippocampus*, *3*, 317–330.
- Olsen, S. M. (2001). Adaptive model theory: A simulation study of speed-accuracy tradeoff in the execution of reaching movements. Master of Engineering Cybernetics thesis, Faculty of Electrical Engineering and Telecommunication, Norwegian University of Science and Technology, Norway and School of Electrical Engineering and Telecommunications, The University of New South Wales, Australia.
- Oytam, Y., Neilson, P. D., & O’Dwyer, N. J. (1998). Characteristics of coordination and performance in visuo-motor coupling. *Australian Journal of Psychology*, *50*, 9.
- Oytam, Y., Neilson, P. D., & O’Dwyer, N. J. (2005). Degrees of freedom and motor planning in purposive movement. *Human Movement Science*, *24*, 710–730.
- Padsha, S. M., & Stein, R. B. (1973). The bases of tremor during a sustained posture. In R. B. Stein, K. G. Pearson, R. S. Smith, & J. G. Redford (Eds.) *Control of Posture and Locomotion*, (pp. 415–419). New York: Plenum.
- Partridge, L. D. (1966). Signal-handling characteristics of load-moving skeletal muscle. *American Journal of Physiology*, *210*, 1178–1191.
- Pashler, H. (1984). Processing stages in overlapping tasks: Evidence for a central bottleneck. *Journal of Experimental Psychology: Human Perception and Performance*, *10*(3), 358–377.
- Pashler, H. (1992). Dual-task interference and elementary mental mechanisms. In D. E. Meyer, & S. Kornblum (Eds.) *Attention and performance XIV: Synergies in*

- experimental psychology, artificial intelligence, and cognitive neuroscience*, (pp. 245–264). Cambridge, MA: MIT.
- Perkins, J. F. (1945). The role of the proprioceptors in shivering. *American Journal of Physiology*, *145*, 264–271.
- Piper, H. (1907). On rhythmical muscle contractions. *Pflügers Archiv European Journal of Physiology*, *119*, 301–338.
- Plamondon, R. (1998). A kinematic theory of rapid human movements: Part III. Kinetic outcomes. *Biological Cybernetics*, *78*, 133–145.
- Plamondon, R., & Alimi, A. M. (1997). Speed/accuracy trade-offs in target-directed movements. *Behavioral and Brain Sciences*, *20*, 279–349.
- Plamondon, R., & Djioa, M. (2006). A multi-level representation paradigm for handwriting stroke generation. *Human Movement Science*, *25*, 586–607.
- Pohja, M., & Salenius, S. (2003). Modulation of cortex-muscle oscillatory interaction by ischaemia-induced deafferentation. *Neuroreport*, *14*, 321–324.
- Proudlock, F. A., & Scott, J. (2003). Tremor in the human hand following peripheral nerve transection and reinnervation. *Brain Research*, *989*, 238–245.
- Raethjen, J., Lemke, M. R., Lindemann, M., Wenzelburger, R., Krack, P., & Deuschl, G. (2001). Amitriptyline enhances the central component of physiological tremor. *Journal of Neurology, Neurosurgery, and Psychiatry*, *70*, 78–82.
- Raethjen, J., Lindemann, M., Schmaljohann, H., Wenzelburger, R., Pfister, G., & Deuschl, G. (2000). Multiple oscillators are causing parkinsonian and essential tremor. *Movement Disorders*, *15*, 84–94.
- Reed, E. S. (1982). An outline of a theory of action systems. *Journal of Motor Behavior*, *14*(2), 98–134.
- Rietz, R. R., & Stiles, R. N. (1974). A viscoelastic-mass mechanism as a basis for normal postural tremor. *Journal of Applied Physiology*, *37*(6), 852–860.
- Sakamoto, K., Nishida, K., Zhou, L., Itakura, N., Seki, K., & Hamba, S. (1992). Characteristics of physiological tremor in five fingers and evaluations of fatigue of fingers in typing. *Annals of Physiological Anthropology*, *11*, 61–68.

- Salenius, S., Portin, K., Kajola, M., Salmelin, R., & Hari, R. (1997). Cortical control of human motoneuron firing during isometric contraction. *Journal of Neurophysiology*, 77, 3401–3405.
- Salmelin, R., & Hari, R. (1994). Spatiotemporal characteristics of sensorimotor neuromagnetic rhythms related to thumb movement. *Neuroscience*, 60, 537–550.
- Saltzman, E., & Kelso, J. A. S. (1987). Skilled actions: A task-dynamic approach. *Psychological Review*, 94(1), 84–106.
- Sardesai, M., Figge, C., Bodner, M., Crosby, M., Hansen, J., Quillfeldt, J. A., Landau, S., Ostling, A., Vuong, S., & Shaw, G. L. (2001). Reliable short-term memory in the trion model: Toward a cortical language and grammar. *Biological Cybernetics*, 84, 173–182.
- Schmidt, R. A. (1975). A schema theory of discrete motor skill learning. *Psychological Review*, 82(4), 225–260.
- Schmidt, R. A. (1976). Control processes in motor skills. *Exercise and Sport Sciences Reviews*, 4, 229–261.
- Schmidt, R. A. (1985). The search for invariance in skilled movement behavior. *Research Quarterly For Exercise and Sport*, 56(2), 188–200.
- Schmidt, R. A., & Lee, T. D. (Eds.) (1999). *Motor control and learning: A behavioral emphasis*. Champaign, IL: Human Kinetics, 3rd ed.
- Schmidt, R. A., Zelaznik, H., Hawkins, B., Frank, J. S., & Quinns, J. T. (1979). Motor-output variability: A theory for the accuracy of rapid motor acts. *Psychological Review*, 86(5), 415–451.
- Sears, T. A., & Stagg, D. (1976). Short-term synchronization of intercostal motoneurone activity. *Journal of Physiology*, 263, 357–381.
- Shapiro, D. C., & Walter, C. B. (1986). An examination of rapid positioning movements with spatiotemporal constraints. *Journal of Motor Behavior*, 18(4), 373–395.

- Shaw, G. L., & Silverman, D. J. (1988). Simulations of the trion model and the search for the code of higher cortical processing. In R. M. J. Cotterill (Ed.) *Computer simulation in brain science*. Cambridge: Cambridge University.
- Singer, W. (1999). Neuronal synchrony: A versatile code for the definition of relations? *Neuron*, *24*, 49–65.
- Smeets, J. B., Brenner, E., & Biegstraaten, M. (2002). Independent control of the digits predicts an apparent hierarchy of visuomotor channels in grasping. *Behavioural Brain Research*, *136*, 427–432.
- Smeets, J. B. J., & Brenner, E. (1999). A new view on grasping. *Motor Control*, *3*, 237–271.
- Smeets, J. B. J., Erkelens, C. J., & Denier van der Gon, J. J. (1990). Adjustments of fast goal-directed movements in response to an unexpected inertial load. *Experimental Brain Research*, *81*, 303–312.
- Soechting, J. F., & Lacquaniti, F. (1981). Invariant characteristics of a pointing movement in man. *Journal of Neuroscience*, *1*(7), 710–720.
- Sowman, P. F., & Türker, K. S. (2005). Methods of time and frequency domain examination of physiological tremor in the human jaw. *Human Movement Science*, *24*, 657–666.
- Sparrow, W. A., & Newell, K. M. (1998). Metabolic energy expenditure and the regulation of movement economy. *Psychonomic Bulletin and Review*, *5*(2), 173–196.
- Stark, L. (Ed.) (1968). *Neurological control systems: Studies in bioengineering*. New York: Plenum.
- Stiles, R. N. (1976). Frequency and displacement amplitude relations for normal hand tremor. *Journal of Applied Physiology*, *40*(1), 44–54.
- Stiles, R. N. (1980). Mechanical and neural feedback factors in postural hand tremor of normal subjects. *Journal of Neurophysiology*, *44*, 40–59.
- Stiles, R. N., & Randall, J. E. (1967). Mechanical factors in human tremor frequency. *Journal of Applied Physiology*, *23*(3), 324–330.

- Taub, E. (1976). Movement in nonhuman primates deprived of somatosensory feedback. *Exercise and Sport Sciences Reviews*, 4, 335–374.
- Taylor, A. (1962). The significance of grouping of motor unit activity. *Journal of Physiology*, 162, 259–269.
- Telford, C. W. (1931). The refractory phase of voluntary and associative responses. *Journal of Experimental Psychology*, 14(1), 1–36.
- Timmer, J., Lauk, M., Pflieger, W., & Deuschl, G. (1998). Cross-spectral analysis of physiological tremor and muscle activity. II. Application to synchronized EMG. *Biological Cybernetics*, 78, 359–368.
- Topka, H., Mescheriakov, S., Boose, A., Kuntz, R., Hertrich, I., Seydel, L., Dichgans, J., & Rothwell, J. (1999). A cerebellar-like terminal and postural tremor induced in normal man by transcranial magnetic stimulation. *Brain*, 122, 1551–1562.
- Travis, L. E. (1929). The relation of voluntary movement to tremors. *Journal of Experimental Psychology*, 12, 515–524.
- Uno, Y., Kawato, M., & Suzuki, R. (1989). Formation and control of optimal trajectory in human multijoint arm movement. *Biological Cybernetics*, 61, 89–101.
- Vallbo, Å. B., & Wessberg, J. (1993). Organization of motor output in slow finger movements in man. *Journal of Physiology*, 469, 673–691.
- van Beers, R. J., Baraduc, P., & Wolpert, D. M. (2002). Role of uncertainty in sensorimotor control. *Philosophical Transactions of the Royal Society B: Biological Sciences*, 357, 1137–1145.
- van Beers, R. J., Haggard, P., & Wolpert, D. M. (2004). The role of execution noise in movement variability. *Journal of Neurophysiology*, 91, 1050–1063.
- Vince, M. A. (1948). The intermittency of control movements and the psychological refractory period. *British Journal of Psychology*, 38, 149–157.
- Viviani, P., & Terzuolo, C. (1982). Trajectory determines movement dynamics. *Neuroscience*, 7(2), 431–437.

- von Hofsten, C. (1980). Predictive reaching for moving objects by human infants. *Journal of Experimental Child Psychology*, 30, 369–382.
- von Seelen, W., Mallot, H. A., Krone, G., & Dinse, H. (1986). On information processing in the cat's visual cortex. In G. Palm, & A. Aertsen (Eds.) *Brain theory*, (pp. 49–79). Berlin: Springer.
- Wadman, W. J., Denier van der Gon, J. J., Geuze, R. H., & Mol, C. R. (1979). Control of fast goal-directed arm movements. *Journal of Human Movement Studies*, 5, 3–17.
- Wallace, S. A., & Newell, K. M. (1983). Visual control of discrete aiming movements. *Quarterly Journal of Experimental Psychology*, 35A, 311–321.
- Welford, A. T. (1967). Single-channel operation in the brain. *Acta Psychologica*, 27, 5–22.
- Welford, A. T. (1980). The single-channel hypothesis. In A. T. Welford (Ed.) *Reaction Times*, (pp. 215–252). London: Academic.
- Welsh, J. P., Lang, E. J., Sugihara, I., & Llinás, R. (1995). Dynamic organization of motor control within the olivocerebellar system. *Nature*, 374, 453–457.
- Welsh, J. P., & Llinás, R. (1997). Some organizing principles for the control of movement based on olivocerebellar physiology. *Progress in Brain Research*, 114, 449–461.
- Wessberg, J. (1996). Significant left-right synchronisation of pulsatile motor output in a human bimanual finger movement task. *Society for Neuroscience Abstracts*, 22, 428.
- Wessberg, J., & Kakuda, N. (1999). Single motor unit activity in relation to pulsatile motor output in human finger movements. *Journal of Physiology*, 517, 273–285.
- Wessberg, J., & Vallbo, Å. B. (1995a). Coding of pulsatile motor output by human muscle afferents during slow finger movements. *Journal of Physiology*, 485, 271–282.

- Wessberg, J., & Vallbo, Å. B. (1995b). Human muscle spindle afferent activity in relation to visual control in precision finger movements. *Journal of Physiology*, *482*, 225–233.
- Wessberg, J., & Vallbo, Å. B. (1996). Pulsatile motor output in human finger movements is not dependent on the stretch reflex. *Journal of Physiology*, *493*, 895–908.
- Wickens, C. D. (1984). Processing resources in attention. In R. Parasuraman, & D. R. Davies (Eds.) *Varieties of attention*, (pp. 63–102). Orlando, FL: Academic.
- Widrow, B., & Stearns, S. D. (1985). *Adaptive signal processing*. Englewood Cliffs, NJ: Prentice-Hall.
- Wolpert, D. M., Ghahramani, Z., & Jordan, M. I. (1995). Are arm trajectories planned in kinematic or dynamic coordinates? An adaptation study. *Experimental Brain Research*, *103*, 460–470.
- Woodworth, R. S. (1899). The accuracy of voluntary movement. *Psychological Review*, *3*(Monograph suppl. 2), 1–119.
- Wright, C. E., & Meyer, D. E. (1983). Conditions for a linear speed-accuracy trade-off in aimed movements. *Quarterly Journal of Experimental Psychology*, *35A*, 279–296.
- Yap, C. B., & Boshes, B. (1967). The frequency and pattern of normal tremor. *Electroencephalography and Clinical Neurophysiology*, *22*, 197–203.
- Zelaznik, H. N. (1993). Necessary and sufficient conditions for the production of linear speed-accuracy trade-offs in aimed hand movements. In K. M. Newell, & D. M. Corcos (Eds.) *Variability and motor control*, (pp. 91–115). Champaign, IL: Human Kinetics.
- Zelaznik, H. N., Mone, S., McCabe, G. P., & Thaman, C. (1988). Role of temporal and spatial precision in determining the nature of the speed-accuracy trade-off in aimed-hand movements. *Journal of Experimental Psychology: Human Perception and Performance*, *14*(2), 221–230.

- Zelaznik, H. N., Schmidt, R. A., & Gielen, S. C. (1986). Kinematic properties of rapid aimed hand movements. *Journal of Motor Behavior*, 18, 353–372.
- Zelaznik, H. N., Shapiro, D. C., & McColsky, D. (1981). Effects of a secondary task on the accuracy of single aiming movements. *Journal of Experimental Psychology: Human Perception and Performance*, 7, 1007–1018.



---

## APPENDIX A

### Properties of logarithmic functions

---

#### A.1 Changing the base of a logarithm

For each strictly positive real number  $a$  and  $b$ , different from 1, we have

$$\log_a(x) = \frac{1}{\log_b(a)} \log_b(x) \quad (\text{A.1})$$

We will prove that

$$\log_b(a) \log_a(x) = \log_b(x) \quad (\text{A.2})$$

Let

$$\log_b(a) = u \quad (\text{A.3})$$

$$\log_a(x) = v \quad (\text{A.4})$$

$$\log_b(x) = w \quad (\text{A.5})$$

Then

$$b^u = a \quad (\text{A.6})$$

$$a^v = x \quad (\text{A.7})$$

$$b^w = x \quad (\text{A.8})$$

From Equations A.7 and A.8 we have

$$a^v = b^w \quad (\text{A.9})$$

Using Equation A.6,

$$(b^u)^v = b^{uv} = b^w \quad (\text{A.10})$$

Therefore,

$$uv = w \quad (\text{A.11})$$

or

$$\log_b(a) \log_a(x) = \log_b(x) \quad (\text{A.12})$$

□

## A.2 Logarithm of a fraction

We have

$$\log_a\left(\frac{x}{y}\right) = -\log_a\left(\frac{y}{x}\right) \quad (\text{A.13})$$

We will prove that

$$\log_a\left(\frac{x}{y}\right) = \log_a(x) - \log_a(y), \quad (\text{A.14})$$

and thus, by analogy,

$$\begin{aligned} \log_a\left(\frac{y}{x}\right) &= \log_a(y) - \log_a(x) \\ &= -(\log_a(x) - \log_a(y)) \\ &= -\log_a\left(\frac{x}{y}\right) \end{aligned} \quad (\text{A.15})$$

Let

$$\log_a(x) = u \quad (\text{A.16})$$

$$\log_a(y) = v \quad (\text{A.17})$$

Then

$$a^u = x \tag{A.18}$$

$$a^v = y \tag{A.19}$$

Therefore

$$\begin{aligned} \log_a \left( \frac{x}{y} \right) &= \log_a a^{u-v} \\ &= u - v \\ &= \log_a(x) - \log_a(y) \end{aligned} \tag{A.20}$$

□

---

## APPENDIX B

### Block diagrams of the simulator

---

This appendix provides a brief explanation of the various components of the BUMP model simulator. In the following, readers may refer to Chapter 2 for details on the SA, RP, and RE systems and their interaction. While this thesis is particularly concerned with the RP system, a detailed overview of all three systems can be found in Neilson & Neilson (2005b).

#### B.1 Simulator used for Study I

Fig. B.1 shows a block diagram of the Simulink implementation of the BUMP model used for Study I in Chapter 3. This chapter dealt with speed-accuracy tradeoffs and velocity profiles in aimed movements. Therefore, the simulator was set up to make discrete movements to a stationary target. In engineering terms, this is equivalent to tracking of a step signal. In Fig. B.1 the **Step**<sup>1</sup> block provides such a step signal with unity magnitude. The step signal is then (optionally) scaled by the **Gain** block and fed through the **MAD Stimulus Predictor block**, which predicts the future state of the **stimulus** signal. Naturally, for a stationary stimulus this prediction is very simple.

The RP system consists of the **Response Planner** and the **Prediction Horizon** blocks. Given sensory information about the state of the response (**zoh position** and **zoh velocity**), the part of the response estimated to be due to noise (**disturbance prediction**), and the predicted future state of the stimulus

---

<sup>1</sup>Names of blocks and signals in the diagram are denoted in boldface.

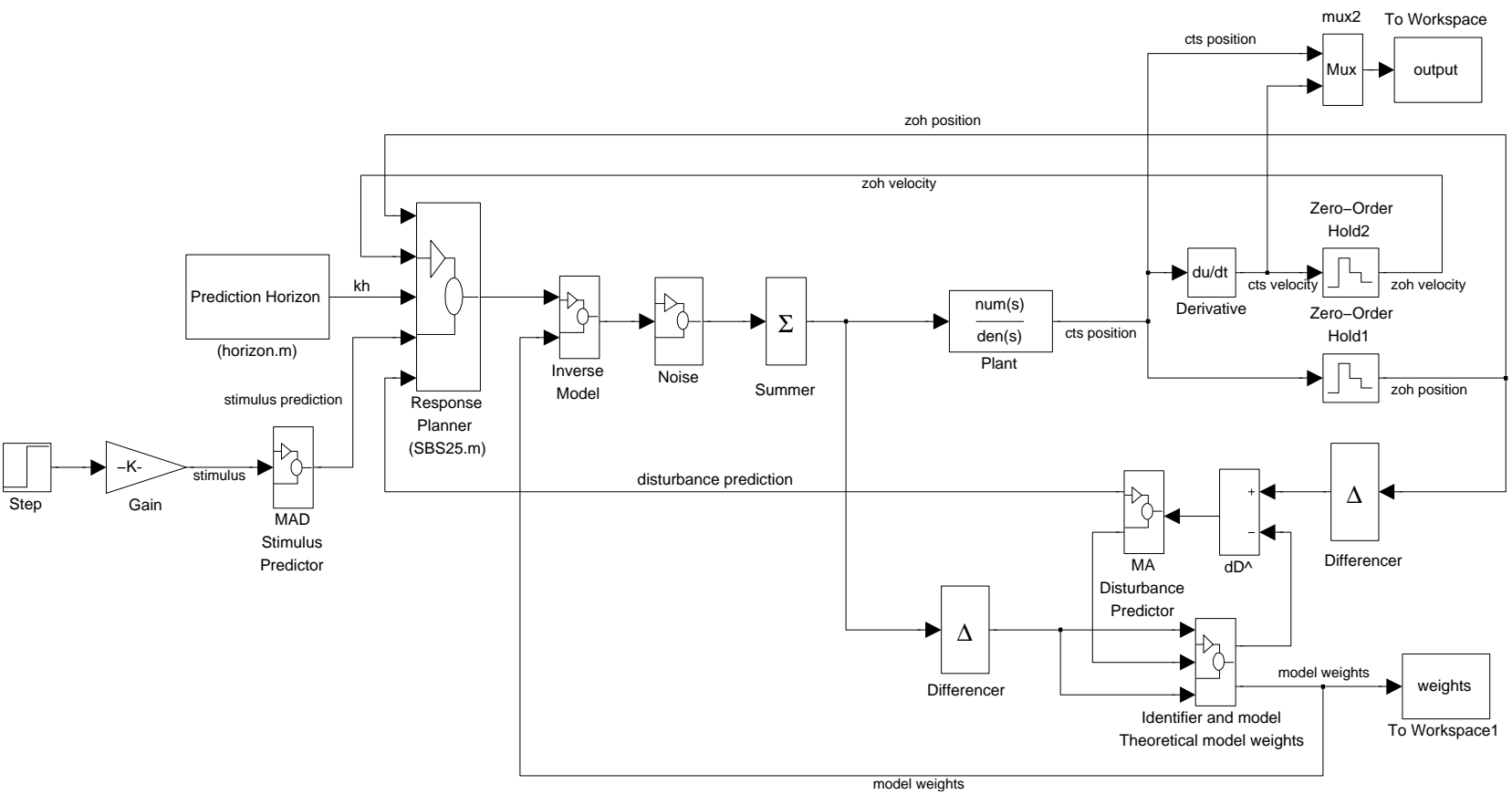


Figure B.1: Simulink block diagram of the BUMP model simulator used for Study I in Chapter 3.

(**stimulus prediction**), the RP system plans an optimal trajectory with a prediction horizon (**kh**), or duration, provided by the **Prediction Horizon** block.

When the RP system has finished calculating an optimal desired trajectory after an RP interval of 100 ms, it passes the first-differences of the desired position trajectory to the RE system, which in turn transforms these signals into appropriate first-differenced motor commands through an **Inverse Model**. The first-differenced motor commands have signal-dependent noise added to them by the **Noise** block before being transformed to positional motor commands through the postural **Summer**. The postural summer holds the motor commands on line such that only changes in the motor commands need to be processed centrally. This reduces the demand on resources as it allows unchanged motor commands to be supplied to all those muscles that maintain fixed aspects of posture in a task. The summed control signal from the **Summer** block is fed to the **Plant**, which consists of a wired-in synergy generator, the musculoskeletal system, and the external world lumped together. When the inverse model is perfectly accurate, the motor commands will force the output of the plant to track the desired response and any deviation will be solely due to signal-dependent noise. The ZOH position and velocity output is fed back to the RP system as sensory feedback and another optimal trajectory can be generated during the next planning interval.

The output of the plant as well as an efference copy of the motor commands are converted to first-difference signals through **Differencer** blocks and fed into a modelling network containing a forward model of the plant. Thus, this modelling network performs adaptive tuning of the inverse model of the plant based on signals with statistical properties similar to those that they will ultimately transform. Experimental observations concerning the accuracy of internal models support the inclusion of postural summers and the associated use of first-difference signals for the formation of models (Davidson, Jones, Sirisena, & Andreae, 2000; Ghous & Neilson, 2002).

To simulate a highly skilled subject, the inverse model is set to perfectly cancel the dynamics of the plant and the modelling network is turned off to ensure that the inverse model remains unchanged. To simulate a less skilled subject, the inverse model is first set to be highly inaccurate and the modelling network is turned on. Running a simulation for a period of time, the inverse model is gradually tuned and becomes more accurate. When the desired accuracy is reached, the inverse model is stored and the modelling network is turned off. The simulator can then be run with the inverse model obtained during adaptation.

## B.2 Simulator used for Study II

Fig. B.2 shows a block diagram of the Simulink implementation of the BUMP model used for Study II in Chapter 4. The simulator is identical to the one depicted in Fig. B.1 with two exceptions: First, Chapter 4 dealt with the simulator's ability to reproduce physiological tremor in a human ramp movements. Therefore, the **Step** block in Fig. B.1 is replaced with a **Signal Builder** containing a set of stimulus, or tracking, signals consisting of sequences of ramp and hold movements. A **Multipoint Switch** and an **inputsig** block provides the ability to select a particular tracking signal.

Second, there is an inherent limitation in Simulink with respect to calculating correct continuous-time derivatives. This problem is overcome by feeding the plant's ZOH velocity signal through a  $\Phi$  block in series with a gain and a derivative block. The  $\Phi$  block contains a simple mathematical operation that together with the gain and derivative blocks produce the mathematically correct acceleration signal of the plant, consisting of rectangular 50 ms acceleration pulses as described in Chapter 2. These pulses are then integrated once and twice to obtain the velocity and position signal, respectively, at any sampling rate desirable. In Study II, the sampling rate was set to 100 Hz, more than sufficient for frequency analysis of 10 Hz physiological tremor.

For more details on the implementation of the simulator, please refer to MATLAB and Simulink source files contained on the CD-ROM accompanying this thesis (see Appendix C for CD-ROM content).



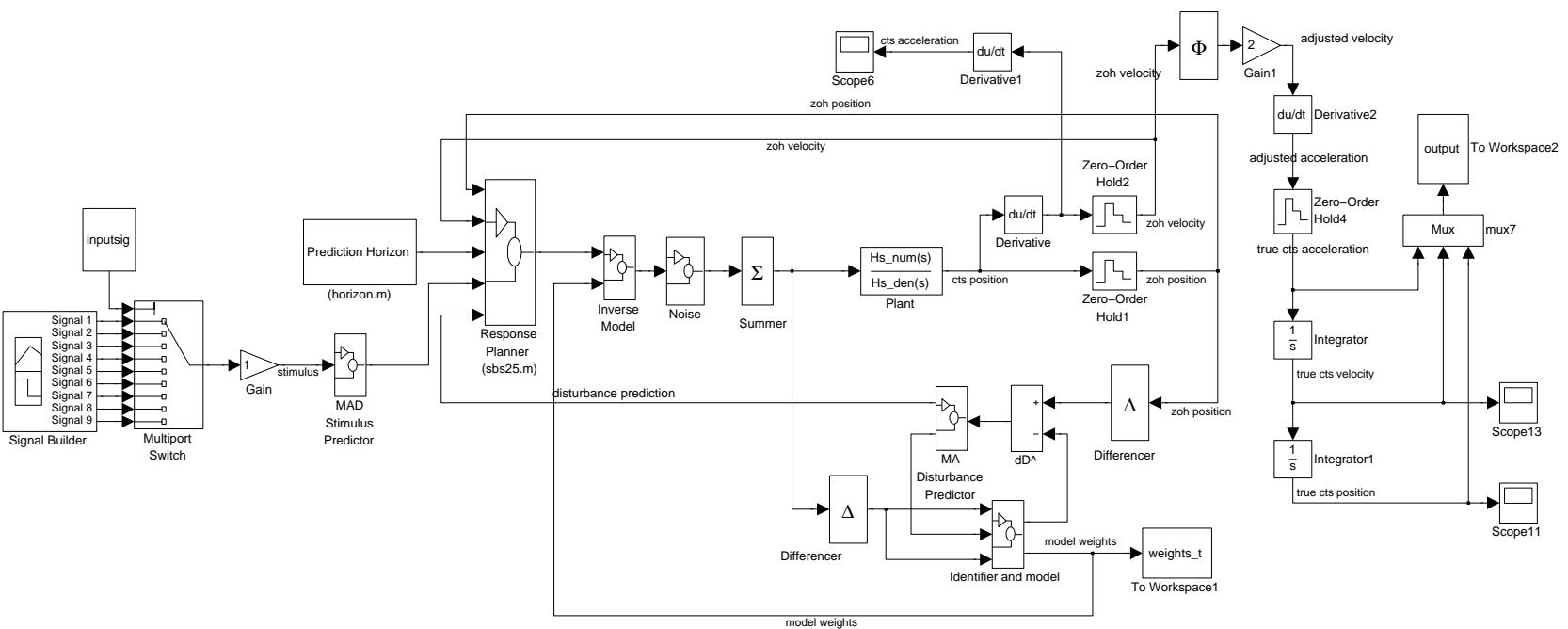


Figure B.2: Simulink block diagram of the BUMP model simulator used for Study II in Chapter 4.

---

## APPENDIX C

### CD-ROM content

---

The accompanying CD-ROM contains the following directories:

**LaTeX** contains the  $\text{\LaTeX}$  development for this thesis.

**MATLAB** contains MATLAB and Simulink files used for simulation, analysis, and illustration.

**Papers** contains digital copies of most of the references as well as other researched material of partial relevance.

**PhDthesis.pdf** is this document.